An intrinsically disordered region of OSBP controls membrane contact site geometry and dynamics

Denisa Jamecna

UNIVERSITÉ CÔTE D'AZUR

ÉCOLE DOCTORALE
SCIENCES DE LA VIE ET DE LA SANTÉ

THÈSE DE DOCTORAT

Une région intrinsèquement désordonnée dans OSBP contrôle la géométrie et la dynamique du site de contact membranaire

Denisa JAMECNA

Institut de Pharmacologie Moléculaire et Cellulaire, CNRS, UMR 7275

Présentée en vue de l'obtention du grade de docteur en Sciences de l'Université Côte d'Azur

Mention : Interactions moléculaires et cellulaires

Dirigée par Bruno ANTONNY / Joëlle BIGAY

Soutenue le 12 Décembre 2018, devant le jury composé de :

Laurent COUNILLON	Professeur, Université Côte d'Azur, LP2M, Nice	Président du jury
Anne-Claude GAVIN	Directrice de Recherche, EMBL, Heidelberg, Allemagne	Rapportrice
Vesa OLKKONEN	Professeur, Université de Helsinki, Helsinki, Finlande	Rapporteur
Daniel LÉVY	Directeur de Recherche, CNRS, Institut Curie, Paris	Examinateur
Bruno ANTONNY	Directeur de Recherche, CNRS, IPMC, Valbonne	Directeur de thèse
Joëlle BIGAY	Chargée de Recherche, CNRS, IPMC, Valbonne	Directrice de thèse

sbcf Société de Biologie Cellulaire de France

FEBS

ipmc

cnrs

SIGNALIFE

Une région intrinsèquement désordonnée dans OSBP contrôle la géométrie et la dynamique du site de contact membranaire

An intrinsically disordered region of OSBP controls membrane contact site geometry and dynamics

Jury:

Président du jury

Laurent COUNILLON, Professeur de l'UCA, LP2M, CNRS-UMR 7370

Rapporteurs

Anne-Claude GAVIN, equivalent Directrice de Recherche, EMBL, Heidelberg

Vesa OLKKONEN, Professeur de l'Université de Helsinki, Finlande

Examinateur

Daniel LÉVY, Directeur de Recherche, Institut Curie, Paris

Directeurs de thèse

Bruno ANTONNY, Directeur de Recherche, IPMC, CNRS-UMR 7275

Joëlle BIGAY, Directrice de Recherche, IPMC, CNRS-UMR 7275

Une région intrinsèquement désordonnée dans OSBP contrôle la géométrie et la dynamique du site de contact membranaire

Résumé

La protéine OSBP est un transporteur de lipides qui régule la distribution cellulaire du cholestérol. OSBP comprend un domaine PH, deux séquences « coiled coil », un motif FFAT (deux phénylalanines dans un environement acide), et un domaine de liaison de lipides (ORD) à son extrémité C-terminale. Le domaine PH interagit avec le PI(4)P et la petite protéine G Arf1-GTP au niveau du Golgi, alors que le motif FFAT interagit avec la protéine VAP-A, résidente du réticulum endoplasmique (RE). En liant simultanément tous ces déterminants, OSBP stabilise des sites de contact membranaire entre RE et Golgi, permettant ainsi un contre-échange cholestérol / PI(4)P par l'ORD.

OSBP contient également une longue séquence N-terminale d'environ 80 aa, intrinsèquement désordonnée, composée principalement de glycine, proline et d'alanine. Nous démontrons que la présence de ce N-terminus désordonné augmente le rayon de Stoke de OSBP tronquée du domaine ORD, et limite sa densité d'association sur la membrane portant le PI(4)P. La protéine dépourvue du N terminus favorise l'agrégation symétrique des liposomes PI(4)P (mimant la membrane du Golgi) par les deux domaines PH du dimère OSBP, alors que la présence de la séquence désordonnée empêche cette association symétrique. De même, nous observons que la distribution d'OSBP sur la membrane de vésicules unilamellaires géantes (GUV) varie selon la présence ou l'absence du N-terminus. En présence de la séquence désordonnée, la protéine est répartie de manière homogène sur toute la surface du GUV, alors que la protéine sans N-terminal a tendance à s'accumuler à l'interface entre deux GUV de type Golgi. Cette accumulation locale ralentit fortement la mobilité de la protéine à l'interface. Un effet similaire du N-terminal sur la dynamique des protéines est observé lorsque l'association de membranes de type ER et Golgi est assuré par des protéines monomériques (dépourvue du coiled coil) en présence de Vap-A.

Les résultats de nos expériences in vitro ont été confirmés en cellules vivantes, où la séquence intrinsèquement désordonnée contrôle le recrutement d'OSBP sur les membranes Golgiennes, sa mobilité et sa dynamique d'activité au cours des cycles de transfert de lipides. La plupart des protéines de la famille d'OSBP contiennent des séquences N-terminales de faible complexité, suggérant un mécanisme général de régulation.

Mots clés : protéine intrinsèquement désordonnée, protéine de transfert de lipides, OSBP, diffusion membranaire, site du contact membranaire, tethering de membranes

An intrinsically disordered region of OSBP controls membrane contact site geometry and dynamics

Abstract

Oxysterol binding protein (OSBP) is a lipid transfer protein that regulates cholesterol distribution in cell membranes. OSBP consists of a pleckstrin homology (PH) domain, two coiled-coils, a "two phenylalanines in acidic tract" (FFAT) motif and a C-terminal lipid binding **O**SBP-**R**elated **D**omain (ORD). The PH domain recognizes PI(4)P and small G protein Arf1-GTP at the Golgi, whereas the FFAT motif interacts with the ER-resident protein VAP-A. By binding all these determinants simultaneously, OSBP creates membrane contact sites between ER and Golgi, allowing the counter-transport of cholesterol and PI(4)P by the ORD.

OSBP also contains an intrinsically disordered ~80 aa long N-terminal sequence, composed mostly of glycine, proline and alanine. We demonstrate that the presence of disordered N-terminus increases the Stoke's radius of OSBP truncated proteins and limits their density and saturation level on PI(4)P-containing membrane. The N-terminus also prevents the two PH domains of OSBP dimer to symmetrically tether two PI(4)P-containing (Golgi-like) liposomes, whereas protein lacking the disordered sequence promotes symmetrical liposome aggregation. Similarly, we observe a difference in OSBP membrane distribution on tethered giant unilamellar vesicles (GUVs), based on the presence/absence of N-terminus. Protein with disordered sequence is homogeneously distributed all over the GUV surface, whereas protein without N-terminus tends to accumulate at the interface between two PI(4)P-containing GUVs. This protein accumulation leads to local overcrowding, which is reflected by slow in-plane diffusion. The effect of N-terminus is also manifested in monomeric OSBP-derived proteins that tether ER-like and Golgi-like membranes in the presence of VAP-A.

Findings from our *in vitro* experiments are confirmed in living cells, where N-terminus controls the recruitment of OSBP on Golgi membranes, its motility and the on-and-off dynamics during lipid transfer cycles. Most OSBP-related proteins contain low complexity N-terminal sequences, suggesting a general effect.

Keywords : intrinsically disordered protein, lipid transfer protein, OSBP, membrane diffusion, membrane contact site, membrane tethering

To my teachers:

Mgr. Mária Birošíková (ZŠ Suľkov, Kysucké Nové Mesto)

Mgr. Ivan Balek (ZŠ Suľkov, Kysucké Nové Mesto)

RNDr. Magdaléna Fiflíková (Hotelová akadémia, Žilina)

SUMMARY

TABLE OF ILLUSTRATIONS

List of Abbreviations

25-OH	25-hydroxycholesterol
aa	amino acid
ABC	ATP-binding cassette transporters
ALPS	Amphipathic lipid packing sensor
AP2	Adaptor protein 2
AP180	Adaptor protein 180
Arf1	ADP-ribosylation factor 1
ArfGAP1	ADP-ribosylation factor GTPase-activating protein 1
ATP	adenosine triphosphate
Bcl-2	B-cell lymphoma-2
BH3	Bcl-2 homology domain
BMP	bis(monoacylglycero)-phosphate
BSA	Bovine serum albumin
CaMKII	Calcium/calmodulin-dependent kinase II
Cdc50	Cell division control protein 50
CERT	Ceramide transfer protein
CFTR	Cystic fibrosis transmembrane conductance regulator
CI2	chymotrypsin inhibitor 2
COPI (or II)	Coat protein I or II
DAG	diacylglycerol
EEA1	Early endosome antigen 1
ENTH	epsin NH2-terminal homology domain
ER	endoplasmic reticulum
ERGIC	ER-Golgi intermediate compartment
Fab1	IP_3 5-kinase Fab1
FAPP2	four-phosphate adaptor protein 2
FCS	fluorescence correlation spectroscopy
FFAT	Two phenylalanines in an acidic tract
Gabarapl2	Gaba(A) receptor-associated protein-like 2
GATE-16	Golgi-associated ATPase enhancer of 16 kDa
GOLPH3	Golgi phosphoprotein 3
GPI	glycosylphosphatidylinositol
GPL	glycerophospholipid
Grp75	glucose-regulated protein 75
IDP	Intrinsically disordered protein
IDPR	Intrinsically disordered protein region
IgG2A	Immunoglobulin gamma-2A
INSIG	Insulin induced gene
IP_3	inositol trisphosphate
IPTG	Isopropyl-β-D-1-thiogalactopyranoside
Ist2	Increased sodium tolerance protein 2
LAF-1	Long after far-red light 1
LE	late endosome
LNS2	Lipin/Nde1/Smp2 domain
LTP	lipid transfer protein
LXR	liver X receptor
MAM	mitochondria-associated membrane
MCS	Membrane contact site
Mfn2	mitofusin-2
MYO18A	Myosin XVIIIa
NMR	Nuclear Magnetic Resonance
ORD	OSBP-related domain
ORP	OSBP-related protein
OSBP	Oxysterol Binding Protein
Osh	OSBP homolog
P4-ATPases	Type 4 P-type ATPases (flippases)
p53	tumor protein p53
PA	phosphatidic acid
PC	phosphatidylcholine
PDB	Protein Data Bank
PE	phosphatidylethanolamine
PH	Pleckstrin homology domain
PI	phosphatidylinositol

PI4KIIα	phosphatidylinositol 4-kinase type 2-alpha
PIs	phosphoinositides
PKA	Protein kinase A
PLC	Phospholipase C
PM	plasma membrane
PONDR	Predictor of Natural Disordered Regions
PS	phosphatidylserine
PTPIP	protein tyrosine phosphatase-interacting protein 51
PVP	polyvinylpyrrolidone
PX	phox-homology
Rab5	Ras-related protein Rab5
RILP	Rab-interacting lysosomal protein
RNA	ribonucleic acid
RNP	ribonucleoprotein
RXR	retinoid X receptor
S100B	S100 calcium binding protein B
SCAP	SREBP cleavage-activating protein
Scs	suppressor of Ca^{2+} sensitivity protein
SD model	Saffman-Delbrück model
Sir2	NAD-dependent protein deacetylase sirtuin 2
SM	sphingomyelin
SMS2	sphingomyelin synthase 2
SREBP	Sterol regulatory element-binding protein
StAR	Steroidogenic Acute Regulatory Protein
StART	StAR-related lipid transfer
Tcb 1 – 3	tricalbin 1 – 3
TGN	*trans*-Golgi network
Vac1	Vacuolar segregation protein pep7
VAMP	Vesicle-associated membrane protein
VAP-A, B	VAMP-associated protein A, B
WT	wild type

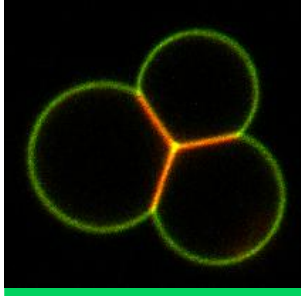

Introduction
&
Working Hypothesis

INTRODUCTION

PART 1: INTRINSICALLY DISORDERED REGIONS

A. DISCOVERY OF INTRINSICALLY DISORDERED PROTEINS

After the discovery of X-rays in 1895 by Wilhelm Röntgen, they were used as a tool to study structure of materials in technology and to visualise tissues under clinical conditions in medicine. X-ray crystallography of biological molecules took off with Dorothy Hodgkin during her PhD in Bernal lab in 1934, where the first X-ray photographs of hydrated protein crystals were taken. Of note, D. Hodgkin also solved the structure of cholesterol (1937) and other biochemical substances, for which she was awarded a Nobel Prize in 1964. During late 1950s, the atomic structure of proteins by X-ray crystallography began to be solved by Sir John Cowdery Kendrew (who crystallized myoglobin in 1959) and by Max Perutz (who solved the structure of haemoglobin in the same year) - for which they shared a Nobel Prize in 1962. Over the oncoming decades, evidence accumulated that a well-defined 3D structure is a prerequisite for protein function, and authors exquisitely relied on the *structure-function paradigm* in biology and biochemistry textbooks for many years. However, some deviations from this paradigm were apparent since the very beginning – in X-ray datasets, many protein regions could not be assigned a fixed, unique position relative to the crystal lattice, indicating that these regions occupy multiple positions, which average out in the electron density maps. Similarly, nuclear magnetic resonance (NMR) spectroscopy demonstrated the presence of large flexible amino acid sequences in solved structural ensembles. Therefore, while there was no doubt that protein structure and function are closely linked, there was also a growing awareness that not all biologically functional proteins fold spontaneously into stable structures (Boesch et al., 1978; Daniels et al., 1978), and that missing regions of electron density of several proteins likely carried out important functions (Gast et al., 1995; Huber and Bennett, 1983). Only around the turn of the millennium, several authors raised that many protein regions are intrinsically

unstructured (later called “disordered”) under native conditions (Tompa, 2002; Wright and Dyson, 1999).

Currently, Protein Data Bank (PDB) contains more than 130000 protein structures solved by X-ray crystallography and more than 12000 protein structures solved by NMR. Thousands of them have been shown to contain disordered regions, and the extent of intrinsic disorder varies from protein to protein. In this thesis, the term intrinsically disordered protein (IDP) refers both to proteins that are completely intrinsically disordered and to those that mostly consist of disordered residues, with few ordered regions. The term intrinsically disordered protein region (IDPR) refers to a sequence of disorder within a folded protein.

The identification of many IDPs/IDPRs enabled the development of sophisticated bioinformatic algorithms for predicting disorder from amino acid sequence. In 1997, the first Predictor Of Natural Disordered Regions (PONDR) was developed which further advanced the field (Romero et al., 1997). Since 1997, more than 70 different structure predictors have been developed based on different principles (He *et al.*, 2009; Li *et al.*, 2015). They have shown that a significant fraction of every proteome is occupied by proteins that do not form a unique 3D structure - around 10 - 35% of prokaryotic and 15 - 45% of eukaryotic proteins contain disordered regions of at least 30 residues in length (Tompa, 2012).

B. CHARACTERISTICS AND FUNCTIONS OF INTRINSICALLY DISORDERED PROTEINS AND PROTEIN REGIONS

Structural and functional properties of proteins are encoded by the alphabet of 20 naturally occurring amino acids. One of the characteristics of IDPs and IDPRs is the presence of low sequence complexity and a bias in the amino acid composition. Disordered sequences tend to display relatively low proportion of bulky hydrophobic (Val, Leu, Ile) and aromatic residues (Phe, Trp and Tyr), which usually form the hydrophobic core of a globular protein, and a high proportion of charged and polar residues (Glu, Ser, Gln, Lys, Gly and Ala). The highest level of abundance and conservation in IDPs/IDPRs is exhibited by a hydrophobic, yet structure breaking

proline (Pro). Proline is unique in that it is the only imino acid – the backbone nitrogen is bound to two alkyl carbons, it lacks the usual proton and creates a distinctive cyclic structure which renders the backbone conformation more rigid than in any other amino acid. Also, proline does not contain backbone amide hydrogen atoms at physiological pH, and is therefore not able to form stabilizing hydrogen bonds in α-helices or β-sheets. Hence, IDPs contain, on average 1.8-times more prolines than folded proteins (Theillet *et al.*, 2013). The second most disorder-promoting residue is glutamic acid (Glu), due to the presence of the carboxylic functional group. Glutamic acid has a large polar surface (121 $Å^2$ vs 69 $Å^2$ of nonpolar surface) and the estimated hydrophobic effect associated with the burial of this residue is 1.74 kcal/mol. Therefore, glutamic acid is 1.49-times more enriched in disordered regions, and 93% of glutamic acid residues in folded proteins are located on the surface so that they have access to the solvent (Karplus, 1997; Uversky, 2013). Of note, the third most disorder-promoting residue is serine due to the presence of its hydroxyl group and large polar surface (56 $Å^2$ vs 59 $Å^2$ of nonpolar surface) (Uversky, 2015; see **Figure 1**).

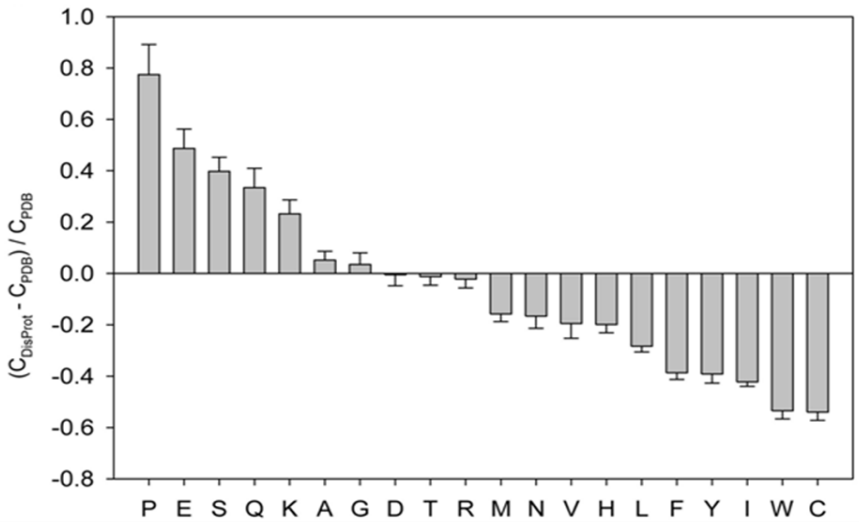

Figure 1: Amino acid determinants define structural and functional differences between ordered and intrinsically disordered proteins

Residue-specific compositional profile between typical IDPs from the DisProt database and a set of completely ordered proteins is shown. The compositional profile was evaluated as $(C_{DisProt} - C_{PDB})/C_{PDB}$, where $C_{DisProt}$ is the content of a given amino acid in a DisProt database, and C_{PDB} is the corresponding content in the data set of fully ordered proteins. Positive bars correspond to residues abundant in IDPs, whereas negative bars correspond to residues depleted in IDPs. Histogram from Uversky, 2015.

Computational analyses of sequences and atomistic simulations have revealed that amino acid composition affects the conformational states of IDPRs and can determine whether they adopt totally extended or rather compact conformation (Das *et al.*, 2015; Mao *et al.*, 2010). At least 75% of known IDPs are polyampholytes, e.g. they contain both cationic and anionic residues, and the fraction of charged residues discriminates between weak and strong polyampholytes. Especially in strong polyampholytes the charge patterning is an important factor - linear sequence distribution of oppositely charged residues influences the extended/collapsed conformation of IDPs, as illustrated in **Figure 2** (Das and Pappu, 2013).

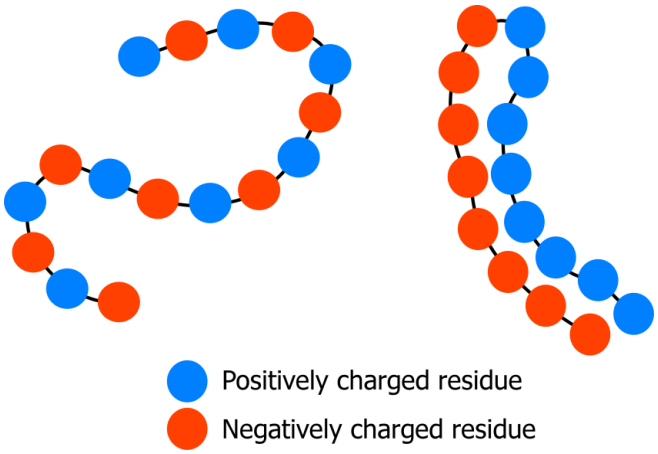

Figure 2: Conformations of IDPs are influenced by linear sequence distribution of oppositely charged residues

The conformational preferences of strong polyampholytic proteins are determined by a combination of fraction of charged residues and the linear sequence distribution of oppositely charged residues. The conformational properties of sequences with balanced distribution of positive and negative residues are, on average, similar to self-avoiding random coils, whereas sequences with high charge asymmetry sample hairpin-like (collapsed) conformations.

Distribution of disorder within proteins is not homogeneous – protein tails are usually more likely to be disordered than centrally placed residues (Uversky, 2013b). Of note, many IDPs can fold into a defined 3D structure upon binding to their cognate partners (Demarest *et al.*, 2002; Dyson and Wright, 2005). Under these circumstances,

either whole disordered sequence folds into a domain, or part of it remains highly dynamic in the complex, leading to formation of fuzzy complexes (Fuxreiter, 2012; Sharma *et al.*, 2015; Tompa and Fuxreiter, 2008). Folding and binding of IDPRs in fuzzy complexes facilitates the interaction with their partners via transient interactions with low affinity but relatively high specificity (Babu, 2016).

In the following chapters, selected functions of intrinsically disordered proteins will be illustrated to highlight their functional versatility.

1. IDPs AS MEDIATORS OF PROTEIN-PROTEIN INTERACTIONS

IDPs and IDPRs are involved in numerous biological processes, where their function results from the conformational plasticity associated with lack of stable 3D structure. Considering that up to 45% of eukaryotic proteins contain large IDPRs, it is not surprising that these proteins hold key positions in the protein-protein interaction networks. Intrinsic disorder is a common feature of hub proteins that are able to interact with unusually large number of interaction partners (Dosztányi *et al.*, 2006; reviewed in Gsponer and Madan Babu, 2009). Interactome networks around hub proteins are generally resistant to removal of any part of the network but are extremely sensitive to removal of the hub. A good demonstrative example is p53, a well-known hub protein with two large disordered regions at the N-terminus (transactivation domains and proline rich region) and C-terminus (oligomerization and regulatory domains). The STRING database-derived interactome of p53 includes 302 nodes and 1884 edges, underlining the extreme binding promiscuity of p53 (Tompa *et al.*, 2016; Uversky, 2016). As a result, altered expression or mutations in p53 have been associated with severe pathological conditions such as cancer (Avantaggiati *et al.*, 1997; Levine *et al.*, 1991).

Disordered regions frequently expose short linear motifs (3-10 amino acids long) that mediate protein-protein interactions, usually characterized by fast association and dissociation rates. Short motifs permit interaction of the same protein in a functionally promiscuous manner or assembly of multiple proteins by serving as a scaffold. An excellent example from the membrane traffic field is the AP2 adaptor protein. AP2

contains a trunk domain that binds to cargo and lipids, and two appendage domains, positioned on flexible linkers. The appendage domains form the protein interaction surface for accessory proteins, when concentrated in emerging coated pits. The adaptor protein complexes do not self-polymerize, so their concentration and stabilization in the pits occurs via binding partners. Appendage domains can bind many different binding partners, which in turn can interact with each other and indirectly with clathrin (Praefcke *et al.*, 2004).

Similarly, disordered regions can also harbour short structured binding motifs, as it is the case in the clathrin binding domain of adaptor protein AP180. The domain is predominantly unstructured but contains 12 short structured clathrin binding elements. The observations of Zhuo *et al.* (2010) show that weak binding by multiple clathrin binding elements regularly dispersed throughout a largely unstructured domain allows efficient recruitment of clathrin to endocytic sites and dynamic assembly of the clathrin lattice (**Figure 3**). In the final coated vesicle, most appendage binding partners are absent, indicating that the function of the unstructured domains of adaptor proteins as an interaction hub is temporal, transitory, and provides directionality to vesicle assembly (Schmid and McMahon, 2007).

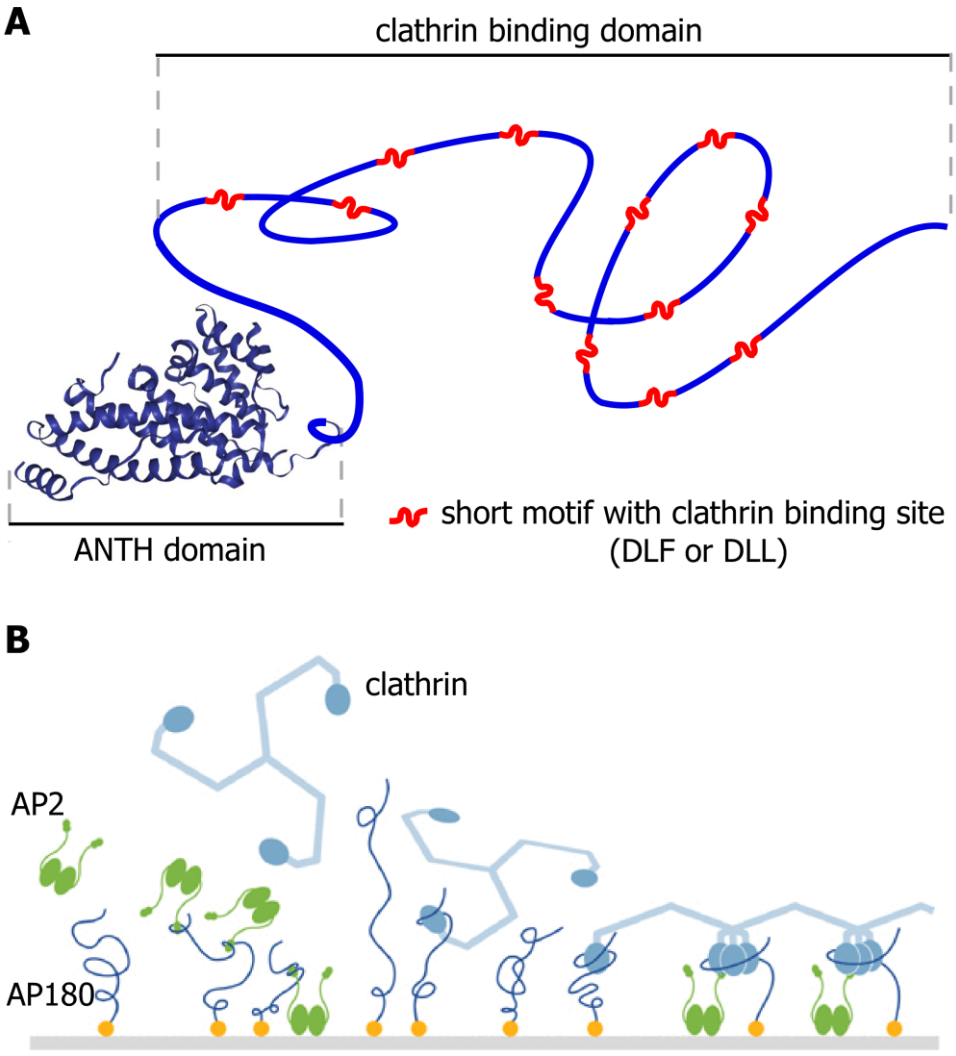

Figure 3: Domain structure of AP180 and early events in clathrin-mediated endocytosis

(A) AP180 is a clathrin assembly protein with a structured N-terminal ANTH domain that interacts with membrane phospholipids, namely PI(4,5)P_2 (PDB ID: 1HX8, Ford *et al.,* 2001; Mao *et al.*, 2001). AP180 contains an unstructured clathrin binding domain with putative clathrin binding motifs DLF or DLL (shown in red) **(B)** Early events in clathrin-mediated endocytosis depend on IDPRs. After binding to the membrane, the long flexible domains of AP180 bind several sites on AP2 and clathrin. In combination with the self-assembly of clathrin triskelions, this would result in highly cooperative assembly mechanism (Kalthoff *et al.,* 2002; Dafforn and Smith, 2004). The process of clathrin recruitment by the IDPRs of AP2/AP180 is described by some authors as "protein fishing" (Evans, 2002).

2. PROTEIN TRAFFICKING AND SUBCELLULAR LOCALIZATION ARE REGULATED BY INTRINSIC DISORDER

Many proteins are shuttled through several membrane compartments during biogenesis and later in their degradation via the lysosomal or ubiquitin-dependent proteasomal pathway. The signals regulating transport are often located in IDPRs in the form of short linear motifs. Their interactions can be modulated by flanking residues outside the motif and via posttranslational modifications, primarily phosphorylation (described in the paragraph below). Some well characterized sorting signals targeting proteins to different compartments of the endocytic and post-Golgi secretory pathways include the cytosolic dilysine KKXX or dileucine-based motifs (D/E)XXXL(L/I), luminal KDEL motifs for ER retention/retrieval and tyrosine based sorting signals such as YXXØ, where Ø is a bulky hydrophobic residue (Bonifacino and Dell'Angelica, 1999; Kozik *et al.*, 2010). A recent peptide-based proteomic screen of Meyer *et al.* reports that mutations in disordered cytosolic regions of three transmembrane proteins (GLUT1, ITPR1 and CACNA1H) can create dileucine motifs, leading to increased clathrin recruitment and mistrafficking of proteins (Meyer *et al.*, 2018).

3. IDPRS HARBOUR POSTTRANSLATIONAL MODIFICATIONS

Conformational flexibility of IDPs greatly increases the accessibility of a modifying enzyme to the modification sites. Consequently, IDPRs are frequent target of diverse posttranslational modifications, which expand their functional scope. Posttranslational modifications on regulatory IDPRs can affect protein interaction with binding partners or its conformation, as in the case of cystic fibrosis transmembrane conductance regulator (CFTR). CFTR is a dimeric chloride channel that opens upon phosphorylation on nine PKA phosphorylation sites localized in a regulatory loop. Multiple phosphorylation excludes the regulatory IDPRs from the dimer interface, which facilitates gating of the channel (Bozoky *et al.*, 2013).

Posttranslational modifications can also lead to a complete switch between disordered and folded states. For instance, multisite phosphorylation induces folding of

intrinsically disordered factor 4E-BP2, which is involved in regulation of mRNA translation (Bah *et al.*, 2015).

4. *DISORDER-TO-ORDER TRANSITION IN AMPHIPATHIC HELICES*

Many studies have suggested that when binding to a partner, IDPs and IDPRs may undergo disorder-to-order transitions, i.e. folding upon binding. This means that instead of an ensemble of conformations, IDPs adopt a stable, well-defined structure. Final conformations of IDPs bound to partner can differ depending on partner protein. For example, the disordered C-terminal domain of p53 can fold and bind as a strand (Avalos *et al.*, 2002), a helix (Rustandi *et al.*, 2000) or a coil (Lowe *et al.*, 2002) when interacting with Sir2, S100B(ββ) and cyclin A, respectively. In other cases, an IDP can form the same structure regardless of the binding partner, as when disordered BH3-only proteins bind to BCL-2 family proteins form a single helix (Crabtree *et al.*, 2018).

An interesting case occurs when the interaction partner of IDPs/IDPRs is not another protein but rather a polar-apolar interface – as it is the case of amphipathic helices. Many amphipathic helices are unfolded in ionic buffer (although they can be found in stably folded proteins), contain charged (polar) residues and display segregation of hydrophobic and polar residues between two opposite faces of the α-helix (Giménez-Andrés *et al.*, 2018). Mechanistic studies on amphipathic peptides suggest that membrane binding occurs in three steps: First, unfolded sequence is attracted to negatively charged membranes via long-range electrostatic interactions. Second, hydrophobic residues are inserted between the lipid acyl chains due to the hydrophobic effect. Last, a disorder-to-order transition occurs to reduce the energy penalty of having exposed peptide bonds in a hydrophobic environment. The last step accounts for 50-60% of the free energy of binding (**Figure 4A**, Seelig, 2004). As example, perilipin 4 is a giant amphipathic helix that is unfolded in solution but adopts a helical structure on the surface of lipid droplets where it can serve as a coat replacing the phospholipid monolayer (Čopič *et al.*, 2018).

A special group of amphipathic helices are the ALPS motifs (Amphipathic Lipid Packing Sensor). What distinguishes ALPS motifs from classical amphipathic helices is the absence of charged residues in their polar face and their lack of structure in solutions. In ALPS the polar face is usually not cooperating with the hydrophobic face in breaking cohesive forces between lipids and inserting helix into the membrane (Drin and Antonny, 2010). Therefore, ALPS motifs rely on imperfections in the geometrical arrangement of membrane lipids, i.e. lipid packing defects, which expose hydrophobic chains of lipids and are frequent in curved membranes (Bigay and Antonny, 2012). ALPS motifs have been shown to respond very strongly to changes in membrane curvature, especially in the range of R = 30-100nm. They are present in a variety of membrane interacting proteins, such as ArfGAP1 or golgin GMAP-210 (**Figure 4B**, (Bigay et al., 2005; Magdeleine et al., 2016; Uversky and Eliezer, 2009).

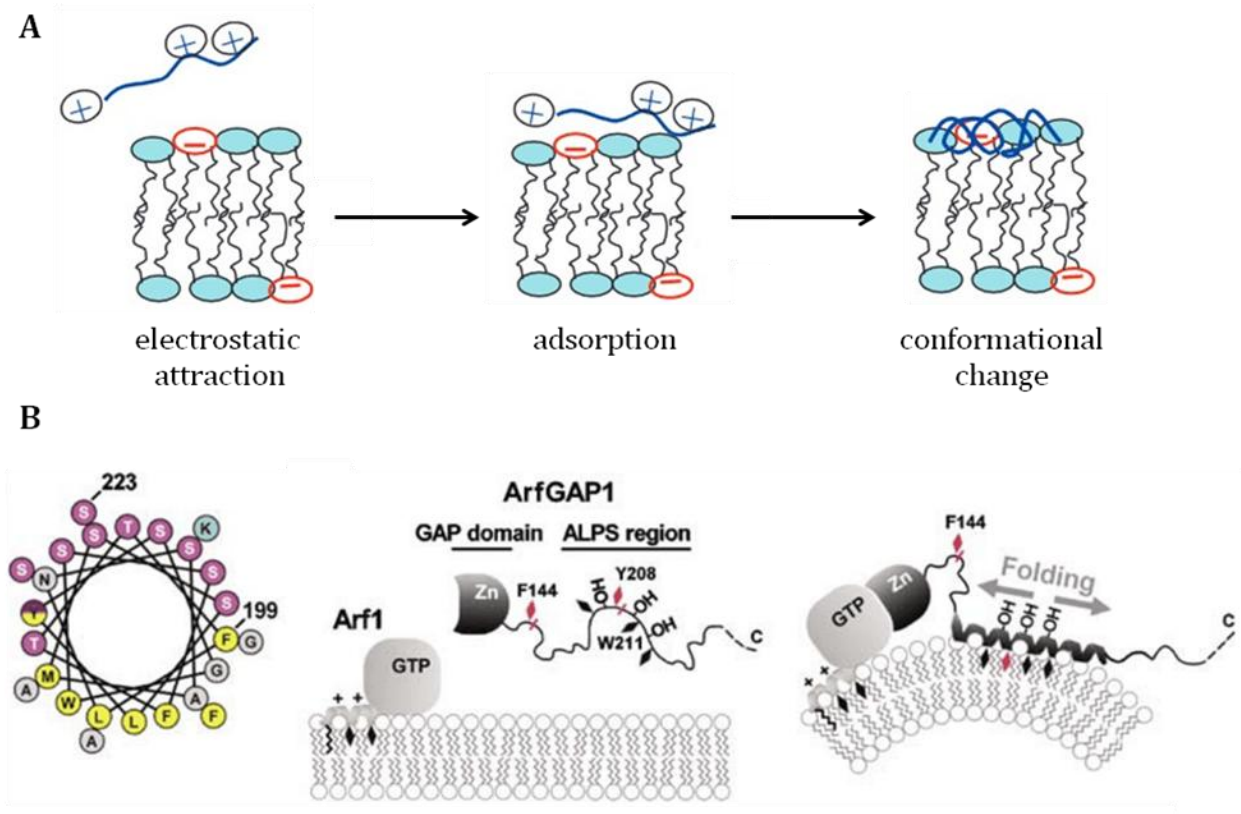

Figure 4: Amphipathic helix insertion into a membrane vs ALPS motif recognition of curved membranes

(A) Amphipathic helix inserts into membrane in three steps **(B)** Left – sequence composition of ArfGAP1 ALPS motif; Right – ArfGAP1 does not interact with flat membranes but recognizes lipid packing defects in curved membranes. Illustration A modified from Seelig, 2004; Illustration B from Bigay *et al.*, 2005.

5. IDPRs IN MEMBRANELESS ORGANELLES AND LIQUID-LIQUID PHASE SEPARATION

Many cell types contain various organelles that can maintain structural integrity without being enclosed in a membrane. These organelles typically range in size from tens of nm to tens of μm, they display liquid-like properties (e.g. ability to flow under restrained conditions and to fuse) and they consist of components cycling rapidly between the organelle and surrounding environment. Membraneless organelles include Cajal bodies, nucleoli, nuclear speckles, processing bodies (P bodies) and germ like granules. They consist of both RNA and proteins (therefore are also referred to as ribonucleoprotein (RNP) bodies or granules) and they mostly specialize in various aspects of gene regulation and mRNA metabolism. Study of Darling *et al.*, 2018 revealed that low complexity sequences and intrinsic disorder are overrepresented within proteins in these organelles – for example, the 200 amino acid long N-terminal arginine/glycine-rich domain of RNA helicase LAF-1 is both necessary and sufficient for the liquid-liquid phase separation and formation of P granule-like particles in vitro (Elbaum-Garfinkle *et al.*, 2015). NMR analysis of proteins within liquid droplets did not provide evidence of folding upon binding, suggesting that the low complexity regions preserve their conformational flexibility within the liquid phase, likely contributing to the dynamic, liquid-like properties of RNP bodies (Li *et al.*, 2012; Nott *et al.*, 2015).

The regulatory effect of liquid phase separation has also been demonstrated on clusters of synaptic vesicles. These clusters form a reservoir from which vesicles are exocytosed during neuronal activity. Several scaffolding proteins could participate in capturing and assembling vesicles into clusters but a special importance of synapsin has been recently highlighted (Milovanovic and De Camilli, 2017). Synapsin contains a C-terminal IDPR with multiple SH3 domain binding motifs and can phase-separate to form a distinct liquid phase in aqueous environment. Importantly, the synapsin phase rapidly disassembles upon phosphorylation by calcium/calmodulin-dependent kinase II (CaMKII). This mimics the dispersion of synapsin at presynaptic buttons upon neuronal stimulation and it suggests that liquid-liquid phase separation may apply to the clustering of synaptic vesicles (**Figure 5**). Moreover, clusters of other membranous organelles may self-organize according to similar principles without the need for a surrounding membrane or protein-based structure to confine them (Milovanovic *et al.*, 2018).

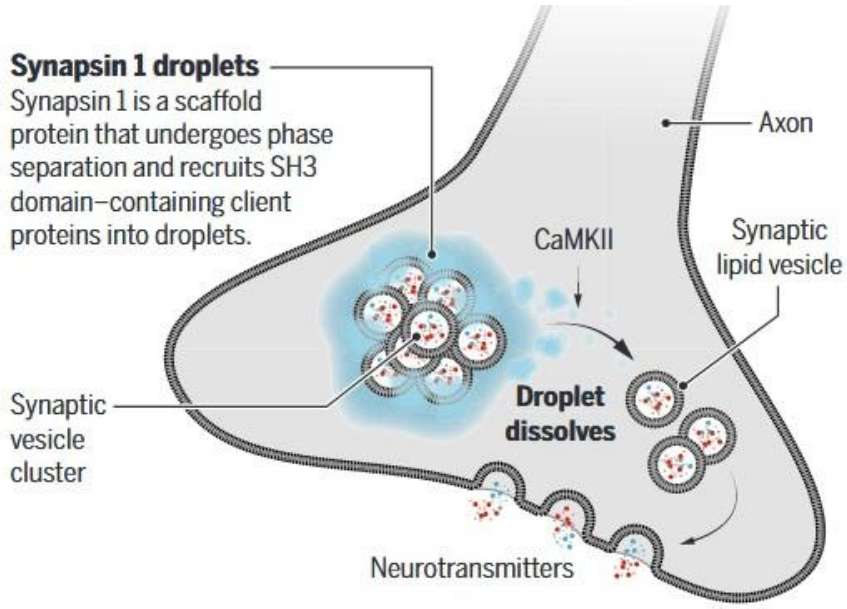

Figure 5: Synapsin liquid-liquid phase separation promotes clustering of synaptic vesicles

Upon synapsin phosphorylation by CaMKII, the clusters dissolve, leading to the release of synaptic vesicles to the membrane for fusion. Illustration from Boczek and Alberti, 2018.

6. *Regulation of function of membrane embedded domains by IDPRs*

While not essential to the basic function of transmembrane proteins, the IDPRs modulate their activity, allowing them to react to changes in intracellular environment, as frequently observed in ion channels and transporters. For example, voltage-gated ion channels use a desensitizing mechanism called ball-and-chain inactivation, initially proposed for voltage-gated sodium channels (**Figure 6**) and later verified in voltage-gated potassium channel Shaker B. Shaker B consists of transmembrane channel subunit and intrinsically disordered plug subunit (Hoshi *et al.*, 1990). The Shaker channel opens when membrane potential drops, allowing outflow of potassium ions. Potassium outflow re-establishes the membrane potential, thus enabling recovery from the action potential. The rapid inactivation of Shaker channel is critical, due to millisecond duration of action potentials, and it is determined by how quickly the plug subunit blocks the channel pore. The plug ("ball"), made of 11 hydrophobic and 8 hydrophilic residues, is tethered to the channel via a 60 amino acid long, flexible linker

("chain") that provides the dynamic properties necessary for fast channel pore blocking, thus acting as an entropic clock (Zhou *et al.*, 2001).

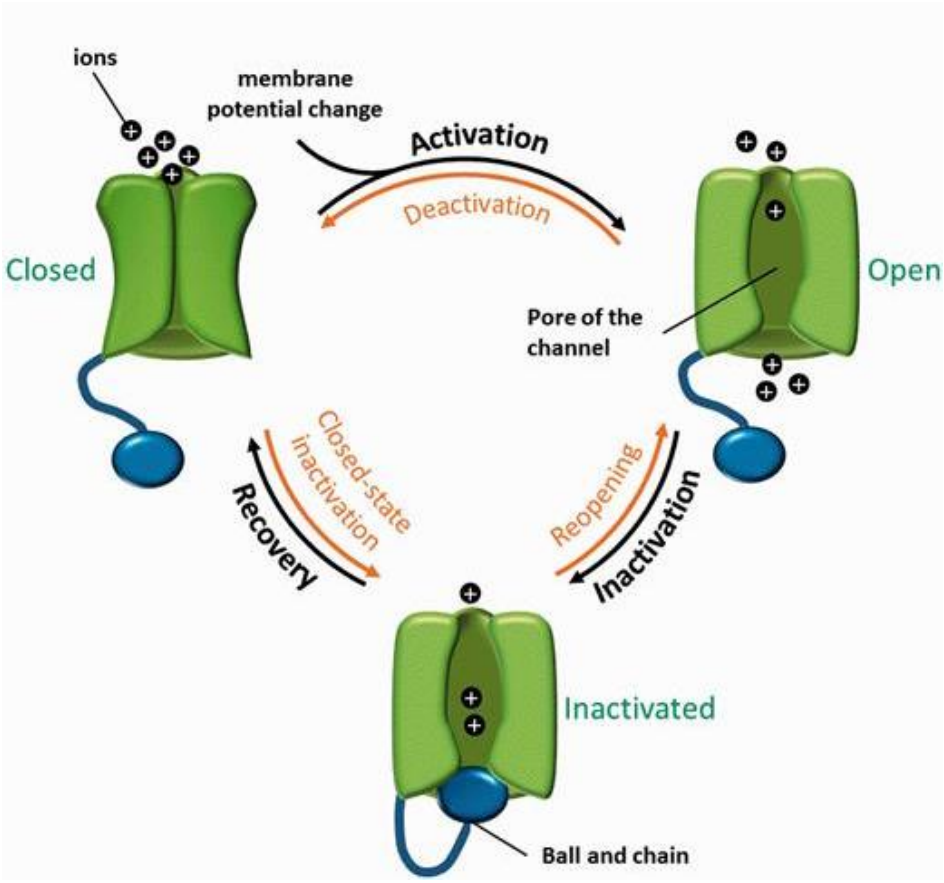

Figure 6: "Ball and chain" model of inactivation of voltage-gated ion channels

The rapid inactivation step enables channel recovery after action potential, and it is facilitated by an intrinsically disordered plug domain. llustration from Hinard *et al.*, 2016.

PART 2: LIPIDS, MEMBRANES AND MEMBRANE PROTEINS

Lipids are organic molecules insoluble in water due to their long non-polar hydrocarbon chain. In aqueous environment, some lipids form aggregates, like for instance oil drops in water. In addition to the non-polar chain ("tail"), some lipid molecules also contain a polar moiety ("head") that, unlike the tail part, can be hydrated. This particular feature is called amphipathicity (or amphiphilicity, respectively) and it has an intriguing effect: amphipathic molecules in aqueous environment do not form drops, but rather organize themselves into micelles or vesicles (**Figure 7**).

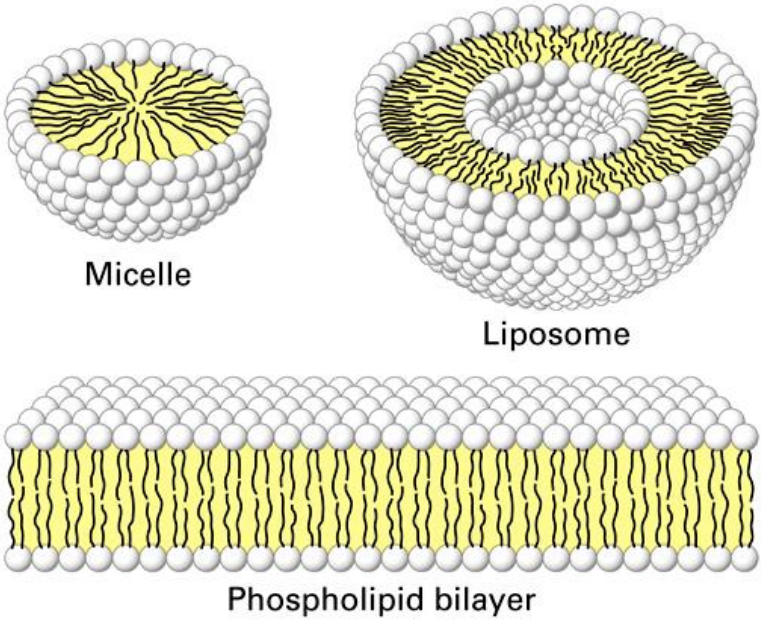

Figure 7: Self-organization of lipids into micelles, liposomes and lipid bilayers in aqueous environment

In micelles, tails of lipids interact with each other, forming spheres of a diameter ~2x the length of one lipid molecule. In liposomes, the internal and external environments are separated from each other by a lipid bilayer i.e. two sheets of lipids. Biological membranes are mostly formed as phospholipid bilayers. It is noteworthy that in apolar environment amphipathic lipids can organize into inverted micelles or bilayers with inverted geometry (= lipid tail facing the apolar solvent). Figure ©2011 the M. P. Mingeot-Leclerq lab (Université Catholique de Louvain).

Lipid bilayers together with transmembrane and membrane-associated proteins form biological membranes essential for life. Cell membranes represent not only the boundaries between subcellular compartments, they also harbour many essential functions - they protect unique cellular contents from dilution and uncontrolled mixing, they prevent oxidation and maintain electrochemical gradients. In addition, they mediate communication with the environment (allowing signal transduction systems to greatly amplify an incoming stimulus), they facilitate transport of molecules and perform certain metabolic functions.

The consensual model to depict the structure and functions of biological membranes is called the "fluid mosaic" model and it was formulated by Singer and Nicholson in the early 1970s. In this model, the lipid components are organized as a bilayer in which hydrophobic tails face each other in the core of the structure, whereas the hydrophilic heads interact with the surrounding aqueous environment. Of note, a small fraction of lipids may also specifically interact with membrane proteins. The integral membrane proteins are a heterogeneous ensemble of amphipathic structures and also follow the same constraints – the highly polar groups protrude from the membrane into the aqueous phase, and the nonpolar groups are largely buried in the hydrophobic interior of the membrane bilayer. The fluid mosaic structure is therefore formally analogous to a 2D solution of transmembrane or membrane-associated proteins in the viscous phospholipid bilayer solvent (Harayama and Riezman, 2018; Singer and Nicolson, 1972). The "mosaic" term in this model refers to the mixture of different lipids and different membrane proteins, and the components are also "fluid" because they can move laterally, allowing diffusion of components in the plane of the lipid bilayer i.e. lateral diffusion (**Figure 8**).

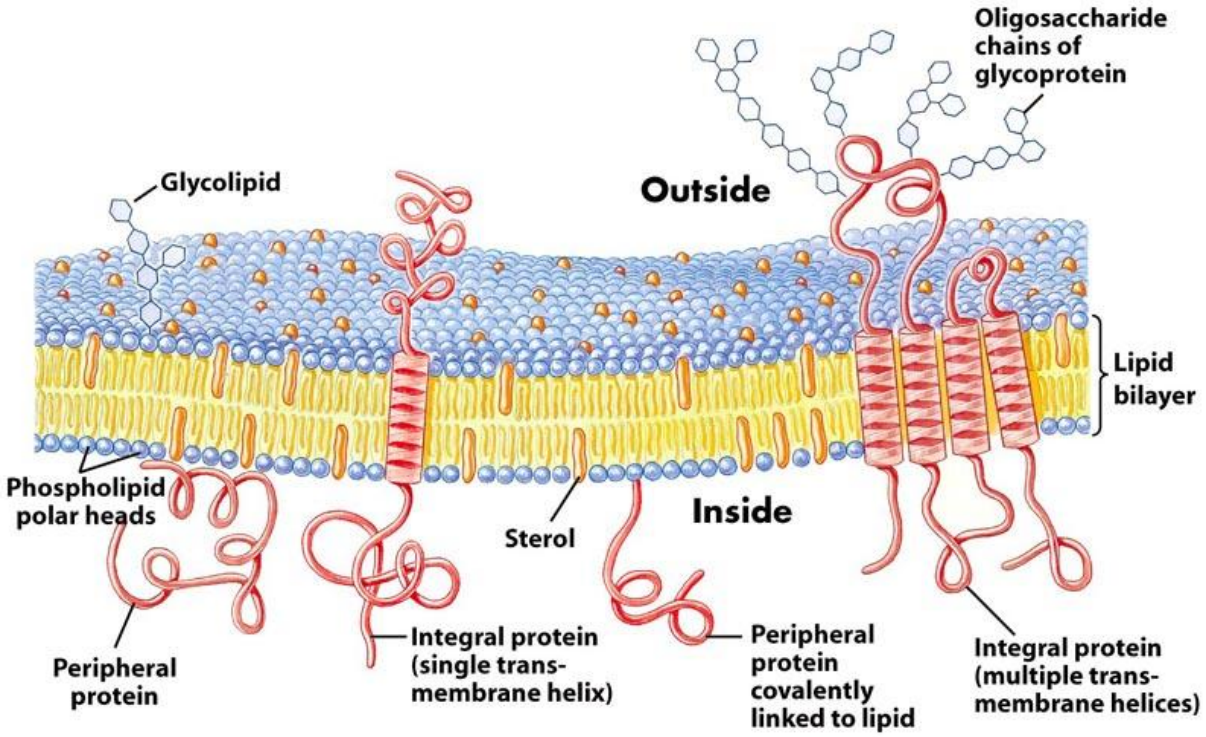

Figure 8: The fluid mosaic model for lipid membrane structure

Both proteins and lipids can move laterally in the plane of the bilayer, but movement of either from one face of the bilayer to the other is restricted (figure from Lehninger Principles of Biochemistry by D. Nelson and M. Cox).

A. COMPOSITION OF CELLULAR MEMBRANES – MEMBRANE LIPIDS

Biological membranes are extremely complex, particularly due to the fact that they are built by numerous lipid species. Of note, the three kingdoms of life (Archea, Bacteria and Eukaryotes) have different lipidomes, i. e. their membranes are formed by different lipid species. As this work focuses on proteins in mammalian membranes, only the lipid species of Eukaryotes will be more closely described. However, we have to keep in mind that during evolution, the ancestors of eukaryotic cells absorbed protobacteria that later became their cellular organelles, namely mitochondria, peroxisomes and, in plants, plastids. These organelles have a lipidome that is very different from the lipidome of the surrounding cell, and to preserve this difference, organelles synthesise their own, organelle-specific lipids such as cardiolipin and

phosphatidylglycerol in mitochondria. The eukaryotic membranes consist primarily of three classes of lipids: glycerophospholipids, sphingolipids and sterols (**Figure 9**).

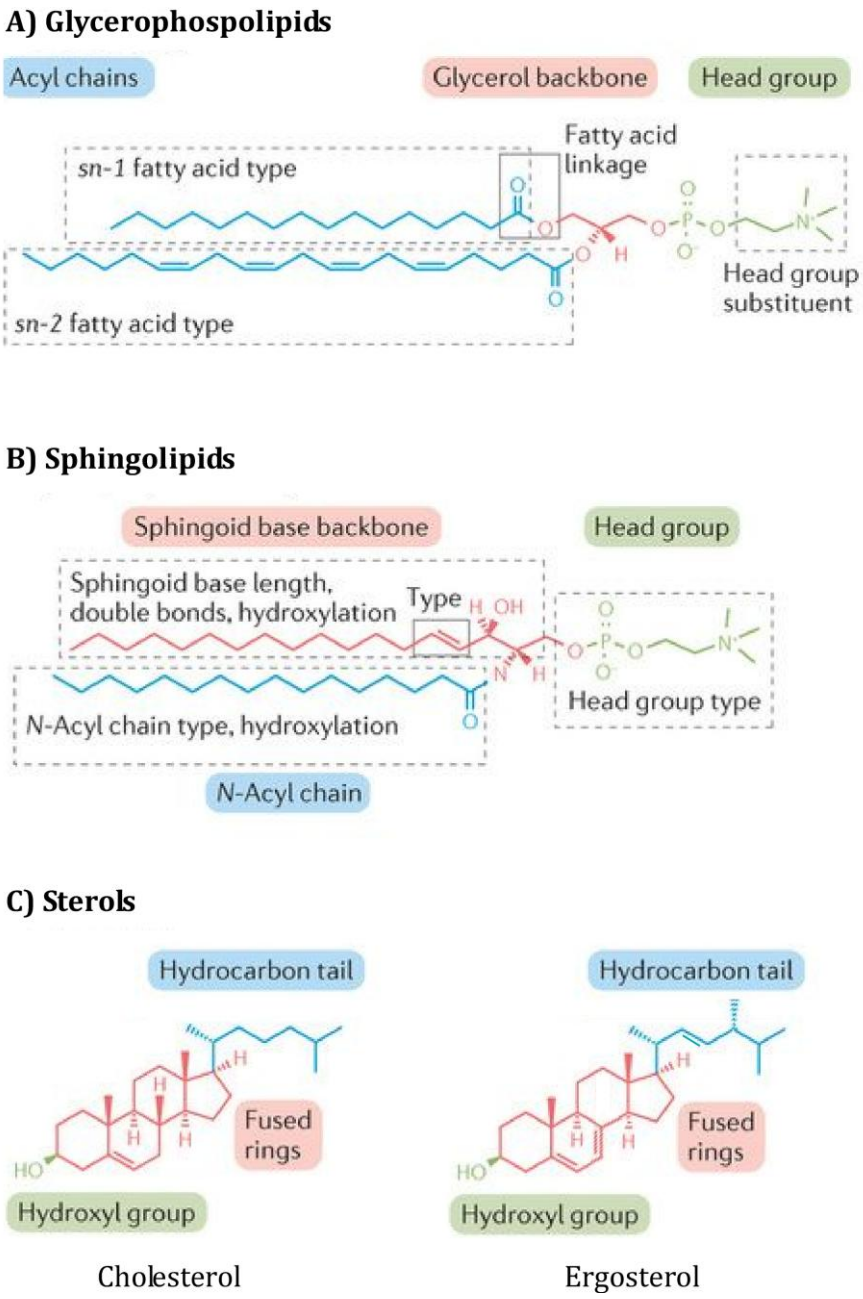

Figure 9: Schematic representation of structural lipid diversity

(A, B) Boxed parts of the GPLs and sphingolipids represent building blocks that confer diversity, for example via addition of different head group substituent or via different fatty acid linkage **(C)** The major mammalian sterol, cholesterol, and its yeast analog, ergosterol. llustration modified from Harayama and Riezman, 2018.

1. GLYCEROPHOSPHOLIPIDS

Glycerophospholipids (GPLs, usually referred to as phospholipids) are the most common components of cellular lipid bilayers. They are derived from diacylglycerol (DAG), that is formed by two acyl chains linked by an ester bond to a glycerol "backbone" at the *sn*-1 and *sn*-2 positions. Glycerol moiety is further modified by adding different "head groups" to build individual phospholipids (**Figure 10**). Head groups can differ in charge and volume - the simplest phospholipid is phosphatidic acid (PA), in which the DAG moiety is phosphorylated on its *sn*-3 hydroxyl group (having thus one negative charge under physiological conditions). Esterification of the *sn*-3 phosphate with different moieties gives the remaining GPLs: phosphatidylcholine (PC), phosphatidylethanolamine (PE), phosphatidylserine (PS) and phosphatidylinositol (PI). PC and PE (polar heads formed of choline and ethanolamine, respectively) are the most abundant species. Both PC and PE are zwitterionic with zero net charge (as the negative phosphate group balances the positive charge of choline/ethanolamine). In PS, the headgroup is formed by zwitterionic *L*-serine and in PI by neutral *myo*-inositol (thus both PS and PI have negative net charge). Phosphorylation of PI on one (or more) hydroxyl groups on the inositol ring gives rise to phosphoinositides (PIPs) that are scarce and do not serve as major building blocks of membranes. However, they perform key functions in lipid signaling, as well as organelle identification (van Meer *et al.*, 2008, also see the "Phosphatidylinositides in organelle identity" paragraph in Part3 of Introduction). The acyl chains in GPLs are described by the number of carbons (16 – 22 in most abundant GPLs) and by the number of double bonds they contain. They can thus be fully saturated (no double bond), mono- (one double bond) or polyunsaturated (two – four double bonds; Schneiter *et al.*, 1999). Adding a concrete example to this description, an 18 carbons-long acyl chain with a single double bond is noted as C18:1.

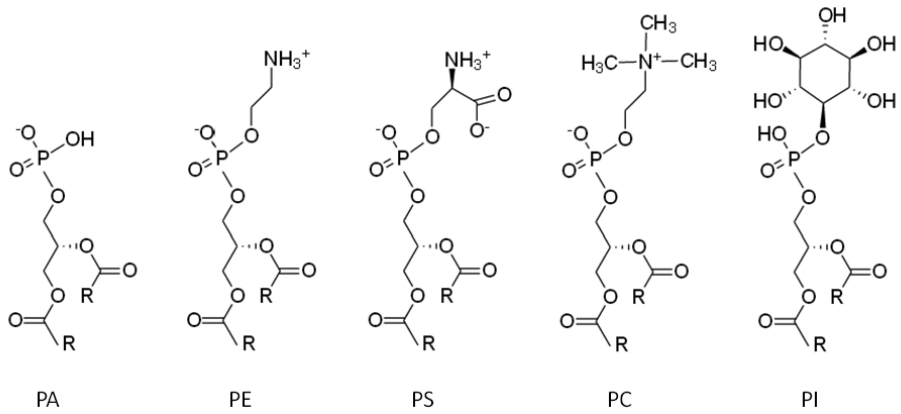

Figure 10: The most abundant phospholipid classes

Different head group substituents are illustrated. (PA) Phosphatidic acid, (PE) phosphatidylethanolamine, (PS) phosphatidylserine, (PC) phosphatidylcholine and (PI) phosphatidylinositol.

2. *SPHINGOLIPIDS*

Sphingolipids have a backbone derived from serine and palmitic acid, forming the sphingosine backbone. Sphingosine backbone is therefore simultaneously the backbone and hydrophobic tail, as shown in Figure 8 B). Sphingosines can be N-acetylated with a very long chain fatty acyl (24 or 26 carbons), forming ceramide. Ceramide can be phosphorylated on its 1-OH group, and additional moieties can be added to form complex sphingolipids such as sphingomyelins (SMs) and glycosphingolipids (cerebrosides, gangliosides and globosides). Sphingolipids usually display long saturated acyl chains (C24:0 or C26:0) and they have an important role in biological membranes, mainly due to their affinity for sterols (Schneiter *et al.*, 1999).

3. *STEROLS*

Sterols are essential building blocks of eukaryotic membranes, although, in contrast to phospholipids and sphingolipids, they display quite unconventional features. Their polar headgroup is tiny and neutral (such as 3-OH group in cholesterol), and they

do not contain long flexible acyl chains. Instead, they are formed by a planar four ringed structure (steroid backbone), comprised of 30 carbons, and a short hydrocarbon tail. The orientation of cholesterol (and its yeast variant ergosterol) in membrane is governed by interactions between its 3-OH headgroup and neighbouring phospholipid headgroups and by interactions of the hydrocarbon ring with hydrophobic acyl chains of membrane lipids. Sterols play key role in maintaining both membrane structural integrity and fluidity – model membranes without sterol undergo a transition from fully rigid, gel phase ("solid ordered") at low temperatures to a very fluid state at high temperatures ("liquid disordered"). In the presence of sterols, the high order at low temperatures is slightly reduced and the low order at high temperatures is markedly increased (**Figure 11**). This ordering-disordering action of sterols promotes a "liquid ordered" phase, which defines a delicate balance between a loose membrane too fluid and akin to great permeability and a rigid membrane forbidding any transfer across the bilayer (Dufourc, 2008).

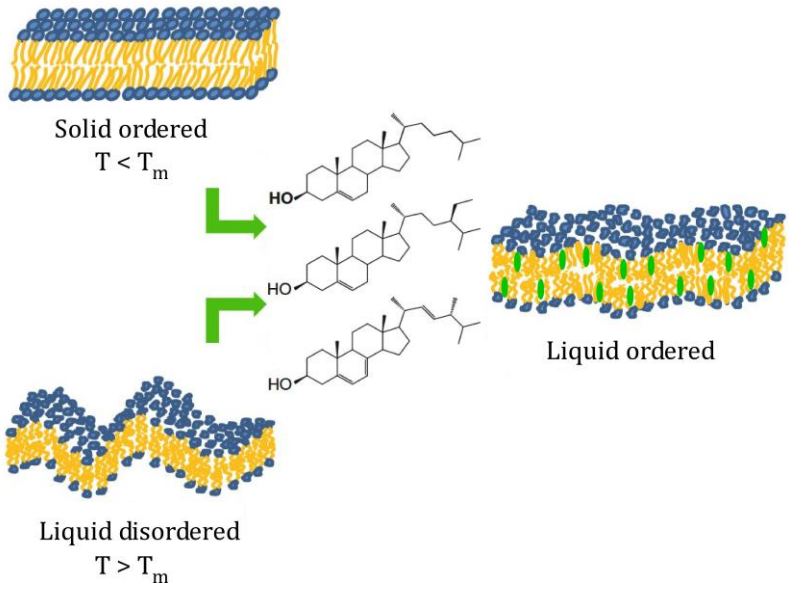

Figure 11: Sterols as regulators of membrane dynamics

Presence of sterols in membrane promotes the formation of liquid-ordered phase. Sterol structures from mammals, fungi and plants are illustrated. Modified from Dufourc, 2008.

4. FUNCTIONS OF LIPIDS BEYOND MEMBRANE BUILDING

Although fatty acid-based lipids and sterols are the building units of cell membranes, it is nonetheless noteworthy that they fulfill some additional functions. For instance, fatty acids can also serve as storage for lipids in the form of triacylglycerols in lipid droplets or as energy source. They can also act as signaling molecules or precursors for biosynthesis of signaling molecules, such as eicosanoids (prostaglandins, thromboxanes, leukotrienes etc). Steroid molecules play major roles unrelated to membrane assembly: sterol metabolites include bile acids, steroid hormones, and vitamin D. Oxygenated derivatives of cholesterol (oxysterols) influence a variety of biological processes, as detailed in the following chapter.

5. OXYSTEROLS

Naturally, oxysterols are present in mammalian cells in very low concentrations as they serve as regulators of numerous signaling pathways. They regulate cholesterol synthesis by preventing the transcriptional activity of sterol regulatory element binding protein (SREBP), and activating the transcription of liver X receptor (LXR) target genes (Luu et al., 2016; Radhakrishnan et al., 2007; **Figure 12**). On the posttranscriptional level, oxysterols accelerate the degradation of rate-limiting enzymes in cholesterol synthesis, such as HMG-CoA reductase (DeBose-Boyd, 2008). Oxysterols are also implicated in Hedgehog signaling pathway, as 25-hydroxycholesterol (25-OH) and 7-ketocholesterol have been found to directly act on Hedgehog receptor Smoothened and to activate Hedgehog target gene transcription (Nachtergaele et al., 2012). In addition, oxysterols affect immune system, for example as endogenous ligands of receptor EBI2, which is essential in B cell function. Oxysterols are implicated in many pathological conditions, notably neurodegenerative diseases (Alzheimer's, Huntington's and Parkinson's disease), atherosclerosis, Niemann-Pick type C disease and cancers (reviewed in Luu et al., 2016).

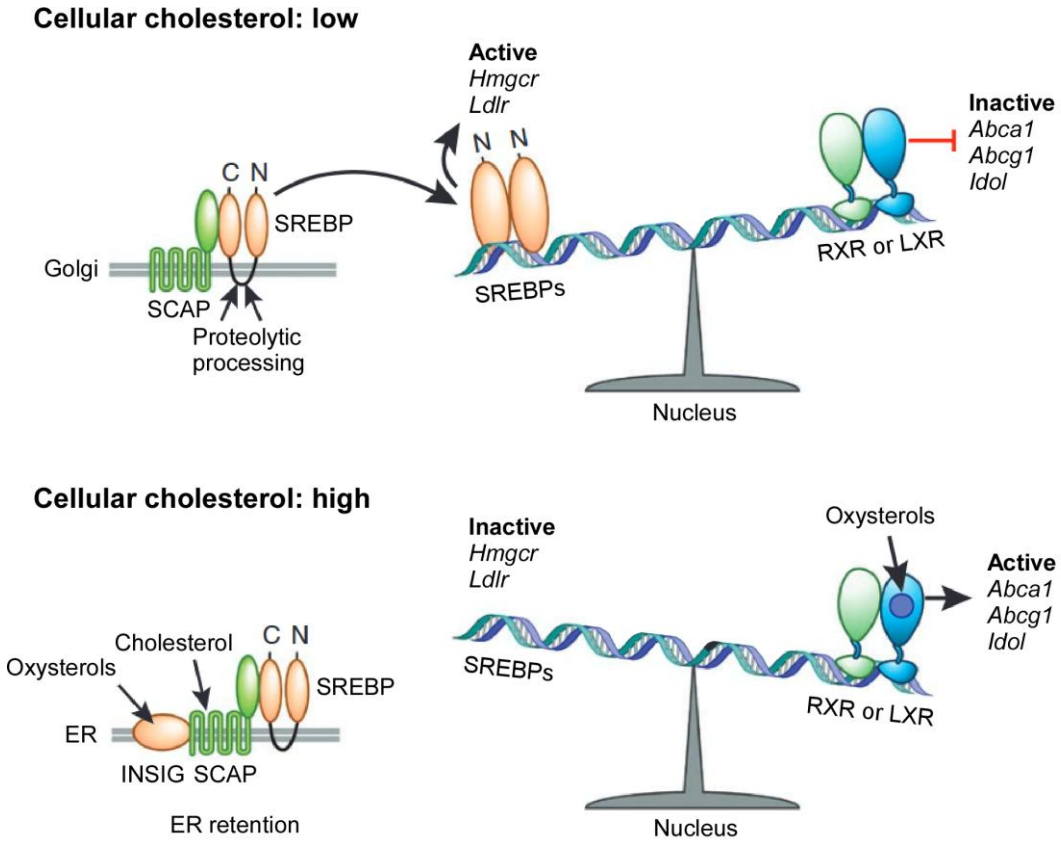

Figure 12: Regulation of cholesterol homeostasis by SREBPs, LXRs and oxysterols.

Under conditions of low cholesterol, SREBP precursors are transported by SCAP to the Golgi where they are proteolyzed. Subsequently, active SREBPs migrate to the nucleus and activate transcription of target genes encoding enzymes required for synthesis and uptake of cholesterol, such as HMG-CoA reductase (*Hmgcr*) and the LDL receptor (*Ldlr*). Under these circumstances, LXRs repress genes that encode proteins mediating cholesterol efflux (*Abca1, Abcg1*) and degradation of the LDL receptor (*Idol*), resulting in an increase in cellular cholesterol content. Under conditions of high cholesterol concentration, cholesterol and its byproducts, oxysterols, sequester SREBP-SCAP-Insig complexes in the ER. At the same time, oxysterols directly bind to and activate LXRs, which induce transcription of ABCA1, ABCG1 and Idol, leading to a decrease in cellular cholesterol content. RXR – retinoid X receptor, SCAP – SREBP cleavage-activating protein, INSIG – insulin-induced gene. Figure modified from Spann and Glass, 2013.

B. THE DIVERSE YET UNIQUE COMPOSITIONS OF ORGANELLE MEMBRANES

Membrane-bound organelles in eukaryotic cells have characteristic morphologies. Some organelles are mostly spherical (lysosomes and peroxisomes) but others are much more complex. For example, the ER forms a continuous network of interconnected tubules and sheets, extending throughout the cell. Mitochondria form a tubular network, and Golgi apparatus is shaped as a stack of flattened cisternae with dilated rims. The differences in organelle shapes are based on different lipid composition and on the interaction of lipid membranes with shape-forming proteins (McMahon and Gallop, 2005). Brief characteristics of lipid composition of several organelles will be discussed below, with emphasis on the ER and Golgi as central organelles in lipid synthesis and transport. Special paragraph will be dedicated to description of phosphoinositides as markers of organelle identity.

1. THE ENDOPLASMIC RETICULUM – MAIN ORGANELLE FOR LIPID SYNTHESIS

The ER is the largest organelle (accounting for more than 50% or total cell membrane in some cell types), and ER-localized enzymes synthesize the vast majority of structural phospholipids, cholesterol and ceramide. From the ER, newly synthesized lipids are transported to other organelles. ER membranes contain high levels of PC and PE and low levels of cholesterol and sphingolipids, which is synonymous with liquid disordered phase and looser membrane packing (Bigay and Antonny, 2012; Harayama and Riezman, 2018). This is consistent with the function of ER in insertion and transport of newly synthesised lipids and proteins.

Lipid-synthesizing enzymes are mostly transmembrane proteins and several studies report their enrichment in fractions of ER membrane that interact with other organelles (Jain and Holthuis, 2017). For example, the PS-synthesising enzymes are particularly abundant in mitochondria-associated membranes of mammalian cells (Kannan *et al.*, 2017; Rusiñol *et al.*, 1994; Stone and Vance, 2000), suggesting that lipid synthesis may be subcompartmentalized (**Figure 13**).

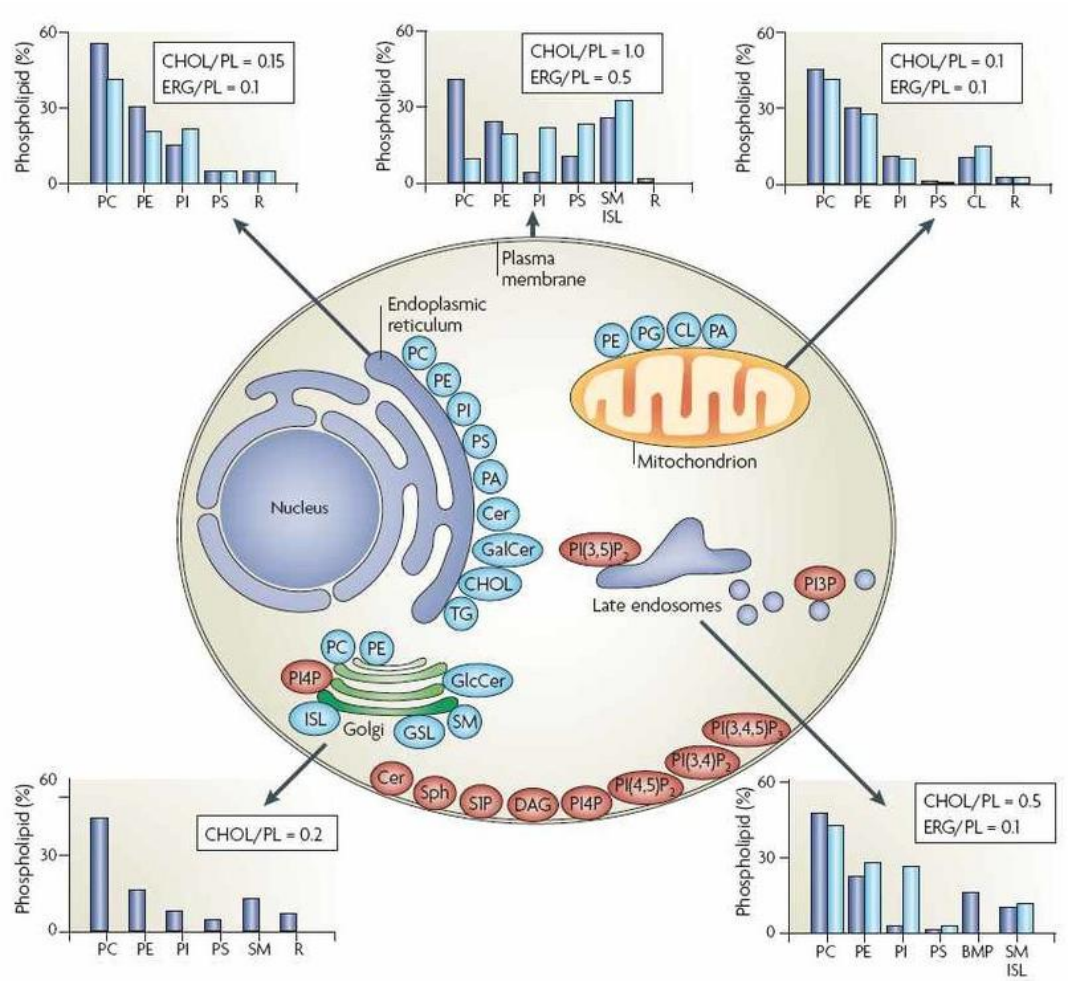

Figure 13: Lipid synthesis and steady-state composition of cell membranes

The lipid composition of cellular membranes varies throughout the cell. The lipid compositional data are expressed as a percentage of total phospholipid (PL) in mammals (blue) and yeast (light blue). In small panels, the molar ratio of cholesterol (CHOL) in mammals or ergosterol (ERG) in yeast to phospholipid is indicated. On the cell drawing, major phospholipids are shown in blue and lipids involved in signalling and organelle recognition are shown in red. Illustration from van Meer *et al.*, 2008.

2. THE GOLGI APPARATUS – A CENTRAL STATION FOR SORTING AND TRANSPORT OF BIOMOLECULES

The organization of Golgi as stack of flat cisternae reflects the logic for its biochemical activities - its function is at the interface of lipid metabolism and membrane trafficking, and it exhibits remarkable dynamics and capacity for self-organisation. Significant levels of lipid synthesis and modification occur in the Golgi. For example, ceramide synthesised in the ER is transported to the Golgi, where it is converted to sphingomyelin, glucosyl- and lactosylceramide and more complex glycosphingolipids, designated for export mainly to the plasma membrane (Futerman and Riezman, 2005). Similarly, the Golgi-specific PA phosphatase can play a role in controling the levels of DAG, which in turn facilitates membrane deformations due to its extreme inverted cone shape. These deformations have been shown to regulate vesicle budding at multiple steps in the vesicular trafficking pathways (Kearns *et al.*, 1997; Litvak *et al.*, 2005), and in some cases DAG directly regulates the activity of protein components of the trafficking machinery (Asp *et al.*, 2009; Baron and Malhotra, 2002). In addition, the two leaflets of (post-) Golgi membrane bilayers have different lipid compositions. This is called bilayer asymmetry (see following chapter for more details). The sphingolipids (except glucosylceramide) are synthesized on the luminal surface of the Golgi, whereas the phospholipid PS and PE are actively concentrated in the cytosolic leaflet (Bretscher, 1973; D'Angelo *et al.*, 2007; Simons and Van Meer, 1988).

It is important to mention that in addition to structural lipids, phosphoinositides are an important signaling component of all post-Golgi membranes - and as such, they will be discussed in a separate subchapter 5.

3. THE PLASMA MEMBRANE AS PROTECTIVE BARRIER

The plasma membrane (PM) is enriched in cholesterol and sphingolipids, which are tightly packed to resist mechanical stress, creating a protective barrier. Although he PM does not autonomously synthesize structural lipids, it can metabolize sphingomyelin at rates high enough to (re)synthetize it again from ceramide by PM-resident sphingomyelin synthase SMS2 (Tafesse *et al.*, 2007).

A key feature of plasma membrane (but also other biological membranes) is that it is compositionally asymmetric (van Meer *et al.*, 2008). In case of PM, the majority of (anionic) aminophospholipids reside in the inner leaflet, with sphingomyelin and choline phospholipids primarily in the outer leaflet (Nickels *et al.*, 2015). The distribution of cholesterol is debated – some authors suggest cholesterol enrichment in the outer leaflet (S.-L. Liu et al., 2017) whereas others suggest higher concentration in the inner leaflet (Courtney et al., 2018; Gibson Wood et al., 2011; Mondal et al., 2009). The bilayer asymmetry is tied to numerous biological functions – for example, phosphatidylserine (PS) is exclusively located at the cytoplasmic side, as exposure of PS on cell surface is a general feature of apoptosis, and it triggers specific recognition and removal by phagocytes (Fadok *et al.*, 1992; Martin, 1995). Bilayer asymmetry results from ATP-dependent translocation of PS and PE between bilayer leaflets. This underlines its importance, as cells invest considerable amount of energy to generate and maintain asymmetric phospholipid distribution. Transbilayer lipid transfer is mediated by P4-ATPases ("flippases"), which belong to the superfamily of P-type ATP pumps whose members usually transport ions rather than lipids. A study of Lenoir *et al.*, 2009 revealed that a specific interaction between P4-ATPases and cell division cycle (Cdc50) proteins might underlie their distinct transport specificity.

Of note, the negative charge of PS in the inner leaflet of PM (where it represents 10-20% of all surface lipids) plays an important part in recruiting proteins with polybasic (polycationic) PM-targeting motifs via electrostatic interactions (Vance and Steenbergen, 2005; Yeung *et al.*, 2008).

4. *LIPIDS IN THE ENDOCYTIC COMPARTMENTS*

Early endosomes have lipid composition similar to plasma membranes but during maturation to late endosomes, the concentration of sterols and PS decreases, while there is a dramatic increase in bis(monoacylglycero)phosphate (BMP). BMP is a negatively charged GPL with acyl chains in an unusual *sn*-1; *sn*-1' configuration. It functions in multivesicular body generation, fusion processes and sphingolipid hydrolysis (Matsuo, 2004; van Meer *et al.*, 2008).

5. PHOSPHOINOSITIDES AS HALLMARKS OF ORGANELLE IDENTITY

Phosphoinositides (PIs) regulate a wide variety of cellular functions by interacting with proteins that either reside in the membrane, such as ion channels and transporters, or with proteins that get reversibly recruited to the membrane, such as clathrin or lipid transfer proteins. PIs are present in minor pools in subcellular compartments (**Figure 14**), where they act, together with small G-proteins, as specific organellar signposts to facilitate their recognition (Balla, 2013). For example, PI(4)P marks mainly the *trans*-Golgi, although functionally distinct pools have also been detected in the PM and endosomal fractions. Golgi-localized PI(4)P is commonly recognized by three groups of effectors: clathrin adaptors, such as AP-1, AP-3 and GGA (Wang *et al.*, 2007, 2003); lipid binding proteins, such as ORP/Osh proteins (Levine and Munro, 2001, 1998), the ceramide transfer protein CERT (Hanada *et al.*, 2003) and the glucosylceramide transfer protein FAPP2 (Godi *et al.*, 2004). For more details please see chapter "Lipid transfer proteins at membrane contact sites". A third kind of PI(4)P effector is the GOLPH3 protein that has been demonstrated to control Golgi morphology by connecting Golgi membranes with the actin cytoskeleton through its binding to unconventional myosin, MYO18A (Dippold *et al.*, 2009). In this case, the link between Golgi morphology and actin cytoskeleton was unexpected, given the well-documented importance of the microtubular rather than the actin network in the maintenance of Golgi structure (Balla, 2013).

Plasma membrane contains the bulk of $PI(4,5)P_2$ and $PI(3,4,5)P_3$. Upon phospholipase C activation by G protein-coupled receptors, $PI(4,5)P_2$ is the precursor of IP_3 and DAG and hence it has a pivotal role for early signaling from cell surface receptors (Berridge and Irvine, 1984). $PI(4,5)P_2$ itself is essential for proper activity of numerous ion channels and transporters (Suh *et al.*, 2010; Wu *et al.*, 2002; Xie *et al.*, 2011). Furthermore, rapid depletion of PM pools of $PI(4,5)P_2$ in intact cells results in dramatic loss of clathrin puncta, demonstrating that clathrin-mediated endocytosis requires $PI(4,5)P_2$ (Zoncu *et al.*, 2007).

PI(3)P and $PI(3,5)P_2$ localize mainly to early and late endosomal membranes, respectively, where they act as key lipid regulators of endocytic trafficking. PI(3)P is recognized by a cysteine-finger FYVE domain present in numerous proteins, including

the Fab1 and Vac1 in yeast and EEA1 in mammals (Stenmark *et al.*, 1996) as well as by the phox-homology (PX) domains found in sorting nexins (Xu *et al.*, 2001). It has been firmly established that PI(3)P, together with Rab5 proteins, controls fusion between early endosomes (Simonsen *et al.*, 1998). PI(3,5)P_2 is synthesised from PI(3)P at the late endosomal/lysosomal system and it is targeted by certain members of the epsin family containing an epsin NH2-terminal homology (ENTH) domain (Chidambaram *et al.*, 2004; Mayinger, 2012).

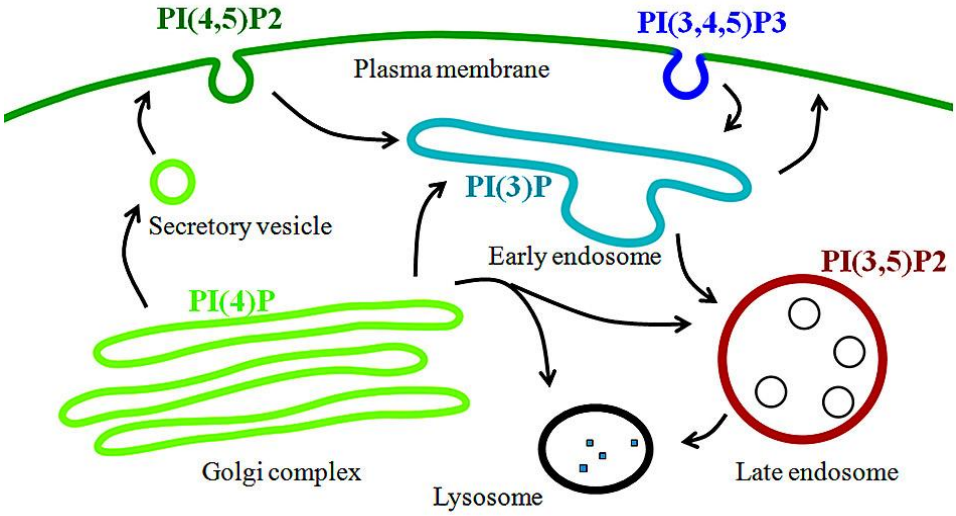

Figure 14: Phosphoinositide distribution in cellular organelles

Post-Golgi organelles contain distinct phosphoinositides to hallmark their identity. Illustration ©2018 The Y. Mao Lab (Cornell university).

C. COMPOSITION OF CELLULAR MEMBRANES – MEMBRANE PROTEINS

Membrane proteins represent a large and diverse group of proteins associated with cellular membranes and carrying out a wide range of functions. Cellular metabolism and communication heavily rely on membrane proteins – more than 30% of all proteins interact with membranes at some stage of their functional activity (Almén *et al.*, 2009). Membrane proteins include integral and peripheral proteins. Integral (transmembrane) proteins are permanently inserted into the membrane and span across the bilayer with one or several hydrophobic domains. Peripheral membrane proteins interact

transiently with membrane surface, either via an (amphipathic) α-helix parallel to the membrane; via a covalently attached lipid (some examples include the GPI-anchored proteins or palmitoylated PI4KIIα; Lu *et al.*, 2012; Zurzolo and Simons, 2016); via interaction with particular membrane lipids (such as PH domains, which recognize phosphoinositides); via a hydrophobic loop or via electrostatic interactions (**Figure 15**). The dynamics of membrane lipids and proteins is an important determinant of intermolecular interactions, downstream signal transduction and local membrane mechanics. The mode of membrane protein mobility can range from random diffusion to immobility and from confined or restricted motion to actively directed motion. In the following chapter, I will more closely focus on diffusion of membrane proteins.

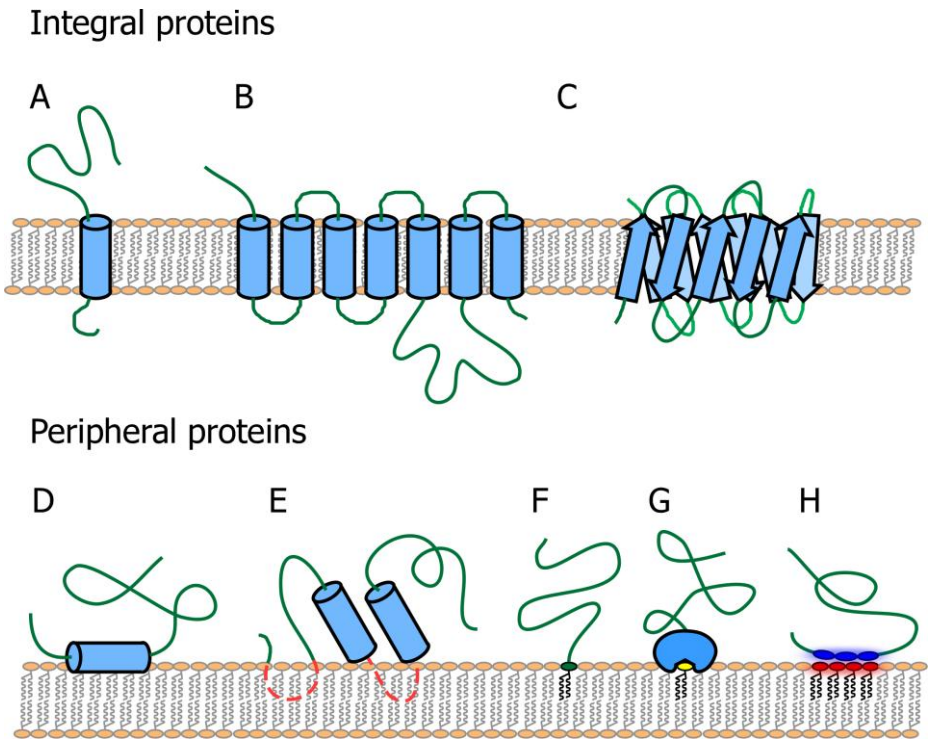

Figure 15: Integral and peripheral proteins

(A,B) Integral proteins can span across lipid bilayer with single (A) or multiple (B) transmembrane domains/helices **(C)** β-barrel structure of a transmembrane protein – typical for ion channels and porins in the outer membrane of bacteria, mitochondria and plastids (Höhr *et al.*, 2015). Peripheral proteins can interact with membrane in various ways: **(D)** via an α-helix, **(E)** with one or several loops inserted into the bilayer **(F)** proteins can be covalently linked to a lipid or they can transiently bind a lipid **(G)**. **(H)** some proteins are recruited to membranes via electrostatic interactions.

D. PRINCIPLES OF PROTEIN DIFFUSION IN SOLUTION AND IN MEMBRANE

1. DIFFUSION CHARACTERISTICS OF SOLUBLE PROTEINS

In the microscopic world, anything that is immersed in a fluid environment will move in an undirected way. In 1820s, this was discovered by R. Brown while looking through a microscope at suspension of pollen grains in water. The observed random motion of the particles is referred to as Brownian motion or diffusion, and it has been described as a consequence of thermal fluctuations in a paper published in 1905 by A. Einstein (making it one of his first big contributions to science). Thermal fluctuations result in thermal force that makes the solvent molecules move around randomly and collide with the particles, causing their displacement. Particles of smaller size (mass), such as insulin (5kDa) have larger displacement, and therefore large diffusion coefficient *D*, whereas larger particles, such as immunoglobulin IgG2A (~150 kDa), are more difficult to displace, resulting in smaller diffusion rate (**Figure 16**). As a result, the diffusion of a soluble protein strongly depends on its Stoke's radius and hydrodynamic interactions (Roosen-Runge *et al.*, 2011).

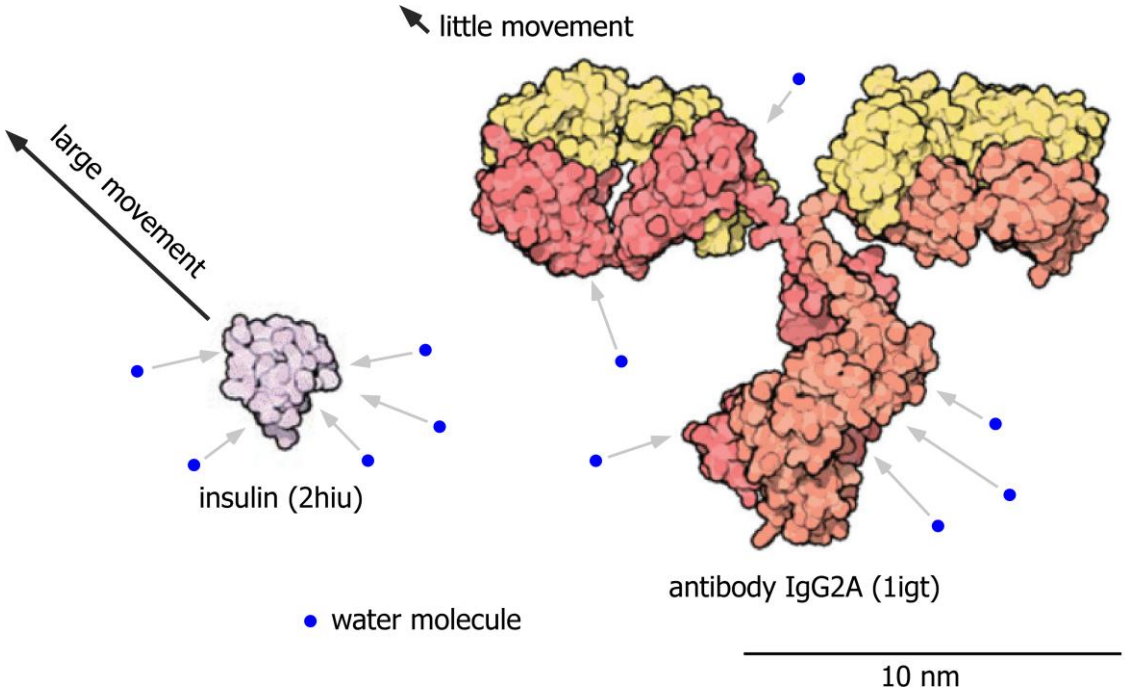

Figure 16: Principle of protein diffusion in aqueous solution

Large particles absorb the water molecules collisions, whereas small particles are moved by those collisions. Proteins are shown on the same scale (modified from book.bionumbers.org; courtesy of D. Goodsell), in parentheses are the PDB structure IDs.

Diffusion of proteins in dilute solutions (total protein concentration is less than 10 mg/ml) is described by the Stokes-Einstein Law

$$D_t = \frac{k_B T}{6\pi\eta r}$$

where D_t is translational diffusion coefficient, k_B is the Boltzmann constant, T is temperature, η is the solution viscosity, and r is the radius of protein being studied. However, the cytosolic environment is rich in macromolecules, which occupy up to 30% of cellular volume and reach concentrations of 100 to 400 mg/ml (Luby-Phelps, 2013). Macromolecular crowding is expected to cause deviations from the Einstein-Stokes Law, as in a crowded fluid, each molecule is excluded from much of the total volume by the presence of other biomolecules (Konopka *et al.*, 2006; Muramatsu and Minton, 1988).

In this context, diffusive behaviour of IDPs has attracted some attention. Using NMR spectroscopy, Wang *et al.,* compared the translational diffusion of a larger IDP (Parkinson's disease related protein α-synuclein, 14 kDa) with a smaller globular protein chymotrypsin inhibitor 2 (CI2, 7.4 kDa). In simple solvent, CI2 diffuses approximately 2x faster than α-synuclein, which is consistent with the Stokes-Einstein relation, and it can be explained by three reasons: first, CI2 has a smaller molecular weight; second, CI2 is folded and compact, making its hydrodynamic radius smaller than that of α-synuclein. Lastly, when the radius of a protein is comparable to or greater than the radius of the co-solute (e.g., glycerol) a larger protein will diffuse more slowly, although the addition of glycerol slows down the diffusion of both proteins (Wang *et al.*, 2010). However, in solutions crowded with "crowder" macromolecules such as PVP or BSA, a larger, disordered protein diffuses faster than a smaller, globular protein, demonstrating that macromolecular crowding affects the diffusion of globular and disordered proteins differently, as indicated in **Figure 17** (Wang *et al.*, 2012).

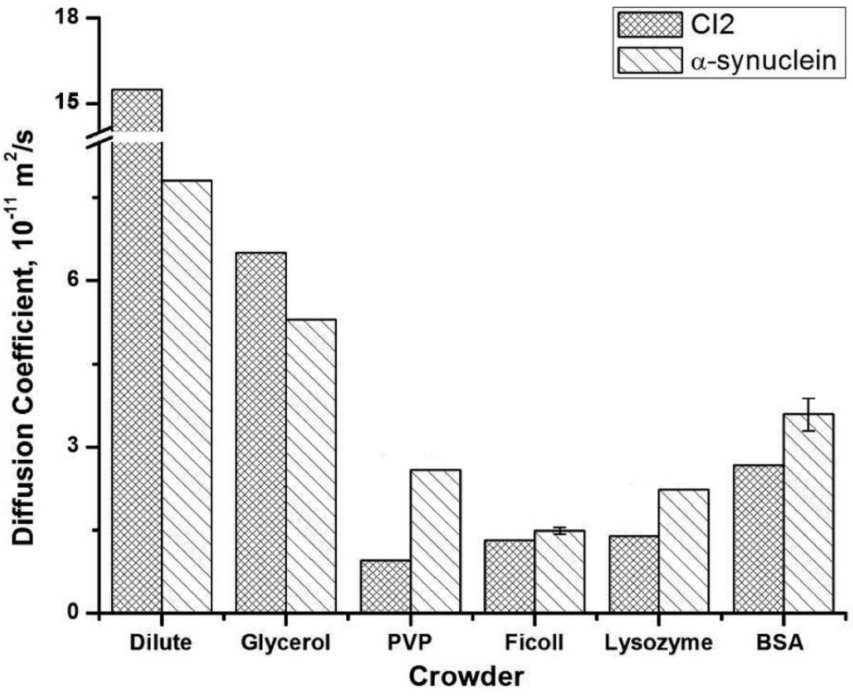

Figure 17: Diffusion of disordered and globular proteins differs in dilute and crowded environment

Histogram showing the translational diffusion coefficient of CI2 and α-synuclein in dilute solution, 300 mg/ml solution of glycerol and 300 mg/ml solution of crowding agents such as polyvinylpyrrolidone (PVP), Ficoll 70, lysosyme and bovine serum albumin (BSA) at 25°C. Figure is adapted from Wang *et al.*, 2012.

2. LATERAL DIFFUSION OF MEMBRANE PROTEINS

Biological membranes are extremely complex fluids, crowded with proteins with typical protein to lipid molar ratios being around 1:50 – 1:100 (Jeon et al., 2016; Metzler et al., 2016). The theoretical investigation of protein diffusion within membranes continues since 1970s, when P. G. Saffman and M. Delbrück investigated the hydrodynamic forces acting on a particle suspended in membrane, when the membrane is described as a 2D fluid sheet of viscosity μ_m embedded within a less viscous fluid of viscosity η (Saffman and Delbrück, 1975). In this model the lateral Brownian diffusion of proteins in lipid membranes depends on the viscosity of the membrane and of the surrounding solvent. Regarding the influence of protein size, the Saffman-Delbrück (SD) model predicts a weak, logarithmic dependence of the diffusion coefficient D_0 on the protein radius,

$$D_t = \frac{k_B T}{4\pi\mu_m h}\left[\ln\left(\frac{2L_{sd}}{r}\right) - \gamma\right]$$

where $\mu_m h$ are membrane parameters (μ_m – membrane viscosity, h – membrane thickness), L_{sd} is Saffman-Delbrück length, calculated as a ratio between membrane parameters and viscosity of surrounding fluid,

$$L_{sd} = \frac{\mu_m h}{2\eta}$$

and $\gamma \approx 0.577$ is the Euler-Mascheroni constant.

However, a study of Gambin *et al.* (2006) on diffusion of various peptides and transmembrane proteins incorporated into giant unilamellar vesicles or in model bilayers of tunable thickness sparked a controversy in the field. They found that the D_0 is strongly linked to the protein dimensions, with a Stokes-like expression for D, ($D \propto 1/R$). Soon after, several authors argued that the SD model may fail for some proteins because they can locally deform the membrane which leads to new hydrodynamic stresses on the protein-membrane complex and to suppression of its mobility (Naji *et al.*, 2007). This idea has been subsequently debated by researchers who argued that although local membrane deformation can change the effective membrane viscosity, the

effect on protein mobility is only weak (<30%), and it does not change the scaling of the diffusion coefficient D_t (Guigas and Weiss, 2008). Fluorescence Correlation Spectroscopy (FCS) of Ramadurai *et al.* (2009) with integral membrane proteins reconstituted in GUVs showed protein diffusion in membranes to comply with the SD model, and similar results were obtained by Weiß *et al.* (2013) using 2-Focus FCS. One possible explanation of controversy in this field could be that the SD model originally predicts lateral diffusion in protein-poor membranes, whereas native cell membranes are crowded with proteins – according to estimations, membrane area fraction occupied by proteins ranges from 15 – 35% (Dupuy and Engelman, 2008), implying that diffusing objects may be hindered in their mobility by constant colliding with one another. Consistently, number of studies on simple membrane systems, both experimental (Dix and Verkman, 2008; Peters and Cherry, 1982; Ramadurai *et al.*, 2009) and computational (Domański *et al.*, 2012; Goose and Sansom, 2013; Javanainen *et al.*, 2013; McGuffee and Elcock, 2010) have indicated that crowding induces anomalous (slower) diffusion in lipid membranes.

In conclusion, in the protein-poor context, diffusion of proteins is fairly well understood, with experimental and computational studies providing compelling evidence that for a membrane protein of lateral radius (R), D_t scales logarithmically as $D_t \propto \ln(1/R)$, agreeing with Saffman-Delbrück model. However, in the crowded case, deviations from the model have been repeatedly observed, with a crossover from the $D_t \propto \ln(1/R)$ behavior to the Stokes-like $D_t \propto 1/R$ relation (**Figure 18**). Hence, in the crowded case, there could be an order of magnitude difference between the diffusion coefficients of the smallest proteins and large protein complexes, and the dynamics in the crowded setting could be radically different from protein-poor conditions (Javanainen *et al.*, 2018).

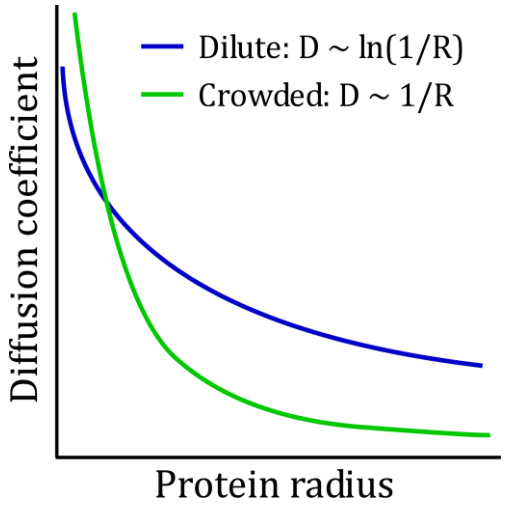

Figure 18: Crowding affects the lateral diffusion of integral membrane proteins

In protein-poor membranes, relation between diffusion and protein size follows the Saffman-Delbrück equation (blue curve) with diffusion coefficient weakly depending on protein radius. In contrast, diffusion in crowded membranes might follow the Stoke's-Einstein law, and protein radius becomes a more significant factor (green curve).

Vast majority of studies focused on the diffusion of folded transmembrane proteins (such as receptors). However, a lot of questions remain open regarding the diffusion properties of membrane-associated proteins that are not integral part of biological membranes, but interact with them transiently. Similarly, very little is known about the membrane diffusion of large intrinsically disordered proteins or proteins with considerable proportions of intrinsic disorder. And lastly, protein diffusion in cell membranes is further complicated by numerous barriers, such as mesh of cytoskeleton components or components of extracellular matrix, poorly mobile intramembraneous clusters of proteins and lipids, membrane curvature or hydrophobic mismatch between short-tailed and long-tailed lipids (Trimble and Grinstein, 2015). Taken together, there is still much to learn about the complex features of protein diffusion on a membrane and within membrane contact sites.

PART 3: LIPID TRANSPORT, MEMBRANE CONTACT SITES AND OSBP-RELATED PROTEINS

A. INTRACELLULAR LIPID TRANSPORT

Lipids as membrane building units lack intrinsic motifs or trafficking signals that could specify their intracellular location. However, as detailed above, each organelle maintains its characteristic lipid composition, evident even at the level of individual leaflets of the bilayer. This astonishing lipid compartmentalization evokes a question: How can specific lipids be delivered to a certain organelle?

Our current understaning of intracellular lipid transport is based on the evidence of efficient and well-controlled lipid fluxes within the cell, and these fluxes are known to occur via four major mechanisms, illustrated in **Figure 19**:

- Lateral diffusion of lipids along membrane bilayers and possibly between very closely apposed membrane leaflets
- Lipid flip-flop from one leaflet of a bilayer to the other one catalyzed by specific integral membrane proteins
- Lipid transport in the form of transport vesicles/tubular carriers in membrane trafficking
- Lipid transport by specialized lipid binding/transfer proteins (LTPs)

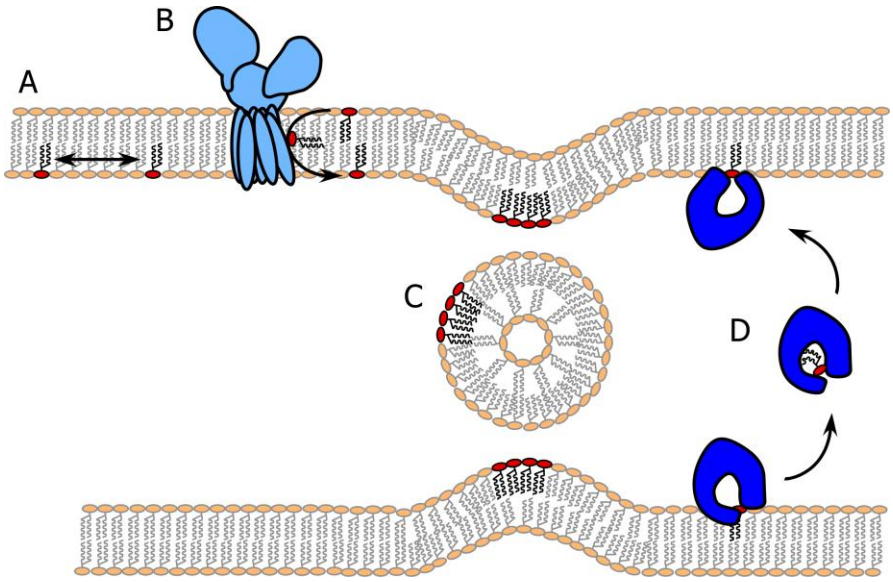

Figure 19: The mechanisms of intracellular lipid transport

(A) lipid diffusion laterally within a leaflet **(B)** Flip-flop of a lipid between the two leaflets of a bilayer **(C)** vesicular lipid transport **(D)** transport mediated by lipid binding/transfer proteins.

Diffusion of lipids within membrane is a passive process closely related to the membrane structure – since cellular membranes are substantially complex systems, lipid diffusion is influenced by the presence of lipid clusters (micro- and nanodomains or rafts), proteins and interactions with cytoskeleton (Dietrich *et al.*, 2002; Trimble and Grinstein, 2015). Free diffusion of lipids between membranes is a very slow process, and it can be neglected for lipid homeostasis.

Movement of lipids from one leaflet to the other is mediated by proteins called P4-ATPases or "flippases" (Jensen *et al.*, 2017; Lopez-Marques *et al.*, 2014). Flippases contribute to the transbilayer asymmetry, a feature important for multiple cellular processes, as detailed before (Part2, chapter B.3). Lipid transport in the opposite direction is catalyzed by some members of the ABC transporter family. These proteins are called also "floppases", and both flippases and floppases require energy in the form of ATP for their function (Hankins *et al.*, 2015). In contrast, other proteins, called scramblases, are ATP-independent and act to randomize lipid distribution by bidirectionally translocating lipids without ligand specificity (Sahu *et al.*, 2007).

1. LIPID TRANSPORT BY VESICULAR TRAFFICKING

1.1 THE SECRETORY PATHWAY

Eukaryotic cells transport material from the "synthesis-and-modification" locations (ER and Golgi) to the "release" location (PM) via secretory pathway. Proteins are synthesised on ribosomes of the rough ER, and they enter or cross the ER membrane cotranslationally - during their synthesis. Soluble proteins are localized in the luminal part of ER whereas transmembrane proteins are inserted into the ER membrane. Subsequently, both are incorporated into either the lumen or membrane of budding vesicles formed by the COPII coat protein machinery. The vesicles fuse with the ER-Golgi Intermediate Compartment (ERGIC) and cargo destined for anterograde transport is targeted towards the *cis*-Golgi for post-translational modification. From both ERGIC and *cis*-Golgi, certain proteins (mainly those containing an ER-retention motif) are retrieved to the ER via a different set of retrograde transport vesicles, coated by COPI. The rest of material advances through the *medial*- towards the *trans*-Golgi. Currently, there are two models describing the cargo transport through the Golgi: first model assumes anterograde transport of vesicles through static Golgi cisternae (Dunlop *et al.*, 2017; Dunphy and Rothman, 1985). In the second model, called cisternal progression (or cisternal maturation), a new *cis*-Golgi stack with its cargo physically moves from the *cis* position towards the *trans* position, successively becoming first a *medial*- and then a *trans*-Golgi cisterna. As this happens, Golgi-resident enzymes and other proteins are constantly being retrieved from later to earlier Golgi cisternae by small retrograde transport vesicles (Losev *et al.*, 2006; Morré and Ovtracht, 1977). Ultimately, cargo reaches the TGN from where it can be sorted to different loci in the cell. Material destined to endosomes and lysosomes is transported in clathrin-coated vesicles, whereas material for PM is sorted into uncoated secretory vesicles that fuse with the PM. Clathrin-mediated endocytosis from TGN and PM allows retrieval of missorted proteins and uptake of exogenous molecules into the cell, respectively. Endocytic vesicles from PM are first targeted to tubulo-vesicular early endosomes, located in the periphery of the cell. Here, some endocytosed cargo such as surface receptors, recycle back to the cell surface via recycling endosomes. Other cargo proceeds to late endosomes. Late endosomes are mainly spherical and contain smaller

vesicles that bud from the perimeter membrane into the endosome lumen. This leads to their multivesicular appearance, and so they are also called multivesicular bodies. From late endosomes, endocytosed material is either delivered to TGN for further processing and sorting, or to lysosomes for degradation (Bonifacino and Glick, 2004; G. Liu et al., 2017), as illustrated in **Figure 20**.

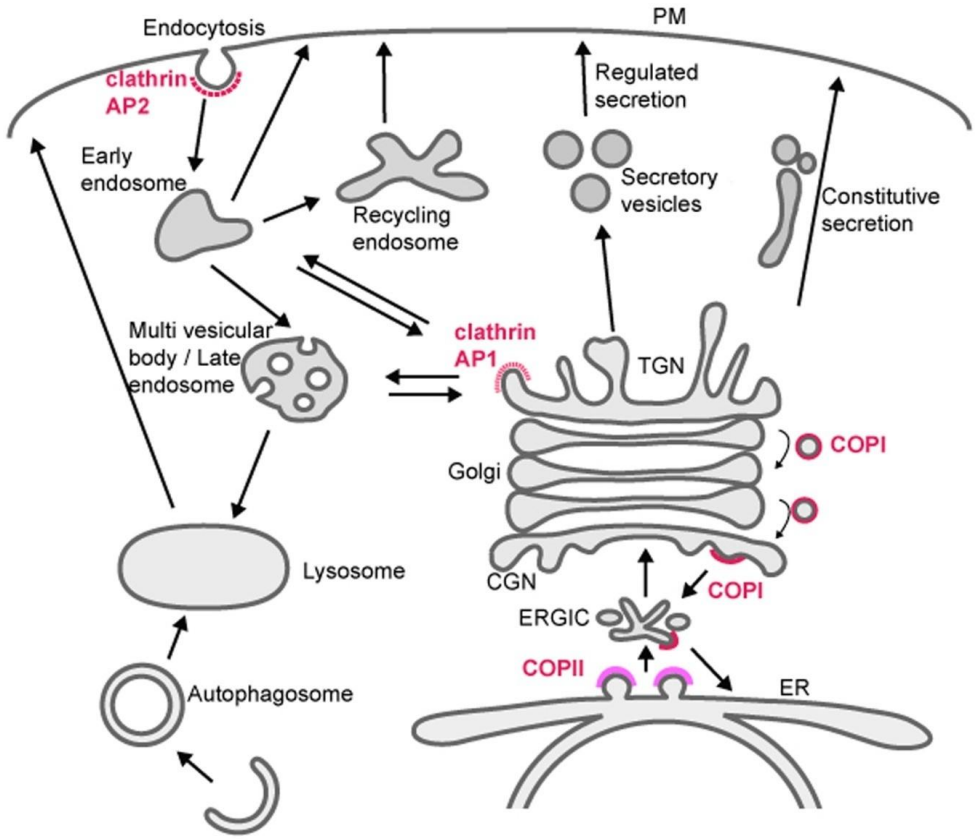

Figure 20: The secretory pathway

Transport is mediated by budding and fusion of transport carriers (vesicles or tubules), by fusion of organelles or by their maturation. Budding of some transport carriers is mediated by coat proteins (indicated by colors) and merging of a vesicle with other vesicles or cell membrane is mediated by specialized proteins, such as SNAREs. Illustration from (Sato et al., 2014).

1.2 CHALLENGES OF LIPID SORTING

Vesicular trafficking exchanges large amount of membrane material between organelles and is thus essential for bulk lipid transport. At the same time, organelles maintain their lipid-based identity, as lipid composition changes progressively throughout the secretory pathway. Therefore, several authors attempted to elucidate lipid selectivity in vesicular trafficking by following if vesicles are enriched in or depleted of lipids that are more or less abundant in the target membrane (Deng *et al.*, 2016; Moreau *et al.*, 1993; Sorre *et al.*, 2009). One model in the field is that lipid clustering of sterols and sphingolipids into microdomains contributes to sorting processes at TGN. One of the first studies of sphingomyelin sorting in polarized epithelial cells incubated with fluorescently labelled short-chain ceramide has shown that fluorescent lipids accumulated to a higher level in the apical membrane domain, suggesting that sphingolipids are enriched in apically targeted secretory vesicles (van Meer *et al.*, 1987). Consistently, a more recent study on lipids in yeast using immunoprecipitation of transport vesicles via Myc-tagged FusMidp protein in combination with quantitative lipidomics has demonstrated that FusMidp-vesicles comprised more ergosterol and sphingolipids, compared to TGN/endosomes extract. Furthermore, lipid analysis also documented differences in other lipid classes – PA was elevated in FusMidp-vesicles, whereas PS, PE and PC were depleted (Klemm *et al.*, 2009).

However, what is missing are the factors responsible for microdomain clustering in TGN and in budding vesicles – inspite of the fact that several luminal or cytosolic proteins have been postulated as candidates for microdomain coalescence (Proszynski *et al.*, 2005). It is also noteworthy that there are organelles that are not connected to the endomembrane system, such as peroxisomes, mitochondria and plastids (in plants). Their lipid homeostasis thus cannot be explained by vesicular lipid trafficking. And ultimately, lipid transfer between subcellular compartments still occurs in conditions where vesicular trafficking is blocked, suggesting that non-vesicular lipid transfer is required for maintaining lipid homeostasis (Lev, 2010).

B. LIPID TRANSPORT AT MEMBRANE CONTACT SITES

1. *BRIEF HISTORY OF MEMBRANE CONTACT SITES*

Membrane contact sites (MCS) have been noted since cells first began to be visualized. In 1959, Copeland and Dalton observed cells of the pseudobranch gland of a teleost and noted "a highly specialized tubular form of endoplasmic reticulum in association with the mitochondria and apparently in turn, with the vascular border of the cell" (Copeland and Dalton, 1959; EM image shown in **Figure 21**).

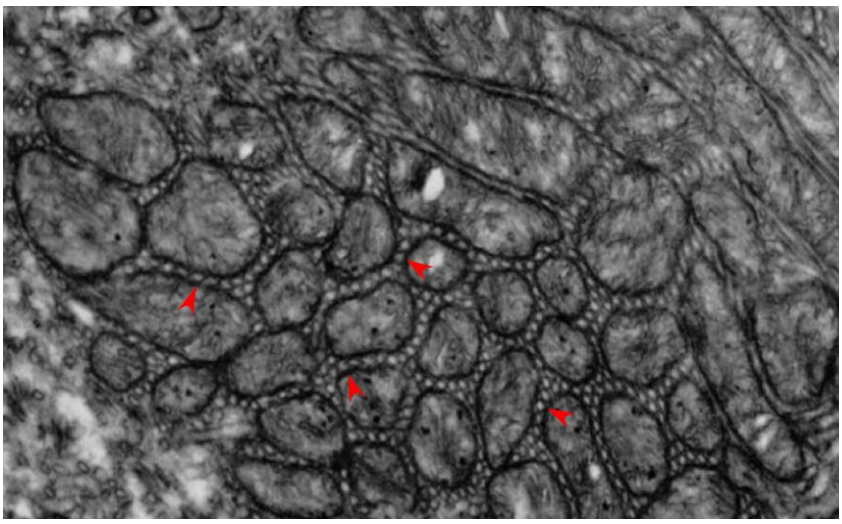

Figure 21: MCS between mitochondria and ER in a pseudobranch gland cell

Note the association of tubular form of ER with mitochondria (red arrows). Electron micrograph from Copeland and Dalton, 1959.

MCS are regions of close appositions (10 – 30nm) between two organelles. Since the endoplasmic reticulum (ER) is the most extensive cellular membrane network, it is not surprising that MCS mostly form between the ER and a second organelle, such as the plasma membrane (PM), mitochondria, Golgi, lysosomes, endosomes and lipid droplets. Of note, MCS between mitochondria and other organelles also began to be studied. True MCS are characterized by four features: they are created by membranes of two organelles tethered to each other with intermembrane distance of 30nm or less; the membranes do not fuse; MCS are enriched in specific proteins and/or lipids and the

formation of MCS affects the function or composition of at least one of the two organelles participating in the contact (Prinz, 2014).

MCS were first functionally characterized due to their critical roles in the intracellular exchange of lipids and calcium, since the ER is both the main site of lipid synthesis and the main store of intracellular Ca^{2+}. However, MCS display a wide variety of functions including regulation of organelle dynamics and trafficking, immune response and apoptosis. MCS are established and maintained by a protein or protein complexes that simultaneously bind the two aposed membranes - such proteins are called tethers, and in most cases, there are several tethers colocalizing at the same MCS (Prinz, 2014). The clarification of whether a protein is a genuine tether, necessary to establish and maintain a MCS, or whether it just functions at MCS but is not necessary for sustaining a contact, is a challenging issue to the field. For instance, the studies of Manford *et al.* (2012) and Stefan *et al.* (2011) on the junction of ER and PM in *Saccharomyces cerevisiae* have demonstrated that there are at least six ER resident transmembrane proteins that need to be eliminated in order to dramatically reduce the contacts between ER and PM. These proteins include calcium and lipid binding domain proteins 1–3 (Tcb 1-3), increased sodium tolerance protein 2 (Ist2) and two suppressors of Ca^{2+} sensitivity proteins (Scs2 and Scs22, homologues of mammalian VAPs). Tcb 1-3 and Ist2 contain cytosolic domains that interact with the plasma membrane lipids (Fischer *et al.*, 2009; Toulmay and Prinz, 2012), whereas Scs2 and Scs22 bind proteins containing “two phenylalanines in an acidic tract” (FFAT) motifs (Loewen *et al.*, 2003).

Many MCS tethering complexes have additional functions. For example, mitofusin-2 (Mfn2) is a dynamin-like protein that mediates mitochondrial fusion. Although it is largely localized to the outer mitochondrial membrane, a small fraction is also present on the ER membranes, and it has been proposed that the interaction between Mfn2 in the mitochondria and Mfn2 in the ER tethers these organelles (de Brito and Scorrano, 2008).

In the following chapters I will briefly depict the key functions of MCS in Ca^{2+} homeostasis and signaling as well as in organelle division. Thereafter, more attention will be given to lipid transfer occurring at MCS and especially the role of LTPs.

2. MCS IN Ca^{2+} HOMEOSTASIS AND SIGNALING

ER-PM and ER-mitochondria MCS also harbour key functions in intracellular Ca^{2+} homeostasis and signalling in mammalian cells, as evidenced on the example of skeletal and cardiac muscle cells. PM of these cells forms deep invaginations, called T (transverse)-tubules, which form extensive contacts with the ER (called sarcoplasmic reticulum in muscle cells, SR). These contacts are maintained by tethers called junctophilins. Junctophilins are SR-transmembrane proteins containing a large cytosolic domain that interacts with the PM. Expression of junctophilins in cells lacking them induces ER-PM contacts (Takeshima *et al.*, 2000) and junctophilin-deficient muscle cells display abnormal SR-PM MCS. These defects correlate with defects in Ca^{2+} signaling (Hirata *et al.*, 2006) because SR-PM contacts enable direct interaction between channels in the PM, called dihydropyridine receptors (DHPRs), and channels in SR, called ryanodine receptors (RyRs), which allows coordinated opening of both channels in response to muscle excitation (Fabiato, 1983; Nakada *et al.*, 2018; Rebbeck *et al.*, 2011).

ER-PM contacts also play a role in regulating Ca^{2+} levels in non-excitable cells in a process known as store-operated Ca^{2+} entry (SOCE). Ca^{2+} ions enter the cell via channel called Orai1, and the sensor of Ca^{2+} concentration in the ER is an integral membrane protein stromal interaction molecule-1 (STIM1). When Ca^{2+} concentration in the ER is low, STIM1 oligomerizes (**Figure 22**). Oligomerization exposes a polybasic segment in its intrinsically disordered C-terminus, which interacts with $P(4,5)P_2$ in the PM (Zhou *et al.*, 2013). STIM1 can also bind and activate Orai1 (Kawasaki *et al.*, 2009) and more recently, this interaction has been discovered to be modulated by cholesterol in the PM (Pacheco *et al.*, 2016). Activated STIM1 forms number of puncta, which are regions where the ER and PM are closely apposed. The PM and ER MCS allows Ca^{2+} to move from extracellular environment directly into the lumen of the ER without significant elevation of cytosolic Ca^{2+} levels (Jousset *et al.*, 2007). Of note, these MCS frequently accommodate the sarco/endoplasmic reticulum Ca^{2+} ATPase (SERCA) pump, which may interact directly with STIM1, thus more effectively channeling the Ca^{2+} ions into the ER lumen (Manjarrés *et al.*, 2011).

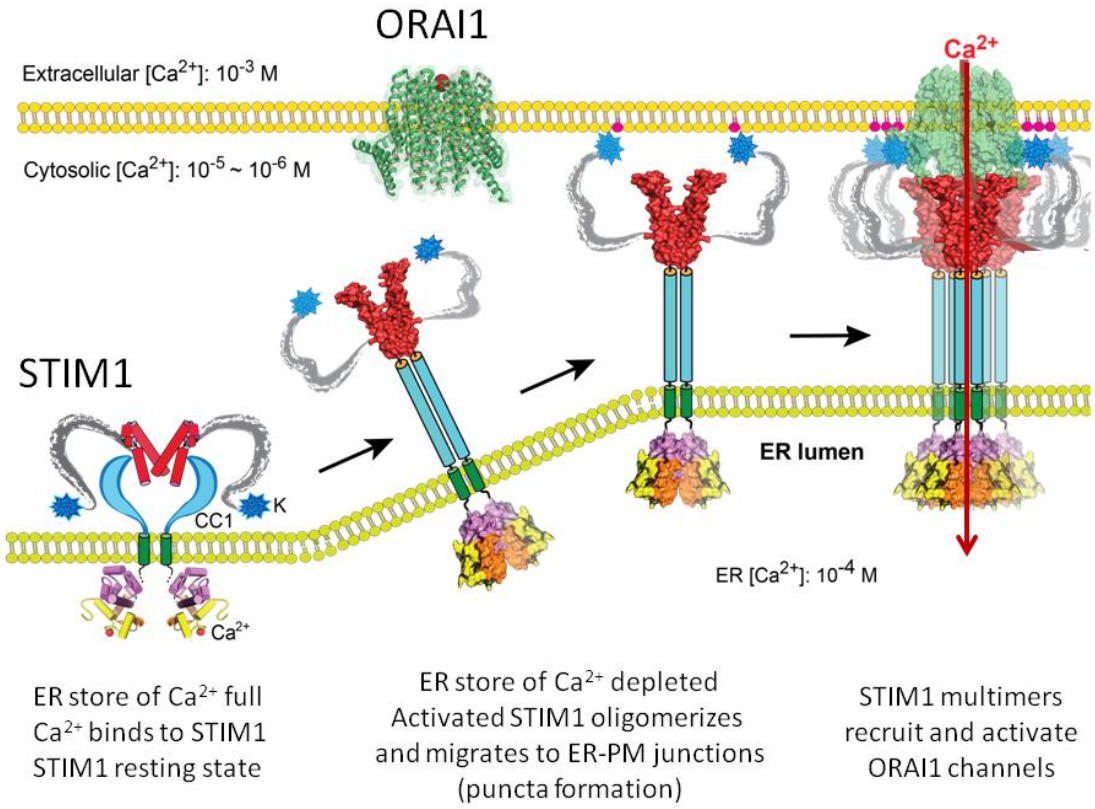

Figure 22: Activation of STIM1 and recruitment of ORAI1 to ER-PM contact sites

Blue asterisk "K" on STIM1 - polybasic aa segment; PM lipid shown in pink is $PI(4,5)P_2$, CC1 – predicted coiled coil. Illustration modified from Zhou *et al.*, 2013.

Similarly, Ca^{2+} influx into mitochondria is regulated by Ca^{2+} channels interacting with each other at ER-mitochondria MCS. The channel in the ER is called the inositol triphosphate receptor (IP3R), while the channel in the outer mitochondrial membrane is the voltage-dependent anion channel (VDAC). These proteins, together with the cytosolic chaperone Grp75, form a complex connecting ER and mitochondria and enabling Ca^{2+} flux between these organelles (Szabadkai *et al.*, 2006).

3. MCS AND ORGANELLE DIVISION AND INHERITANCE

In 2011, a study of Friedman et al. identified a new function of MCS between the ER and mitochondria: the ER encircles mitochondria at sites where mitochondrial scission will occur (Friedman *et al.*, 2011). Sites of close contacts between ER and mitochondria promote the multimerization of Dnm1/Drp1 in the outer mitochondrial membrane by a yet unknown mechanism. According to the current hypothesis, the ER circle may constrict the mitochondria to a diameter that allows the assembly of Dnm1/Drp1. The force necessary for constriction may come from actin polymerisation, mediated by protein called inverted formin-2 (Korobova *et al.*, 2013). An alternative hypothesis is that an unknown factor could constrict mitochondria from the inner mitochondrial membrane (**Figure 23**).

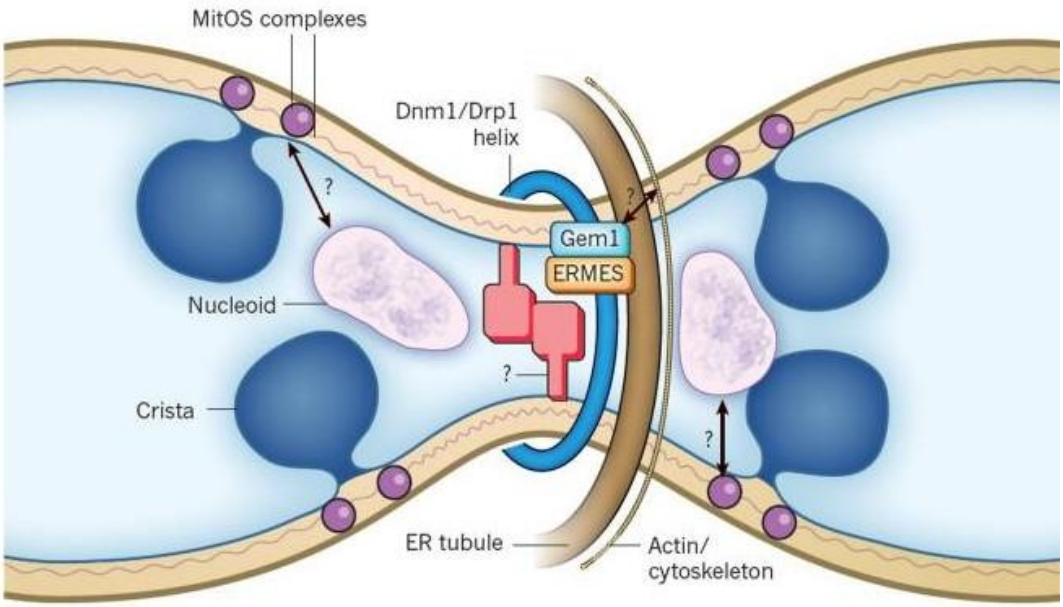

Figure 23: Molecular model for mitochondrial fission at mitochondria-ER MCS

In yeast, the ER-mitochondria encounter structure (ERMES) and the conserved Miro GTPase Gem1 are linked to ER-associated mitochondrial division site, together with a subset of nucleoids that are actively replicating and segregate before mitochondria fissions. Unknown mitochondrial factor and/or cytoskeletal components may also participate in membrane constriction before Dnm1/Drp1 recruitment. Nucleoid

placement at sites of division could be mediated by the MitOS scaffold complex. Illustration from Friedman and Nunnari, 2014.

Of note, similar mechanism of ER-mediated organelle division has been discovered recently in endosomes. When endosomes undergo fission for cargo sorting, actin regulator Coronin 1C at endosome buds recruits an ER-resident protein called transmembrane and coiled-coil domain family 1 (TMCC1) to regulate ER-associated endosome fission (Hoyer *et al.*, 2018).

4. LIPID TRANSFER PROTEINS AT MEMBRANE CONTACT SITES

Lipid transfer proteins (LTPs) are defined as proteins capable of transferring lipids between different membranes. The discovery of LTPs was a result of studies that investigated how the lipid components of plasma lipoproteins are transferred into the membranes of liver cells in the late 1960s. It soon became apparent that liver cells contain a cytosolic factor that is able to transfer phosphatidylcholine (PC) from one membrane to another (Wirtz and Zilversmit, 1968, 1969), and these studies are considered as first notions of the existence of non-vesicular membrane traffic. Karel Wirtz and Donald Zilversmit discovered that radioactively labelled phospholipids are exchanged between mitochondria and microsomes isolated by centrifugation from rat liver homogenates. Based on the findings that the unknown lipid transfer factor was nondialyzable, inactivated by high temperatures and sensitive to trypsin, the factor was assumed to be a protein. Similar observations followed from other laboratories, and efforts to purify the lipid transfer protein gradually uncovered a variety of proteins that could accelerate the transfer of different phospholipid classes, as well as transfer of less polar lipids (Bloj and Zilversmit, 1977; Noland *et al.*, 1980).

After the discovery of LTPs, it took many years until their role in lipid exchange at MCS has been fully appreciated. A milestone was the description of a region of ER as a membrane fraction associated with the mitochondria (termed “mitochondria-associated membrane, MAM”) and being associated with phospholipid synthesis (Vance, 1990).

However, definitive evidence to show that MCS are involved in the interorganelle transport of lipids was not obtained for a long time.

In the early 2000s, a protein that mediates the inter-organelle transport of ceramide was identified after a functional rescue cloning method (Hanada *et al.*, 2003). The discovery of ceramide transfer protein (CERT) has shown that CERT has functional and structural characteristics not only to catalyze the lipid transfer, but also to act at ER-Golgi MCS. This provided an entity-based model in which LTPs mediate the inter-organelle transport of lipids at organelle MCS in a nonvesicular manner (Kawano *et al.*, 2006). In the past decade, various LTP superfamilies with distinct lipid binding domains have been described (**Figure 24**, reviewed in Chiapparino et al., 2016; Hanada, K, 2018; Lev, 2010). These include for example the STARkin (which involves StART, PITP, PRELI and LAM families), TULIP, SEC14 (CRAL/TRIO), NPC1 and NPC2, which shall be mentioned here but will not be discussed in detail. Instead, major attention will be given to OSBP and its related proteins, ORPs.

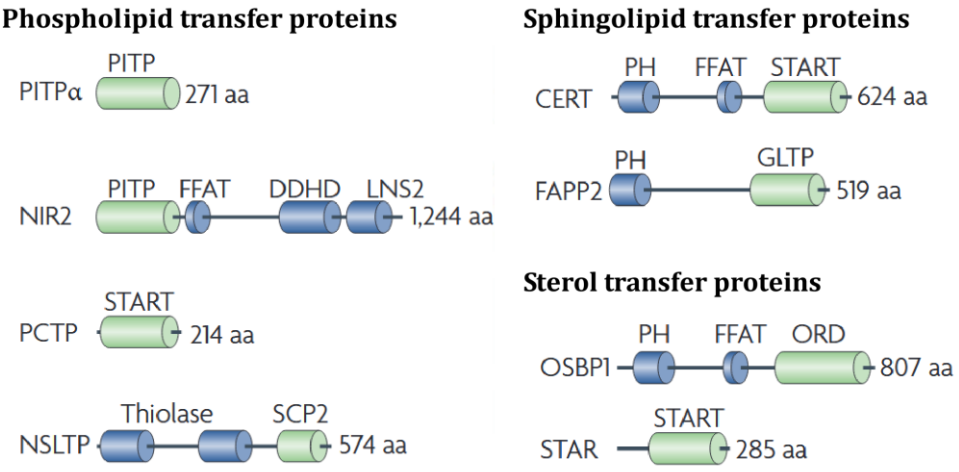

Figure 24: Domain organization of selected LTPs

Domain organization of representatives of major classes of mammalian LTPs. Membrane tethering domains are shown in blue, lipid transfer domains are shown in green. PITP - phosphatidylinositol transfer protein domain, DDHD - ~180 aa long domain in Nir/rdgB proteins containing four conserved residues (DDHD), LNS2 – Lipin/Ned1/Smp2 domain, PCTP – phosphatidylcholine transfer protein, START – StAR-related lipid transfer, NSLTP – non-specific lipid transfer protein, SCP2 – sterol carrier protein 2 domain, FAPP2 – four-phosphate adaptor protein 2, GLTP – glycolipid transfer protein domain, STAR – steroidogenic acute regulatory protein. Figure from Lev, 2010.

C. Oxysterol Binding Protein and OSBP-related proteins

OSBP was identified in 1980s in experiments performed to elucidate mechanisms of sterol synthesis regulation in cultured cells. Kandutsch and Chen (1978) found that oxygenated sterols - oxysterols - are much more (~10 000-fold) active than cholesterol itself in suppressing cholesterol synthesis. The effect is manifested by decreasing the activity of HMG-CoA (3-Hydroxy-3-methylglutaryl-CoA) reductase, a key enzyme in sterol biosynthesis. The decrease in activity was explained by suppression of gene transcription in cultured cells. In particular, 25-OH has been found to be one of the most potent suppressors, and has been used since as general tool to identify sterol-sensitive genes and proteins. Soon after, Kandutch and Thompson found a cytosolic protein whose affinitity for different oxysterols correlated with their ability to suppress HMG-CoA reductase in fibroblasts (Kandutsch and Thompson, 1980). Upon addition of 25-OH, the protein redistributed within the cell and became associated with the Golgi apparatus. Kandutsch and Shown described the sterol-binding properties of this unknown protein and due to its high affinity for oxysterols, they named it Oxysterol binding protein (Kandutsch and Shown, 1981). Its discoverers initially suggested a role for this protein in intracellular sensing of oxysterols and regulating expression of sterol-sensitive genes (Brown and Goldstein, 1997; Kandutsch and Shown, 1981; Lagace et al., 1997; Ridgway, 1992; Taylor and Kandutsch, 1985). Interestingly, the hypothesis that OSBP was involved in sterol-mediated gene regulation was discarded when 25-OH-induced inhibition of HMG-CoA reductase was found to be independent of OSBP (Nishimura *et al.*, 2005).

After the purification of OSBP and identification of OSBP gene by the Brown and Goldstein group (Dawson et al., 1989a, 1989b; Levanon et al., 1990), DNA sequencing- and expressed sequence tags-based screenings revealed that there are several homologs of OSBP in yeast and mammals (Jiang *et al.*, 1994; Laitinen *et al.*, 1999). The novel open reading frames were named OSBP-related proteins (ORPs) and subsequent findings demonstrated that the ORP family is conserved among eukaryotes (Anniss *et al.*, 2002; Lehto *et al.*, 2001; Zhou *et al.*, 2014).

Human genome contains 12 ORP genes, compared to 7 genes encoding the homologous Osh proteins in yeast. Human ORP genes give rise to 16 proteins due to alternative promoter and splice-site usage (**Figure 25**). The resulting "short" ORP variants differ from their "long" counterparts in unique expression pattern and functional properties (Ngo *et al.*, 2010; Olkkonen and Levine, 2004).

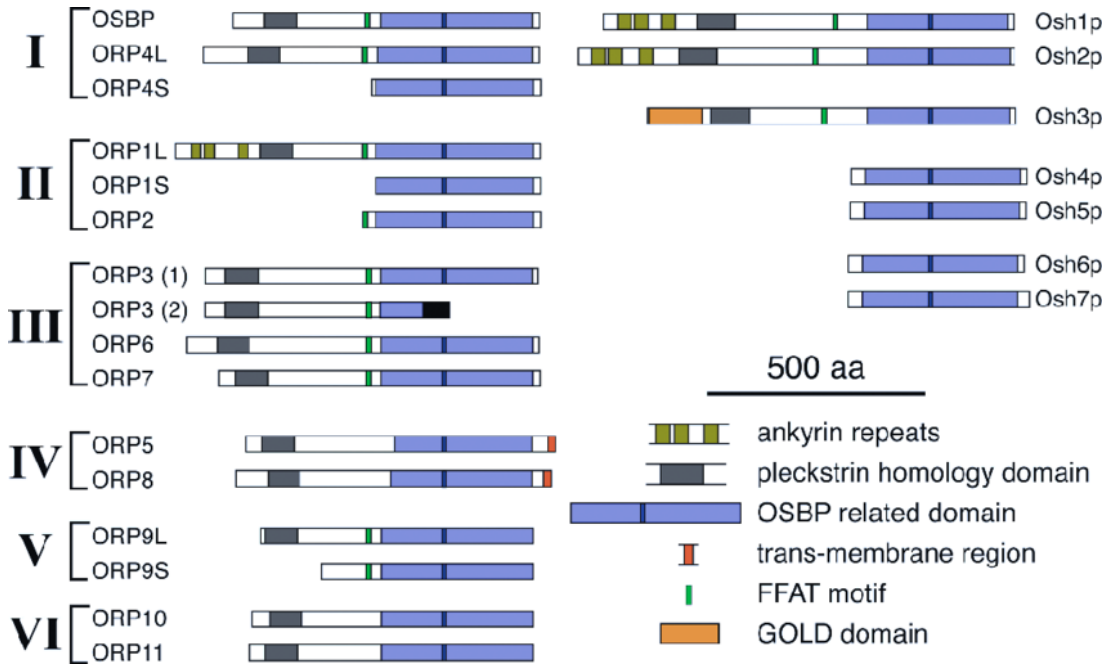

Figure 25: Structural organization of the human ORP and yeast Osh family

Domain structure of the major variants is shown. The dark blue area represents the highly conserved EQVSHHPP motif. Variants containing the PH domain are denoted as long (L) and variants without PH domain as short (S). In the case of ORP3, ORP3 (1) represents the full length variant while ORP3 (2) contains a C-terminal sequence unrelated to ORD (Collier *et al.,* 2003). Illustration from Olkkonen and Levine, 2004.

The hallmark of all ORPs is a well conserved, ~350 aa long lipid transfer domain called OSBP-related domain (ORD), located in the C-terminal half of the proteins. First evidences for the role of ORD in lipid transport come from studies of yeast Osh proteins. Deletion of all seven *OSH* genes was shown to be lethal, and expression of any single Osh protein was sufficient to maintain viability, demonstrating the functional redundancy

and co-operativity of Osh proteins (Beh *et al.*, 2001). Conditional *OSH1-OSH7* mutants displayed severe defects in intracellular sterol distribution and endocytosis (Beh and Rine, 2004). Crystal structure of Osh4 with sterol inside the hydrophobic pocket of the ORD has been determined by Im *et al.* (2005), and detailed studies of *in vitro* sterol transfer activity of Osh proteins provided additional evidence of their functional role in lipid binding. Osh4 has been shown to extract sterols from membranes, which was markedly enhanced by addition of PI(4,5)P_2 or PS in the donor vesicles (Raychaudhuri *et al.*, 2006). Later on, the structure of Osh4 with PI(4)P inside the ORD ligand cavity has been resolved, and it has been suggested that sterols and PI(4)P could be transported along opposite routes: sterol from the ER to late compartments (PM) and PI(4)P backwards (de Saint-Jean *et al.*, 2011). The authors envisioned that - when coupled to PI(4)P metabolism - this model (**Figure 26**) could also explain how an increasing gradient of sterol from the ER to the PM is generated (Ikonen, 2008; Maxfield and van Meer, 2010). The subsequent study of Moser von Filseck *et al.* (2015) clearly demonstrated that Osh4 can transport sterol against its concentration gradient by dissipating the energy of a PI(4)P gradient, concluding that Osh4 is far more efficient when it acts as a lipid exchanger rather than a mere transporter. PI(4)P gradients are maintained over time as PI(4)P is continually synthesized on late membranes and hydrolyzed by Sac1 in the ER (Faulhammer *et al.*, 2007; Foti *et al.*, 2001). To date, all members of ORP/Osh protein families have been suggested to bind PI(4)P (Tong *et al.*, 2013), and some ORP/Osh have been shown to recognize a second lipid that is not sterol (Maeda *et al.*, 2013; Moser von Filseck *et al.*, 2015).

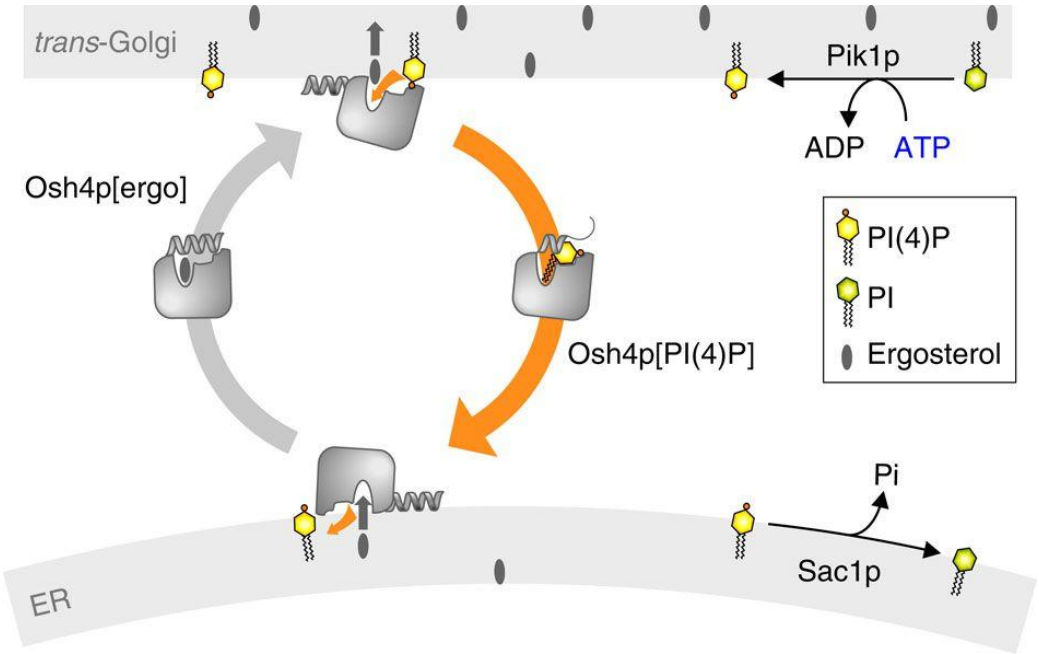

Figure 26: Sterol/PI(4)P exchange by Osh4

ATP-dependent phosphorylation of PI into PI(4)P by Pik1 and hydrolysis of PI(4)P by Sac1 fuel multiple sterol/PI(4)P exchange cycles, give directionality to the lipid exchange and thereby create and maintain sterol gradient. Illustration from Moser von Filseck et al., 2015.

Another conserved sequence feature of ORP/Osh proteins is a plekstrin homology (PH) domain in the N-terminal half of the protein. Most PH domains recognize and target individual phosphoinositides with rather low affinity. Nevertheless, high membrane binding specificity results from cooperativity with additional, mainly anionic lipids (Harlan et al., 1994; Lemmon and Ferguson, 2001; Vonkova et al., 2015). PH domains facilitate protein localisation to PIP-enriched membranes of organelles such as the Golgi (Levine and Munro, 2002, 1998) or plasma membrane (Lehto *et al.*, 2005). With the exception of ORP2 in human and Osh4 – 7 in yeast, the PH domain is found in all ORP/Osh. OSBP and many other ORP/Osh also feature a linear FFAT motif with the consensus sequence EFFDAxE (**Figure 27**). FFAT ("two phenylalanines in an acidic tract") motif has been demonstrated to bind to vesicle-associated membrane protein (VAMP)-associated protein A (VAP-A) located at the ER (Furuita *et al.*, 2010; Kaiser *et al.*, 2005; Wyles and Ridgway, 2004). Some ORPs

which lack the FFAT motif are localized to the ER via their C-terminal transmembrane domain (Du *et al.*, 2011; Yan *et al.*, 2008).

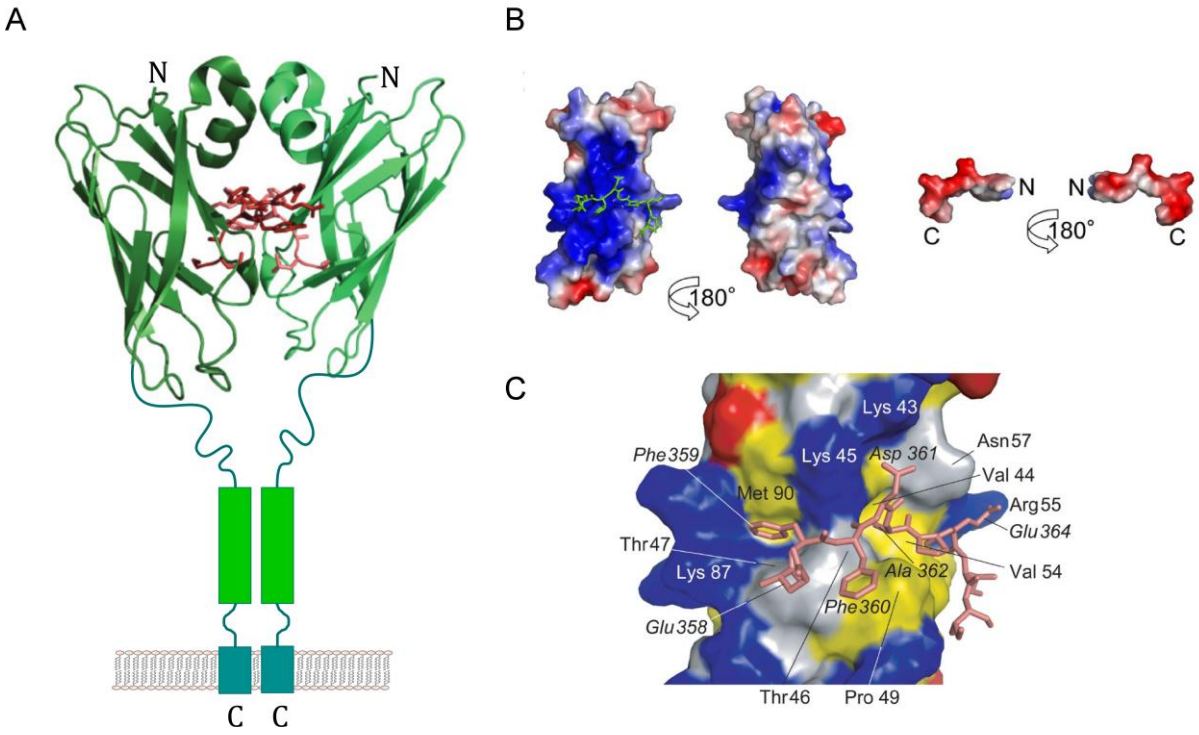

Figure 27: FFAT motif recognition by VAP-A

(A) FFAT motif (red) is recognized by Major Sperm Protein (MSP) domain of VAP-A. Regions of high coiled-coil probability between the MSP and transmembrane domains of VAP-A (light green) as well as between PH domains and ORDs of most ORPs suggest a dimeric 2:2 organization (figure modified from Antonny *et al.*, 2018) **(B)** Electrostatic surfaces of MSP domain (left) and FFAT motif of OSBP (right) coloured by electrostatic potential (red = negative/acidic, blue = positive/basic) **(C)** Details of the interaction. Residues of OSBP are written in *italics*. OSBP FFAT motif is shown as stick model, VAP-A MSP residues are colored according to their charge – red = acidic, blue = basic, yellow = hydrophobic. Models from Furuita *et al.*, 2010.

Based on similarity in amino acid sequence and gene structure, the ORPs were divided into 6 distinct subfamilies (see **Figure 25**). In the subsequent chapters, I will briefly discuss the specific structure/function features of each ORP subfamily.

1. STRUCTURE AND FUNCTION OF OSBP AND OSBP-RELATED PROTEINS

1.1 Subfamily I – OSBP, ORP4 L and ORP4 S

OSBP is ubiquitously expressed (although the levels of expression may vary between different tissues/cell types) and its structural elements correspond to its function in membrane tethering and selective lipid exchange. OSBP contains a PH domain that has been shown to recognize a small G-protein Arf1-GTP and phosphoinositide PI(4)P at the *trans*-Golgi membrane (Godi *et al.*, 2004; Levine and Munro, 2002, 1998), illustrated in **Figure 28**.

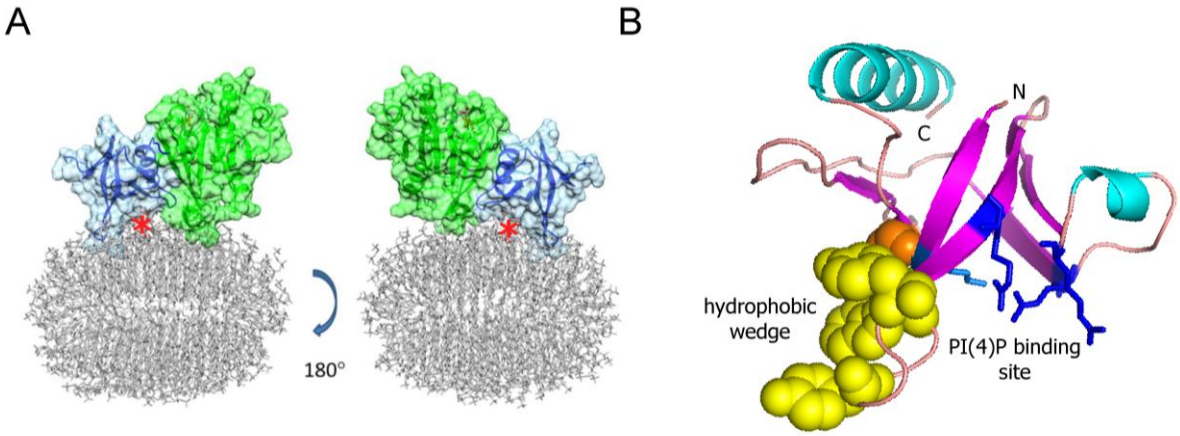

Figure 28: Recognition of Arf1-GTP and PI(4)P by PH domains of LTPs

(A) Model of interaction of PH domain of FAPP1 (blue) with Arf1 (green) and PI(4)P (binding site indicated by red asterisk) at a small bicelle surface (Liu et al., 2014) **(B)** PH domain of OSBP modeled according to the crystal structure of FAPP1 PH domain. Yellow residues indicate hydrophobic residues likely inserted into membrane, i.e. hydrophobic wedge. PI(4)P binding site is located within a cluster of basic residues. Note the positions of the N-terminal and C-terminal ends. Upstream of the N-terminal end is located the disordered region (not shown).

PH domain is followed by two coiled-coils that mediate formation of OSBP dimers as well as heterodimerization with its close homolog, OSBP2/ORP4 (Ridgway, 1992; Wyles et al., 2007). OSBP also contains a canonical linear FFAT motif that

mediates its binding with ER-resident transmembrane proteins VAP-A and VAP-B (Loewen *et al.*, 2003; Loewen and Levine, 2005, **Figure 27**). The C-terminal half of the protein comprises the lipid transfer domain – ORD, which has a hydrophobic pocket that can accommodate two very distinct lipids: cholesterol and PI(4)P, as shown in **Figure 29** (de Saint-Jean *et al.*, 2011; Mesmin *et al.*, 2013). Structural studies show that residues recognizing PI(4)P are conserved among the ORPs/Oshs, suggesting a common mechanism by which PI(4)P would be specifically exchanged for another lipid (Tong *et al.*, 2016).

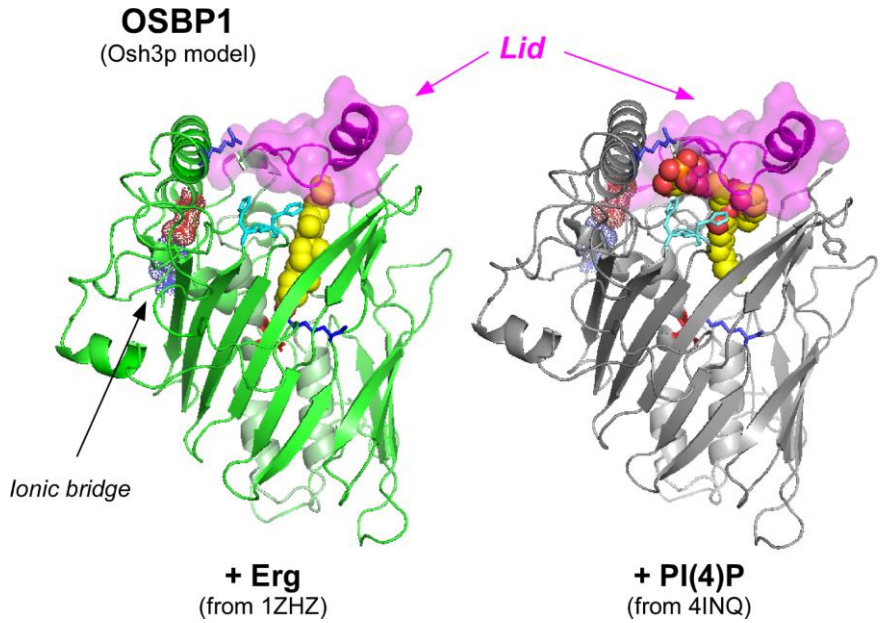

Figure 29: Model of the ORD domain of OSBP

Models were created according to the structure of Osh3p, with an ergosterol structure position estimated from Osh4p-based model alignment (left), and with PI(4)P molecule crystallized in the hydrophobic pocket of Osh3p ORD(right). Note the different orientations of sterol and PI(4)P – the polar hydroxyl group of sterol is deep inside the pocket whereas the polar part of PI(4)P is facing the surface. Lid region (pink) covers the hydrophobic pocket and might be stabilized by an ionic bridge in its proximity. Courtesy of J. Bigay.

The architecture of OSBP enabling simultaneous interactions of PH domain with PI(4)P/Arf1-GTP at the trans-Golgi and of FFAT motif with VAP-A at the ER, allows

OSBP to both tether organelles and transport lipids between them. These two activities are part of a four-step cycle described by Mesmin *et al.* in 2013. First, TGN and ER are tethered by PH domain and FFAT motif. Bringing both membranes into close apposition enables sterol transfer from the ER to the Golgi by the ORD. In the opposite direction, a counter-transfer of PI(4)P by the ORD follows. Upon its release into the ER membrane, PI(4)P is hydrolyzed by the ER-localized phosphatase Sac1. The energy provided by hydrolyzis of PI(4)P drives sterol transfer, ensures its directionality and allows negative feedback when PI(4)P pools become limiting (**Figure 30**, Mesmin *et al.,* 2013). A follow-up study has shown that OSBP is a major regulator of PI(4)P turnover, cholesterol distribution and lipid order in living cells. Inhibition of OSBP by a strong inhibitor, OSW-1, causes accumulation of sterols at ER/lipid droplets at the expense of TGN, thereby reducing the gradient of lipid order along the secretory pathway. OSBP activity is fueled by about half of the total cellular pool of PI(4)P (Antonny *et al.*, 2018; Mesmin *et al.*, 2017).

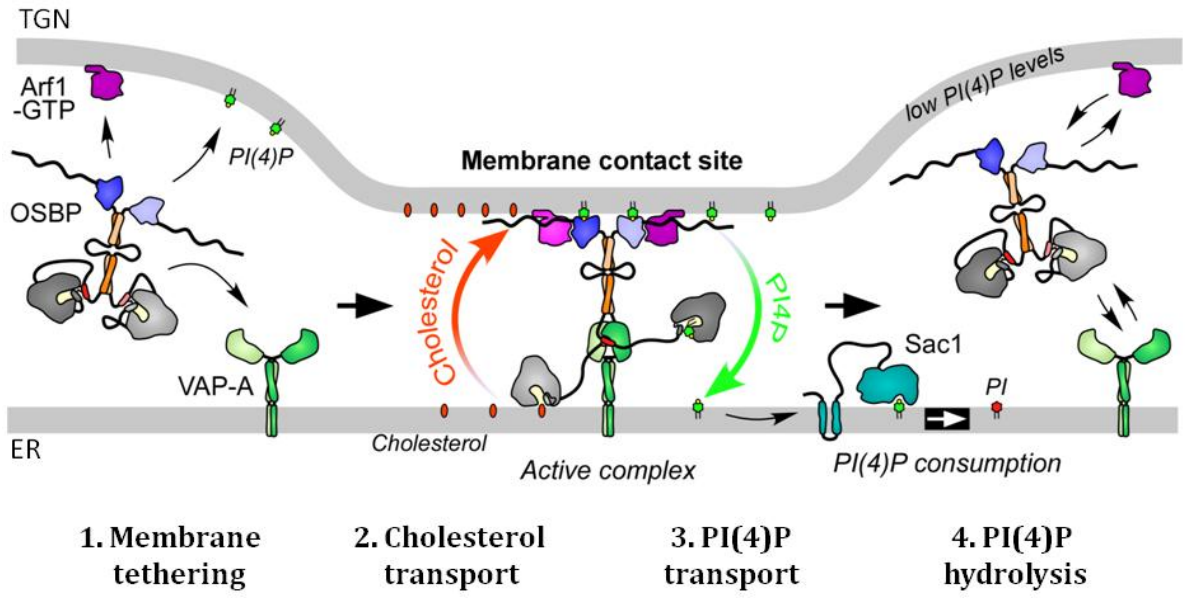

Figure 30: A four-step cycle driven by PI(4)P hydrolyzis directs sterol/PI(4)P exchange by the ER-Golgi tether OSBP

TGN and ER are tethered by PH domain and FFAT motif; this enables sterol transfer by the ORD followed by counter-transfer of PI(4)P by the ORD. Finally, PI(4)P is hydrolyzed in *cis* by the transmembrane phosphatase Sac1 residing in the ER. Figure from Mesmin *et al.,* 2013.

OSBP has also been shown to influence the activity of other LTPs – for example, upon 25-OH treatment, OSBP recruits CERT to the Golgi to enhance flux of ceramides for sphingomyelin synthesis, and concomitant generation of diacylglycerol (DAG) through which the Golgi secretory function is also affected (Perry and Ridgway, 2006). OSBP and CERT cooperate with another LTP, the PI/PC transfer protein Nir2, which also acts to regulate Golgi DAG levels via inhibition of the PC synthesis and stimulation of PI(4)P synthesis (Litvak *et al.*, 2005; Peretti *et al.*, 2008).

Evidence suggests that in addition to its lipid transfer activity and orchestration of other LTPs activity, OSBP could also regulate different signaling pathways in lipid metabolism-dependent manner. For example, Wang *et al.* observed that upon cholesterol binding, OSBP acts as a scaffolding protein for the phosphatases HePTP and PP2A. OSBP, HePTP and PP2A proteins form a high molecular weight complex, in which HePTP and PP2A are spatially organized so that they can cooperate to dephosphorylate the extracellular signal-regulated kinase, pERK. The pERK1/2 phosphatase activity conferred through OSBP is positively regulated by cholesterol and negatively by oxysterols, which gives implication that LTPs may have lipid-specific scaffolding functions that regulate key signaling pathways (Wang, 2005). Other study reports that OSBP also affects the JAK-STAT3 signaling by scaffolding the assembly of JAK2/STAT3 module in a sterol-dependent manner (Romeo and Kazlauskas, 2008). It is noteworthy that both pERK1/2 dephosphorylation and JAK2/STAT3 assembly lead to the activation of genes regulating cell survival and proliferation. Consistently, OSBP has been identified as a strong target of natural compounds that potently and in some cases selectively inhibit the growth of cultured human cancer cell lines. Because of their affinity for OSBP and ORP4L, these compounds have been named ORPphilins, including, for example, OSW1 (Burgett *et al.*, 2011). Of note, some viruses hijack the OSBP lipid transfer machinery to supply cholesterol to viral replication organelles (Ishikawa-Sasaki *et al.*, 2018; Meutiawati *et al.*, 2018; Strating *et al.*, 2015).

OSBP2/ORP4 is a close homolog of OSBP, sharing >60% amino acid identity and differing mainly in the N-terminal region upstream of PH domain. ORP4 has two isoforms, ORP4L and ORP4S. Both bind 25-OH with high affinity and both can extract and transfer cholesterol between liposomes (Charman *et al.*, 2014). The PH domain of ORP4L can also bind PI(4)P in the Golgi but contrary to OSBP, ORP4L does not localize

to the Golgi apparatus in response to sterol treatment nor does it affect sphingolipid regulation (Wang *et al.*, 2002). ORP4 tissue expression is restricted to testis, brain and heart, suggesting a rather specialized function (Udagawa *et al.*, 2014). Notably, ORP4-deficient mice display male infertility due to severe defects in sperm development and morphology (Udagawa et al., 2014). The ORD domain of ORP4 has been demonstrated to interact with vimentin filaments *in vitro* and, when overexpressed in cells, interacts with and collapses the vimentin network (Wang *et al.*, 2002; Wyles *et al.*, 2007). The functional relevance of ORP4 association with vimentin is unknown, yet ORP4 is required for proliferation and survival of cultured cells (Charman *et al.*, 2014). Consistently, increased levels of ORP4 are detectable in blood leukocytes of patients with chronic myeloid leukemia, suggesting that it may have some implications in cancers (Fournier et al., 1999; Li et al., 2016).

1.2 Subfamily II – ORP1L, ORP1S and ORP2

The *OSBPL1* gene of subfamily II gives rise to two protein variants, ORP1L and ORP1S with distinct tissue expression patterns: ORP1L is abundant in brain, lung and macrophage, whereas ORP1S is found in skeletal muscle and heart (Johansson *et al.*, 2003). The PH domain of ORP1L binds phosphoinositides, and ORP1L N-terminus contains three ankyrin repeats, which mediate its association with GTPase Rab7 on late endocytic compartments. Rab7 interacts with its effector RILP (Rab7-Interacting Lysosomal Protein) which recruits dynein/dynactin microtubule motors and facilitates intracellular motility and distribution of LE compartments (Johansson *et al.*, 2007, 2005), as illustrated in **Figure 31**. Under low cholesterol conditions, ORP1 induces the formation of ER/LE contact sites via its interactions with VAPs and Rab7, respectively, restricting LE motility and preventing LE clustering (Rocha *et al.*, 2009; Vihervaara *et al.*, 2011).

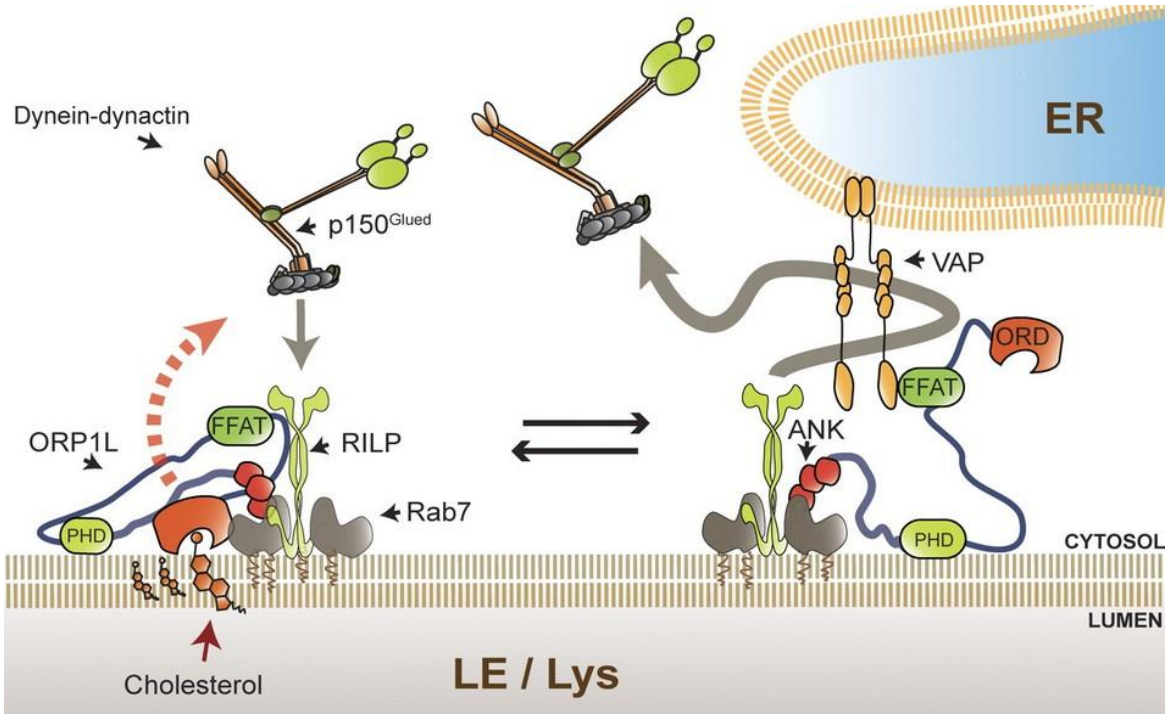

Figure 31: ORP1L senses cholesterol levels in late endosomal compartments and regulates the recruitment of motor protein complexes

Rab7 recruits RILP to late endosomes, where RILP binds the p150^{Glued} subunit of the dynein/dynactin motor. The ORD of ORP1L senses cholesterol, and at low cholesterol levels it adopts a conformation in which the FFAT motif is exposed and ORP1L is recruited to the ER via VAP. Binding with VAP removes p150^{Glued} domain from RILP, thus preventing LE transport and LE clustering. Illustration from Rocha *et al.* 2009.

ORP1S was reported to translocate into the nucleus upon oxysterol ligand stimulation, and suggested to regulate APOE expression via liver X receptor pathway (Lee *et al.*, 2012).

ORP2 only exists in a short variant and is expressed ubiquitously. Its first functional characterisation revealed its involvement in cellular cholesterol efflux (Laitinen *et al.*, 2002). ORP2 localizes at the surface of lipid droplets, and as it possesses a FFAT motif and interacts with VAPs, it was suggested to be a regulator of neutral lipid metabolism (Hynynen *et al.*, 2009; Olkkonen and Li, 2013). More recently, ORP2 has been discovered to regulate hepatocellular energy metabolism as well as actin cytoskeletal functions (Kentala *et al.*, 2018a, 2018b).

1.3 Subfamily III – ORP3, ORP6 and ORP7

ORP3 and ORP7, unlike many other ORPs, have not been studied in the context of lipid metabolism. ORP3 is mainly expressed in kidney, testicular epithelia and immune cells; ORP6 in the central nervous system and ORP7 is most abundant in the epithelia of the gastrointestinal tract (Lehto *et al.*, 2004). ORP3 and ORP7 were found to interact with small GTPase R-Ras, which controls cell adhesion and migration (Goldfinger *et al.*, 2007; Lehto *et al.*, 2008; Weber-Boyvat *et al.*, 2015). ORP7 also interacts with a small ubiquitin-like protein GATE-16/Gabarapl2, which is a chaperone for the Golgi trafficking regulator GS28, and this interaction results in destabilisation of SNARE protein (Zhong *et al.*, 2011).

ORP6 is upregulated in LDL-loaded macrophages, as well as in the livers of both mice and non-human primates that were fed a cholesterol-rich diet (Lehto et al., 2001; Ouimet et al., 2016). Consistently, ORP6 gene has been shown to be tightly regulated by the LXR transcription factors and SREBP2-related post-transcriptional repression mediated by miRNA (Ouimet et al., 2016). Gain- and loss-of-function experiments in the same study demonstrated that ORP6 contributes to cellular cholesterol efflux to apoA1 and HDL. ORP6 has also been studied in cultured mouse neurons, where it co-localized with ORP3 at ER-PM contact sites. Knockdown of ORP6 resulted in increased localisation of a PI(4)P marker at the PM, implicating that ORP6 might be involved at PI(4)P turnover at ER-PM contact sites (Mochizuki *et al.*, 2018).

1.4 Subfamily IV – ORP5 and ORP8

ORP5 and ORP8 share 80% aa sequence identity. ORP5 is ubiquitously expressed, while highest levels of ORP8 were reported in immune cells, spleen, kidney and brain (Yan *et al.*, 2008). ORP5 and ORP8 lack the FFAT motif, but instead they are anchored to ER membranes via a C-terminal transmembrane domain. Both are targeted to the PM via interaction of their PH domain with PI(4)P and/or PI(4,5)P_2. The function of ORP5 as PS transporter was suggested in an interactome study of Maeda *et al.* (2013), and later both ORP5 and ORP8 have been confirmed to countertransport PI(4)P/PS between the ER and the PM in similar mechanism by which OSBP exchanges

PI(4)P/cholesterol at ER-Golgi MCS or by which Osh6/Osh7 exchange PI(4)P/PS at ER-PM contact sites in yeast (Chung *et al.*, 2015; Mesmin *et al.*, 2013; Moser von Filseck *et al.*, 2015). Other studies also noted the localisation of ORP5 and ORP8 to ER-mitochondria contacts (Galmes et al., 2016; Pulli et al., 2018). As mitochondrial membranes do not contain PIs, interaction of ORP5/ORP8 with outer mitochondrial membrane could occur through protein PTPIP51, known to promote ER-mitochondria junctions via VAP-B interaction (Galmes *et al.*, 2016; Stoica *et al.*, 2014).

It is noteworthy that recent study of Ghai *et al.,* has shown that the PH domains of ORP5 and ORP8 can also recognize di- and tri-phosphorylated PIs. In addition, the ORD of ORP8 was able to transport PI(4,5)P_2 between liposomes and a gradient of PI(4,5)P_2 enhanced PS transport, demonstrating that PIs other than PI(4)P can also serve as co-exchangers for the transport by ORPs (Ghai *et al.*, 2017).

Additional function of ORP5 in mTORC1 signaling and stimulation of cell growth has been reported recently (Du *et al.*, 2018), whereas an implication of ORP8 in inhibiting cancer cell proliferation has been suggested (Guo *et al.*, 2017; Zhong *et al.*, 2015).

1.5 Subfamily V – ORP9L and ORP9S

ORP9 is expressed in long and short variants, and ORP9L has been shown to transfer cholesterol between membranes *in vitro*. In cells, it localizes at the ER/Golgi interface, and therefore its function is assumed to involve sterol transfer (Wyles and Ridgway, 2004). ORP9L depletion causes Golgi fragmentation, defects in vesicular transport and accumulation of cholesterol in endosomes/lysosomes, suggesting additional role in maintaining integrity of the early secretory pathway (Ngo and Ridgway, 2009).

1.6 Subfamily VI – ORP10 and ORP11

ORP10 and ORP11 are unique among the ORPs in that they do not have established ER targeting determinants, although both can dimerize with ORP9, which contains the FFAT motif (Nissilä *et al.*, 2012; Zhou *et al.*, 2010). Both proteins have been associated with cardiometabolic diseases (Koriyama *et al.*, 2010; Perttilä *et al.*, 2009). ORP10 has shown affinity for microtubules and partially with Golgi membranes via the affinity of its PH domain for PI(4)P, suggesting that it could play a role in dynamics of carriers in the secretory pathway or juxtapose Golgi elements with microtubules (Nissilä *et al.*, 2012). Consistently, ORP10 was reported to interact with Diaphanous 1, which is a regulator of microfilament and microtubule function (Li *et al.*, 2013).

ORP11 is highly expressed in brain, gonads and adipose tissues (Zhou *et al.*, 2012). Depending on ORP9, ORP11 localizes at the *trans*-Golgi and endosomes. Its overexpression induced the formation of lamellar lipid bodies associated with vacuolar elements or with the Golgi, indicating its involvement in lipid trafficking on the endosome-Golgi axis (Zhou *et al.*, 2010).

WORKING HYPOTHESIS

The ORP family of lipid transfer proteins has been extensively studied in the past. We know that ORPs share a similar domain organization. The most studied of ORPs is OSBP, a founding (first identified) member of the ORP family. From the first notions that OSBP may be implicated in sterol metabolism in 1980s – 1990s (Kandutsch and Thompson, 1980; Taylor *et al.,* 1984), researchers have gradually elucidated its function in binding sterols in the lipid transfer OSBP-related domain (Im *et al.*, 2005; Ridgway, 1992) which has been shown to accommodate not only sterols but also structurally very distinct lipid, PI(4)P (de Saint-Jean *et al.*, 2011). The dimeric structure of OSBP has been reported (Ridgway, 1992), and its PH and FFAT domains have been shown to interact with ER and Golgi membranes (Kaiser *et al.*, 2005; Levine and Munro, 2002, 1998). Later it has been suggested by our group that OSBP may serve as a bridge at the ER-Golgi MCS, counter-transporting lipids by using the chemical gradient of PI(4)P to generate sterol gradient along the secretory pathway (Mesmin *et al.*, 2013). Recently, we have found that OSBP is responsible for continuous exchange of approximately half of *trans*-Golgi PI(4)P pools for cholesterol from the ER, thus being a major regulator of sterol homeostasis and membrane order in cells (Mesmin *et al.*, 2017). It is noteworthy that analogous function in lipid exchange has been simultaneously discovered in other ORPs, confirming the role of PI(4)P as "currency" for vectorial transfer of other lipids such as phosphatidylserine (Maeda *et al.*, 2013; Tong *et al.*, 2013; Antonny *et al.*, 2018). However, until now very little is known about the details of lipid exchange dynamics and topological organization of ORPs (and similarly structured LTPs) within MCS in general.

Vast majority of studies on OSBP has focused on its folded domains. Nevertheless, a big questionmark was the presence of considerably long (50 to 140 aa), variable sequences upstream of PH domains in most ORPs. Particularly in the N-terminal part of OSBP, we noticed a large proportion of glycine, proline and alanine, hinting us to intrinsic disorder. Intrinsically disordered regions are known to display enhanced conformational flexibility. They play unique roles in protein-protein as well as protein-membrane interactions (Babu, 2016; Tompa, 2012). IDPRs also change physico-chemical parameters of proteins, for example inducing phase separation or influencing

protein volume and thereby its diffusion behavior (Lippincott-Schwartz *et al.*, 2001; Wang *et al.*, 2012).

OSBP's natural behavior is cycling between soluble form in cytosol and recruited form transporting lipids at ER-Golgi MCS. MCS are highly specialized zones of material (proteins, lipids, ions, metabolites etc) exchange between organelles. The organisation of MCS creates regions of confined environment (~20 – 30 nm thick) which are co-occupied by many other proteins involved in material transport, signaling or organelle dynamics. Given the high protein density within a narrow space, the regulation of protein dynamics as well as the dynamics of MCS as a whole became a very captivating research issue.

Therefore, we decided to investigate the role of unfolded N-terminal tail in regulating membrane binding and tethering properties of OSBP (and of its very close homolog with a distinct N-terminus, ORP4). We aimed to discover how intrinsic disorder affects recruitment of OSBP to simple flat membranes, as well as how it regulates protein tethering and dynamics within MCS (both artificial ER-Golgi MCS on giant vesicles and natural MCS in in living cells). At the same time, we were appealed by the possibility that N-terminal regions may play a role in lipid transfer properties of ORPs, either directly by regulating lipid exchange activity of the ORD, or indirectly via regulating protein mobility.

As a result, this study links the distinct fields briefly introduced before (intrinsically disordered proteins, lateral diffusion of membrane proteins, MCS and OSBP/ORPs). Using a variety of tools in biochemistry and cell biology, we introduce an innovative view on intrinsically disordered N-terminal sequences upstream of PH domains in ORPs (and possibly other LTPs with similar domain structure) as regulators of protein lateral motility and MCS dynamics. Moreover, we provide an interesting implication of N-terminus of OSBP in regulating MCS geometry by favouring ER-Golgi tethering and preventing aberrant Golgi-Golgi contacts.

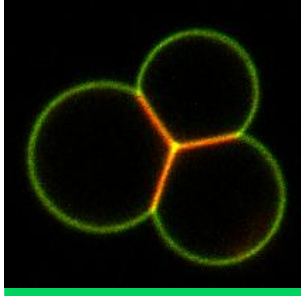

Materials & Methods

MATERIALS AND METHODS

Bioinformatic analysis

We assessed the order/disorder score of different ORPs with Predictor of Natural Disordered Regions (PONDR®) web server (http://www.pondr.com/) (Romero et al., 1997) using VL3-BA and VSL2 predictors. Percentual amino acid composition of selected domains was determined using Expasy/protparam web server (https://web.expasy.org/protparam/) (Gasteiger et al., 2005) and plotted as pie charts to highlight similarities and divergences between domains (N-terminus, PH domain, ORD). Limits of selected domains were as follows:

Human ORP	UNIPROT Accession Number	Total aa	N-ter Seq	PH Seq	ORD Seq
OSBP 1	P22059	1-807	1-91	92-183	410-807
ORP 4	Q969R2	1-878	1-147	148-238	476-878
ORP 1	Q9BXW6	1-950	1-234	235-334	537-950
ORP 3	Q9H4L5	1-887	1-50	51-146	516-887
ORP 6	Q9BZF3	1-934	1-89	90-190	559-934
ORP 7	Q9BZF2	1-842	1-50	51-142	467-842
ORP 5	Q9H0X9	1-879	1-125	126-243	359-748
ORP 8L	Q9BZF1	1-889	1-147	148-265	395-780
ORP 9	Q96SU4	1-736		1-99	365-736
ORP 10	Q9BXB5	1-764	1-73	74-171	387-764
ORP 11	Q9BXB4	1-747	1-58	59-160	357-747

Notably, our ORP4 sequence (gift from N. Ridgway) started at M39 (as referred to UNIPROT Q969R2:ORP4-OSBP2 sequence). Therefore, in this study M1 corresponds to M39 of the UNIPROT reference sequence.

For phylogenetic analysis, protein sequences of higher eukaryotes most similar to human OSBP were obtained from the UniProt database. The phylogenetic tree was created using the Phylogeny.fr server (http://www.phylogeny.fr/) (Dereeper and Guignon *et al.*, 2008). The sequences of each OSBP domain were then aligned and compared to that of the corresponding human domain using Clustal Omega (Sievers *et al.*, 2011). A percent identity matrix was calculated for each domain. For the N-ter,

sequences shorter than 20 amino acids were not included in the identity analysis. The prediction of coiled-coils was done using the NPS@ web server (Combet et al., 2000). Only sequences located between the PH domain and the FFAT motif were evaluated.

Construction, expression and purification of proteins

1. OSBP and ΔN-OSBP

In order to obtain catalytically active protein for our *in vitro* assays, we purified full-length (1-807) human OSBP and ΔN-OSBP (88-807) from baculovirus-infected Sf9 cells. The construct of full-length (1-807) human OSBP in pENTD/R was previously described (Mesmin *et al.*, 2013). For the expression and purification of ΔN-OSBP, we modified the pFastBac™HTA vector from Invitrogen by successive mutations to allow the insertion of a PCR amplified sequence upstream of the 6His-tag. These modifications include: 1) transformation of the original BamHI site into 2 stop codons and insertion of a new BamHI site upstream of the His tag. The insert [OSBP ΔN (88-807) + thrombin site] DNA sequence was PCR amplified using the pENTR/D-(OSBP-FL-thrombin site) as matrix and cloned into the BamHI-digested pFastBac™HTA modified vector using the GeneArt™ Seamless Cloning and Assembly Kit (Invitrogen). Recombinant vectors were then transformed into DH10Bac *E.coli* strain. Recombinant bacmids were selected as described in Bac to Bac^{R} Expression System user manual (Invitrogen) and used to produce recombinant baculovirus.

Full-length OSBP and ΔN-OSBP with a C-terminal 6His-tag were purified from baculovirus-infected Sf9 cells. Cell pellets were resuspended in lysis buffer (20 mM Tris pH 7.5, 300 mM NaCl, 20 mM imidazole, EDTA-free protease inhibitors and phosphatases inhibitors) and lysed with Dounce homogenizer. After ultracentrifugation, OSBP or ΔN-OSBP from the supernatant was adsorbed on an HisPur™ Cobalt Resin (Thermo Scientific), submitted to 3 washes with lysis buffer supplemented with 800, 550, and 300 mM NaCl, respectively, and then eluted with 250 mM imidazole-containing buffer. OSBP fractions were pooled, concentrated on Amicon Ultra centrifugal filter (cut-off 30 kDa) and submitted to thrombin cleavage for 1 hr at 25°C to eliminate the His-tag.

Thrombin-cleaved proteins were purified on a Sephacryl S300 HK16/70 column (GE Healthcare) using an AKTÄ chromatography system (GE Healthcare). All steps were performed at 4°C. The purified protein fractions were pooled, concentrated, supplemented with 10 % glycerol, flash-frozen in liquid nitrogen and stored at -80°C.

2. N-PH-FFAT and PH-FFAT of OSBP and ORP4

N-PH-FFAT and PH-FFAT fragments of both OSBP and ORP4 were expressed in *E. coli* strain BL21 (DE3). The corresponding expression plasmids were prepared using pET.His6.StrepII.TEV.LIC (2HR-T, Addgene plasmid # 29718) and pET.His10.TEV.LIC (2B-T-10, Addgene plasmid # 78173) cloning vectors (gift from Scott Gradia).

OSBP N-PH-FFAT (1-408) and OSBP PH-FFAT (76-408) fragments were first inserted into pET.His6.StrepII.TEV.LIC vector, and then expressed as N-terminal 6His-tag- StrepII-TEV site constructs.

ORP4 N-PH-FFAT (1-475) and PH-FFAT (128-475) fragments were PCR amplified and inserted into the SspI-digested host plasmid pET16b.His10.TEV.LIC using GeneArt™ Seamless Cloning and Assembly Enzyme Mix. Expression plasmids were transformed into *E.coli* and induced with 1 mM IPTG at 20°C overnight. Then, bacteria were lysed with a French Press (SLM AMINCO) and lysates were incubated for 30 min on ice with DNAse and $MgCl_2$ (5mM) before ultracentrifugation (125 000 *g*). His-tagged proteins were purified using HisPur™ Cobalt Resin (Thermo Scientific). Protein fractions were pooled and submitted to TEV protease cleavage at 4°C overnight. Digested proteins were purified on a SourceQ HR 10/10 column (GE Healthcare) with a 0-1M NaCl gradient in 25mM Tris pH7.5 followed by a Sephacryl S200 HK16/70 column (GE Healthcare) equilibrated in 25mM Tris pH7.5, 120 mM NaCl, 2mM DTT. Purified proteins were pooled, concentrated, supplemented with 10% glycerol, flash-frozen in liquid nitrogen and stored at -80°C.

3. N-PH-ΔCC-FFAT and PH-ΔCC-FFAT of OSBP

N-PH-ΔCC-FFAT and PH-ΔCC-FFAT constructs were prepared from pGEX4.T1 (GE Healthcare) plasmids encoding the OSBP (1-408) or (76-408) sequence. A NaeI restriction site was introduced by site directed mutagenesis to remove the coiled coils (207-329) region by digestion / ligation taking advantage of another NaeI site. Proteins were expressed as N-terminally tagged GST-thrombin-site constructs in *E. coli* BL21 (DE3). Purification was performed using Glutathione Sepharose beads (GE Healthcare). GST was removed by thrombin cleavage. The subsequent purification steps were the same as that used for N-PH-FFAT / PH-FFAT. All new construct sequences were verified by sequencing.

4. Other proteins

The preparation of Arf1, NBD-PH_{FAPP1} and VAP-A have been described previously (Franco *et al.*, 1995; Mesmin *et al.*, 2013).

Analytical gel filtration

Purified proteins (100 µl, 5 µM) were applied on a Superose 12™column (GE Healthcare) and eluted at a flow rate of 0.5 ml/min in 25 mM Tris pH 7.5, 120 mM NaCl and 1mM DTT. The column was calibrated using the following standards (MW/Stoke's radius): Apoferritin (443 kDa/6.1 nm), Alcohol dehydrogenase (150 kDa/4.6 nm), Bovine serum albumin (67 kDa/3.5 nm), Carbonic anhydrase (25 kDa/2.1 nm) and Cytochrome C (12.4 kDa/ 1.7 nm). The elution volume and Stoke's radius of the standards were used to establish a first calibration curve, from which the Stoke's radius of the OSBP and ORP4-derived constructs were determined. Thereafter, we plotted the Stoke's radius as a function of MW for both protein standards and for OSBP and ORP4 constructs.

Liposome preparation

To measure transport of lipids between lipid membranes or to assess tethering capacities of described proteins/fragments, we used liposomes prepared from lipid films by suspension in buffer and extrusion throught a porous filter. Most lipids were purchased from Avanti Polar Lipids, except fluorescently labeled lipids and sterols (Texas Red-DOPE and Oregon Green-DOPE were from Thermo Fischer Scientific, Atto390-DOPE was from ATTO-TEC; cholesterol and DHE were from Sigma Aldrich). Lipids solubilized in chloroform or in chloroform:methanol (2:1, in mixtures containing PI(4)P) were mixed at the desired molar ratio and the solvent was removed in a rotary evaporator. For most assays, the lipid films were hydrated in 50 mM HEPES pH 7.2 and 120 mM potassium acetate (HK buffer, which was filtered and degassed before use to eliminate bubbles or large particles that could interfere with our DLS measurements). In the case of sedimentation assay, lipid films were hydrated in degassed 50 mM HEPES pH 7.2, sucrose 210 mM buffer. After hydration, we obtained a suspension of large multilamellar liposomes (lipid concentration: 2-5 mM) which underwent four freeze/thaw cycles in liquid nitrogen and a 40°C water bath, respectively. Multilamellar liposome stocks were stored at -20°C until extruded. Extrusion was performed through 0.1 µm pore size polycarbonate filters using hand extruder (Avanti Polar Lipids). Extruded liposomes were used within 1-2 days.

Liposome sedimentation assay

For sedimentation assays comparing the binding properties of N-PH-ΔCC-FFAT and PH-ΔCC-FFAT, we used sucrose-loaded Golgi-like liposomes containing egg PC / liver PE / brain PS / cholesterol / Rhodamine-PE (61/17/5/10/2 mol%) and increasing amount of brain PI(4)P (0, 1, 2, 5, 8 or 15 mol%) at the expense of liver PI (15, 14, 13, 10, 7 or 0 mol%). Proteins (3 µM) and liposomes (up to 20 µM PI(4)P) were incubated in 50 mM Hepes (pH 7.2), 120 mM potassium acetate and 1 mM $MgCl_2$ (HKM buffer) at room temperature for 30 min in a total volume of 50 μL. The samples were centrifuged at 240 000g in a TLA 120.1 (Beckman) rotor for 1 h. The pellets were resuspended in 50µl HKM buffer before analysis on 13% SDS-PAGE by Sypro Orange staining.

Liposome aggregation measurement by dynamic light scattering (DLS)

Liposome aggregation induced by OSBP or ORP4 fragments was followed in real time by dynamic light scattering (DLS) using a DynaPro instrument (Protein Solutions). Golgi-like liposomes (15 µM) containing 0 - 4% PI(4)P and ER-like liposomes containing 2% DGS-NTA-Ni (15 µM) were mixed in HK buffer supplemented with 1 mM $MgCl_2$ and 1 mM DTT (HKMD buffer) and with VAP-A-His or VAP-A(KM-DD)-His (600 nM) as indicated. 10 DLS autocorrelation curves (= 10 x 10 seconds) were acquired as "baseline" to determine the initial size distribution of liposome suspension. After, 600 nM OSBP or ORP4 fragment was injected and liposome aggregation was followed by acquiring one autocorrelation curve every 10 s. The temperature was set at 30°C. Data were analyzed using the Dynamics v6.1 software (Protein Solutions).

In vitro PI(4)P and DHE transfer assays

We performed the PI(4)P-transfer assays as described previously using purified recombinant proteins and extruded liposomes mimicking ER and Golgi membranes (Mesmin *et al.*, 2013; 2017). In the PI(4)P transfer assay, the lipid composition of ER-like and Golgi-like liposomes was egg PC / brain PS / DGS-NTA-Ni / cholesterol (93/5/2/0-15 mol%) and egg PC / liver PE / brain PS / liver PI / brain PI(4)P / Rhodamine-PE (64/17/5/12-10/0-2/2 mol%), respectively. Measurements were carried out in a Jasco FP-8300 spectrofluorimeter using a cylindrical quartz cuvette (600 µl) equilibrated at 37°C and equipped with a magnetic bar for continuous stirring. PI(4)P transfer from Golgi-like liposomes (2% PI(4)P and 2% Rhodamine-PE) to ER-like liposomes (0 or 15 % cholesterol) was detected via a fluorescent PI(4)P probe: PH domain of FAPP1 protein labeled with the fluorophore NBD (NBD-PH_{FAPP1}). When bound to PI(4)P on the Golgi-like liposomes, the NBD fluorescence is quenched by rhodamine. After transfer of PI(4)P to ER-like liposomes, NBD-PH_{FAPP1} relocates away from rhodamine which results in signal unquenching. In the assay, the cuvette initially contained NBD-PH_{FAPP1} (300 nM) and VAP-A-His (3 µM) in HKM buffer. Golgi-like liposomes (300 µM lipid), ER-like liposomes (300 µM lipid) and OSBP (0.1 µM) were

then sequentially added at indicated times. NBD-PH_{FAPP1} probe fluorescence was detected at 530 nm (excitation wavelength 460 nm).

In the DHE transfer assay, the lipid composition of ER-like and Golgi-like liposomes was egg PC / brain PS / DGS-NTA-Ni / DHE (93/5/2/18 mol%) and egg PC / liver PE / brain PS / liver PI / Dansyl-PE (63.5/19/5/10/2.5 mol%), respectively. We measured the dehydroergosterol (DHE) transfer from ER-like liposomes (containing 18% DHE) to Golgi-like liposomes containing Dansyl-PE by the Förster resonance energy transfer (FRET) signal resulting from the excitation of Dansyl group by the emitted fluorescence of DHE. FRET signal was measured at 525 nm with excitation at 310 nm.

Cryo-electron microscopy experiments

Chloroform-solubilized lipid mixture composed of egg PC / brain PS / brain PI(4)P (85/15/5 mol%, respectively) was dried under a nitrogen flux for 5 min and further dried under vacuum for 60 min. Lipid film was rehydrated in HK buffer and liposomes were formed by vortexing for 2 min. Liposomes (30 μM) were mixed with 600 nM N-PH-FFAT or PH-FFAT and incubated for 5 min. Subsequently, a 5 μl drop of the solution was deposited on a glow discharged lacey carbon electron microscopy grid (Ted Pella, USA). Blotting was carried out on the opposite side from the liquid drop and plunge frozen in liquid ethane (EMGP, Leica, Germany). Samples were imaged using a Tecnai G2 (Thermofisher, USA) microscope operated at 200 kV and equipped with a 4k x 4k CMOS camera (F416, TVIPS). Image acquisition was performed under low dose conditions of 10 $e^-/Å^2$ at a magnification of 50 000 or 29 500 with a pixel size of 2.13 Å or 3 Å, respectively. Cryo-EM was performed in collaboration with the group of Daniel Lévy at the Institut Curie, Paris.

GUV preparation

Giant unilamellar vesicles were generated by electro-formation. Lipid mixtures of selected composition (total lipid concentration 0.5 mg/ml) in chloroform or in (2:1) chloroform:methanol mixture were deposited on indium tin oxide coated glass slides

and dried at room temperature for 45 min to remove all solvents. Lipids were then hydrated in 250 mM sucrose osmotically equilibrated with HKM buffer. GUVs were electroformed in Vesicle Prep Pro instrument (Nanion Technologies) by applying an alternating current electric field (3 V and 5 Hz), at 37 °C for 60 min. After electroformation, GUVs were washed 1x with HKM buffer to remove residual sucrose from the suspension. GUVs were stored in HKM at room temperature and were used within the same day.

Cell culture

HeLa cells were cultured in DMEM medium with GlutaMAX (Gibco) supplemented with 10% fetal calf serum, 1% antibiotics (Zell Shield, Minerva Biolabs) and were incubated at 37°C in a 5% CO_2 humidified atmosphere. For hTERT-RPE1 cells (ATCC Cat# CRL-4000, RRID: CVCL_4388); hereafter RPE1 cells), DMEM was replaced by DMEM/F12 (Gibco). RPE1 cells stably expressing EGFP-PH_{OSBP} were selected using G418 (Sigma). Surviving colonies were isolated using cloning cylinders (Bel-Art), expanded and further sorted by FACS (FACSAria III, BD Biosciences). RPE1 cells stably expressing EGFP-PH_{OSBP}, were cultured in medium supplemented with G418 (500 µg/ml). For microscopy, cells were seeded at suitable density to reach 50-90% confluence on the day of imaging. Insect SF9 cells were cultured at 27°C in SF-900 II media supplemented with 1,5% FCS in absence of antibiotic. For protein expression, SF9 cells were infected at 10^6 cells/ml and at multiplicity of infection ratio of 0.1 in 0.5l CELLSPIN Spinner. After 72h, cells were collected by centrifugation at 300xg for 15 mn, washed in PBS and stored at -20°C.

OSBP silencing and live cell imaging

To silence endogenous OSBP and simultaneously overexpress siRNA-resistant OSBP, RPE-1 cells stably expressing GFP-PH_{OSBP} were electroporated using Amaxa Nucleofector™ Solution (Lonza). Nucleofection mix contained 90 pmol siRNA (ON-TARGETplus Human OSBP siRNA; GE Healthcare; target sequence:

GCAAUGACUUGAUAGCUAA), 0.5 μg siRNA-resistant OSBP plasmid and 0.5 μg Golgi marker BFP-GalT plasmid. After nucleofection, cells were plated on 6-well plate or on μ-Dish^{35mm} (Ibidi). After 18-24 hours, cells were used for live cell imaging in time-lapse microscopy.

Time-lapse widefield microscopy was performed using an Olympus IX83 inverted microscope equipped with a Z-drift compensator, a scanning stage SCAN IM (Märzhäuser) and an iXon3 camera (Andor). Cells plated in μ-Dish^{35mm} (Ibidi) were put into a stage chamber set at 37°C (Okolab). BFP, EGFP and mCherry signals were detected using Chroma fluorescence filter sets (ref. 49000, 39002, 39010). Multidimensional acquisition and analysis was performed with MetaMorph software (Molecular Devices).

Confocal microscopy, FRAP assays

Confocal microscopy with fixed cells was performed with a LSM780 microscope run by ZEN software using a Plan-Apochromat 63X/1.4 Oil objective (Carl Zeiss). Confocal microscopy of liposomes or GUVs was performed using the same microscope.

Fluorescence recovery after photobleaching recordings were performed with a Zeiss LSM780 microscope or with a Nicon Eclipse Ti microscope equipped with an UltraVIEW VoX spinning disc imaging system (PerkinElmer) operated by Volocity software, and using a CFI Plan Apo 100X/1.4 Oil objective (Nikon). Cells were placed in phenol red-free medium supplemented with HEPES (Gibco) and FRAP assays were carried out at 37°C. Photobleaching was performed on circular areas of 3 μm diameter within perinuclear regions positive for BFP-GalT signal. FRAP assays with GUVs were performed using the same mircoscope. GUVs were gently suspended in buffer containing 50mM HEPES, 120mM potassium acetate and 1mM $MgCl_2$ (HKM buffer) with fluorescent proteins. Photobleaching was performed on circular areas of 2 μm diameter in the middle of GUV-GUV contacts.

Electron microscopy

For transmission electron microscopy, RPE1 cells were transfected with mCherry-tagged N-PH-FFAT or PH-FFAT *wt* constructs or their respective FF/AA mutants using the Amaxa® Nucleofector™ technology (Lonza) to obtain high efficiency of transfection. Cells were fixed in 1.6% glutaraldehyde in 0.1 M phosphate buffer, rinsed in 0.1 M cacodylate buffer and postfixed for 1 hr in 1% osmium tetroxide and 1% potassium ferrocyanide in 0.1 M cacodylate buffer to enhance membrane staining. The cells were then rinsed in distilled water, dehydrated in alcohols and embedded in epoxy resin. Contrasted ultrathin sections (70 nm) were analyzed under a JEOL 1400 transmission electron microscope mounted with a Morada Olympus CCD camera. Electron microscopy was performed by Sandra Lacas-Gervais from the Centre Commun de Microscopie Appliquée (CCMA) at the University of Nice-Sophia Antipolis.

Image analysis

To determine the Golgi/cytosol ratio of mCherry-tagged protein construct in living/fixed cells we used the ImageJ 1.50b software. Two circular regions of the same area (20 pixels) were applied in the Golgi (identified by the BFP-GalT marker) and in the cytosol. The average mCherry fluorescence was determined for each region and the ratio was then calculated. Alternatively, mean Golgi/total cell ratios were also determined by applying masks to calculate mean fluorescence intensity in total cell and mean fluorescence intensity on Golgi.

Kymographs were generated using the Metamorph software (Molecular Devices) from a line drawn on the image stack and projected across time of the complete time series. The lines were 72 pixels long (ca. 20 µm) with a width set to 10 pixels (ca. 3 µm), from which pixel values were averaged. Scan lines quantification on GUVs were generated using Image J software.

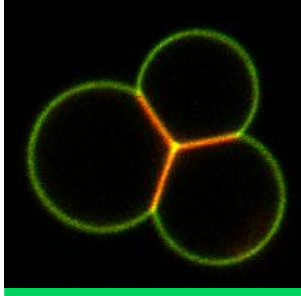

Results

RESULTS

1. OSBP AND RELATED PROTEINS CONTAIN PREDICTED INTRINSICALLY DISORDERED SEQUENCES UPSTREAM OF THEIR PH DOMAINS

Most members of mammalian ORP family share similar domain organisation, as illustrated before (Introduction, Figure 24). The N-terminal half (from PH domain to FFAT motif) has been shown to mediate membrane tethering, whereas the C-terminal half (ORD) is responsible for lipid transfer activity (Mesmin *et al.*, 2013). Most ORPs, namely OSBP, ORP3 - ORP8, ORP10 and ORP11, contain a 50 to 140 aa long sequence upstream of their PH domain. First, we noticed the low complexity of N-terminus in the case of OSBP. To find out if similar low complexity sequences exist in other ORPs, we compared the amino acid compositions of their N-termini using their respective PH domains and ORDs as references (because of their high degree of conservation). We observed that the aa contents of PH and ORD domains are well balanced between 20 common amino acids, which is a general characteristic of folded, globular domains. In contrast, N-termini display a strong compositional bias towards few amino acids and a considerable variability between each other, as shown on pie charts below (**Figure 32**).

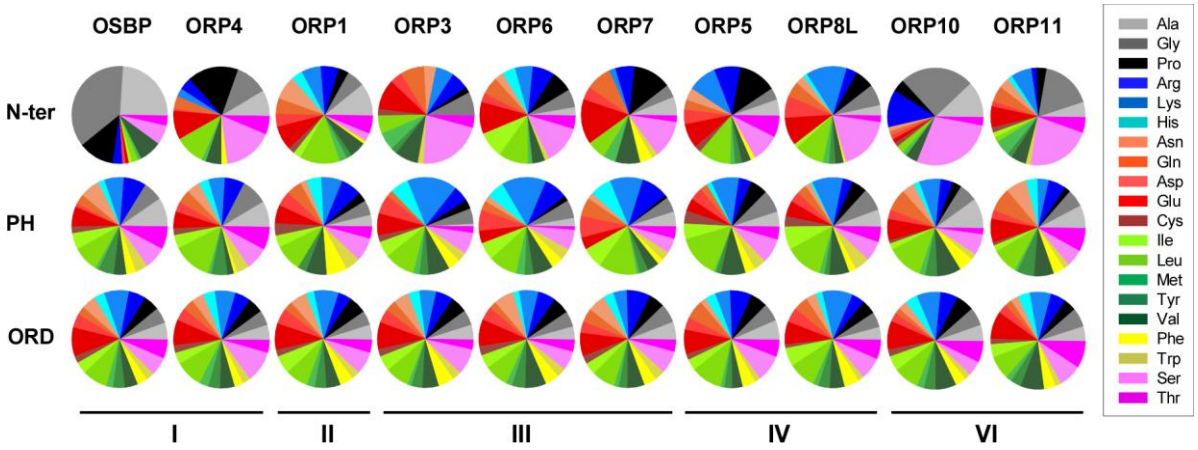

Figure 32: Amino acid distribution in N-termini, PH and ORD domains of ORPs

Note the composition bias towards Pro, Gly, Ala and Ser in the N-terminal sequences. Following ORP sequences were used (Uniprot access numbers): OSBP1 (P22059), OSBP2/ORP4 (Q969R2), ORP1 (Q9BXW6), ORP3 (Q9H4L5), ORP6 (Q9BZF3), ORP7

(Q9BZF2), ORP5 (Q9H0X9), ORP8L (Q9BZF1), ORP10 (Q9BXB5), ORP11 (Q9BXB4). ORP2 was not involved in the analysis, as it only consists of the ORD domain, and ORP9 (Q96SU4) does not possess any N-terminal disordered sequence. Notably, our ORP4 sequence (gift from N. Ridgway) started at M39 (as referred to UNIPROT Q969R2:ORP4-OSBP2 sequence), therefore, in all this study M1 corresponds to M39 of the UNIPROT reference sequence. Exact amino acid range of all domains is indicated in Materials & Methods.

Compared to folded PH and ORD domains, most N-terminal tails are enriched in residues such as Pro, Gly, Ala and Ser (black, grey and pink) whereas other, mainly large hydrophobic amino acids such as Phe, Trp, Ile and Leu (yellow and green), are underrepresented. Scarcity of hydrophobic residues and higher content of proline, the strongest disorder-promoting residue, and serine, which is after proline and glutamic acid the third most disorder-promoting residue, are hallmarks of protein regions not prone to fold (Theillet *et al.*, 2013; Uversky *et al.*, 2015). Therefore, we assessed the order/disorder distribution along the ORP sequences using Predictor of Naturally Disordered Regions (PONDR®) (**Figure 33**). PONDR® offers several algorithms, from which we selected VL3 and VSL2. They were both trained against a set of disordered and ordered protein sequences verified from crystallographic data, therefore PONDR® has a low error rate, especially when it predicts a long disordered region (Linding et al., 2003). The attributes used by these algorithms include amino acid frequencies, sequence complexity, ratio of net charge/hydrophobicity and averaged flexibility.

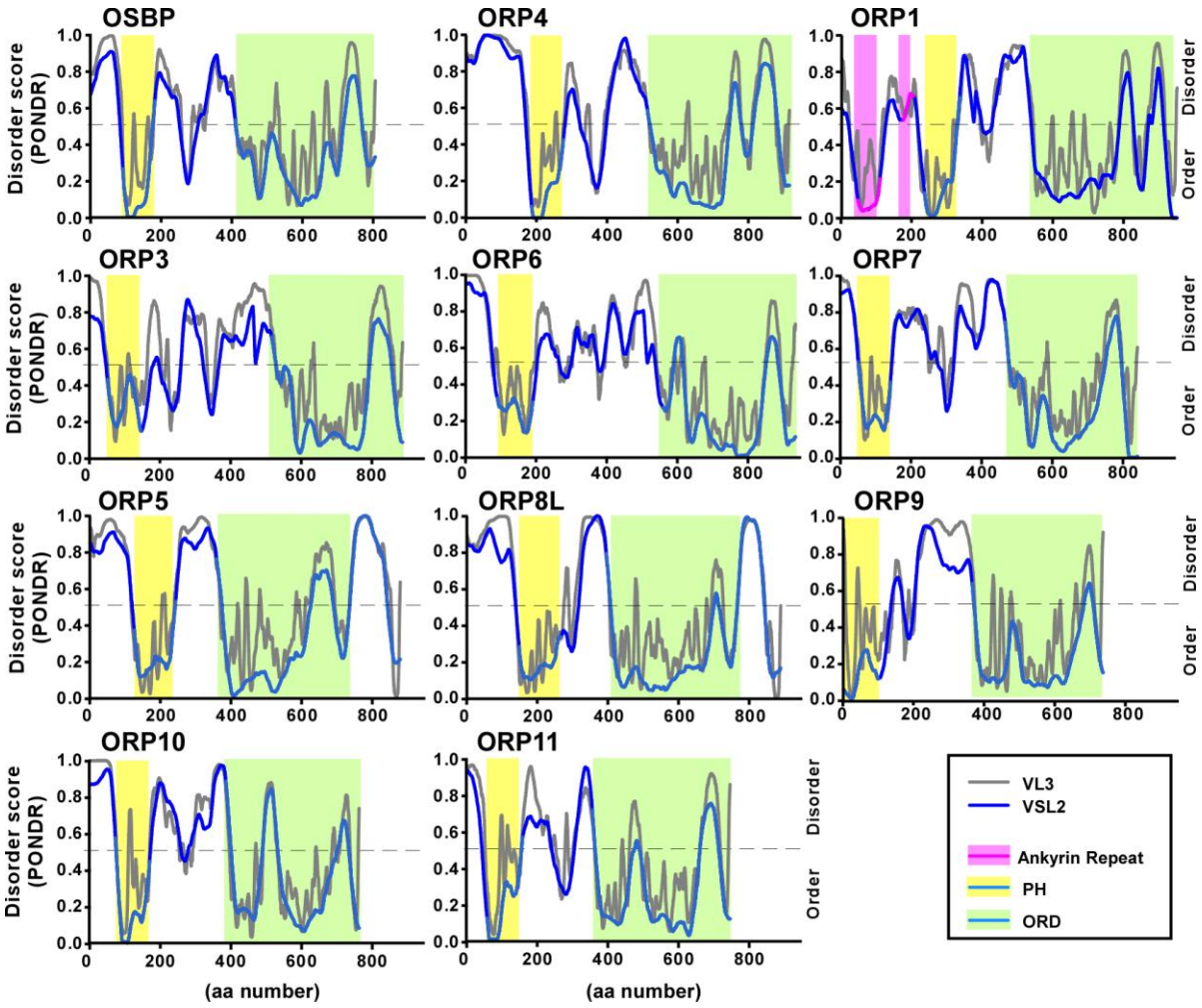

Figure 33: Disorder/order prediction of ORP family

Scores obtained with PONDR® web server using full sequences of ORPs. Regions corresponding to PH domains, ORDs and ankyrin repeats (in ORP1) are highlighted in yellow, green and pink, respectively.

The N-termini of OSBP, ORP3 - ORP8, ORP10 and ORP11 have a high disorder score (>0.8), contrasting to the low disorder scores of PH domain (yellow) and ORD (green). The low disorder score of ORP1 correlates with the presence of three ankyrin repeats (pink), which interact with small GTPase Rab7 on late endosomes (Johansson et al., 2005). Interestingly, PONDR® found other regions of high disorder located between PHs and ORDs. We identified these positions as linear FFAT motifs and predicted coiled-coils. In this case, the high disorder score can be explained by the fact that composition bias is frequently found in coiled-coils, as well as in non-globular, yet ordered proteins, such as collagen (Nassa et al., 2012). PONDR® predicts intrinsic disorder from amino

acid frequency and sequence complexity and therefore it is not able to discriminate between loops with low complexity and coiled-coils.

Upon prediction of disordered N-termini in most ORPs, we were interested in elucidating the evolution of N-terminus of OSBP (as a representative ORP) compared to the conservation of other protein components (PH domain, coiled-coils and ORD). Phylogenetic analysis performed by web software *phylogeny.fr* (Dereeper et al., 2008) on selected OSBP sequences from different species revealed that N-terminus is rather a recent feature, emerging with late chordates, Amniota (branch including turtles, lizards, snakes, crocodiles, birds, marsupials and placentals), and being well conserved among placentals (mammals; **Figure 34**). Interestingly, we noticed its co-appearance with coiled-coil 1 (corresponding to aa 200 – 225 in human OSBP), indicating possible relationship between dimerisation and presence of N-terminal disorder.

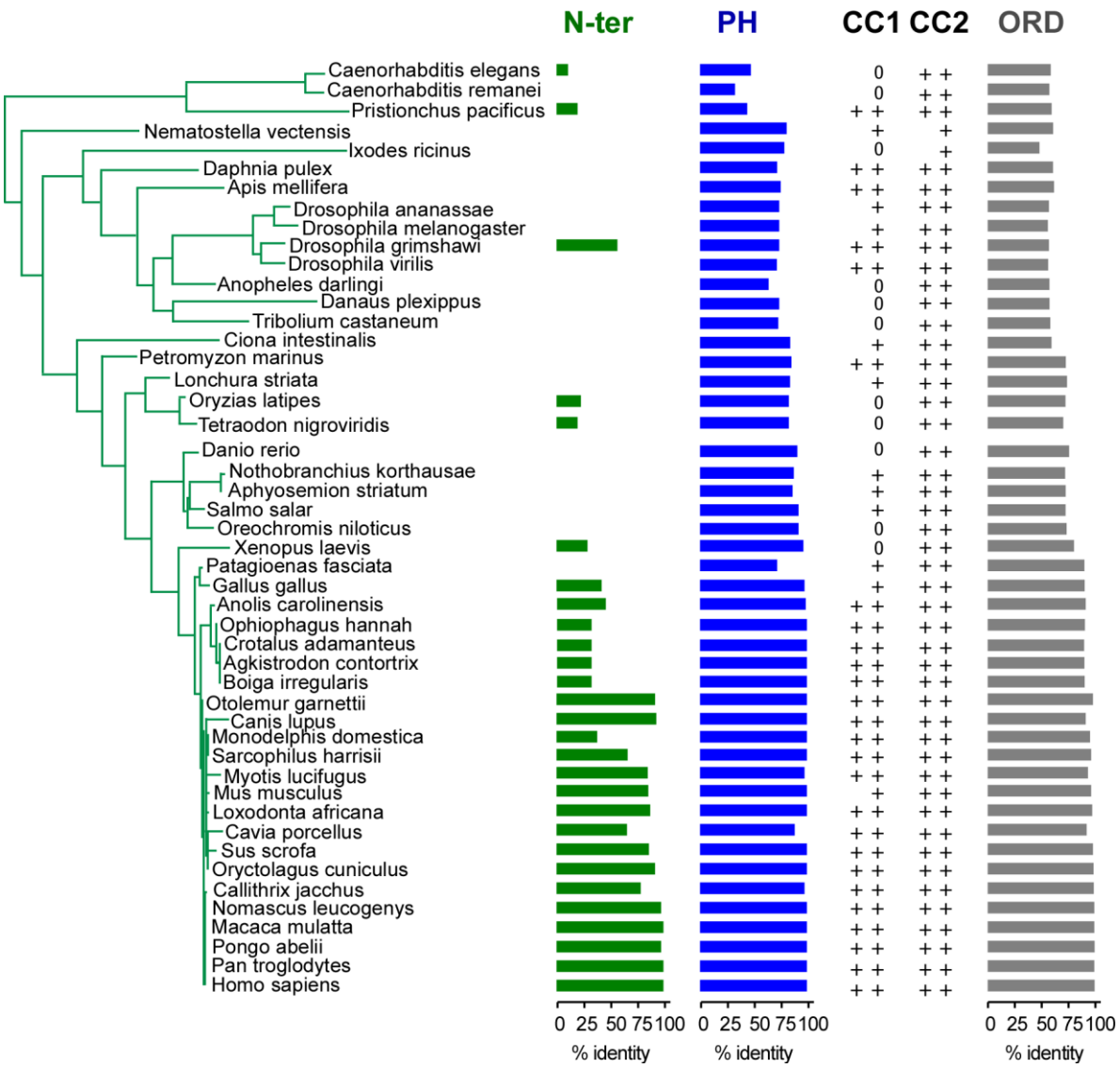

Figure 34: Phylogenetic tree of OSBP in higher eukaryotes

Bar plots show amino acid identity of the N-terminus, PH and ORD domains in selected species with the N-terminus, PH and ORD of human OSBP. N-terminal sequences shorter than 20 amino acids are not included in the analysis (blank rows). Column showing the probability of coiled-coil formation between PH and FFAT motif was created by scanning the corresponding sequences in the coiled coil prediction NPS@ software (Combet et al., 2000): (++) at least two scanning windows (14 – 21- 28 aa) give a region with coiled-coil probability score >0.5; (+) only one scanning window gives a coiled-coil probability >0.5; (0) no scanning window gives a probability >0.5.

Taken together, amino acid composition and disorder scores predicted by PONDR® suggest that most ORPs contain long intrinsically disordered N-terminal sequences. Based on phylogenetic tree of OSBP, these sequences are a recent feature,

possibly co-evolving with coiled-coil 1. In further experiments, we decided to study the function of these domains on two very close ORP homologs, OSBP and OSBP2 (ORP4). This choice was motivated by two reasons. First, OSBP and ORP4 are very similar (>60% amino acid identity in total length of the protein; 75% identity in the PH and 68% in the ORD domains), but they differ remarkably in their N-termini (~28 % identity, see below **Figure 35**). Second, numerous *in vitro* and cell culture assays have been developed for OSBP in the lab previously (Mesmin *et al.*, 2013; 2017) which greatly facilitated our analysis.

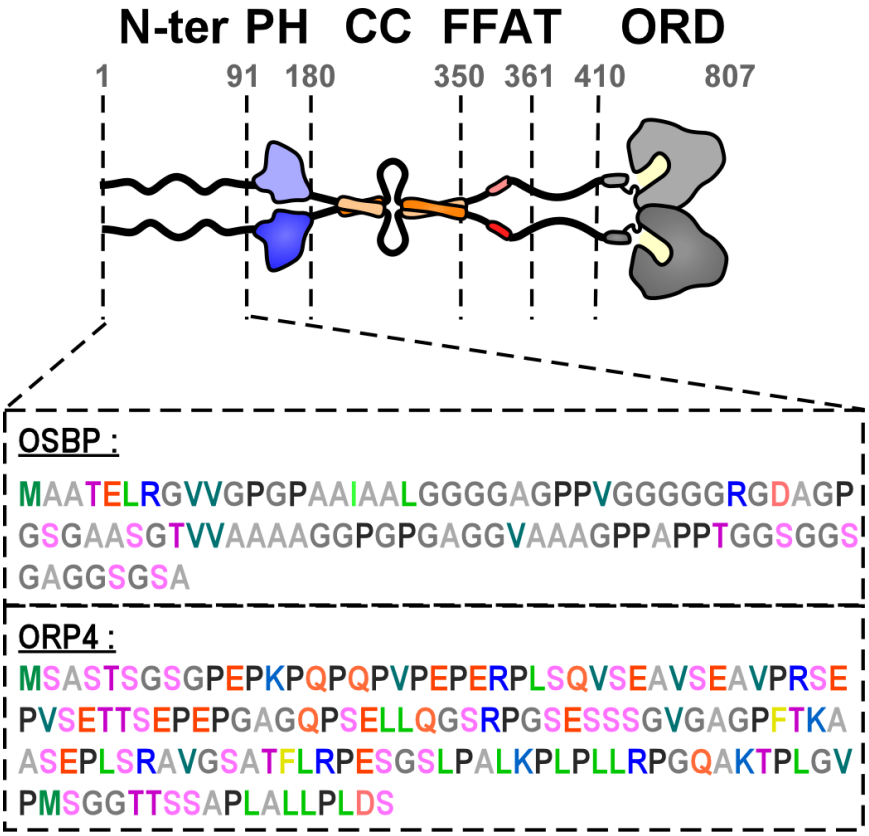

Figure 35: Domain organization and amino acid composition of N-termini of OSBP and ORP4

OSBP contains approximately 90 aa long region rich in Gly (dark grey), Ala (light grey) and Pro (black) whereas ORP4 has a ~140 aa long N-terminus containing Pro (black), Ser (pink) and a variety of charged residues (red and blue).

2. N-terminal regions of OSBP and ORP4 strongly increase their hydrodynamic radii

Disordered regions occupy a larger volume than structured sequences of the same aa length, as evidenced by the increase in hydrodynamic radii (R_h) of folded proteins during denaturation (Borzova et al., 2016; Dutta and Bhattacharyya, 2001; Wilkins et al., 1999). To estimate the contributions of N-termini to protein size, we performed analytical gel filtration chromatography. Initially, we calibrated the Superose 12™ column with well-folded protein standards so we could determine the elution volume/Stoke's radius reference line for globular proteins (protein standards Apoferritin, Alcohol dehydrogenase, BSA, Carbonic anhydrase and Cytochrome C). Subsequently, we determined the elution volumes of several protein constructs derived from OSBP and ORP4 (**Figure 36 A, B**). These include the full length proteins (OSBP FL *vs* ΔN), truncated dimeric proteins lacking the ORD (N-PH-FFAT *vs* PH-FFAT) and monomeric constructs lacking the coiled-coils between PH domain and FFAT motif (N-PH-ΔCC-FFAT *vs* PH-ΔCC-FFAT). Comparing the elution volumes of individual construct with the reference line, we extrapolated the Stoke's radius of OSBP and ORP4 constructs and plotted it as function of molecular weight in the graph shown in **Figure 36 C, D**.

In all cases, the N-terminus had a large impact on overall protein size, increasing the Stoke's radius by ~0.5 – 1 nm for OSBP (OSBP FL vs ΔN, N-PH-FFAT vs PH-FFAT and N-PH-ΔCC-FFAT vs PH-ΔCC-FFAT). For ORP4, which has a longer N-ter sequence, the increase was by ~1.3 nm (ORP4 N-PH-FFAT vs ORP4 PH-FFAT). Compared to the calibration curve obtained with protein standards (**Figure 36 C,** black line), the increase in size upon addition of N-terminus is approximately two-fold steeper (dashed line), which is consistent with the bulky nature of IDPs/IDPRs. In conclusion, our hydrodynamic analysis suggests that the N-termini of both OSBP and ORP4 are indeed intrinsically disordered.

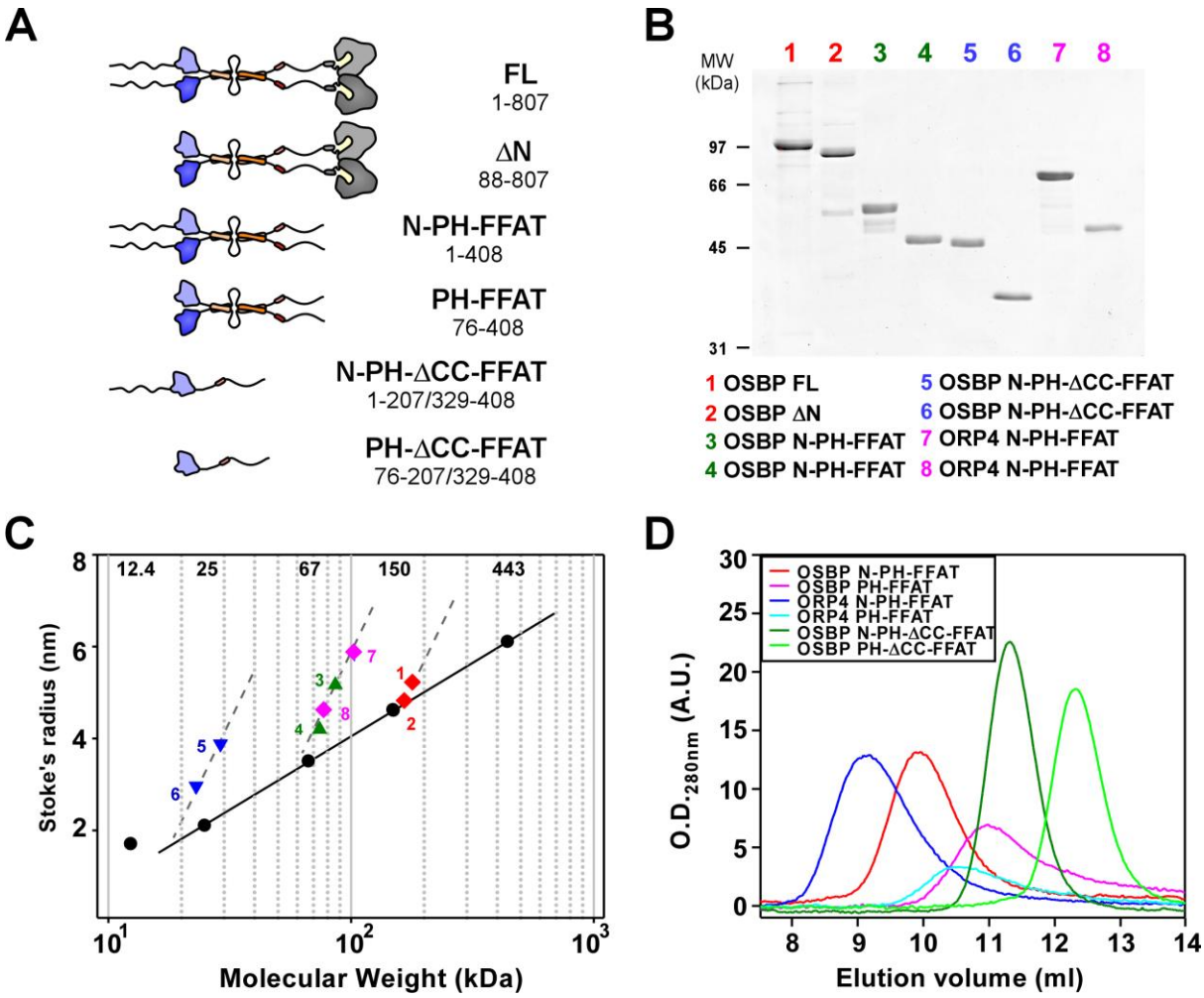

Figure 36: Disordered N-termini increase the hydrodynamic radii of OSBP- and ORP4-derived constructs

(A) Schematic representation of OSBP- and ORP4-related constructs used throughout this study **(B)** SDS PAGE analysis of purified OSBP- and ORP4 constructs. Staining performed with Sypro Orange. Please note the presence of contaminants with lower molecular weight in N-PH-FFAT of OSBP **(C)** Stoke's radius *vs* molecular weight comparison of OSBP and ORP4 constructs (colored symbols) with globular protein standards (black circles) as determined by gel filtration. The N-terminus increases the Stoke's radius by a factor two-fold larger than what is expected for a folded domain **(D)** Elution profiles of short (without the ORD) OSBP and ORP4 constructs.

3. The N-terminus limits membrane recruitment of PH domain via a crowding effect

Given the position of the disordered region upstream of the PH domain and its effect on the R_h of OSBP- and ORP4-derived proteins, we hypothesized that N-terminus could have a simple steric effect, controling the density of OSBP on PI(4)P-containing membranes by limiting the surface concentration of PH domains. To test this, we labeled the simplest monomeric OSBP constructs (N-PH-ΔCC-FFAT and PH-ΔCC-FFAT) with a fluorophore Alexa488 and we tested their binding to giant unilamellar vesicles (GUVs) of Golgi-like lipid composition (64.9 mol% egg PC, 20 mol% liver PE, 6 mol% liver PI, 5 mol% brain PS, 4 mol% brain PI(4)P and 0.1% Atto390-DOPE for visualisation). The GUVs were incubated with increasing concentrations of N-PH-ΔCC-FFAT and PH-ΔCC-FFAT, ranging from 50 to 600 nM (**Figure 37**). N-PH-ΔCC-FFAT always displayed lower recruitment on GUVs compared to equimolar PH-ΔCC-FFAT and saturated the membrane at lower protein concentration, as indicated by the smaller increase in signal intensity with concentration and a stagnation of fluorescence signal above 400 nM. Therefore, we concluded that N-terminus limits the surface occupancy of OSBP on PI(4)P-containing membrane.

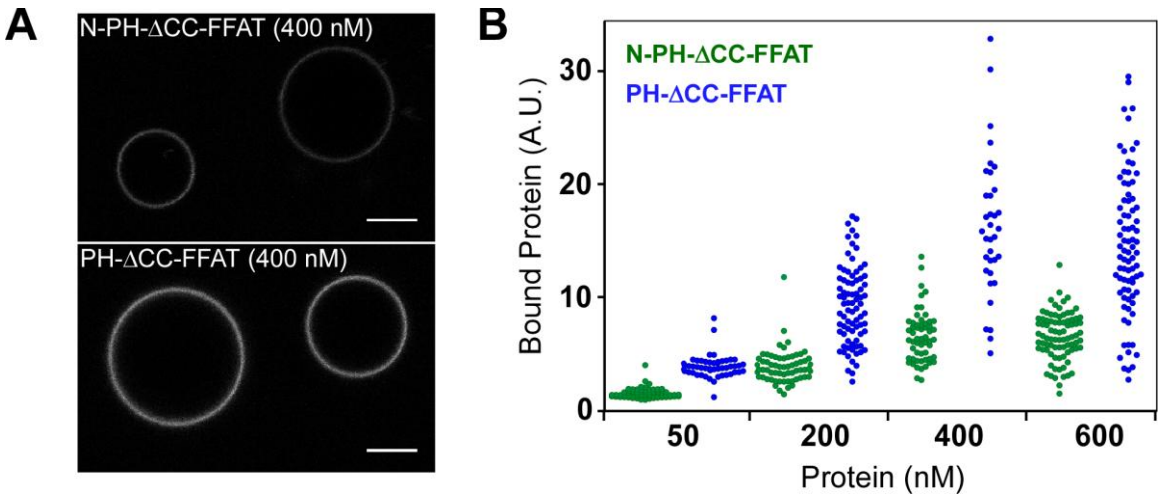

Figure 37: N-terminus limits OSBP density on PI(4)P-containing membranes

(A) For illustration, images of 400 nM N-PH-ΔCC-FFAT (top) and 400 nM PH-ΔCC-FFAT (bottom) on Golgi-like GUVs are shown. Scale bar = 5 μm **(B)** Quantification of fluorescence signal (=bound protein, A.U.) from one representative experiment similar

to the one shown in (A). Experiments were repeated two times with consistent results. Each point corresponds to one GUV.

To further examine the effect of N-terminus on protein density, we performed a complementary assay using sedimentation of Golgi-like liposomes with bound proteins. In this case, the concentration of N-PH-ΔCC-FFAT and PH-ΔCC-FFAT was equal in all conditions (3 μM), as was the total concentration of PI(4)P (20 μM). What we manipulated was the surface density of PI(4)P in liposomes, as indicated in **Figure 38.** PI(4)P density increased from 1, 2, 5, 8 to 15 mol%, while the liposome concentration reciprocally decreased from 2, 1, 0.4, 0.25 to 0.13 mM. After incubating liposome populations with our proteins for 30 min and subsequent centrifugation, we quantified the amount of bound protein. N-PH-ΔCC-FFAT and PH-ΔCC-FFAT were equally recruited on liposomes without PI(4)P (background binding) or with lowest PI(4)P density (1 mol%), showing that the intrinsic disorder likely did not affect the affinity of PH domain for PI(4)P. However, with an increase in PI(4)P density, N-PH-ΔCC-FFAT binding decreased more than that of PH-ΔCC-FFAT. In summary, our assays with fluorescently labeled proteins on GUVs and with proteins bound to sedimented liposomes both support the hypothesis that N-terminus limits the membrane density of OSBP on membranes via a crowding effect.

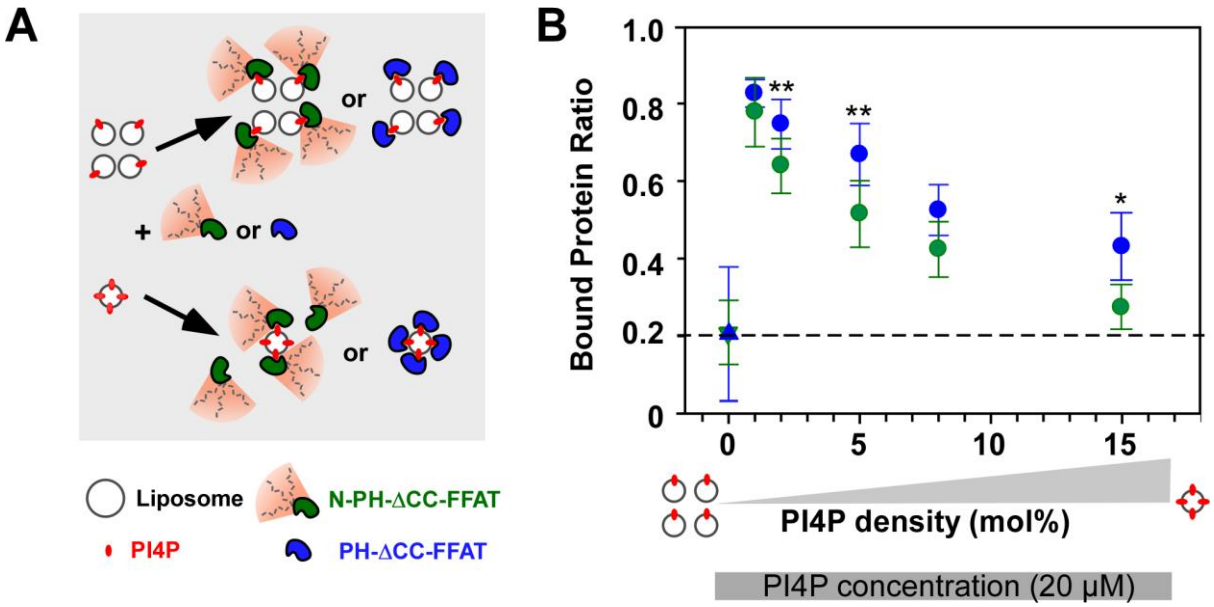

Figure 38: N-terminus limits OSBP density on PI(4)P-containing membranes via a crowding effect

(A) Schematic representation of the liposome sedimentation assay. Total PI(4)P concentration was held constant (20 μM) but across conditions, PI(4)P surface density gradually increased and, inversely, liposome concentration decreased **(B)** Result of the liposome sedimentation assay from 5 independent experiments. After 30 min of incubation, liposomes were centrifuged and bound proteins were quantified on SDS-PAGE by Sypro Orange staining. At low concentrations of PI(4)P (1 mol%), PH-FFAT and N-PH-FFAT displayed similar binding. With increasing PI(4)P density, N-PH-FFAT recruitment was significantly reduced compared to that of PH-FFAT.

4. MCS TETHERING GEOMETRY IS REGULATED BY N-TERMINUS *IN VITRO*

In cells, OSBP is able to interact with both the ER and the Golgi via its FFAT motif and PH domain, respectively (Levine and Munro, 1998; Loewen et al., 2003). To determine whether the presence of intrinsic disorder around PH domain affects OSBP and ORP4 tethering activities, we reconstituted MCS *in vitro* with two liposome populations and purified proteins. Liposomes were prepared with lipid compositions corresponding to that of the ER (93 mol% egg PC, 5 mol% brain PS, 2% DGS-NTA-Ni) and Golgi (65 mol% egg PC, 20 mol% liver PE, 6 mol% liver PI, 5 mol% brain PS, 4 mol% brain PI(4)P). The presence of DGS-NTA-Ni on ER-like liposomes allowed the attachment of His-tagged VAP-A (aa 8 - 212). In a typical experiment, we mixed the two liposome populations with or without 600nM VAP-A (600 nM), added tethering protein (600 nM) and followed liposome aggregation over time by dynamic light scattering (DLS, **Figure 39**).

When all tethering determinants were present in the DLS cuvette (Golgi + ER + VAP-A + N-PH-FFFAT or PH-FFAT), there was no difference in the tethering acivity between tethering proteins. Nevertheless, when we removed VAP-A or when we replaced it with a mutant unable to interact with FFAT motif (VAP-A *KM/DD*) we observed a striking difference between the two constructs: PH-FFAT was able to tether liposomes independently of VAP-A, whereas N-PH-FFAT was not.

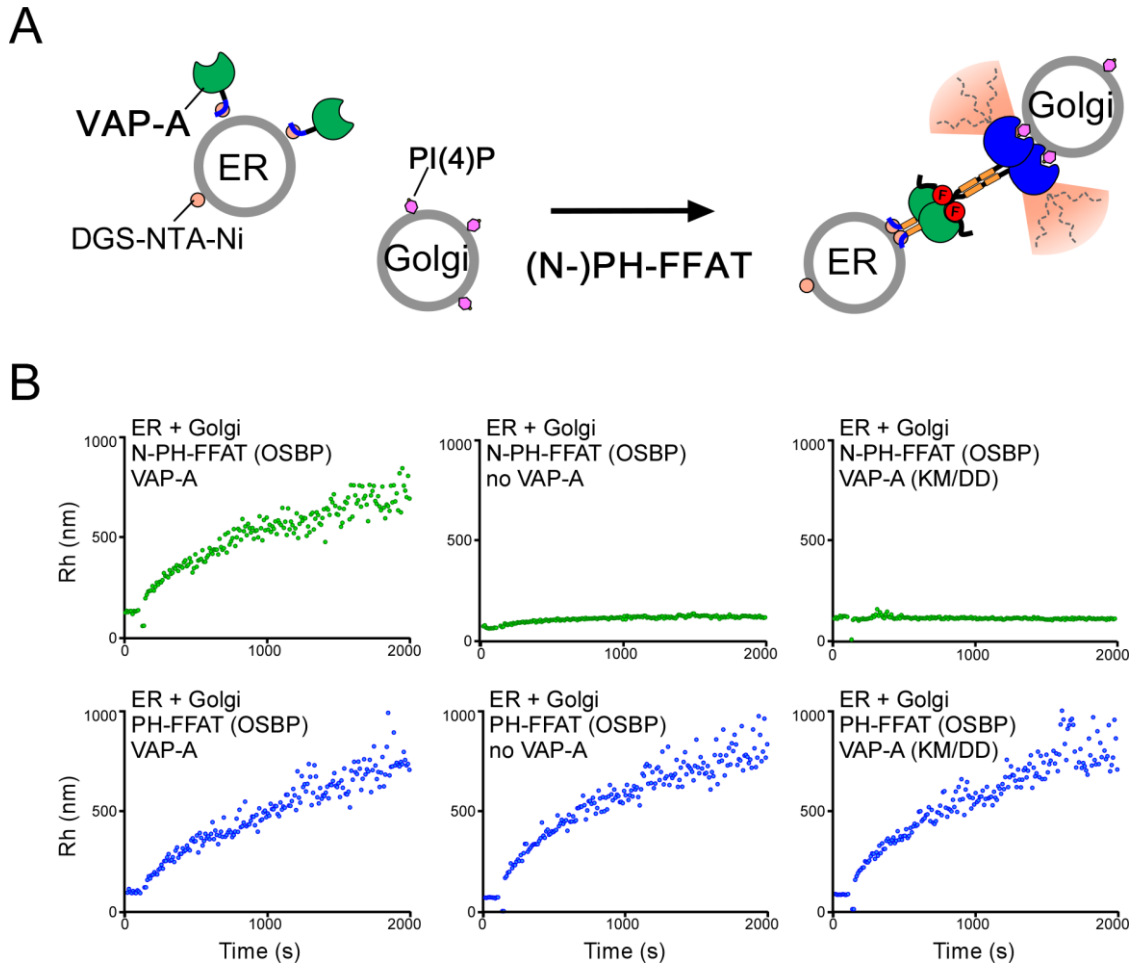

Figure 39: Tethering independent of VAP-A is observed in construct lacking N-terminal sequence

(A) Schematic representation of the liposome tethering assay in standard conditions. The DLS samples contained 15μM of ER-like liposomes (2% DGS-NTa-Ni), 15 μM of Golgi-like liposomes (4% PI(4)P) and either 600nM *wt* VAP-A, 600nM mutant VAP-A (*KM/DD*) or no VAP-A **(B)** At t = 100 s, 600nM tethering protein was added and liposome aggregation was followed over time. N-PH-FFAT only tethered liposomes in the presence of *wt* VAP-A, whereas PH-FFAT could promote aggregation independently of VAP-A.

We imagined that, in the absence of VAP-A, ER-like liposomes cannot be included in the aggregates created by PH-FFAT. Therefore, it is most likely that only Golgi-like liposomes are tethered in a homotypic (Golgi-like with Golgi-like) manner. To confirm our hypothesis we labeled the Golgi-like liposomes with Texas Red-DOPE and the ER-

like liposomes with Oregon Green-DOPE (Ho and Stroupe, 2015). Fluorescently labeled liposomes enabled us to visualise aggregates by confocal microscopy, so we could easily distinguish homotypic (Golgi-Golgi) vs heterotypic (Golgi-ER) tethering after each DLS measurement, as illustrated in **Figure 40**.

We observed that with VAP-A, both N-PH-FFAT and PH-FFAT of OSBP and ORP4 promoted heterotypic (Golgi-like with ER-like) liposome tethering (evidenced by yellow aggregates). Without VAP-A, both N-PH-FFATs did not tether any liposome population, whereas PH-FFATs selectively aggregated only Golgi liposomes.

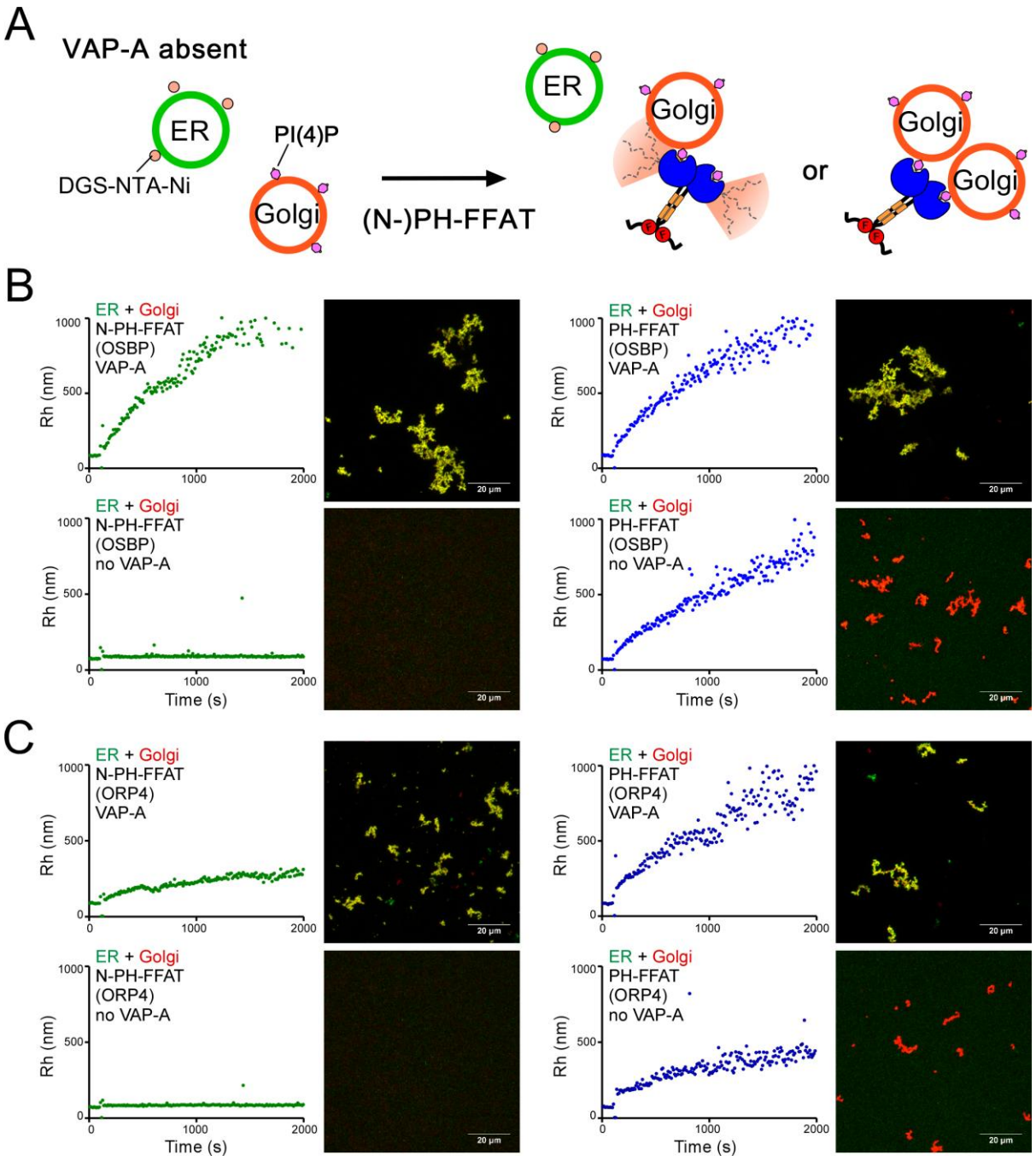

Figure 40: Membrane tethering geometry is regulated by the disordered N-terminus

(A) Schematic representation of the DLS assay coupled with confocal microscopy in the absence of VAP-A. **(B, C)** N-PH-FFAT of both OSBP and ORP4 only tethered in the ER-Golgi manner in the presence of VAP-A, whereas PH-FFAT of both OSBP and ORP4 aggregated Golgi-Golgi liposomes independently of VAP-A. Note the lower tethering activity of ORP4-derived constructs.

To verify and elucidate the mechanism of homotypic tethering in more detail, we performed additional experiments, this time with fluorescent Golgi-like liposomes only. We tested the PH-FFAT-mediated tethering in conditions when both red and green liposomes contained PI(4)P, when only red or only green liposomes contained PI(4)P and when none contained PI(4)P. We observed that Golgi-Golgi tethering depends on PI(4)P, as we only saw aggregation of PI(4)P-containing liposomes (**Figure 41 A**).

In the next step, based on our phylogenetic analysis, we assessed the role of protein dimerization. We repeated the experiment setup with fluorescent Golgi-like liposomes with/without PI(4)P but this time we replaced the dimeric PH-FFAT by an equivalent construct lacking the coiled-coil, PH-ΔCC-FFAT. As we did not observe any aggregation in this case, we concluded that both the presence of PI(4)P as well as the ability to dimerize play essential roles in the ability of PH-FFAT to promote homotypic tethering (**Figure 41 B**).

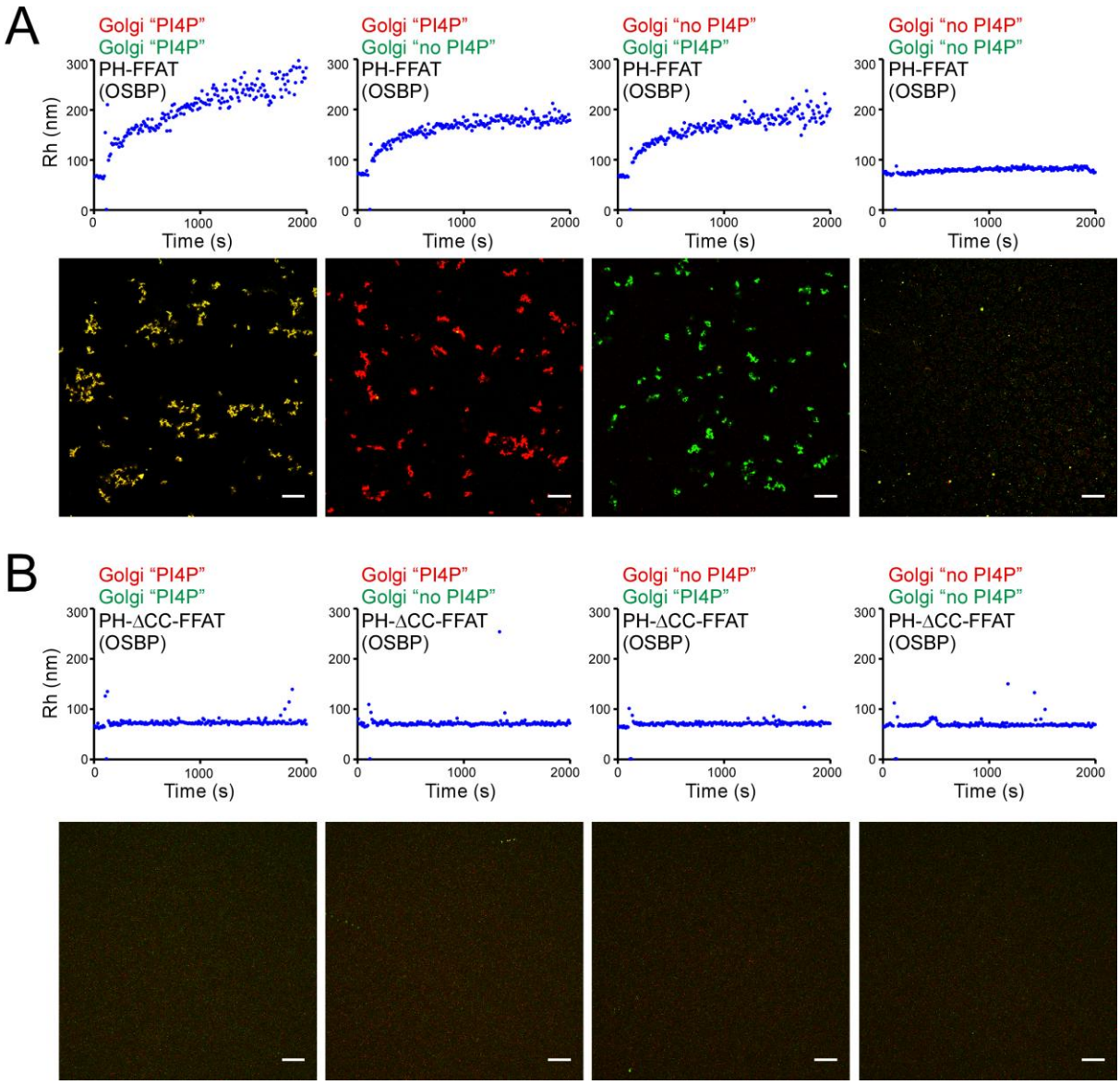

Figure 41: PH-FFAT mediated tethering depends on PI(4)P and on the ability of PH-FFAT to dimerize

(A) Golgi-like liposomes with 4% or 0% PI(4)P were labeled with different fluorescent lipids. Aggregates contained only liposomes containing PI(4)P. **(B)** Same as in (A) with monomeric construct PH-ΔCC-FFAT. No tethering was observed regardless of presence/absence of PI(4)P. Scale bar = 20 μm.

We also assessed the heterotypic, ER-Golgi tethering ability of monomeric constructs with/without VAP-A. We noticed that both constructs can only promote VAP-dependent tethering in the ER-Golgi orientation (**Figure 42**). This finding was very useful as we took advantage of it in a GUV experiment, as described a few chapters later.

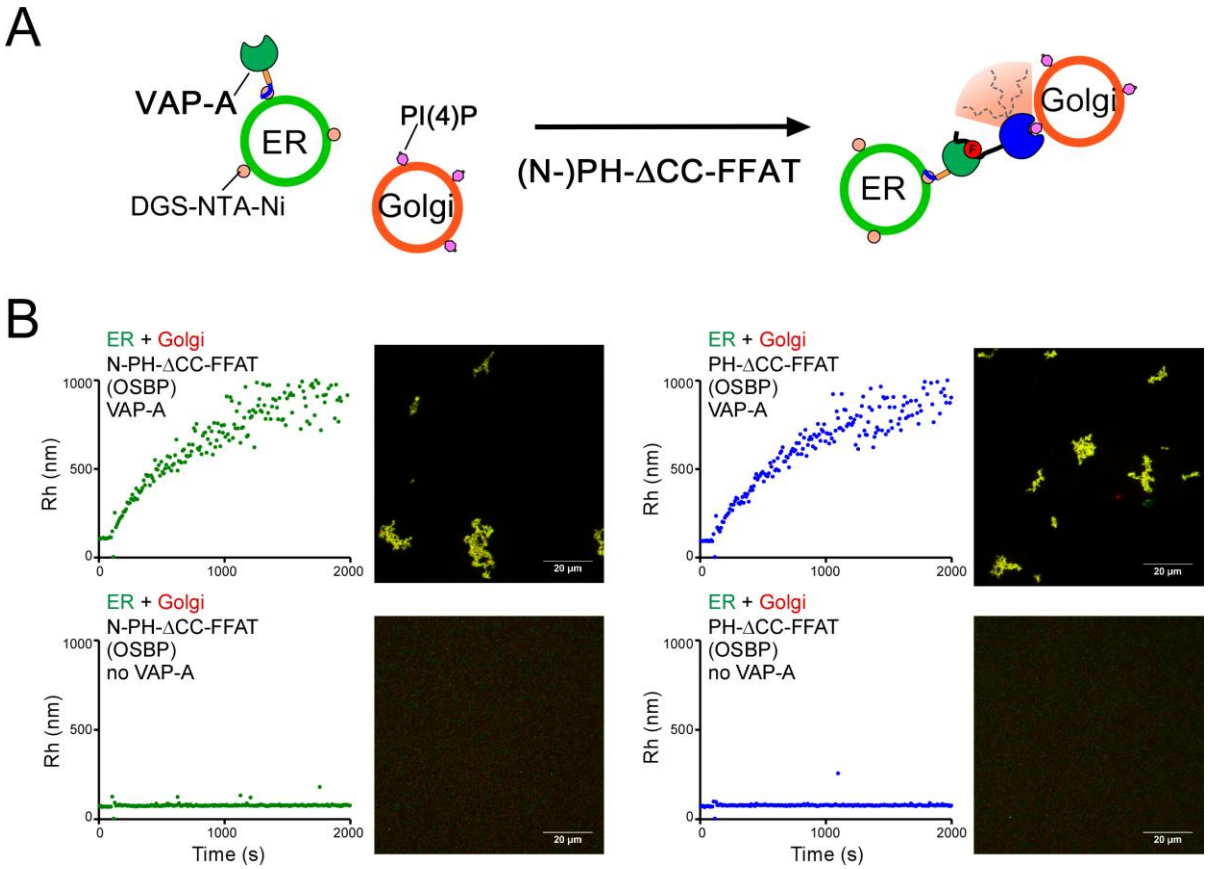

Figure 42: Monomeric constructs can only mediate ER-Golgi aggregation in the presence of VAP-A

(A) Schematic representation of the assay. Same condition as in Figure 39 **(B)** DLS measurement results – monomeric (ΔCC) constructs are only capable of heterotypic tethering in the presence of VAP-A.

Lastly, we investigated whether homotypic tethering by PH-FFAT can also be mediated via the interaction of PH domain with its second interaction partner, Arf1-GTP (Levine and Munro, 2002). We prepared Golgi-like liposomes without PI(4)P and loaded them with Arf1-GTP according to a protocol described previously (Franco *et al.*, 1995). We detected weak liposome aggregation by PH-FFAT but not by N-PH-FFAT (**Figure 43**), suggesting that the N-terminal tail also prevents homotypic tethering mediated by interaction of PH domains with Arf1-GTP. Additionally, we demonstrated that the Arf1-GTP/PH domain interaction alone is able to promote homotypic membrane tethering.

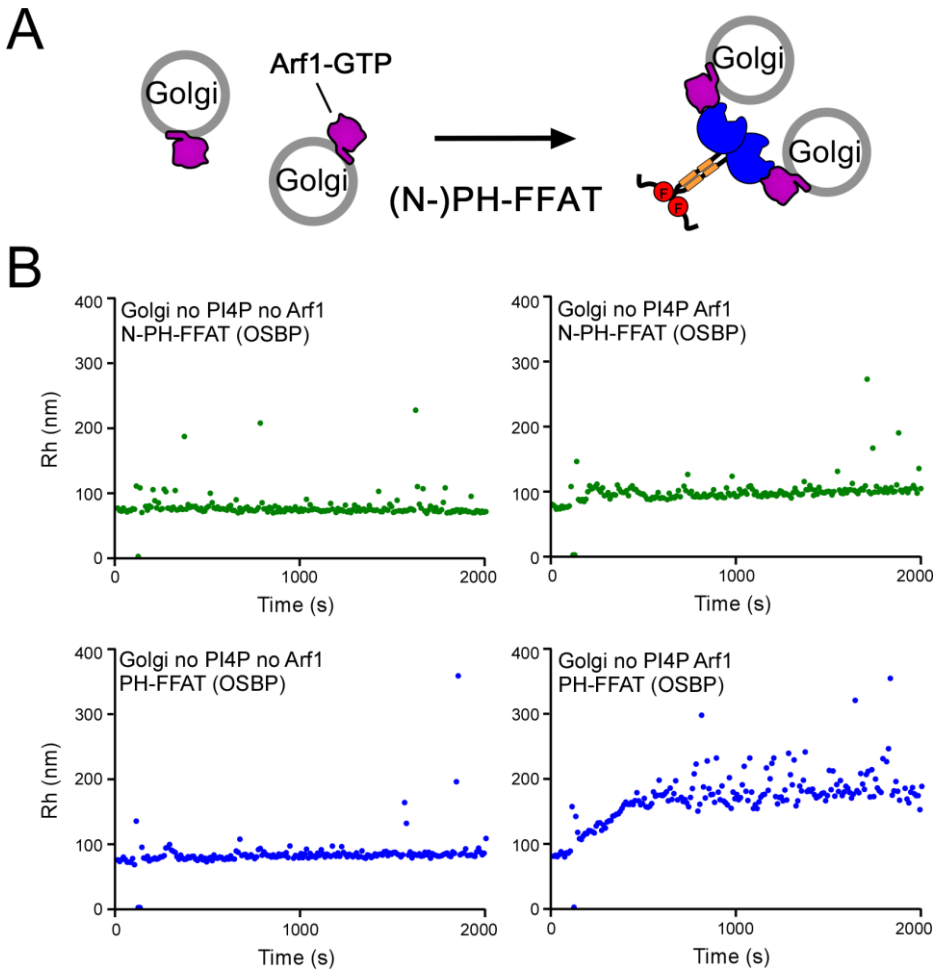

Figure 43: Homotypic tethering mediated by PH-Arf1GTP interaction in PH-FFAT

(A) Schematic representation of homotypic tethering mediated by PH-FFAT via interaction with Arf1-GTP **(B)** DLS measurement on Golgi liposomes without PI(4)P, loaded (or not) with Arf1-GTP and mixed with N-PH-FFAT (green) or PH-FFAT (blue).

DLS measurements and confocal microscopy results confirmed our hypothesis that the two PH domains of PH-FFAT dimer can simultaneously bind two PI(4)P- or Arf1-GTP-containing membranes, thereby causing homotypic tethering. When the PH domains are flanked by disordered bulky N-terminus, homotypic membrane tethering is prevented, whereas heterotypic tethering is not affected.

5. OSBP N-terminus regulates protein distribution and diffusion at homotypic GUV-GUV membrane interfaces

Although DLS provided us with valuable information about how membrane tethering properties of OSBP and ORP4 are impacted by their N-termini, at the same time new questions arose: Does N-terminal sequence manifest the same impact on tethering geometry when large, flat PI(4)P-containing surfaces are used instead of small, curved liposomes? Is the crowding effect observed on GUVs and in liposome sedimetation assay also apparent when proteins accumulate within an artificial membrane contact site?

To facilitate our inquiry, we took advantage of several GUV-based assays carried out under the two main conditions identified in DLS, i. e. in homotypic and heterotypic tethering. All experiments consisted in adding electroformed GUVs of defined lipid composition (Golgi-like vs ER-like) to solutions of fluorescent proteins. Of note, the GUVs assays, although providing unique information about protein distribution and dynamics in a large membrane interface, are less quantitative in terms of tethering activity than DLS, as it is difficult to master the GUV concentration and therefore the protein/lipid ratio.

In the first set of experiments, we incubated Golgi-like GUVs (containing 2 to 4% PI(4)P and visualized by Atto390-DOPE) with either N-PH-FFAT or PH-FFAT, labeled with Alexa568 or Alexa488. PH-FFAT promoted the formation of GUV-GUV contacts, manifested by mutual deformation of tethered GUVs and creation of large membrane alignment at the interface (**Figure 44 B**). Surprisingly, we also observed GUV-GUV tethering with N-PH-FFAT, which initially seemed very contradictory to the outcomes of DLS assays. However, after a closer examination, we realized that our N-PH-FFAT protein stock was not perfectly pure. On SDS-PAGE, we visualized 2 contaminants with a lower molecular weight than the major band. A Western blot with antibody recognizing an epitope just at the very end of FFAT motif showed that all 3 bands have the C-terminal epitop, indicating that N-PH-FFAT was contaminated at a level of about 16% by fragments with a truncated N-terminus (**Figure 44 D, Figure 36 B**). This could explain the tendency of N-PH-FFAT to form GUV-GUV contacts. Yet despite this contamination, we could see a clear difference between N-PH-FFAT and PH-FFAT:

whereas PH-FFAT was mainly accumulated at the GUV-GUV interface, N-PH-FFAT decorated all membrane surfaces with only slight enrichment at the interface (which could still be rather due to the contaminating short fragments, **Figure 44 C**). The distinct protein distribution indicated that disordered N-terminal sequence favors a balanced, wide-spread protein occupancy on membranes, whereas shorter and smaller construct tends to overaccumulate at GUV-GUV contact site.

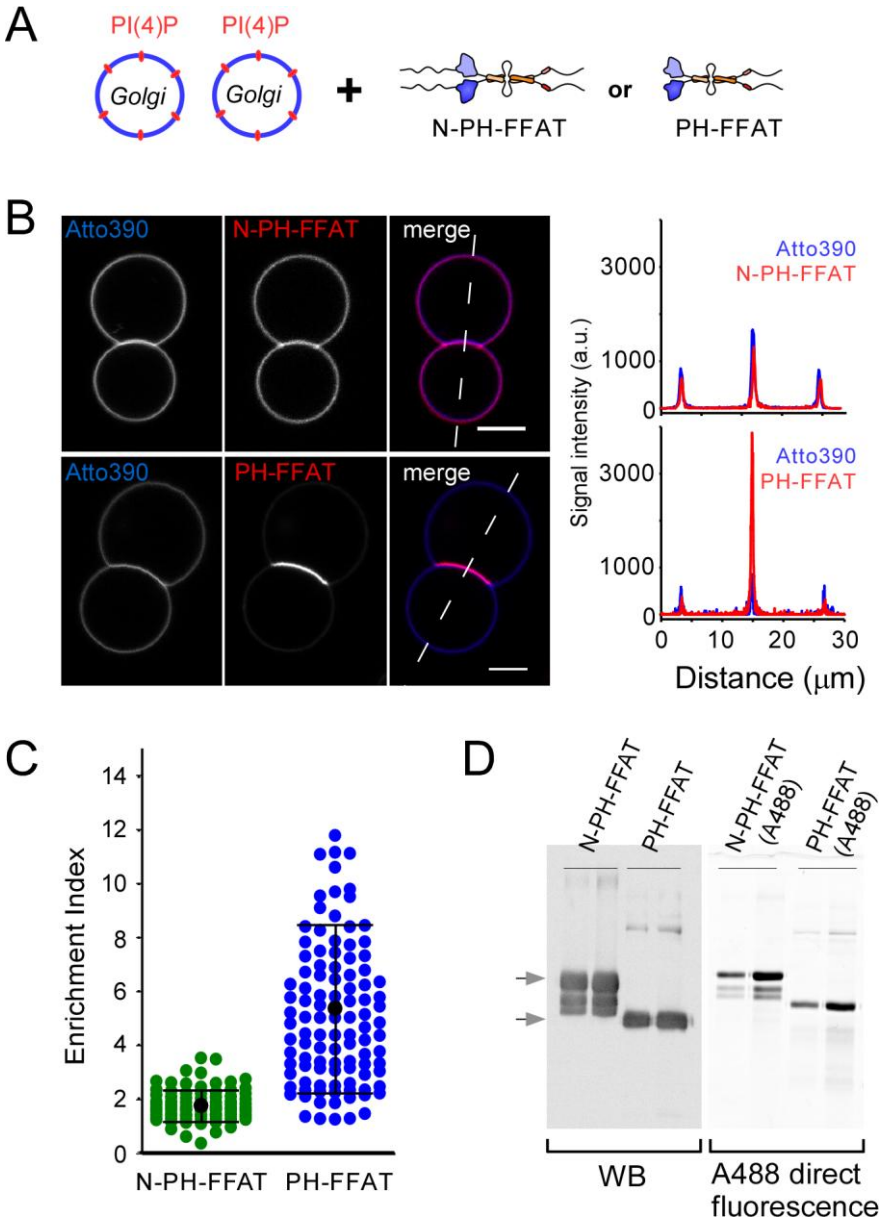

Figure 44: The N-terminus controls OSBP membrane distribution

(A) Schematic representation of GUV-based assay. GUVs of Golgi-like composition (2% PI(4)P, labeled with Atto390-DOPE) were added into solution of 100 nM tethering protein labeled with fluorescent dyes (Alexa568 and Alexa488) **(B)** N-PH-FFAT distributes over all membrane surfaces, whereas PH-FFAT accumulates at the GUV-GUV

interface. On the right side, linescans corresponding to dashed lines are shown **(C)** N-terminus has a large impact on protein enrichment at membrane interface. Enrichment index was calculated from experiments with Alexa568-labeled proteins as a ratio between fluorescence signal intensity at the interface and a sum of fluorescence intensities on the outer surfaces of tethered GUVs (according to Schmid et al., 2016). Experiments with proteins labeled with Alexa488 gave accordant results **(D)** N-PH-FFAT stock contamination by shorter fragments. Arrows indicate the positions of N-PH-FFAT and PH-FFAT. Western blot with antibody against FFAT motif (left) and direct fluorescence visualization of labeled proteins (right).

The overaccumulation of PH-FFAT indicated possible protein crowding at membrane interface. To test this, we compared the fluorescence recovery after photobleaching (FRAP) rates of labeled OSBP-derived constructs on tethered GUVs (**Figure 45 A**). The circular bleaching area was located either at the surface of tethered GUVs or in the middle of the GUV-GUV contact. When bleaching the free, outer surface, we observed an instantaneous fluorescence recovery for both constructs (**Figure 45 D**). In contrast, at the interface we recorded much slower recovery, and we could also recognize a remarkable difference between tethering proteins. Recovery of N-PH-FFAT was much quicker compared to that of PH-FFAT (recovery time of $\sim$ 1 s and >>100 s, respectively), implying that the disordered region significantly accelerated the protein diffusion on artificial homotypic membrane contact sites, possibly due to the reduced crowding of N-PH-FFAT.

Given the clear difference in distribution and fluorescence recovery between the two OSBP-derived constructs, we wondered if the effect of N-terminus would also be evident when both proteins occupy the same interface. Previous studies with fluorescent binding and nonbinding model proteins at GUV-GUV interface reported that small proteins which are able to bind each other *in trans* can establish a membrane contact site and exclude larger, non-binding proteins (Schmid et al., 2016). This exclusion is size-dependent, but also influenced by protein crowding. Therefore, we tried to analyze membrane distribution of N-PH-FFAT (labeled with Alexa568) and PH-FFAT (labeled with Alexa488) in equimolar concentrations on the same GUV-GUV contacts. We noted a clear segregation between the two proteins: PH-FFAT accumulated at membrane interface, whereas N-PH-FFAT was rather excluded and localized on the

free GUV surface (**Figure 45 B**). This experiment provided evidence that the presence of N-terminus upstream of the PH domain is an effective way of regulating protein crowding or exclusion at artificial MCS.

To investigate the influence of N-terminus on crowding and size-dependent exclusion in non-equimolar conditions, we compared the ability of N-PH-FFAT and PH-FFAT to invade a membrane interface that was already occupied by the other protein. First, we mixed GUVs with either N-PH-FFAT or PH-FFAT labeled with one dye, and 30 minutes later we added an excess of the counterpart protein (PH-FFAT or N-PH-FFAT, respectively), labeled with a different dye. After another 30 min incubation period, the GUVs were visualised. Whereas N-PH-FFAT could not invade PH-FFAT-occupied contacts, PH-FFAT was able to invade and eventually replace N-PH-FFAT (**Figure 45 C**). This finding further emphasizes the impact of intrinsic disorder near the PH domain on localisation preference of OSBP constructs at GUV-GUV contact sites.

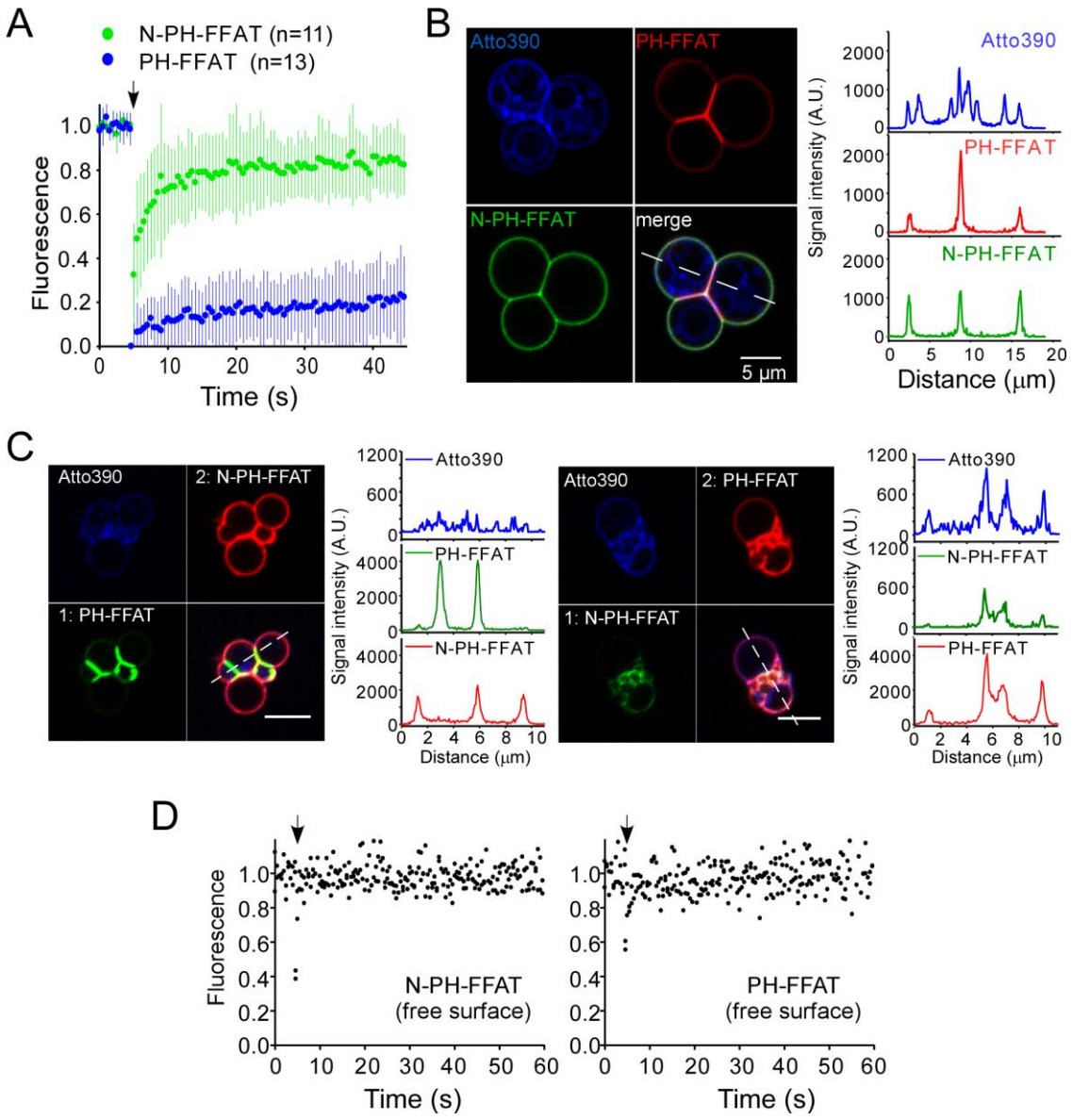

Figure 45: N-terminus regulates diffusion rate of OSBP on artificial membranes

(A) FRAP measurements of N-PH-FFAT (green trace) and PH-FFAT (blue trace). Photobleaching was performed on a circular area (2µm diameter) on the interface between tethered GUVs. FRAP on proteins labeled with Alexa488 and Alexa568 gave consistent results. Means ± SD of one representative experiment is shown. At least two independent experiments in each color were performed. n = number of recordings per condition **(B)** Segregation of N-PH-FFAT (Alexa488) and PH-FFAT (Alexa568) over time. Proteins were mixed in equimolar concentrations (50 nM) and incubated with Golgi-like GUVs (2% PI(4)P, Atto390-DOPE) for approximately 4 hours. Experiment was also performed with inverse color combination with similar results. **(C)** Golgi-like GUVs were mixed with 50 nM of N-PH-FFAT or PH-FFAT (Alexa488) and incubated for 30 min. Then, 100 nM of PH-FFAT or N-PH-FFAT (Alexa568) were added, respectively, and incubated for another 30 min. Scale bar = 5 µm **(D)** Control FRAP measurements on the outer surface of tethered GUVs. Two measurements are shown in each condition.

6. Cryo-EM visualisation of homotypic tethering

To obtain a more detailed view of homotypic membrane tethering, we visualized by cryo-EM liposomes (2% PI(4)P) incubated with N-PH-FFAT or PH-FFAT of OSBP. In both cases, dotted electron densities were apparent on the outer leaflets, indicating the presence of membrane-bound proteins (**Figure 46**, top right inset). However, liposomes incubated with N-PH-FFAT were not deformed and did not form any contacts, whereas in PH-FFAT condition, large regions of membrane aposition between two liposomes were observed. These contact sites displayed a parallel structure, with well-defined intermembrane distance of 15 ± 1 nm. Electron-dense signal was detected at the center of the membrane interface, spanning the entire length of the interface, suggesting that PH-FFAT adopts symmetrical conformation to mediate homotypic membrane tethering (red arrow).

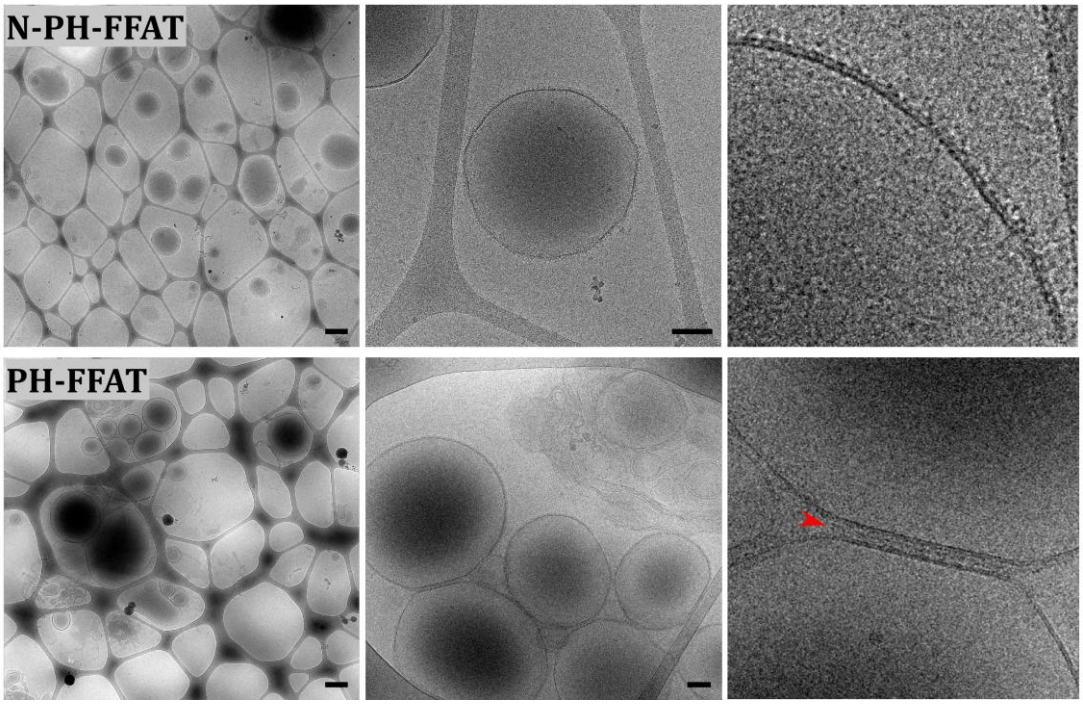

Figure 46: Liposomes visualised by cryo-EM

In N-PH-FFAT incubation, no membrane contacts are present. Instead, we can clearly identify dotted electron densities on the outer leaflet of membrane (inset). In PH-FFAT incubation, liposomes form large parallel regions of membrane juxtaposition, with electron densities present in the middle (red arrow), suggesting tethering mediated by symmetrically arranged PH-FFAT constructs. Scale bars: left - 500 nm, middle - 100 nm.

7. Regulation of protein diffusion by the disordered region at heterotypic membrane interfaces

Previous experiments elucidate the behavior of OSBP-derived constructs with or without N-terminus in the context of Golgi-Golgi tethering. However, the physiological function of OSBP is to bridge Golgi and ER membranes (Mesmin *et al.*, 2013). Therefore, we investigated conditions of heterotypic tethering by mixing OSBP constructs with two populations of GUVs: ER-like (containing 2-3% DGS-NTA-Ni) and Golgi-like (containing 2-4% PI(4)P). We distinguished the two populations by confocal microscopy, as Golgi-like GUVs were labeled with Atto390-DOPE, whereas ER-like GUVs were not labeled, and thus only "visible" when interacting with Golgi-like GUVs or when decorated by a fluorescent protein (VAP-A, labeled with A488). Initially, we performed the assay with dimeric N-PH-FFAT and PH-FFAT. We noticed that these constructs created complex assemblies with VAP-A and both populations of GUVs underwent both homotypic and heterotypic tethering. This made the analysis impossible. In order to simplify the system, we took advantage of the monomeric N-PH-ΔCC-FFAT and PH-ΔCC-FFAT constructs labeled with Alexa568. From DLS we know that OSBP monomers are only able to tether in the ER-Golgi manner. Furthermore, their monomeric nature necessarily decreased the number of putative interactions which should favour protein recycling and therefore facilitate our FRAP analysis (**Figure 47 A**).

Confocal microscopy of heterotypic N-PH-ΔCC-FFAT/VAP-A and PH-ΔCC-FFAT/VAP-A complexes on GUVs revealed a modest, not very obvious disorder-dependent differences in membrane distribution – in both cases, we rather observed a massive enrichment of VAP-A and N-PH-ΔCC-FFAT or PH-ΔCC-FFAT at the ER-Golgi GUV-GUV interface (**Figure 47 B - E**). However, FRAP analysis showed that N-PH-ΔCC-FFAT recovery happened quickly (within seconds) whereas PH-ΔCC-FFAT signal recovered very slowly (**Figure 47 F, G**). In a complementary FRAP experiment, in which we followed the fluorescence of VAP-A, we observed the same difference in signal recoveries, suggesting that mobility of VAP-A was imposed by the corresponding OSBP-derived construct. Therefore, N-terminus controls OSBP density and mobility in heterotypic conditions when engaged in a dual interaction with VAP-A on one membrane and with PI(4)P on the other.

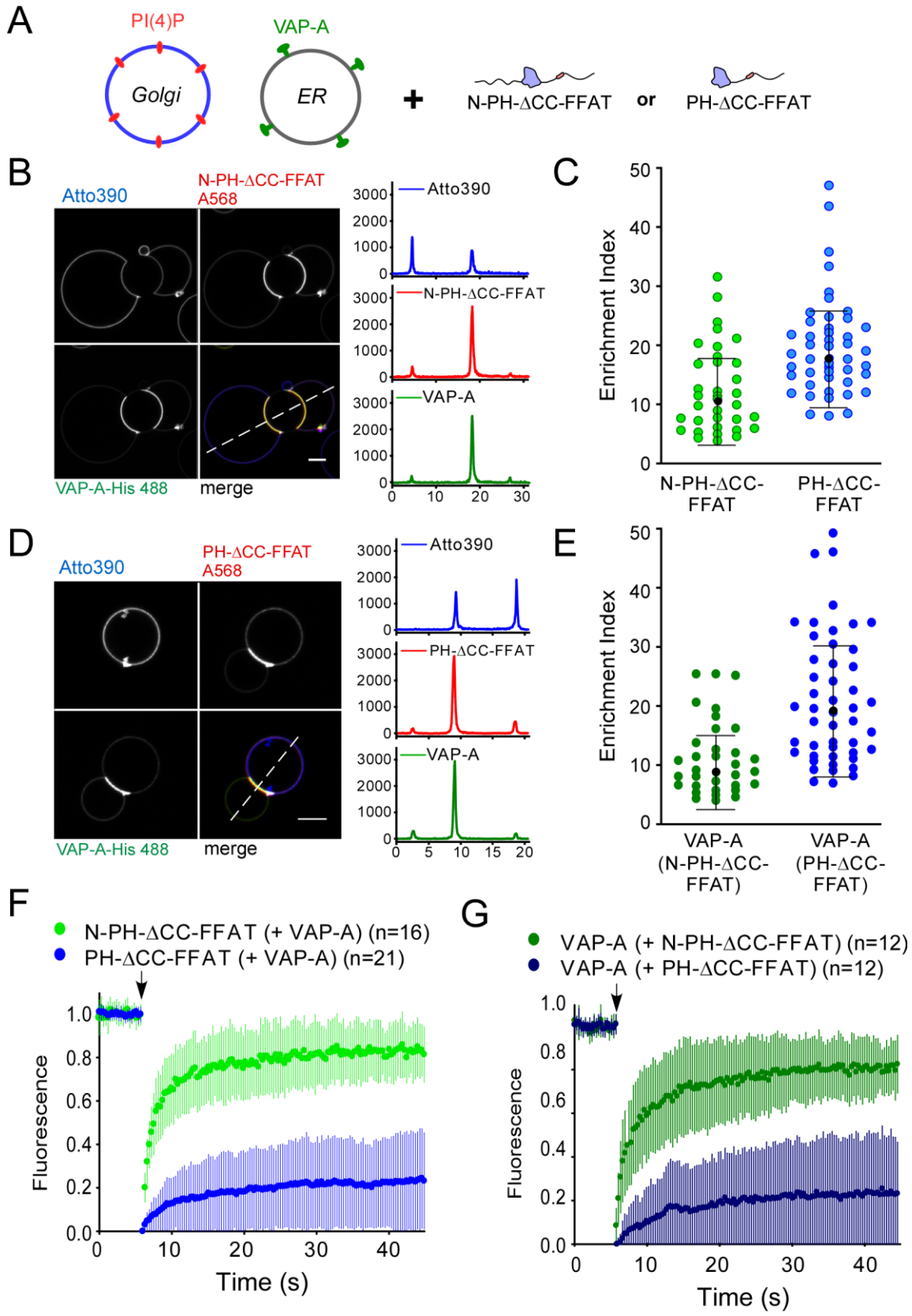

Figure 47: Effect of N-terminal sequence on protein difusion within heterotypic membrane interface

(A) Schematic representation of the assay. ER-like GUVs (2% DGS-NTa-Ni, no color) and Golgi-like GUVs (2% PI4P, Atto390-DOPE) were incubated with mixtures of 50 nM VAP-A (Alexa488) and 50 nM N-PH-ΔCC-FFAT or PH-ΔCC-FFAT (Alexa568), respectively **(B - E)** Visualisation of heterotypic ER-Golgi membrane interfaces and enrichment index quantification. Both proteins and associated VAP-A greatly accumulate at membrane interface. N-ter-dependent differences in enrichment index are modest. Enrichment of OSBP constructs **(C)** positively correlates with the enrichment of their associated VAP-A **(E)**. Scale bar = 5 μm **(F)** A representative FRAP experiment with bleaching of Alexa568, showing the N-PH-ΔCC-FFAT/VAP-A (light green trace) *vs* PH-ΔCC-FFAT/VAP-A (light blue trace) signal recovery **(G)** A complementary FRAP on Alexa488 (=VAP-A). N-PH-ΔCC-FFAT/VAP-A trace in dark green, PH-ΔCC-FFAT/VAP-A trace in dark blue. n = number of measurements per condition. In both **(F)** and **(G)**, one representative experiment from two independent experiments is shown.

8. Lipid transfer activity of OSBP is not influenced by the N-ter

To address the role of N-terminus on OSBP lipid transfer, we performed liposome-based lipid transfer assays with catalytically active proteins containing the lipid binding ORD domain. We followed the transfer of naturally fluorescent analog of cholesterol, the dehydroergosterol (DHE), from ER-like to Golgi-like liposomes. Conversely, we also followed the translocation of PI(4)P from Golgi-like liposomes (4 mol% PI(4)P) to ER-like liposomes by monitoring the increase in fluorescence of a dequenched PI(4)P probe (NBD-labeled PH_{FAPP1}). OSBP was used in catalytic amount compared to PI(4)P (1 OSBP for ~30 accessible PI(4)P molecules) but in large excess over the liposomes (~60 OSBP molecules for one liposome). Thus, the equilibration of PI(4)P between the donor and acceptor liposomes required OSBP to undergo multiple rounds of lipid exchange on the same liposomes, without the need for OSBP to translocate between different liposomes. As shown in **Figure 48 A and B**, OSBP FL and ΔN-OSBP were very similar in their DHE transfer activity. This similarity also applied in the PI(4)P transfer assay **(Figure 48 C and D)**, either with or without cholesterol present in the ER liposomes. Cholesterol considerably accelerated the rate of PI(4)P transfer due to coupling between forward cholesterol transfer and backward PI(4)P transfer (Mesmin *et al.*, 2017; Moser von Filseck *et al.*, 2015b). We concluded that the N-terminal region is not directly involved in the mechanism of sterol/PI(4)P exchange by OSBP.

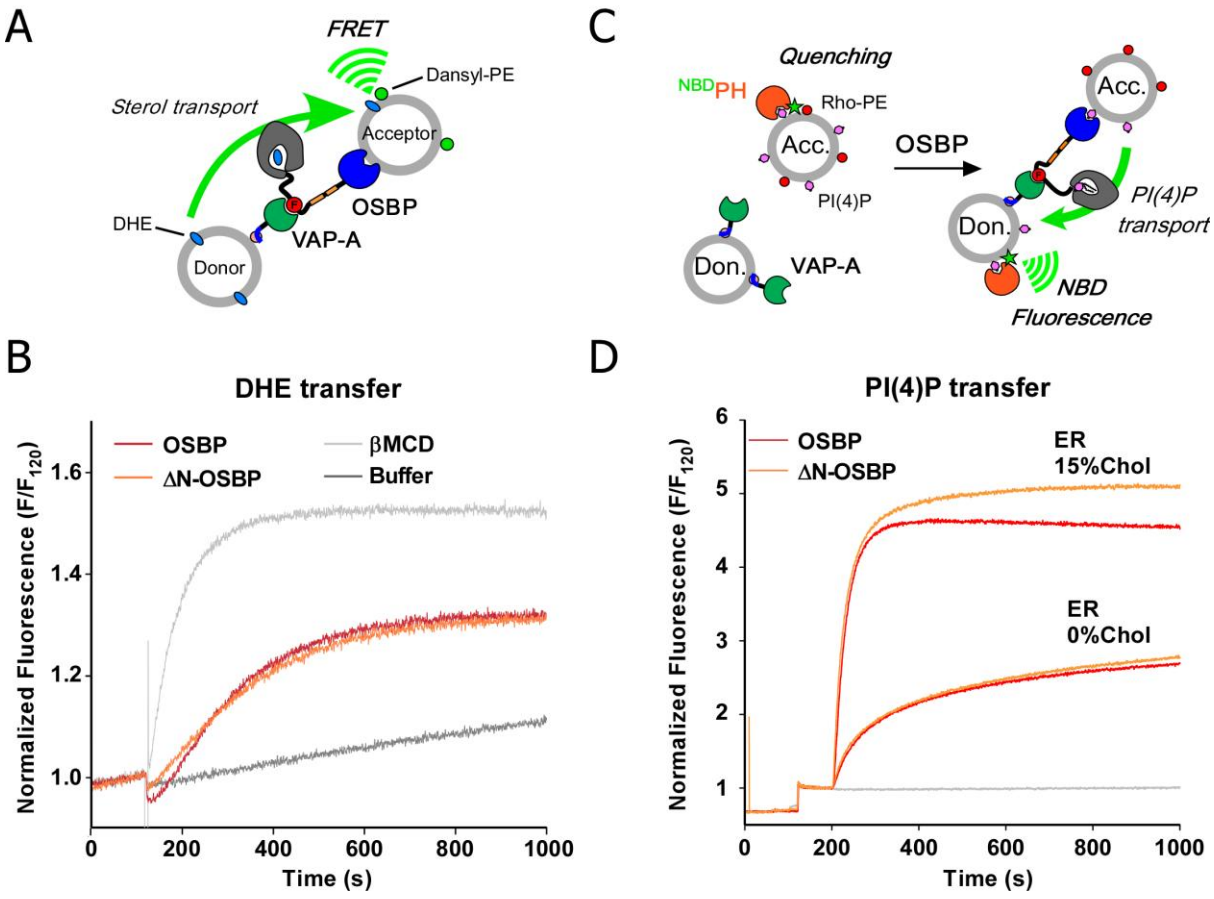

Figure 48: N-terminus does not affect the lipid transfer activity of OSBP

(A) Schematic representation of the DHE transfer assay. Donor liposomes (65 μM) contain 10% of DHE (a naturally fluorescent cholesterol analog), acceptor liposomes contain 2.5% Dansyl-PE. Upon DHE transfer, a FRET occurs between DHE and Dansyl group, and the Dansyl fluorescence can be detected at 510 nm **(B)** Time course of DHE transfer from donor (ER-like) to Acceptor (Golgi-like) liposomes by 100 nM OSBP (red) or ΔN-OSBP (orange trace) **(C)** Scheme of PI(4)P transfer assay. PI(4)P on donor (Golgi-like) liposomes (6 mol%) is recognized by NBD-labelled PH_{OSBP}. Rhodamine-PE on the same liposomes quenches NBD fluorescence. Upon PI(4)P translocation, NBD-PH_{OSBP} relocates to acceptor (ER-like) liposomes and its fluorescence can be detected at 536 nm **(D)** Time course of PI(4)P transfer by 100 nM OSBP (red) or ΔN-OSBP (orange). The assay was performed either in absence or in presence of cholesterol (15 mol%) in the ER-like (acceptor) liposomes. Transfer assay was repeated also with liposomes containing 1 or 2 mol% PI(4)P (donor) and 5 mol% cholesterol (acceptor) with similar results.

9. N-terminus regulates Golgi localisation of OSBP in living cells

After assessing *in vitro* effect of N-terminus on protein localisation on membranes, we also decided to look into the role of N-terminus in living HeLa and RPE1 cells. First, we investigated the subcellular localization of four C-terminally mCherry-tagged constructs: OSBP, ΔN-OSBP, N-PH-FFAT and PH-FFAT (**Figure 49 A**). In both cell types, OSBP localized mainly to the Golgi complex (as evidenced by the colocalisation with the Golgi marker BFP-GalT). Weak mCherry fluorescence was also observed at structures decorated by EGFP-Rab7, which likely correspond to late endosomes (**Figure 49 B**). This observation fits with previous study of Dong et al. (2016), which has shown that OSBP can bind PI(4)P in the endosomal membranes. However, a large fraction of OSBP was also found in cytosol. Compared to full length OSBP, ΔN-OSBP displayed a 2-fold higher Golgi/cytosol ratio. On the contrary, both N-PH-FFAT and PH-FFAT were highly localized to the Golgi, with tiny cytosolic fractions. This high Golgi recruitment of catalytically inactive constructs lacking the ORD is due to the absence of a negative feedback effect faciliated by the ORD – by relocating PI(4)P away from Golgi membrane, ORD removes a "recruiting" lipid that is recognized by the PH domain, which leads to destabilization of the interaction of OSBP with membranes (Mesmin *et al.*, 2013).

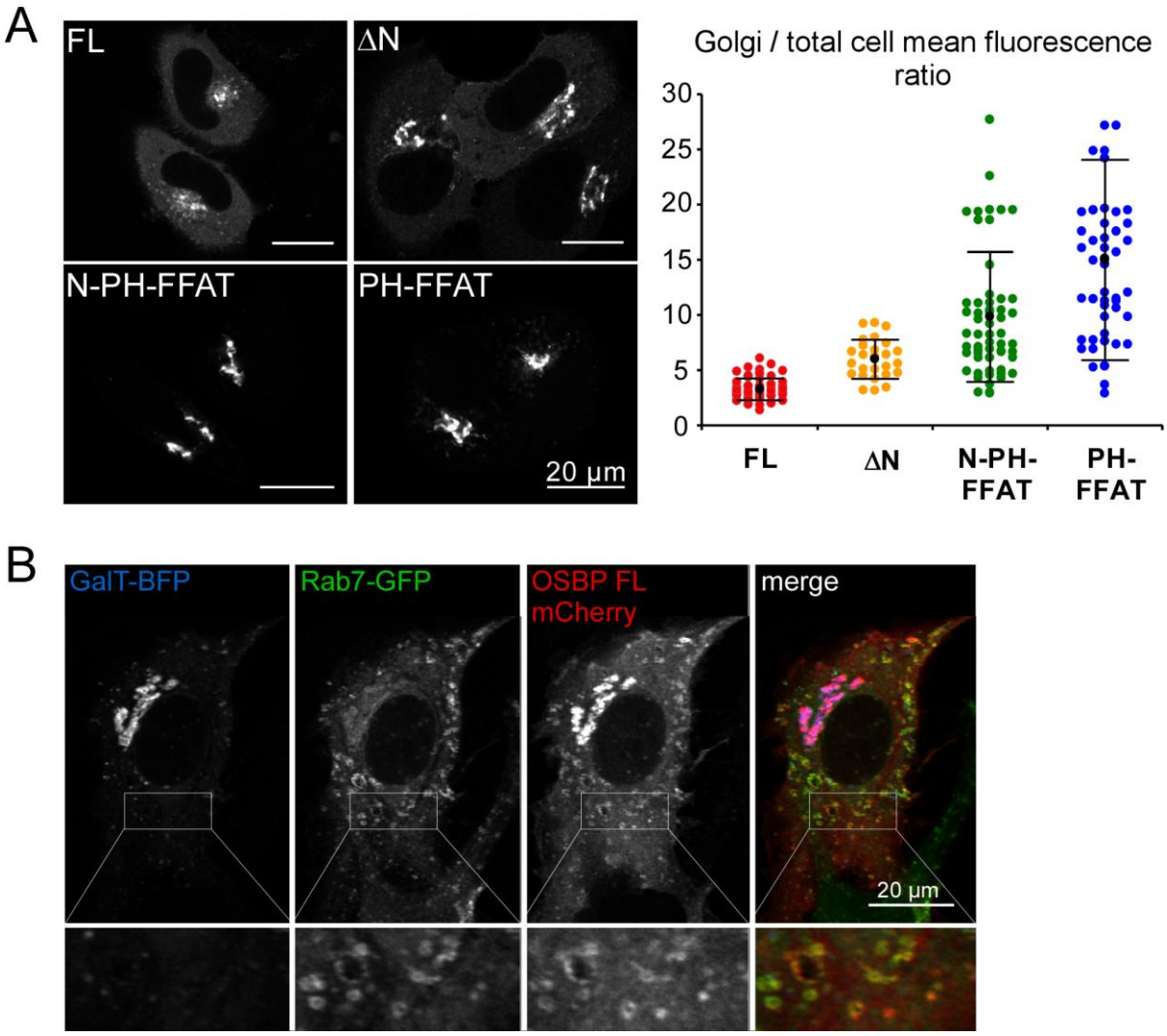

Figure 49: Subcellular distribution of OSBP-derived constructs expressed in HeLa cells

(A) C-terminal mCherry-tagged proteins were co-transfected in cultured cells together with the Golgi marker BFP-GalT. Subcellular distribution of OSBP constructs was measured as the ratio between mean fluorescence intensity at the Golgi and mean total cell fluorescence intensity **(B)** full length OSBP colocalisation with Golgi marker BFP-GalT and a weak but recognizable colocalisation with endosomal marker EGFP-Rab7.

Similar experiments were performed with corresponding four ORP4-derived proteins (**Figure 50**). In agreement with previous report (Wang et al., 2002), ORP4 constructs containing the ORD co-localized with intermediate filaments, as shown by the vimentin staining in cells. These constructs only modestly stained the Golgi, which did not enable us to do a proper Golgi/cytosol analysis and suggested that the main

functional role of full length ORP4 in HeLa or RPE1 cells may not necessarily consist in lipid transfer at ER-Golgi MCS. Therefore, we focused on ORP4 N-PH-FFAT and PH-FFAT, which only partitioned between the cytosol and the Golgi - N-PH-FFAT displayed both cytosolic and Golgi signal, whereas PH-FFAT highly localized to the Golgi. However, the Golgi/cytosol ratios were lower than that of corresponding OSBP-derived proteins, in consistence with the lower recruitment to the Golgi (which was also seen by lower tethering activity in DLS), suggesting a minor (if any) role of ORP4 in lipid transfer at the ER-Golgi MCS. Nevertheless, we could still conclude that N-terminus regulates the Golgi membrane partitioning of OSBP and truncated ORP4 proteins in cultured cells.

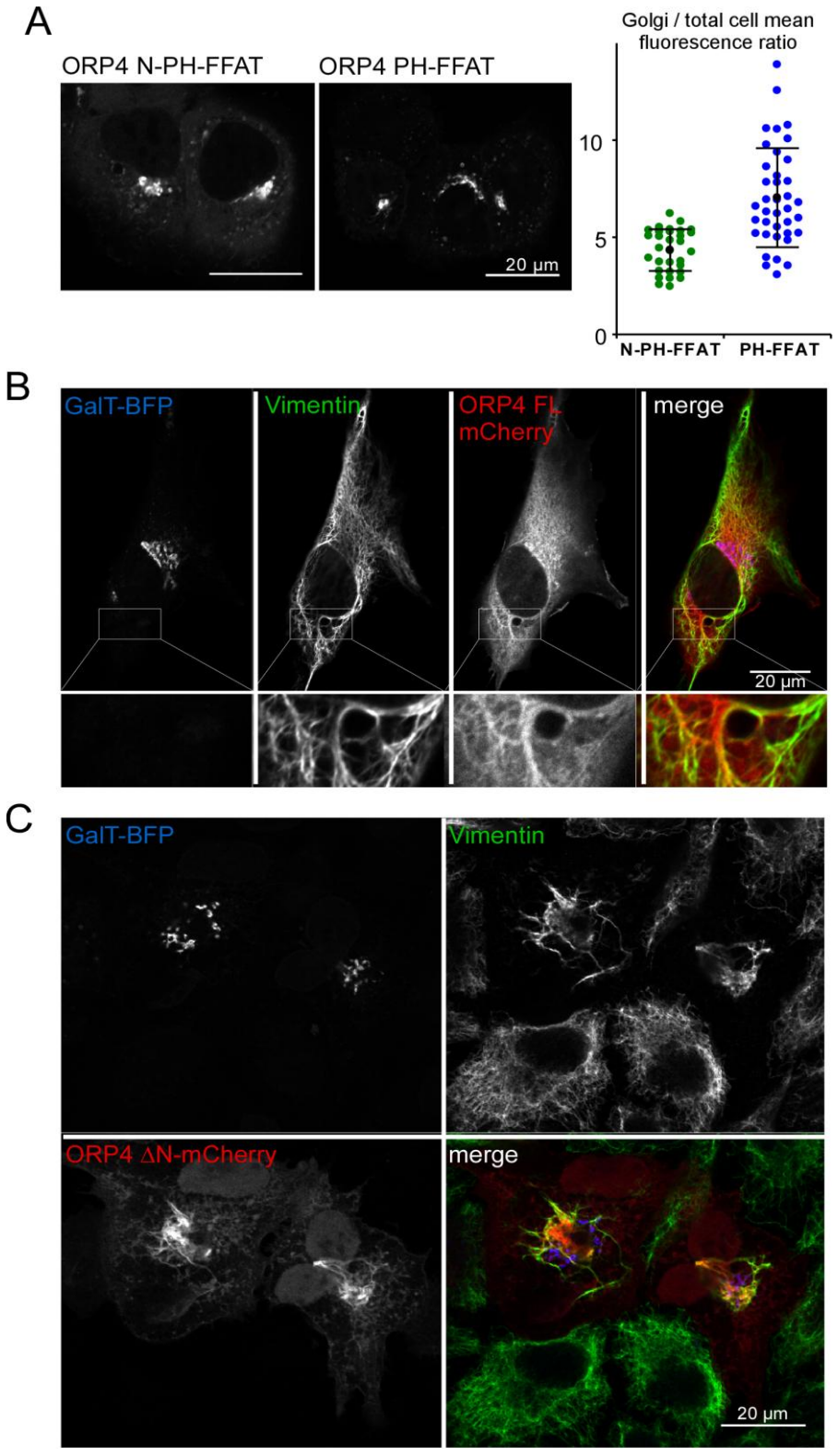

Figure 50: Subcellular distribution of ORP4 constructs expressed in HeLa cells

(A-C) C-terminal mCherry-tagged ORP4 constructs were co-transfected with GalT-BFP. As reported previously, ORP4 FL and ΔN co-localized with vimentin filaments and did not show major Golgi recruitment. Note the collapse of vimentin filaments when overexpressing ORP4 ΔN.

To examine whether the dynamics of OSBP and ORP4 at the Golgi was also affected, we performed FRAP experiments by bleaching small circular areas at the Golgi. As shown for a representative experiment on **Figure 51**, the fluorescence recovery rate inversely correlated with the Golgi partitioning of proteins: full length > ΔN-OSBP > N-PH-FFAT > PH-FFAT. In addition, the recovery kinetics of OSBP-derived constructs were systematically slower that those of related ORP4 constructs, consistent with the higher Golgi recruitment of OSBP *vs* ORP4. Importantly, all constructs with N-terminus manifested faster (~3-5-fold) fluorescence recovery compared to corresponding ΔN-constructs. This indicates that the N-termini facilitate protein lateral motility at the membrane surface and/or exchange with the cytosolic pool.

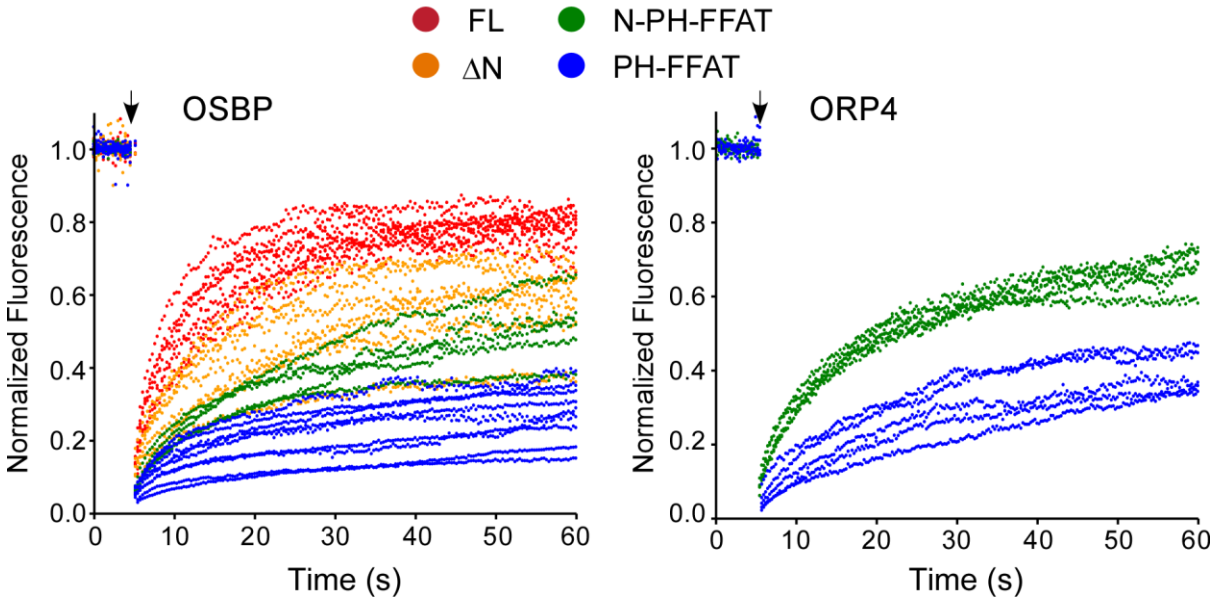

Figure 51: Fluorescence recovery of OSBP and ORP4 constructs at the Golgi

Both OSBP- and ORP4-derived proteins that contain N-terminal disordered sequence display higher FRAP recovery rate. Photobleaching was performed on a circular area (3μm diameter) at the Golgi apparatus.

In our further investigations, we also aimed to elucidate the possibility of homotypic tethering in living cells. At first, we transfected RPE1 cells with mCherry-tagged N-PH-FFAT and PH-FFAT and looked at the morphology of Golgi apparatus by electron microscopy. We did not observe any unusual features (data not shown). However, we realized that in cells, an important role in regulating the MCS geometry is likely played by VAP-A, which is embedded in the ER membranes in large quantities (Kulak et al., 2014). Therefore, we decided to take advantage of short OSBP constructs with disabled FFAT motif (FF/AA substitution) to prevent interaction with VAP-A. Under these circumstances, in some RPE1 cells transfected with PH-FFAT (FF/AA) we could clearly observe anomalies in the TGN, especially in the form of "swollen" cisternae with large alignments of membranes (**Figure 52**, red arrows). However, we could not exclude possible involvement of ER or other membranes in these alignments and we observed similar (although not so frequent and no so severe) anomalies also in N-PH-FFAT (FF/AA) overexpressing cells. Therefore, the question whether Golgi-Golgi tethering occurs in living cells cannot be answered doubtlessly for now.

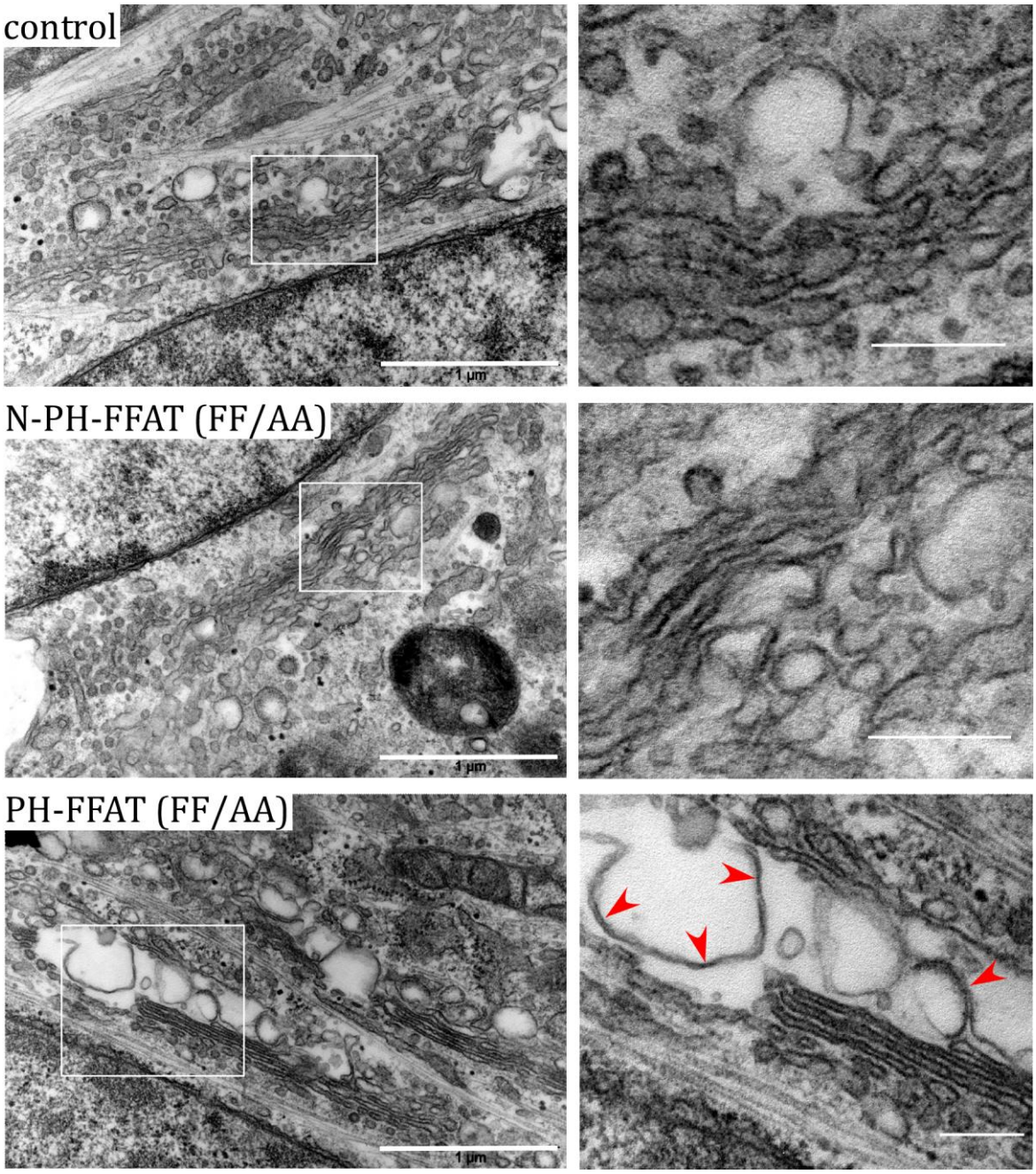

Figure 52: Electron microscopy of (N-)PH-FFAT (FF/AA) expressing cells

Top row: Electron micrograph of mock-transfected cell. Middle row: RPE1 cell overexpressing N-PH-FFAT (FF/AA), displaying a regular Golgi morphology, similar to non-transfected cells and representing the majority of cells transfected by N-PH-FFAT (FF/AA). Bottom row: Cell overexpressing PH-FFAT (FF/AA). Note the swollen Golgi stacks in the TGN area and the excessive membrane alignments (red arrows), whereas the *cis*- and *medial*- Golgi seem to stay unaffected. Scale bar on the left: 1 µm, right: 200 nm.

10. N-TERMINUS OF OSBP HAS NO EFFECT ON ITS LIPID TRANSFER ACTIVITY IN CELLS

Although *in vitro* lipid transfer assays produced negative results, we attempted to investigate whether N-terminus could affect lipid transport by OSBP in cultured cells. We visualized PI(4)P by a probe that mainly marks the Golgi pool of PI(4)P/Arf1 (GFP-PH_{OSBP}, **Figure 53 A**). To avoid possible artifacts due to the presence of mCherry-tag at the ORD, we compared PI(4)P signals in cells expressing C-terminally- and N-terminally-tagged full-length OSBP. This control experiment showed that oppositely tagged proteins manifest similar lipid transfer activity (**Figure 53 B**). Subsequently, we could perform a series of steady-state experiments where we analyzed the consequences of overexpressing C-terminally-tagged OSBP or ΔN-OSBP during long (24h) and short (7h) expression period (**Figure 53 C**). Both constructs strongly diminished PI(4)P levels at the Golgi, without any major difference between FL or N-ter-truncated OSBP, which confirmed our assumption based on *in vitro* data: N-terminus is most likely not affecting the lipid transfer activity of the ORD domain.

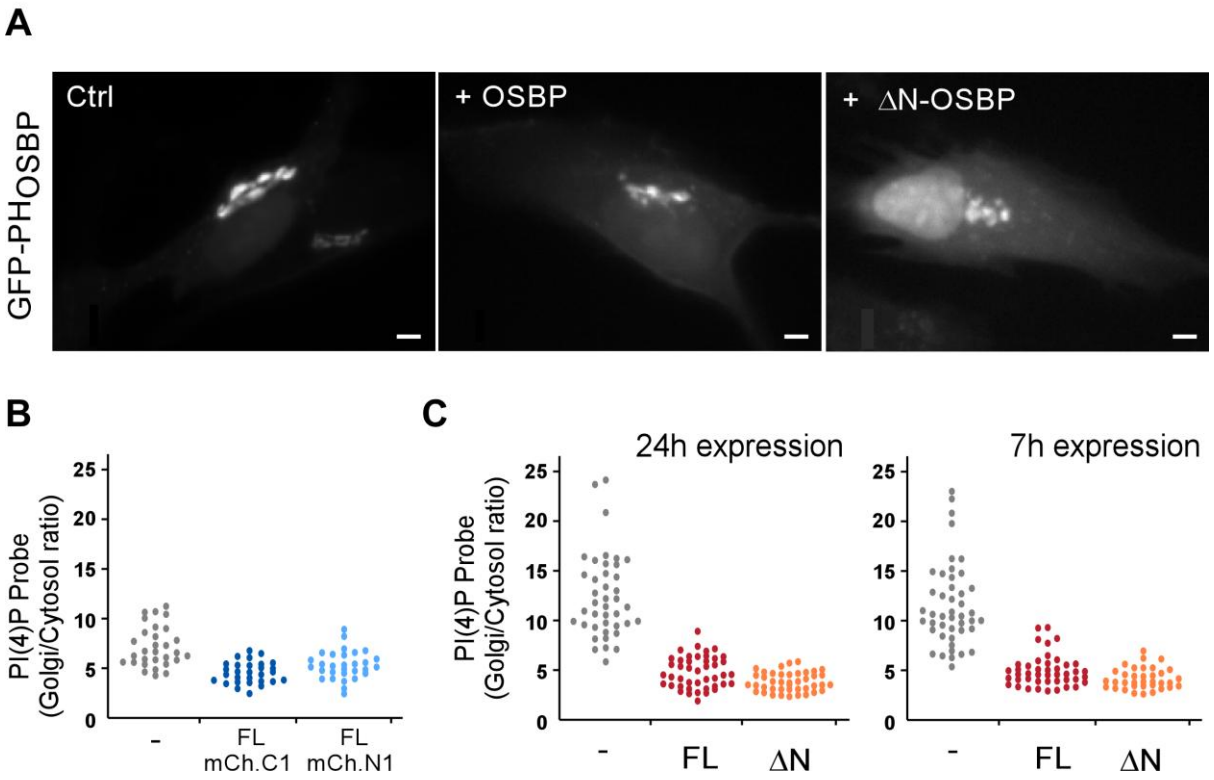

Figure 53: Lipid transfer activity of OSBP is not affected by the N-terminus in cells

(A) GFP-PH_{OSBP} probe in mock-transfected cells (Ctrl) and cells expressing C-terminally mCherry-tagged FL OSBP *vs* ΔN-OSBP **(B)** Position of the mCherry-tag does not affect lipid transfer activity of full-length OSBP **(C)** FL OSBP and ΔN-OSBP display similar lipid transfer activity in living cells. In all experiments, cells were co-transfected with Golgi marker BFP-GalT. Live cell imaging was performed 7 or 24 hours post-transfection and GFP-PH_{OSBP} Golgi/cytosol signal ratio was measured as described in Materials and Methods.

11. N-TERMINUS FACILITATES OSBP RECYCLING UPON CONDITIONS OF RESTRICTED PI4P SYNTHESIS

From the FRAP experiments with different OSBP- and ORP4-derived constructs that were described in previous parts of this work, we concluded that N-terminus is a major regulator of protein mobility on Golgi membranes. To further assess its role in OSBP dynamics, we took advantage of a live-cell assay developed recently in the lab (Mesmin *et al.*, 2017). When RPE1 cells stably overexpressing PI(4)P/Arf1 probe (PH_{OSBP}) are treated with PI4KIIIβ inhibitor (PIK93), PI(4)P probe displays oscillations ("travelling waves") across the TGN. These waves probably reflect the dynamics of OSBP-mediated contact sites after restricting the synthesis of local pools of PI(4)P by PI4KIIIβ. As PI(4)P becomes limited, MCS move towards PI(4)P-rich regions that are likely generated by remote PI4-kinases, not colocalizing with OSBP. These waves display a remarkable regularity, due to which they are well-suited for precise dynamics measurement (Mesmin *et al.*, 2017).

In our assay, we silenced endogenous OSBP using specific siRNA. After OSBP silencing, PIK93 no longer induced travelling waves of PH_{OSBP} indicating that OSBP is largely involved in PI(4)P turnover at the Golgi (**Figure 54 A-C**). In the following rescue experiments, we overexpressed either siRNA-resistant OSBP or ΔN-OSBP (OSBP-*res*-mCherry and ΔN-OSBP-*res*-mCherry, respectively). ΔN-OSBP-*res*-mCherry was more associated with the TGN than OSBP-*res*-mCherry, as evidenced by the stronger fluorescence (**Figure 54 D *vs* E**). Upon PIK93 treatment, OSBP-*res*-mCherry restored the appearance of PH_{OSBP} waves (green signal) with amplitude and period similar to endogenous OSBP. In addition, we also observed that OSBP-*res*-mCherry itself was oscillating across the Golgi (red signal), in phase with waves of PH_{OSBP}. In contrast, ΔN-OSBP-*res*-mCherry did not rescue the siRNA phenotype – upon PIK93 addition, we observed a sharp decrease of PH_{OSBP} signal at the TGN (suggesting that ΔN-OSBP-*res*-mCherry was able to consume PI(4)P) but the decrease was followed by waves of much smaller amplitude than that observed with full length OSBP (**Figure 54 F, G**). This experiment clearly demonstrated that although the N-terminus does not affect the lipid transfer activity of OSBP *per se*, it has a strong effect on OSBP dynamics during lipid transfer cycles at the TGN.

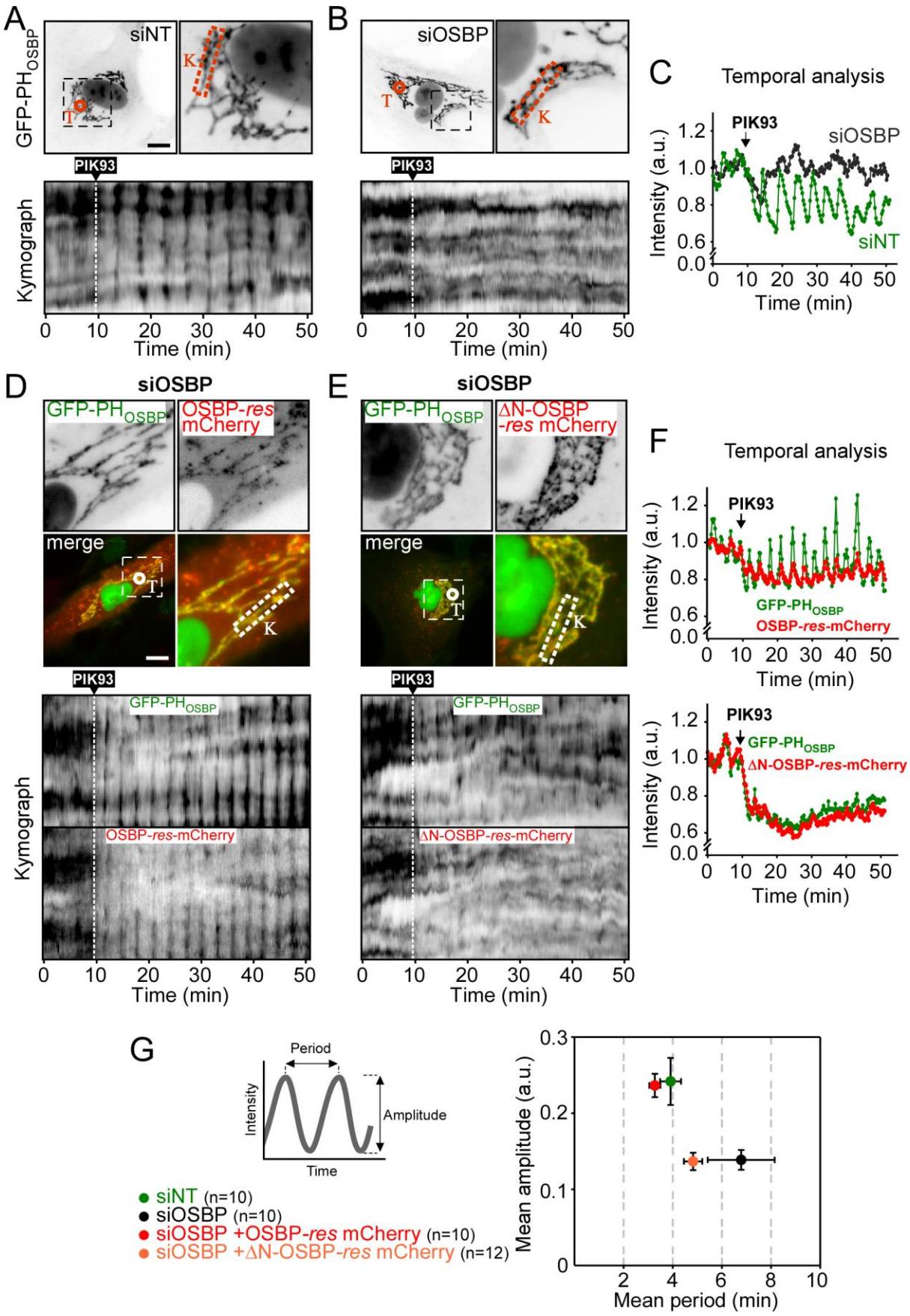
A
siNT
GFP-PH$_{OSBP}$
T
K
PIK93
Kymograph
Time (min)
B
siOSBP
C
Temporal analysis
PIK93
siOSBP
siNT
Intensity (a.u.)
Time (min)
D
siOSBP
GFP-PH$_{OSBP}$
OSBP-*res* mCherry
merge
E
ΔN-OSBP -*res* mCherry
F
Temporal analysis
OSBP-*res*-mCherry
ΔN-OSBP-*res*-mCherry
G
Period
Amplitude
Intensity
Time
siNT (n=10)
siOSBP (n=10)
siOSBP +OSBP-*res* mCherry (n=10)
siOSBP +ΔN-OSBP-*res* mCherry (n=12)
Mean amplitude (a.u.)
Mean period (min)

Figure 54: N-terminus regulates OSBP dynamics during lipid transfer cycles in living cells

(A, B) RPE1 cells stably expressing GFP-PH_{OSBP} probe were treated with control siRNA (siNT) or siRNA agains OSBP (siOSBP). When indicated, 500 nM of PIK93 was added into the cell medium. Top: snapshots of cells taken at t = 0 using an inverted grayscale lookup table (fluorescence in black). Scale bar = 20 μm. Bottom: kymograph taken from a rectangular TGN region ("K", ~ 20 x 3 μm). Silencing of endogenous OSBP abolishes GFP-PH_{OSBP} oscillations **(C)** Temporal analysis of siNT- and siOSBP-treated cells. Graph shows normalized mean fluorescence intensity measured on a circular area ("T", diameter 8 μm) from images A and B over time. **(D, E)** RPE1 cells stably expressing GFP-PH_{OSBP} and treated with siOSBP were transfected with siRNA-resistant OSBP constructs (OSBP-*res*-mCherry or ΔN-OSBP-*res*-mCherry) for 24 hours before imaging. In time-lapse videos, both GFP and mCherry signals were monitored, as shown in kymographs **(F)** Temporal analysis shows the rescue of GFP-PH_{OSBP} waves by full length of OSBP, in contrast to ΔN-OSBP which does not rescue the *wt* phenotype **(G)** Quantification of mean GFP-PH_{OSBP} oscillation amplitude and period from recordings similar to that shown in **(C)** and **(F)**

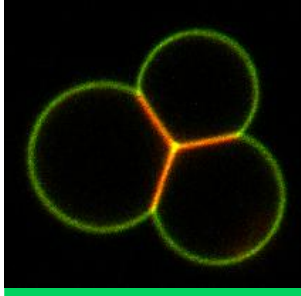

Discussion, Conclusion & Perspectives

DISCUSSION

Membrane contact sites are closely apposed domains that facilitate exchange of considerable amount of material (such as ions, metabolites and lipids) as well as information between two distinct organelles. Therefore, MCS can be viewed as platforms harboring specialized membrane-associated proteins (ion channels, transporters, enzymes, receptors, adaptors etc.), playing a crucial role in regulation of numerous cellular processes. Intermembrane distances at MCS usually vary between 10 and 30 nm (West et al., 2011), implying that individual protein components must operate within a narrow space densely occupied by other proteins. This confinement effect could substantially complicate the dynamics and function of MCS.

A major group of MCS-localized proteins are lipid transfer proteins (LTPs) which act as mediators of nonvesicular lipid transfer. LTPs include several protein families. Among them, the OSBP-related proteins (ORPs) are major regulators of cellular lipid distribution and homeostasis (Mesmin *et al.*, 2013; 2017). This PhD study identified a key role for the N-terminal tail of OSBP in regulating protein density and diffusion within MCS as well as in maintaining proper OSBP dynamics during lipid transfer cycles without directly affecting the lipid transfer activity of the ORD. In addition, N-terminus restricts the OSBP tethering geometry *in vitro* by favoring the ER-Golgi (heterotypic) orientation and countering the aberrant Golgi-Golgi (homotypic) tethering. Based on our observations we propose a model in which N-terminus acts as a regulator of MCS geometry and dynamics (**Figure 55**).

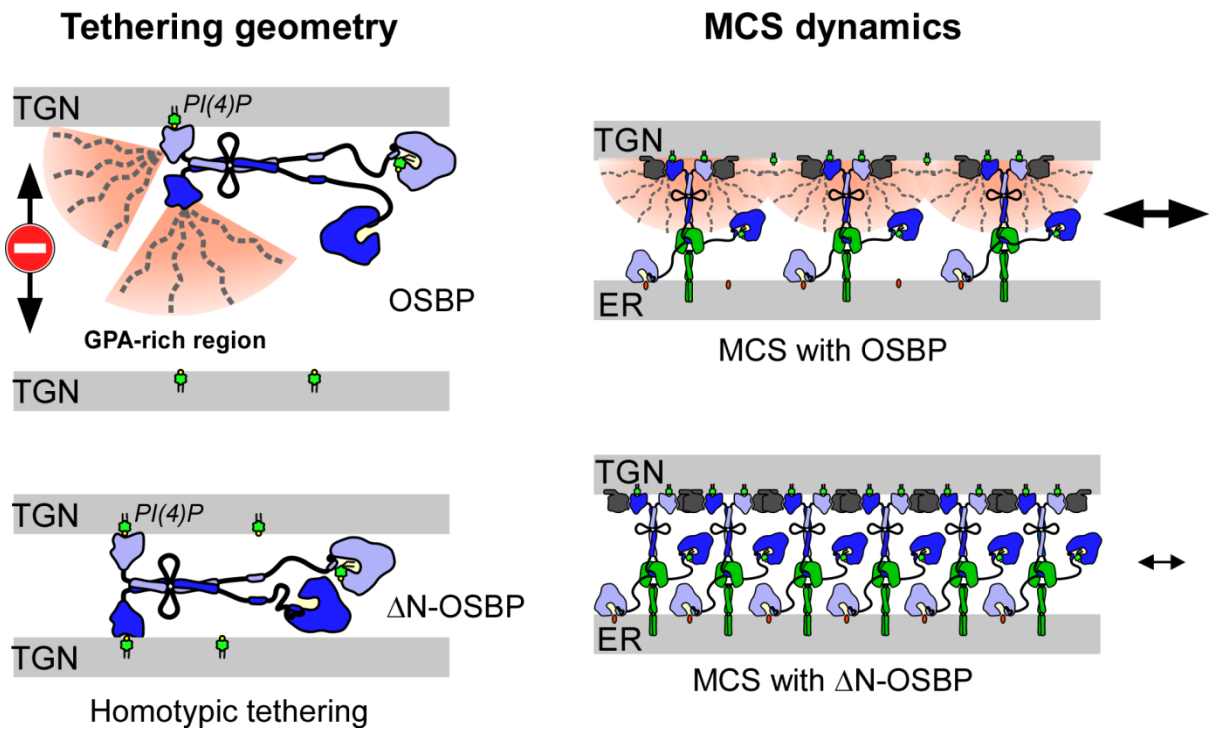

Figure 55: N-terminus of OSBP regulates membrane tethering geometry and MCS dynamics

Intrinsically disordered N-terminus acts as an entropic "shield" preventing two PH domains of dimeric OSBP to simultaneously bridge two PI(4)P/Arf1-GTP containing membranes. N-terminal tail also limits membrane protein density within MCS, thus facilitating protein mobility and proper MCS dynamics during lipid transfer cycles by OSBP.

Long (50 to 140 aa) intrinsically disordered regions display remarkable flexibility and ability to shift within a large variety of possible conformations over time, occupying approximately two-fold larger volume (R_h) compared to folded domains of the same residue count. We suggest that such disordered tail around a membrane-bound PH domain could create an entropic "shield" and likely regulate several important properties of ORPs. In this study, we used lipid vesicles of defined size and lipid composition to demonstrate that N-terminus reduces (and eventually limits) the amount of protein able to bind to PI(4)P-rich membrane via protein crowding.

Protein crowding is an important factor influencing lateral diffusion of integral membrane proteins (Zhou, 2009). In contrast to free diffusion in solution (3D), the reduction in dimensionality to 2D on a membrane means a similar level of crowding is

achieved with far fewer proteins. This has an important consequence: cells must carefully regulate the amount of proteins that can be recruited to biological membranes in order to ensure proper dynamics of membrane-associated reactions and signaling events. Therefore, the presence of a bulky tail in most abundant proteins might protect a balanced protein density on membrane and also compensate for the lack of disorder in less abundant proteins that co-localize to the same membrane/MCS (**Figure 56**).

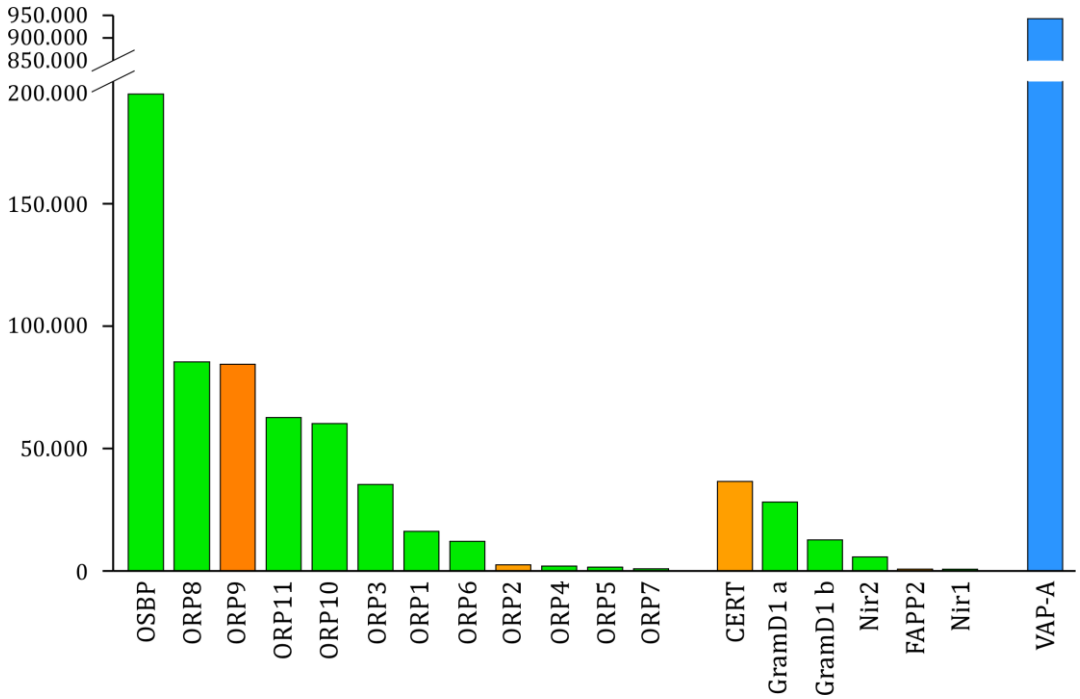

Figure 56: Protein copy number of selected LTPs in HeLa cells

Quantification of protein copy number in HeLa cells is from Kulak *et al.* (2014) and was performed by mass spectrometry-based proteomics in single, enclosed cell lysate volume to eliminate contamination or loss of proteins. Selected LTPs are shown. Green bars correspond to proteins that contain N-terminus, orange bars are proteins without N-terminus. Blue bar illustrates the abundance of VAP-A.

As N-terminus affects the protein density on membrane via protein crowding, it necessarily impacts lateral diffusion. The extent of this impact can be measured by FRAP with fluorescently labeled proteins on GUVs with known lipid composition, using proteins without lipid transfer activity, namely dimeric N-PH-FFAT and PH-FFAT (in homotypic MCS) or monomeric derivatives N-PH-ΔCC-FFAT and PH-ΔCC-FFAT

(interacting with VAP-A in heterotypic MCS). Our study showed that the presence of N-terminal tail greatly accelerates the fluorescence recovery both in homotypic and heterotypic condition. Fitting the recovery curves of N-PH-FFAT and N-PH-ΔCC-FFAT suggests apparent diffusion coefficients in the range of 0.15 $\mu m^2/s$, whereas no or very slow recovery was observed with constructs lacking the N-terminus. Moreover, N-terminal tail of monomeric OSBP construct imposed the mobility also on the interaction partner, VAP-A, indicating a general effect on the dynamics of MCS.

This effect is striking both by its trend and by its magnitude. In general, increasing protein size (volume) leads to a decrease in mobility, in both dilute and crowded environments. In soluble phase this is mainly due to higher friction between the solvent-accessible surface area of a protein and solvent molecules, and in case of integral membrane proteins due to higher friction between the surface of transmembrane segment and surrounding lipid bilayer. The effect of protein size tends to be modest, as volume increases as the cube of linear dimension, whereas surface increases as the square. Therefore, for spherical proteins moving in 3D, doubling the molecular weight leads only to a 1.25-fold reduction in diffusion coefficient (Lippincott-Schwartz et al., 2001). In membrane proteins diffusing in 2D, the effect is even smaller: large proteins with five to seven transmembrane helices are ~1.5-fold slower than a protein with single membrane-spanning helix (Ramadurai et al., 2009). These comparisons underline the surprising effect of OSBP N-terminus: although it occupies large volume around PH domains, instead of slowing down diffusion, it leads to an increase in apparent mobility by almost an order of magnitude. Possible explanation of this phenomenon consists in the very nature of N-terminal tail, in its intrinsic disorder.

In dilute solutions, an unfolded model protein diffuses slower than a folded protein of similar molecular weight due to its expanded surface area which leads to higher amount of collisions with solvent molecules. However, in solutions crowded with other proteins or crowding agents, a disordered protein diffuses faster due to its flexibility and ability to shift between different shapes (Wang *et al.*, 2017, 2012, 2010). This may explain the higher apparent mobility of proteins decorated by regions of intrinsic disorder *in vitro*. We monitored a similar behavior also in living cells expressing dimeric proteins with and without the ORD. We report that both short and long proteins lacking the N-terminus display a higher Golgi localization and slower

fluorescence recovery, suggesting that even in the context of MCS in living cells, N-terminus impacts membrane recruitment of OSBP. However, in these experiments, the complex arrangement of Golgi membranes makes a more detailed interpretation of FRAP recovery curves difficult (Lippincott-Schwartz *et al.*, 2001), mainly because the signal recovery could occur not only by lateral diffusion within ER-TGN contacts but as well by exchange with cytosolic pool of soluble protein. In addition, OSBP constructs carrying a functional ORD have lipid transfer activity, which establishes a negative feedback loop by consuming PI(4)P, thus weakening its own association with the TGN (Mesmin *et al.*, 2013; 2017).

It has been described that PH domain of OSBP can bind PI(4)P with very high affinity (Levine and Munro, 2002). As OSBP is proposed to counter-exchange lipids in homodimeric conformation, the presence of two unshielded PH domains grants an opportunity to bridge PI(4)P containing membranes in a homotypic Golgi-Golgi manner. Such tethering geometry would not favor a directional lipid transfer, as it could cause unproductive relocating of PI(4)P molecules between the membranes of TGN and thereby disturb the cellular lipid distribution. In the context of possibly dangerous homotypic tethering, protein dimerization must be detailed. There are two predicted coiled-coils between the PH domain and FFAT motif of OSBP, and they are most likely dispensable for both membrane tethering and lipid transfer activity. For example, Osh3 protein displays similar domain architecture like OSBP (PH domain – FFAT – ORD) but it lacks the coiled-coils. Instead, the sequence between PH domain and FFAT is a 37 nm-long loop (Tong *et al.*, 2013). In OSBP phylogeny, N-terminus and coiled-coils (especially CC1) are both recent features, compared to highly conserved PH and ORD. In contrast to flexible loops, coiled-coils adopt a more solid, rod-like structure that could allow the precise setting of intermembrane distance at MCS. As coiled-coils and N-terminal disordered regions seem to co-evolve, we hypothesize that OSBP in higher organisms is adapted to fine-tune intermembrane distance without the risk of creating aberrant symmetrical MCS tethering.

After the creation of MCS by tethers of certain length, other membrane-interacting molecules can enter the forming MCS, as long as their length does not exceed the intermembrane distance (Schmid *et al.*, 2016). In the initial steps, this helps the forming of a functional MCS but over time the increasing amount of proteins

accumulating at the same interface could impair protein mobility and function. In this context, N-terminal disordered sequence of OSBP could also act as a general entropic barrier, regulating protein spacing within the confined environment of MCS. This regulation would not necessarily follow only the "spatial needs" of OSBP but also of other neighboring proteins inhabiting the same contact site. Indeed, it has been shown that OSBP is involved in the regulation of ceramide transport by CERT (Perry and Ridgway, 2006). Simultaneously, PI(4)P production necessary for the Golgi targeting of OSBP and CERT depends on the PI/PC transfer activity of Nir2 (Peretti *et al.*, 2008), which partly occupies the same ER-TGN contacts as OSBP and CERT (**Figure 57**).

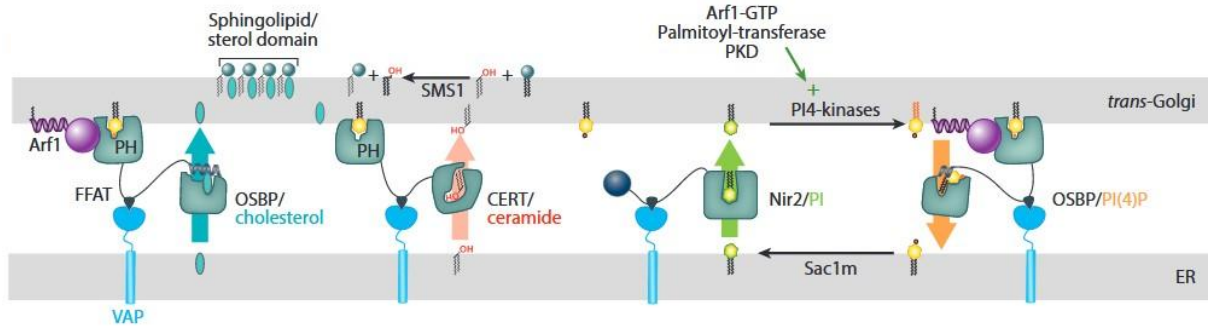

Figure 57: Spatial and functional cooperation of LTPs at ER-Golgi contact site

Several LTPs co-occupy the same MCS. OSBP bridges ER and *trans*-Golgi and delivers sterol into the Golgi membranes, activating PI4KIIα (Lu et al., 2012). The production of PI(4)P by PI4KIIα facilitates the recruitment of CERT at the same MCS (Banerji et al., 2010). Nir2 supplies Golgi apparatus with PI and promotes the formation of PI(4)P by PI4-kinases IIα and IIIβ. Anterograde transport of PI by Nir2 and retrograde transport of PI(4)P by OSBP and CERT provide energy and directionality for cholesterol and ceramide transfer and control the life-time of MCS through PI(4)P degradation by Sac1 in the ER. To prevent protein overcrowding as well as to keep proper MCS dynamics, LTPs may rely on their intrinsically disordered regions. Illustration from Drin, 2014.

Given the importance of N-terminus in membrane tethering and protein dynamics, as well as its prevalence in ORPs, an important question arises: is the presence of disordered terminal region a general feature of MCS-associated LTPs? Indeed, many LTPs contain low complexity terminal regions. The domain organization

of highly conserved Nir/RdgB protein family displays similar, although inverted features like that of ORPs (N-terminal PI/PC-transfer domain, central FFAT motif and C-terminal Lipin/Nde1/Smp2 (LNS2) domain). Human Nir1-3 have been shown to interact with ER-resident VAP-B (Amarilio *et al.*, 2005). Under steady-state conditions, Nir2 localizes to the Golgi, whereas upon stimulation of PLC-coupled receptors, Nir2 relocates to the PM where its LNS2 domain recognizes phosphatidic acid. Consequently, PI-transfer activity of Nir2 could couple PLC to PI signaling and possibly coordinate both local lipid metabolism as well as PA- and PI-mediated signaling pathways at the ER-PM contact sites (Herdman and Moss, 2016; Kim *et al.*, 2013, 2016). Downstream the PA-interacting LNS2 domain, Nir proteins contain ~80 - 130 aa long disordered regions that could fulfill analogous functions in regulating protein mobility like that of OSBP (see **Figures 57 and 58**).

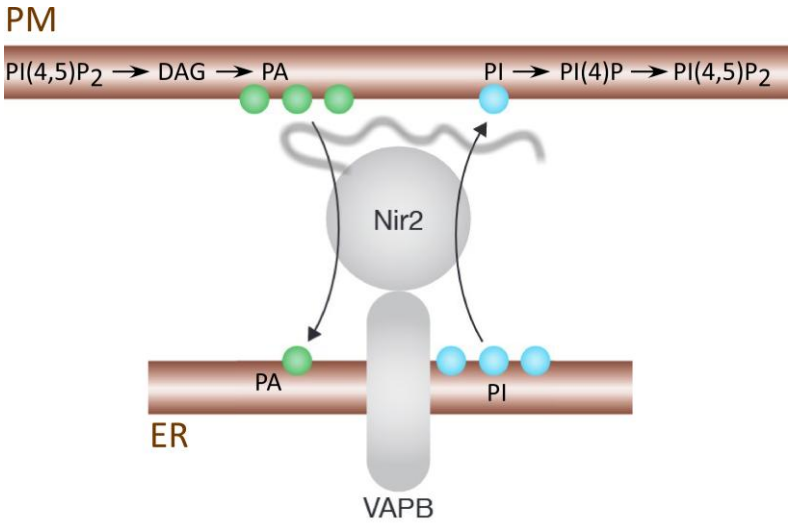

Figure 58: PI/PA exchange activity of Nir2 at ER-PM contact sites

By transporting PA to the ER and PI to the plasma membrane, Nir2 could link PA- and PI- mediated signaling pathways. Upon PLC activation, $PI(4,5)P_2$ is cleaved to DAG and IP_3. IP_3 signaling leads to release of Ca^{2+} from the ER, whereas DAG is converted to PA. PA is transported by Nir2/3 proteins to ER membrane, where it is converted to PI and transported back to PM via Nir2/3. PI is subsequently converted to PI(4)P and $PI(4,5)P_2$. Illustration modified from Krauβ and Haucke, 2016.

Another example is the LAM family of sterol transporters which consists of transmembrane proteins anchored to ER. LAMs contain a PH-like domain that interacts with other membranes such as PM, outer mitochondrial membrane or vacuolar membrane at nuclear-vacuolar junction in yeast. Lipid transfer activity is facilitated by one or two lipid binding StART-like domains. Most LAMs (GRAMD1 a-c in humans and Lam2p, Lam4p, Lam5p, Lam6p in yeast; Gatta *et al.*, 2015; Tong *et al.*, 2018) are decorated with long disordered regions upstream of their PH-like domains (**Figure 59**).

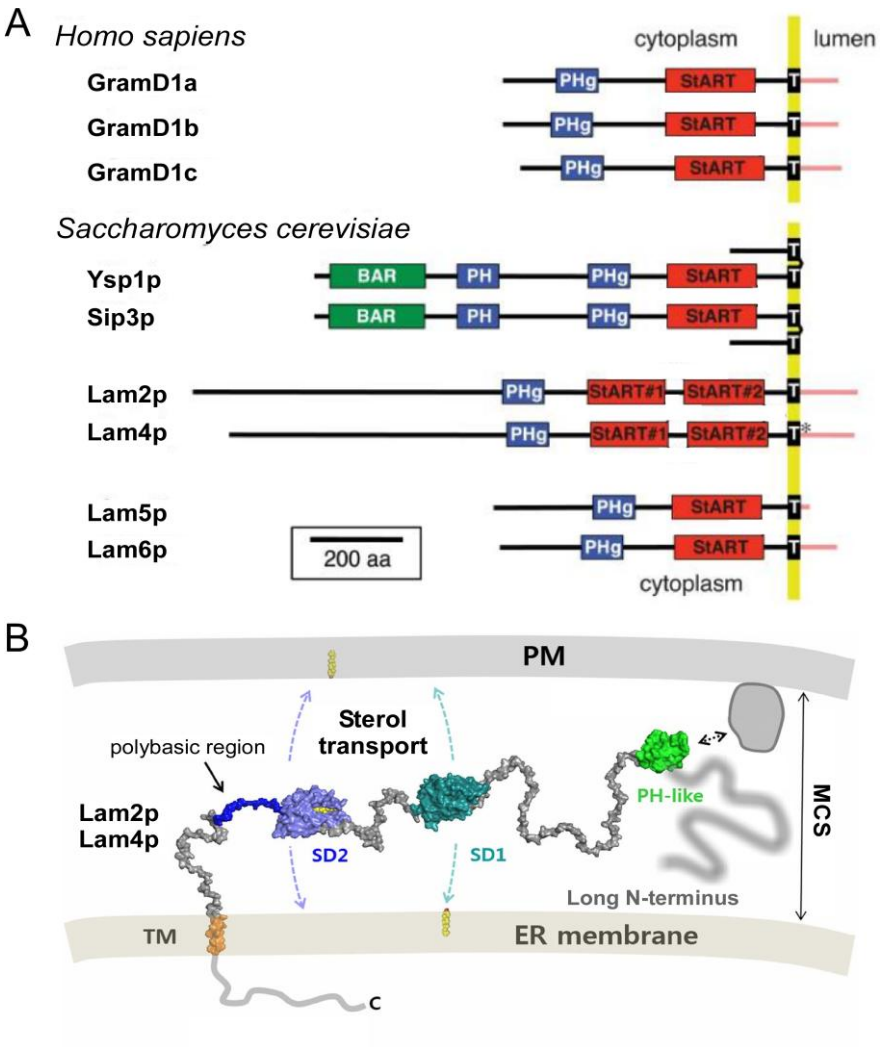

Figure 59: LAM family of LTPs

(A) Schematic representation of LAM family members in human and in yeast. PHg = domains from the plekstrin homology superfamily, T = transmembrane domain (weakly predicted in Lam4p*). Illustration from Gatta *et al.*, 2015 **(B)** Model of LAM function at MCS. LAMs are ER-anchored proteins with two sterol transporting StART-like domains (SD1, SD2), connected by flexible linkers. Several LAM homologs contain polybasic

regions at the end of their second StART-like domain, which might assist in membrane binding of the domain during sterol uptake or release. The binding partner(s) of PH-like domain of Lam2p and Lam4p at the PM are unknown. At the N-terminus, most LAMs contain long regions of predicted disorder. Figure modified from Tong *et al.*, 2018.

On the contrary, certain MCS-localized LTPs seem to perform their function without the necessity of N-terminal tail. These LTPs include sphingolipid transfer proteins CERT and FAPP2. Both display architecture similar to ORPs (PH domain, FFAT motif, lipid transfer StART or GLTP domain, respectively). Whereas in FAPP2, the PH domain and FFAT motifs are not linked by coiled-coils but rather by flexible loop (thus suggesting that FAPP2 might operate as monomer), CERT has a predicted coiled-coil region. However, both proteins colocalise with OSBP and Nir2 at ER-TGN contact sites. Therefore, CERT and FAPP2 might simply benefit from the "entropic shields" of their neighbours.

A particular case is ORP9. This ORP is highly abundant in HeLa cells and has been reported to target ER and Golgi membranes via its FFAT motif and PH domain (Kulak *et al.*, 2014; Liu and Ridgway, 2014; Ngo and Ridgway, 2009; Wyles and Ridgway, 2004). ORP9 can form heterodimers with its close relatives, ORP10 and ORP11, which lack the FFAT motif (Nissilä *et al.*, 2012; Zhou *et al.*, 2010). These observations suggest a role of ORP9 in mediating ER-tethering of ORP10 and ORP11. It is noteworthy that ORP10 and ORP11 are also abundant and both contain long disordered tails, indicating that heterodimeric complexes may indeed be a reciprocal solution for involved proteins to obtain ER-targeting signal (FFAT motif) and keep proper membrane dynamics (disordered N-terminus). Alternatively, the properties of coiled-coils of ORP9 alone may intervene with possible homotypic tethering. Experiments to elucidate the structure and membrane tethering abilities of this peculiar ORP are currently ongoing in our team.

As presented in this study, disordered tails vary considerably between individual LTPs, which may reflect either a weaker degree of sequence conservation (typical for IDPRs) or additional functions of disordered domains. Charge patterns, hydropobicity, amino acid length etc. play an important role in biophysics of IDPRs. Naturally,

variations in these parameters may lead to differences in dynamics (such as diffusion) and protein-protein or protein-membrane interactions by disordered regions.

Regarding protein diffusion and intrinsic disorder, it has been reported that with increasing concentration and size of crowding agents (such as proteins) in solution, intrinsic disorder plays more and more important role in enhancing protein diffusion (Wang *et al.*, 2017). In the context of LTPs, such observation necessarily gives us a hint to an important issue: diffusion behavior of proteins in a confined environment co-occupied by a large amount of neighbouring proteins with distinct properties also depends on the properties of these "neighbours". This means that diffusion behavior of membrane-interacting domains decorated by intrinsic disorder in crowded environments is rather nontrivial and deserves comprehensive theory- and experiment-based understanding, which, however, is still lacking.

Regarding additional functions in protein-protein or protein-membrane interactions of disordered regions in LTPs, we know that IDPs/IDPRs are commonly attributed to functional areas relying on their ability to interact with multiple partners via high-specificity/low-affinity interactions (Uversky *et al.*, 2018). It is therefore tempting to hypothesize that the N-termini of ORPs could be also involved in mentioned interactions. For example, Ghai *et al.* (2017) performed isothermal calorimetry experiments with PH domains of ORP5 and ORP8. They reported no binding to monophosphorylated PIPs and rather modest binding to dually phosphorylated PIPs. When the PH domain of ORP8 was crystallized, its 3D structure revealed an atypical binding site for PIPs away from the canonical binding site, explaining the weak affinity for PIPs. Subsequently, systematic truncation of the N-termini of ORP5 and ORP8 revealed their crucial role in proper PM targeting and it has been postulated that their polybasic regions may serve as coincindence detectors, complementing the weak PIPs binding by certain PH domains with electrostatic interactions on the surface of negatively charged PM (Ghai et al., 2017; Lee and Fairn, 2018). This principle might be similar to the lipid cooperativity that has been observed e.g. for PH domains with weak affinity for single phosphoinositide species. These PH domains coincidentally recognize the presence of other, auxiliary lipids, such as distinct phosphoinositide species, ceramides or phosphatidylserine to recruit peripheral proteins to specific subcellular membranes (Macia et al., 2000; Vonkova et al., 2015).

Similarly, membrane-attached disordered regions could participate in protein-protein interactions and facilitate the formation of multiprotein complexes, as shown for the clathrin adaptor proteins AP180 and AP2 (Kalthoff et al., 2002; Owen et al., 1999). In extreme cases, protein-protein interactions mediated by IDPs/IDPRs may even lead to formation of aggregates, as in the case of α-synuclein-related pathologies (Uversky and Eliezer, 2009). Nevertheless, an opposite aspect must also be kept in mind – N-termini may equally serve to prevent undesirable or excessive interactions. For example, presence of highly flexible regions has been shown to reduce tendency of ordered proteins to aggregate, most likely as a result of conformational entropy (De Simone et al., 2012).

Therefore, we can assume that unfolded terminal regions of LTPs may perform additional functions which may well correspond with their diversity. Even in this PhD work, we may have identified an additional role for the N-terminus of ORP4 as we noticed that overexpression of ΔN-ORP4 in HeLa cells leads to collapsed vimentin network (**Figure 50 C**). Nevertheless, the fact that two different N-termini (OSBP and ORP4) display similar effects on membrane tethering properties *in vitro* and protein mobility in living cells suggests that the control of MCS geometry and protein density on membranes constitutes a plausible unifying function. Taken together, our study brings a novel view on disordered N-terminal regions of OSBP and related proteins as important regulators of protein orientation and dynamics on membrane.

CONCLUSION AND PERSPECTIVES

Most proteins from the mammalian ORP family contain an intrinsically disordered sequence upstream of their PH domains. Moreover, several other LTPs with similar domain architecture also possess a disordered N-terminus. In ORPs, N-termini differ in length (between 50 and 140 residues) and amino acid composition – some are nonpolar (OSBP, ORP10, ORP11) whereas others contain charged residues (ORP4, ORP5, ORP8). One common denominator seems to be the mere presence of intrinsic disorder. Until now, very little attention has been given to the unfolded tail regions of ORPs, and there was no explanation at all for the rather general necessity of intrinsic disorder around the membrane binding domains of several (mostly) dimeric and highly abundant LTPs.

This thesis work provides solid evidence for the role of unstructured N-terminus in regulating OSBP tethering geometry and dynamics at OSBP-mediated contact sites both *in vitro* and in living cells. We show that N-terminal sequence occupies a large volume, thus limiting protein recruitment to PI(4)P-rich membranes. In addition, when two PH domains of dimeric OSBP are not flanked by the N-terminal entropic "shield" they tend to bridge PI(4)P-rich membranes in an aberrant Golgi-Golgi (homotypic/symmetrical) manner. Homotypic tethering depends on the presence of PI(4)P or Arf1-GTP in membrane and on the ability of OSBP-derived constructs to dimerize. This indicates that disordered tail plays a crucial role in regulating membrane tethering geometry of OSBP. Due to its effect on volume extension around the PH domain, N-terminus is an effective regulator of protein density and lateral mobility within the confined environment of MCS, as demonstrated in our *in vitro* and *in cellulo* FRAP assays. Although the change in protein spacing did not initially seem to affect lipid transfer activity, we found that OSBP turnover during assembly/disassembly cycles of MCS in conditions with restricted PI(4)P synthesis is impaired. Thus, we also revealed a function of intrinsic disorder in regulating OSBP dynamics during lipid transfer cycles in living cells.

In addition, our research on N-terminus of OSBP is supported by findings from assays with ORP4, a close homolog of OSBP with remarkably different N-terminus.

Truncated ORP4 constructs lacking the disordered region are, similarly to related OSBP constructs, capable of homotypic tethering. Consistently, in FRAP assays we observed a slower protein recovery. Taken together, we found a unifying role for two very distinct N-termini. This role could possibly extend to disordered tails in many other ORPs and even non-related but similarly organized LTPs (such as Nir proteins or LAMs).

However, there are still many questions that remain open. An important issue to test is, for example, the compatibility between different N-termini within the same MCS. Are N-termini with similar properties preferably distributed in the same environment? Can change in the length of disordered sequence or in its amino acid composition influence the preference of LTPs for certain microenvironments? Can N-terminal tails be interchanged between distinct ORPs without affecting their function? For now, we do not know, but these questions certainly deserve further investigation.

As a final remark, understanding MCS complexity and dynamics in the context of membrane tethering proteins containing large regions of intrinsic disorder is an important topic, which can yield insight into several fields of membrane biology. Our present work represents an instructive framework to study this issue on the example of OSBP and its related proteins at ER-TGN contact sites. The next step forward could be a closer examination of other LTPs or tethering proteins along the lines presented in this thesis.

LIST OF REFERENCES

Almén, M., Nordström, K.J., Fredriksson, R., Schiöth, H.B., 2009. Mapping the human membrane proteome: a majority of the human membrane proteins can be classified according to function and evolutionary origin. BMC Biol. 7, 50. https://doi.org/10.1186/1741-7007-7-50

Andrew Karplus, P., 1997. Hydrophobicity regained: Hydrophobicity regained. Protein Sci. 6, 1302–1307. https://doi.org/10.1002/pro.5560060618

Anniss, A.M., Apostolopoulos, J., Dworkin, S., Purton, L.E., Sparrow, R.L., 2002. An oxysterol-binding protein family identified in the mouse. DNA Cell Biol. 21, 571–580. https://doi.org/10.1089/104454902320308942

Antonny, B., Bigay, J., Mesmin, B., 2018. The Oxysterol-Binding Protein Cycle: Burning Off PI(4)P to Transport Cholesterol. Annu. Rev. Biochem. 87, 809–837. https://doi.org/10.1146/annurev-biochem-061516-044924

Asp, L., Kartberg, F., Fernandez-Rodriguez, J., Smedh, M., Elsner, M., Laporte, F., Bárcena, M., Jansen, K.A., Valentijn, J.A., Koster, A.J., Bergeron, J.J.M., Nilsson, T., 2009. Early Stages of Golgi Vesicle and Tubule Formation Require Diacylglycerol. Mol. Biol. Cell 20, 780–790. https://doi.org/10.1091/mbc.e08-03-0256

Avalos, J.L., Celic, I., Muhammad, S., Cosgrove, M.S., Boeke, J.D., Wolberger, C., n.d. Structure of a Sir2 Enzyme Bound to an Acetylated p53 Peptide. Mol. Cell 13.

Avantaggiati, M.L., Ogryzko, V., Gardner, K., Giordano, A., Levine, A.S., Kelly, K., 1997. Recruitment of p300/CBP in p53-Dependent Signal Pathways. Cell 89, 1175–1184. https://doi.org/10.1016/S0092-8674(00)80304-9

Babu, M.M., 2016. The contribution of intrinsically disordered regions to protein function, cellular complexity, and human disease. Biochem. Soc. Trans. 44, 1185–1200. https://doi.org/10.1042/BST20160172

Bah, A., Vernon, R.M., Siddiqui, Z., Krzeminski, M., Muhandiram, R., Zhao, C., Sonenberg, N., Kay, L.E., Forman-Kay, J.D., 2015. Folding of an intrinsically disordered protein by phosphorylation as a regulatory switch. Nature 519, 106–109. https://doi.org/10.1038/nature13999

Balla, T., 2013. Phosphoinositides: Tiny Lipids With Giant Impact on Cell Regulation. Physiol. Rev. 93, 1019–1137. https://doi.org/10.1152/physrev.00028.2012

Banerji, S., Ngo, M., Lane, C.F., Robinson, C.-A., Minogue, S., Ridgway, N.D., 2010. Oxysterol Binding Protein-dependent Activation of Sphingomyelin Synthesis in the Golgi Apparatus Requires Phosphatidylinositol 4-Kinase II␣. Mol. Biol. Cell 21, 10.

Baron, C.L., Malhotra, V., 2002. Role of diacylglycerol in PKD recruitment to the TGN and protein transport to the plasma membrane. Science 295, 325–328. https://doi.org/10.1126/science.1066759

Beh, C.T., Cool, L., Phillips, J., Rine, J., 2001. Overlapping functions of the yeast oxysterol-binding protein homologues. Genetics 157, 1117–1140.

Beh, C.T., Rine, J., 2004. A role for yeast oxysterol-binding protein homologs in endocytosis and in the maintenance of intracellular sterol-lipid distribution. J. Cell Sci. 117, 2983–2996. https://doi.org/10.1242/jcs.01157

Berridge, M.J., Irvine, R.F., 1984. Inositol trisphosphate, a novel second messenger in cellular signal transduction. Nature 312, 315–321.

Bigay, J., Antonny, B., 2012. Curvature, Lipid Packing, and Electrostatics of Membrane Organelles: Defining Cellular Territories in Determining Specificity. Dev. Cell 23, 886–895. https://doi.org/10.1016/j.devcel.2012.10.009

Bigay, J., Casella, J.-F., Drin, G., Mesmin, B., Antonny, B., 2005. ArfGAP1 responds to membrane curvature through the folding of a lipid packing sensor motif. EMBO J. 24, 2244–2253. https://doi.org/10.1038/sj.emboj.7600714
Bloj, B., Zilversmit, D.B., 1977. Complete exchangeability of cholesterol in phosphatidylcholine/cholesterol vesicles of different degrees of unsaturation. Biochemistry 16, 3943–3948. https://doi.org/10.1021/bi00637a001
Boczek, E.E., Alberti, S., 2018. Phase changes in neurotransmission. Science 361, 548–549. https://doi.org/10.1126/science.aau5477
Boesch, C., Bundi, A., Oppliger, M., WuTHRICH, K., 1978. 1H Nuclear-Magnetic-Resonance Studies of the Molecular Conformation of Monomeric Glucagon in Aqueous Solution. Eur. J. Biochem. 91, 209–214. https://doi.org/10.1111/j.1432-1033.1978.tb20953.x
Bonifacino, J.S., Dell'Angelica, E.C., 1999. Molecular Bases for the Recognition of Tyrosine-based Sorting Signals: Figure 1. J. Cell Biol. 145, 923–926. https://doi.org/10.1083/jcb.145.5.923
Bonifacino, J.S., Glick, B.S., 2004. The Mechanisms of Vesicle Budding and Fusion. Cell 116, 153–166. https://doi.org/10.1016/S0092-8674(03)01079-1
Borzova, V.A., Markossian, K.A., Chebotareva, N.A., Kleymenov, S.Y., Poliansky, N.B., Muranov, K.O., Stein-Margolina, V.A., Shubin, V.V., Markov, D.I., Kurganov, B.I., 2016. Kinetics of Thermal Denaturation and Aggregation of Bovine Serum Albumin. PLOS ONE 11, e0153495. https://doi.org/10.1371/journal.pone.0153495
Bozoky, Z., Krzeminski, M., Muhandiram, R., Birtley, J.R., Al-Zahrani, A., Thomas, P.J., Frizzell, R.A., Ford, R.C., Forman-Kay, J.D., 2013. Regulatory R region of the CFTR chloride channel is a dynamic integrator of phospho-dependent intra- and intermolecular interactions. Proc. Natl. Acad. Sci. 110, E4427–E4436. https://doi.org/10.1073/pnas.1315104110
Bretscher, M.S., 1973. Membrane Structure: Some General Principles. Science 181, 622–629. https://doi.org/10.1126/science.181.4100.622
Brown, M.S., Goldstein, J.L., 1997. The SREBP pathway: regulation of cholesterol metabolism by proteolysis of a membrane-bound transcription factor. Cell 89, 331–340.
Burgett, A.W.G., Poulsen, T.B., Wangkanont, K., Anderson, D.R., Kikuchi, C., Shimada, K., Okubo, S., Fortner, K.C., Mimaki, Y., Kuroda, M., Murphy, J.P., Schwalb, D.J., Petrella, E.C., Cornella-Taracido, I., Schirle, M., Tallarico, J.A., Shair, M.D., 2011. Natural products reveal cancer cell dependence on oxysterol-binding proteins. Nat. Chem. Biol. 7, 639–647. https://doi.org/10.1038/nchembio.625
Charman, M., Colbourne, T.R., Pietrangelo, A., Kreplak, L., Ridgway, N.D., 2014. Oxysterol-binding Protein (OSBP)-related Protein 4 (ORP4) Is Essential for Cell Proliferation and Survival. J. Biol. Chem. 289, 15705–15717. https://doi.org/10.1074/jbc.M114.571216
Chiapparino, A., Maeda, K., Turei, D., Saez-Rodriguez, J., Gavin, A.-C., 2016. The orchestra of lipid-transfer proteins at the crossroads between metabolism and signaling. Prog. Lipid Res. 61, 30–39. https://doi.org/10.1016/j.plipres.2015.10.004
Chidambaram, S., Müllers, N., Wiederhold, K., Haucke, V., von Mollard, G.F., 2004. Specific Interaction between SNAREs and Epsin N-terminal Homology (ENTH) Domains of Epsin-related Proteins in *trans* -Golgi Network to Endosome Transport. J. Biol. Chem. 279, 4175–4179. https://doi.org/10.1074/jbc.M308667200
Chung, J., Torta, F., Masai, K., Lucast, L., Czapla, H., Tanner, L.B., Narayanaswamy, P., Wenk, M.R., Nakatsu, F., De Camilli, P., 2015. PI4P/phosphatidylserine countertransport at ORP5- and ORP8-mediated ER-plasma membrane contacts. Science 349, 428–432. https://doi.org/10.1126/science.aab1370
Combet, C., Blanchet, C., Geourjon, C., Deléage, G., 2000. NPS@: network protein sequence analysis. Trends Biochem. Sci. 25, 147–150.
Copeland, D.E., Dalton, A.J., 1959. An association between mitochondria and the endoplasmic reticulum in cells of the pseudobranch gland of a teleost. J. Biophys. Biochem. Cytol. 5, 393–396.

Čopič, A., Antoine-Bally, S., Giménez-Andrés, M., La Torre Garay, C., Antonny, B., Manni, M.M., Pagnotta, S., Guihot, J., Jackson, C.L., 2018. A giant amphipathic helix from a perilipin that is adapted for coating lipid droplets. Nat. Commun. 9. https://doi.org/10.1038/s41467-018-03717-8

Courtney, K.C., Pezeshkian, W., Raghupathy, R., Zhang, C., Darbyson, A., Ipsen, J.H., Ford, D.A., Khandelia, H., Presley, J.F., Zha, X., 2018. C24 Sphingolipids Govern the Transbilayer Asymmetry of Cholesterol and Lateral Organization of Model and Live-Cell Plasma Membranes. Cell Rep. 24, 1037–1049. https://doi.org/10.1016/j.celrep.2018.06.104

Crabtree, M.D., Mendonça, C.A.T.F., Bubb, Q.R., Clarke, J., 2018. Folding and binding pathways of BH3-only proteins are encoded within their intrinsically disordered sequence, not templated by partner proteins. J. Biol. Chem. 293, 9718–9723. https://doi.org/10.1074/jbc.RA118.002791

D'Angelo, G., Polishchuk, E., Di Tullio, G., Santoro, M., Di Campli, A., Godi, A., West, G., Bielawski, J., Chuang, C.-C., van der Spoel, A.C., Platt, F.M., Hannun, Y.A., Polishchuk, R., Mattjus, P., De Matteis, M.A., 2007. Glycosphingolipid synthesis requires FAPP2 transfer of glucosylceramide. Nature 449, 62–67. https://doi.org/10.1038/nature06097

Daniels, A.J., Williams, R.J.P., Wright, P.E., 1978. The character of the stored molecules in chromaffin granules of the adrenal medulla: A nuclear magnetic resonance study. Neuroscience 3, 573–585. https://doi.org/10.1016/0306-4522(78)90022-2

Darling, A.L., Liu, Y., Oldfield, C.J., Uversky, V.N., 2018. Intrinsically Disordered Proteome of Human Membrane-Less Organelles. PROTEOMICS 18, 1700193. https://doi.org/10.1002/pmic.201700193

Das, R.K., Pappu, R.V., 2013. Conformations of intrinsically disordered proteins are influenced by linear sequence distributions of oppositely charged residues. Proc. Natl. Acad. Sci. 110, 13392–13397. https://doi.org/10.1073/pnas.1304749110

Das, R.K., Ruff, K.M., Pappu, R.V., 2015. Relating sequence encoded information to form and function of intrinsically disordered proteins. Curr. Opin. Struct. Biol. 32, 102–112. https://doi.org/10.1016/j.sbi.2015.03.008

Dawson, P.A., Ridgway, N.D., Slaughter, C.A., Brown, M.S., Goldstein, J.L., 1989a. cDNA cloning and expression of oxysterol-binding protein, an oligomer with a potential leucine zipper. J. Biol. Chem. 264, 16798–16803.

Dawson, P.A., Van der Westhuyzen, D.R., Goldstein, J.L., Brown, M.S., 1989b. Purification of oxysterol binding protein from hamster liver cytosol. J. Biol. Chem. 264, 9046–9052.

de Brito, O.M., Scorrano, L., 2008. Mitofusin 2 tethers endoplasmic reticulum to mitochondria. Nature 456, 605–610. https://doi.org/10.1038/nature07534

de Saint-Jean, M., Delfosse, V., Douguet, D., Chicanne, G., Payrastre, B., Bourguet, W., Antonny, B., Drin, G., 2011. Osh4p exchanges sterols for phosphatidylinositol 4-phosphate between lipid bilayers. J. Cell Biol. 195, 965–978. https://doi.org/10.1083/jcb.201104062

De Simone, A., Kitchen, C., Kwan, A.H., Sunde, M., Dobson, C.M., Frenkel, D., 2012. Intrinsic disorder modulates protein self-assembly and aggregation. Proc. Natl. Acad. Sci. 109, 6951–6956. https://doi.org/10.1073/pnas.1118048109

DeBose-Boyd, R.A., 2008. Feedback regulation of cholesterol synthesis: sterol-accelerated ubiquitination and degradation of HMG CoA reductase. Cell Res. 18, 609–621. https://doi.org/10.1038/cr.2008.61

Demarest, S.J., Martinez-Yamout, M., Chung, J., Chen, H., Xu, W., Dyson, H.J., Evans, R.M., Wright, P.E., 2002. Mutual synergistic folding in recruitment of CBP/p300 by p160 nuclear receptor coactivators. Nature 415, 549–553. https://doi.org/10.1038/415549a

Deng, Y., Rivera-Molina, F.E., Toomre, D.K., Burd, C.G., 2016. Sphingomyelin is sorted at the trans Golgi network into a distinct class of secretory vesicle. Proc. Natl. Acad. Sci. U. S. A. 113, 6677–6682. https://doi.org/10.1073/pnas.1602875113

Dereeper, A., Guignon, V., Blanc, G., Audic, S., Buffet, S., Chevenet, F., Dufayard, J.-F., Guindon, S., Lefort, V., Lescot, M., Claverie, J.-M., Gascuel, O., 2008. Phylogeny.fr: robust phylogenetic analysis for the non-specialist. Nucleic Acids Res. 36, W465-469. https://doi.org/10.1093/nar/gkn180

Dietrich, C., Yang, B., Fujiwara, T., Kusumi, A., Jacobson, K., 2002. Relationship of Lipid Rafts to Transient Confinement Zones Detected by Single Particle Tracking. Biophys. J. 82, 274–284. https://doi.org/10.1016/S0006-3495(02)75393-9
Dippold, H.C., Ng, M.M., Farber-Katz, S.E., Lee, S.-K., Kerr, M.L., Peterman, M.C., Sim, R., Wiharto, P.A., Galbraith, K.A., Madhavarapu, S., Fuchs, G.J., Meerloo, T., Farquhar, M.G., Zhou, H., Field, S.J., 2009. GOLPH3 Bridges Phosphatidylinositol-4- Phosphate and Actomyosin to Stretch and Shape the Golgi to Promote Budding. Cell 139, 337–351. https://doi.org/10.1016/j.cell.2009.07.052
Dix, J.A., Verkman, A.S., 2008. Crowding Effects on Diffusion in Solutions and Cells. Annu. Rev. Biophys. 37, 247–263. https://doi.org/10.1146/annurev.biophys.37.032807.125824
Domański, J., Marrink, S.J., Schäfer, L.V., 2012. Transmembrane helices can induce domain formation in crowded model membranes. Biochim. Biophys. Acta BBA - Biomembr. 1818, 984–994. https://doi.org/10.1016/j.bbamem.2011.08.021
Dong, R., Saheki, Y., Swarup, S., Lucast, L., Harper, J.W., De Camilli, P., 2016. Endosome-ER Contacts Control Actin Nucleation and Retromer Function through VAP-Dependent Regulation of PI4P. Cell 166, 408–423. https://doi.org/10.1016/j.cell.2016.06.037
Dosztányi, Z., Chen, J., Dunker, A.K., Simon, I., Tompa, P., 2006. Disorder and Sequence Repeats in Hub Proteins and Their Implications for Network Evolution. J. Proteome Res. 5, 2985–2995. https://doi.org/10.1021/pr060171o
Drin, G., 2014. Topological Regulation of Lipid Balance in Cells. Annu. Rev. Biochem. 83, 51–77. https://doi.org/10.1146/annurev-biochem-060713-035307
Drin, G., Antonny, B., 2010. Amphipathic helices and membrane curvature. FEBS Lett. 584, 1840–1847. https://doi.org/10.1016/j.febslet.2009.10.022
Du, X., Kumar, J., Ferguson, C., Schulz, T.A., Ong, Y.S., Hong, W., Prinz, W.A., Parton, R.G., Brown, A.J., Yang, H., 2011. A role for oxysterol-binding protein-related protein 5 in endosomal cholesterol trafficking. J. Cell Biol. 192, 121–135. https://doi.org/10.1083/jcb.201004142
Du, X., Zadoorian, A., Lukmantara, I.E., Qi, Y., Brown, A.J., Yang, H., 2018. Oxysterol-binding protein–related protein 5 (ORP5) promotes cell proliferation by activation of mTORC1 signaling. J. Biol. Chem. 293, 3806–3818. https://doi.org/10.1074/jbc.RA117.001558
Dufourc, E.J., 2008. Sterols and membrane dynamics. J. Chem. Biol. 1, 63–77. https://doi.org/10.1007/s12154-008-0010-6
Dunlop, M.H., Ernst, A.M., Schroeder, L.K., Toomre, D.K., Lavieu, G., Rothman, J.E., 2017. Land-locked mammalian Golgi reveals cargo transport between stable cisternae. Nat. Commun. 8, 432. https://doi.org/10.1038/s41467-017-00570-z
Dunphy, W.G., Rothman, J.E., 1985. Compartmental organization of the Golgi stack. Cell 42, 13–21.
Dupuy, A.D., Engelman, D.M., 2008. Protein area occupancy at the center of the red blood cell membrane. Proc. Natl. Acad. Sci. 105, 2848–2852. https://doi.org/10.1073/pnas.0712379105
Dutta, S., Bhattacharyya, D., 2001. Size of Unfolded and Dissociated Subunits versus that of Native Multimeric Proteins. J. Biol. Phys. 27, 59–71. https://doi.org/10.1023/A:1011826525684
Dyson, H.J., Wright, P.E., 2005. Intrinsically unstructured proteins and their functions. Nat. Rev. Mol. Cell Biol. 6, 197–208. https://doi.org/10.1038/nrm1589
Elbaum-Garfinkle, S., Kim, Y., Szczepaniak, K., Chen, C.C.-H., Eckmann, C.R., Myong, S., Brangwynne, C.P., 2015. The disordered P granule protein LAF-1 drives phase separation into droplets with tunable viscosity and dynamics. Proc. Natl. Acad. Sci. 112, 7189–7194. https://doi.org/10.1073/pnas.1504822112
Evans, P., 2002. Endocytosis and vesicle trafficking. Curr. Opin. Struct. Biol. 12, 814–821. https://doi.org/10.1016/S0959-440X(02)00395-0
Fabiato, A., 1983. Calcium-induced release of calcium from the cardiac sarcoplasmic reticulum. Am. J. Physiol. 245, C1-14. https://doi.org/10.1152/ajpcell.1983.245.1.C1

Fadok, V.A., Voelker, D.R., Campbell, P.A., Cohen, J.J., Henson, P.M., n.d. Exposure of phosphatidylserine on the surface of apoptotic lymphocytes triggers specific recognition and removal by macrophages. 11.
Faulhammer, F., Kanjilal-Kolar, S., Knödler, A., Lo, J., Lee, Y., Konrad, G., Mayinger, P., 2007. Growth control of Golgi phosphoinositides by reciprocal localization of sac1 lipid phosphatase and pik1 4-kinase. Traffic Cph. Den. 8, 1554–1567. https://doi.org/10.1111/j.1600-0854.2007.00632.x
Fischer, M.A., Temmerman, K., Ercan, E., Nickel, W., Seedorf, M., 2009. Binding of plasma membrane lipids recruits the yeast integral membrane protein Ist2 to the cortical ER. Traffic Cph. Den. 10, 1084–1097. https://doi.org/10.1111/j.1600-0854.2009.00926.x
Foti, M., Audhya, A., Emr, S.D., 2001. Sac1 lipid phosphatase and Stt4 phosphatidylinositol 4-kinase regulate a pool of phosphatidylinositol 4-phosphate that functions in the control of the actin cytoskeleton and vacuole morphology. Mol. Biol. Cell 12, 2396–2411. https://doi.org/10.1091/mbc.12.8.2396
Fournier, M.V., Guimarães da Costa, F., Paschoal, M.E., Ronco, L.V., Carvalho, M.G., Pardee, A.B., Giumaraes, F.C., 1999. Identification of a gene encoding a human oxysterol-binding protein-homologue: a potential general molecular marker for blood dissemination of solid tumors. Cancer Res. 59, 3748–3753.
Franco, M., Chardin, P., Chabre, M., Paris, S., 1995. Myristoylation of ADP-ribosylation Factor 1 Facilitates Nucleotide Exchange at Physiological Mg Levels. J. Biol. Chem. 270, 1337–1341. https://doi.org/10.1074/jbc.270.3.1337
Friedman, J.R., Lackner, L.L., West, M., DiBenedetto, J.R., Nunnari, J., Voeltz, G.K., 2011. ER tubules mark sites of mitochondrial division. Science 334, 358–362. https://doi.org/10.1126/science.1207385
Friedman, J.R., Nunnari, J., 2014. Mitochondrial form and function. Nature 505, 335–343. https://doi.org/10.1038/nature12985
Furuita, K., Jee, J., Fukada, H., Mishima, M., Kojima, C., 2010. Electrostatic Interaction between Oxysterol-binding Protein and VAMP-associated Protein A Revealed by NMR and Mutagenesis Studies. J. Biol. Chem. 285, 12961–12970. https://doi.org/10.1074/jbc.M109.082602
Futerman, A.H., Riezman, H., 2005. The ins and outs of sphingolipid synthesis. Trends Cell Biol. 15, 312–318. https://doi.org/10.1016/j.tcb.2005.04.006
Fuxreiter, M., 2012. Fuzziness: linking regulation to protein dynamics. Mol BioSyst 8, 168–177. https://doi.org/10.1039/C1MB05234A
Galmes, R., Houcine, A., van Vliet, A.R., Agostinis, P., Jackson, C.L., Giordano, F., 2016. ORP5/ORP8 localize to endoplasmic reticulum-mitochondria contacts and are involved in mitochondrial function. EMBO Rep. 17, 800–810. https://doi.org/10.15252/embr.201541108
Gambin, Y., Lopez-Esparza, R., Reffay, M., Sierecki, E., Gov, N.S., Genest, M., Hodges, R.S., Urbach, W., 2006. Lateral mobility of proteins in liquid membranes revisited. Proc. Natl. Acad. Sci. U. S. A. 103, 2098–2102. https://doi.org/10.1073/pnas.0511026103
Gast, K., Damaschun, H., Eckert, K., Schulze-Forster, K., Maurer, H.R., Mueller-Frohne, M., Zirwer, D., Czarnecki, J., Damaschun, G., 1995. Prothymosin .alpha.: A Biologically Active Protein with Random Coil Conformation. Biochemistry 34, 13211–13218. https://doi.org/10.1021/bi00040a037
Gasteiger, E., Hoogland, C., Gattiker, A., Duvaud, S., Wilkins, M.R., Appel, R.D., Bairoch, A., 2005. Protein Identification and Analysis Tools on the ExPASy Server, in: Walker, J.M. (Ed.), The Proteomics Protocols Handbook. Humana Press, Totowa, NJ, pp. 571–607. https://doi.org/10.1385/1-59259-890-0:571
Gatta, A.T., Wong, L.H., Sere, Y.Y., Calderón-Noreña, D.M., Cockcroft, S., Menon, A.K., Levine, T.P., 2015. A new family of StART domain proteins at membrane contact sites has a role in ER-PM sterol transport. eLife 4. https://doi.org/10.7554/eLife.07253
Ghai, R., Du, X., Wang, H., Dong, J., Ferguson, C., Brown, A.J., Parton, R.G., Wu, J.-W., Yang, H., 2017. ORP5 and ORP8 bind phosphatidylinositol-4, 5-biphosphate (PtdIns(4,5)P 2) and

regulate its level at the plasma membrane. Nat. Commun. 8. https://doi.org/10.1038/s41467-017-00861-5
Gibson Wood, W., Igbavboa, U., Müller, W.E., Eckert, G.P., 2011. Cholesterol asymmetry in synaptic plasma membranes: Brain membrane cholesterol asymmetry. J. Neurochem. 116, 684–689. https://doi.org/10.1111/j.1471-4159.2010.07017.x
Giménez-Andrés, M., Čopič, A., Antonny, B., 2018. The Many Faces of Amphipathic Helices. Biomolecules 8, 45. https://doi.org/10.3390/biom8030045
Godi, A., Campli, A.D., Konstantakopoulos, A., Tullio, G.D., Alessi, D.R., Kular, G.S., Daniele, T., Marra, P., Lucocq, J.M., Matteis, M.A.D., 2004. FAPPs control Golgi-to-cell-surface membrane traffic by binding to ARF and PtdIns(4)P. Nat. Cell Biol. 6, 393–404. https://doi.org/10.1038/ncb1119
Goldfinger, L.E., Ptak, C., Jeffery, E.D., Shabanowitz, J., Han, J., Haling, J.R., Sherman, N.E., Fox, J.W., Hunt, D.F., Ginsberg, M.H., 2007. An experimentally derived database of candidate Ras-interacting proteins. J. Proteome Res. 6, 1806–1811. https://doi.org/10.1021/pr060630l
Goose, J.E., Sansom, M.S.P., 2013. Reduced Lateral Mobility of Lipids and Proteins in Crowded Membranes. PLoS Comput. Biol. 9, e1003033. https://doi.org/10.1371/journal.pcbi.1003033
Gsponer, J., Madan Babu, M., 2009. The rules of disorder or why disorder rules. Prog. Biophys. Mol. Biol. 99, 94–103. https://doi.org/10.1016/j.pbiomolbio.2009.03.001
Guigas, G., Weiss, M., 2008. Influence of hydrophobic mismatching on membrane protein diffusion. Biophys. J. 95, L25-27. https://doi.org/10.1529/biophysj.108.136069
Guo, X., Zhang, L., Fan, Y., Zhang, D., Qin, L., Dong, S., Li, G., 2017. Oxysterol-Binding Protein-Related Protein 8 Inhibits Gastric Cancer Growth Through Induction of ER Stress, Inhibition of Wnt Signaling, and Activation of Apoptosis. Oncol. Res. 25, 799–808. https://doi.org/10.3727/096504016X14783691306605
Hanada, K, 2018. Lipid-transfer proteins rectify inter-organelle flux and accurately deliver lipids at membrane contact sites 69.
Hanada, K., Kumagai, K., Yasuda, S., Miura, Y., Kawano, M., Fukasawa, M., Nishijima, M., 2003. Molecular machinery for non-vesicular trafficking of ceramide. Nature 426, 803–809. https://doi.org/10.1038/nature02188
Hankins, H.M., Baldridge, R.D., Xu, P., Graham, T.R., 2015. Role of Flippases, Scramblases and Transfer Proteins in Phosphatidylserine Subcellular Distribution. Traffic 16, 35–47. https://doi.org/10.1111/tra.12233
Harayama, T., Riezman, H., 2018. Understanding the diversity of membrane lipid composition. Nat. Rev. Mol. Cell Biol. 19, 281–296. https://doi.org/10.1038/nrm.2017.138
Harlan, J.E., Hajduk, P.J., Yoon, H.S., Fesik, S.W., 1994. Pleckstrin homology domains bind to phosphatidylinositol-4,5-bisphosphate. Nature 371, 168–170. https://doi.org/10.1038/371168a0
He, B., Wang, K., Liu, Y., Xue, B., Uversky, V.N., Dunker, A.K., 2009. Predicting intrinsic disorder in proteins: an overview. Cell Res. 19, 929–949. https://doi.org/10.1038/cr.2009.87
Herdman, C., Moss, T., 2016. Extended-Synaptotagmins (E-Syts); the extended story. Pharmacol. Res. 107, 48–56. https://doi.org/10.1016/j.phrs.2016.01.034
Hinard, V., Britan, A., Rougier, J.S., Bairoch, A., Abriel, H., Gaudet, P., 2016. ICEPO: the ion channel electrophysiology ontology. Database 2016, baw017. https://doi.org/10.1093/database/baw017
Hirata, Y., Brotto, M., Weisleder, N., Chu, Y., Lin, P., Zhao, X., Thornton, A., Komazaki, S., Takeshima, H., Ma, J., Pan, Z., 2006. Uncoupling store-operated Ca2+ entry and altered Ca2+ release from sarcoplasmic reticulum through silencing of junctophilin genes. Biophys. J. 90, 4418–4427. https://doi.org/10.1529/biophysj.105.076570
Hoshi, T., Zagotta, W., Aldrich, R., 1990. Biophysical and molecular mechanisms of Shaker potassium channel inactivation. Science 250, 533–538. https://doi.org/10.1126/science.2122519

Hoyer, M.J., Chitwood, P.J., Ebmeier, C.C., Striepen, J.F., Qi, R.Z., Old, W.M., Voeltz, G.K., 2018. A Novel Class of ER Membrane Proteins Regulates ER-Associated Endosome Fission. Cell 175, 254-265.e14. https://doi.org/10.1016/j.cell.2018.08.030
Huber, R., Bennett, W.S., 1983. Functional significance of flexibility in proteins. Biopolymers 22, 261–279. https://doi.org/10.1002/bip.360220136
Hynynen, R., Suchanek, M., Spandl, J., Bäck, N., Thiele, C., Olkkonen, V.M., 2009. OSBP-related protein 2 is a sterol receptor on lipid droplets that regulates the metabolism of neutral lipids. J. Lipid Res. 50, 1305–1315. https://doi.org/10.1194/jlr.M800661-JLR200
Ikonen, E., 2008. Cellular cholesterol trafficking and compartmentalization. Nat. Rev. Mol. Cell Biol. 9, 125–138. https://doi.org/10.1038/nrm2336
Im, Y.J., Raychaudhuri, S., Prinz, W.A., Hurley, J.H., 2005. Structural mechanism for sterol sensing and transport by OSBP-related proteins. Nature 437, 154–158. https://doi.org/10.1038/nature03923
Ishikawa-Sasaki, K., Nagashima, S., Taniguchi, K., Sasaki, J., 2018. Model of OSBP-Mediated Cholesterol Supply to Aichi Virus RNA Replication Sites Involving Protein-Protein Interactions among Viral Proteins, ACBD3, OSBP, VAP-A/B, and SAC1. J. Virol. 92. https://doi.org/10.1128/JVI.01952-17
Jain, A., Holthuis, J.C.M., 2017. Membrane contact sites, ancient and central hubs of cellular lipid logistics. Biochim. Biophys. Acta BBA - Mol. Cell Res. 1864, 1450–1458. https://doi.org/10.1016/j.bbamcr.2017.05.017
Javanainen, M., Hammaren, H., Monticelli, L., Jeon, J.-H., Miettinen, M.S., Martinez-Seara, H., Metzler, R., Vattulainen, I., 2013. Anomalous and normal diffusion of proteins and lipids in crowded lipid membranes. Faraday Discuss 161, 397–417. https://doi.org/10.1039/C2FD20085F
Javanainen, M., Martinez-Seara, H., Metzler, R., Vattulainen, I., 2018. Diffusion of Proteins and Lipids in Protein-Rich Membranes. Biophys. J. 114, 551a. https://doi.org/10.1016/j.bpj.2017.11.3009
Jensen, M.S., Costa, S.R., Duelli, A.S., Andersen, P.A., Poulsen, L.R., Stanchev, L.D., Gourdon, P., Palmgren, M., Günther Pomorski, T., López-Marqués, R.L., 2017. Phospholipid flipping involves a central cavity in P4 ATPases. Sci. Rep. 7, 17621. https://doi.org/10.1038/s41598-017-17742-y
Jeon, J.-H., Javanainen, M., Martinez-Seara, H., Metzler, R., Vattulainen, I., 2016. Protein Crowding in Lipid Bilayers Gives Rise to Non-Gaussian Anomalous Lateral Diffusion of Phospholipids and Proteins. Phys. Rev. X 6. https://doi.org/10.1103/PhysRevX.6.021006
Jiang, B., Brown, J.L., Sheraton, J., Fortin, N., Bussey, H., 1994. A new family of yeast genes implicated in ergosterol synthesis is related to the human oxysterol binding protein. Yeast 10, 341–353. https://doi.org/10.1002/yea.320100307
Johansson, M., Bocher, V., Lehto, M., Chinetti, G., Kuismanen, E., Ehnholm, C., Staels, B., Olkkonen, V.M., 2003. The two variants of oxysterol binding protein-related protein-1 display different tissue expression patterns, have different intracellular localization, and are functionally distinct. Mol. Biol. Cell 14, 903–915. https://doi.org/10.1091/mbc.e02-08-0459
Johansson, M., Lehto, M., Tanhuanpää, K., Cover, T.L., Olkkonen, V.M., 2005. The oxysterol-binding protein homologue ORP1L interacts with Rab7 and alters functional properties of late endocytic compartments. Mol. Biol. Cell 16, 5480–5492. https://doi.org/10.1091/mbc.e05-03-0189
Johansson, M., Rocha, N., Zwart, W., Jordens, I., Janssen, L., Kuijl, C., Olkkonen, V.M., Neefjes, J., 2007. Activation of endosomal dynein motors by stepwise assembly of Rab7–RILP–p150 ^{Glued}, ORP1L, and the receptor βlll spectrin. J. Cell Biol. 176, 459–471. https://doi.org/10.1083/jcb.200606077
Jousset, H., Frieden, M., Demaurex, N., 2007. STIM1 Knockdown Reveals That Store-operated Ca $^{2+}$ Channels Located Close to Sarco/Endoplasmic Ca $^{2+}$ ATPases (SERCA) Pumps Silently

Refill the Endoplasmic Reticulum. J. Biol. Chem. 282, 11456–11464. https://doi.org/10.1074/jbc.M609551200
Kaiser, S.E., Brickner, J.H., Reilein, A.R., Fenn, T.D., Walter, P., Brunger, A.T., 2005. Structural Basis of FFAT Motif-Mediated ER Targeting. Structure 13, 1035–1045. https://doi.org/10.1016/j.str.2005.04.010
Kalthoff, C., Alves, J., Urbanke, C., Knorr, R., Ungewickell, E.J., 2002. Unusual Structural Organization of the Endocytic Proteins AP180 and Epsin 1. J. Biol. Chem. 277, 8209–8216. https://doi.org/10.1074/jbc.M111587200
Kandutsch, A.A., Chen, H.W., 1978. Inhibition of cholesterol synthesis by oxygenated sterols. Lipids 13, 704–707.
Kandutsch, A.A., Shown, E.P., 1981. Assay of oxysterol-binding protein in a mouse fibroblast, cell-free system. Dissociation constant and other properties of the system. J. Biol. Chem. 256, 13068–13073.
Kandutsch, A.A., Thompson, E.B., 1980. Cytosolic proteins that bind oxygenated sterols. Cellular distribution, specificity, and some properties. J. Biol. Chem. 255, 10813–10821.
Kannan, M., Lahiri, S., Liu, L.-K., Choudhary, V., Prinz, W.A., 2017. Phosphatidylserine synthesis at membrane contact sites promotes its transport out of the ER. J. Lipid Res. 58, 553–562. https://doi.org/10.1194/jlr.M072959
Kawano, M., Kumagai, K., Nishijima, M., Hanada, K., 2006. Efficient Trafficking of Ceramide from the Endoplasmic Reticulum to the Golgi Apparatus Requires a VAMP-associated Protein-interacting FFAT Motif of CERT. J. Biol. Chem. 281, 30279–30288. https://doi.org/10.1074/jbc.M605032200
Kawasaki, T., Lange, I., Feske, S., 2009. A minimal regulatory domain in the C terminus of STIM1 binds to and activates ORAI1 CRAC channels. Biochem. Biophys. Res. Commun. 385, 49–54. https://doi.org/10.1016/j.bbrc.2009.05.020
Kearns, B.G., McGee, T.P., Mayinger, P., Gedvilaite, A., Phillips, S.E., Kagiwada, S., Bankaitis, V.A., 1997. Essential role for diacylglycerol in protein transport from the yeast Golgi complex. Nature 387, 101–105. https://doi.org/10.1038/387101a0
Kentala, H., Koponen, A., Kivelä, A.M., Andrews, R., Li, C., Zhou, Y., Olkkonen, V.M., 2018a. Analysis of ORP2-knockout hepatocytes uncovers a novel function in actin cytoskeletal regulation. FASEB J. Off. Publ. Fed. Am. Soc. Exp. Biol. 32, 1281–1295. https://doi.org/10.1096/fj.201700604R
Kentala, H., Koponen, A., Vihinen, H., Pirhonen, J., Liebisch, G., Pataj, Z., Kivelä, A., Li, S., Karhinen, L., Jääskeläinen, E., Andrews, R., Meriläinen, L., Matysik, S., Ikonen, E., Zhou, Y., Jokitalo, E., Olkkonen, V.M., 2018b. OSBP-related protein-2 (ORP2): a novel Akt effector that controls cellular energy metabolism. Cell. Mol. Life Sci. 75, 4041–4057. https://doi.org/10.1007/s00018-018-2850-8
Kim, S., Kedan, A., Marom, M., Gavert, N., Keinan, O., Selitrennik, M., Laufman, O., Lev, S., 2013. The phosphatidylinositol-transfer protein Nir2 binds phosphatidic acid and positively regulates phosphoinositide signalling. EMBO Rep. 14, 891–899. https://doi.org/10.1038/embor.2013.113
Kim, Y.J., Guzman-Hernandez, M.L., Wisniewski, E., Echeverria, N., Balla, T., 2016. Phosphatidylinositol and phosphatidic acid transport between the ER and plasma membrane during PLC activation requires the Nir2 protein. Biochem. Soc. Trans. 44, 197–201. https://doi.org/10.1042/BST20150187
Klemm, R.W., Ejsing, C.S., Surma, M.A., Kaiser, H.-J., Gerl, M.J., Sampaio, J.L., de Robillard, Q., Ferguson, C., Proszynski, T.J., Shevchenko, A., Simons, K., 2009. Segregation of sphingolipids and sterols during formation of secretory vesicles at the trans-Golgi network. J. Cell Biol. 185, 601–612. https://doi.org/10.1083/jcb.200901145
Konopka, M.C., Shkel, I.A., Cayley, S., Record, M.T., Weisshaar, J.C., 2006. Crowding and Confinement Effects on Protein Diffusion In Vivo. J. Bacteriol. 188, 6115–6123. https://doi.org/10.1128/JB.01982-05
Koriyama, H., Nakagami, H., Katsuya, T., Akasaka, H., Saitoh, S., Shimamoto, K., Ogihara, T., Kaneda, Y., Morishita, R., Rakugi, H., 2010. Variation in OSBPL10 is associated with

dyslipidemia. Hypertens. Res. Off. J. Jpn. Soc. Hypertens. 33, 511–514. https://doi.org/10.1038/hr.2010.28
Korobova, F., Ramabhadran, V., Higgs, H.N., 2013. An Actin-Dependent Step in Mitochondrial Fission Mediated by the ER-Associated Formin INF2. Science 339, 464–467. https://doi.org/10.1126/science.1228360
Kozik, P., Francis, R.W., Seaman, M.N.J., Robinson, M.S., 2010. A Screen for Endocytic Motifs. Traffic 11, 843–855. https://doi.org/10.1111/j.1600-0854.2010.01056.x
Krauβ, M., Haucke, V., 2016. Directing lipid transport at membrane contact sites. Nat. Cell Biol. 18, 461–463. https://doi.org/10.1038/ncb3345
Kulak, N.A., Pichler, G., Paron, I., Nagaraj, N., Mann, M., 2014. Minimal, encapsulated proteomic-sample processing applied to copy-number estimation in eukaryotic cells. Nat. Methods 11, 319–324. https://doi.org/10.1038/nmeth.2834
Lagace, T.A., Byers, D.M., Cook, H.W., Ridgway, N.D., 1997. Altered regulation of cholesterol and cholesteryl ester synthesis in Chinese-hamster ovary cells overexpressing the oxysterol-binding protein is dependent on the pleckstrin homology domain. Biochem. J. 326 (Pt 1), 205–213.
Laitinen, S., Lehto, M., Lehtonen, S., Hyvärinen, K., Heino, S., Lehtonen, E., Ehnholm, C., Ikonen, E., Olkkonen, V.M., 2002. ORP2, a homolog of oxysterol binding protein, regulates cellular cholesterol metabolism. J. Lipid Res. 43, 245–255.
Laitinen, S., Olkkonen, V.M., Ehnholm, C., Ikonen, E., 1999. Family of human oxysterol binding protein (OSBP) homologues. A novel member implicated in brain sterol metabolism. J. Lipid Res. 40, 2204–2211.
Lee, M., Fairn, G.D., 2018. Both the PH domain and N-terminal region of oxysterol-binding protein related protein 8S are required for localization to PM-ER contact sites. Biochem. Biophys. Res. Commun. 496, 1088–1094. https://doi.org/10.1016/j.bbrc.2018.01.138
Lee, S., Wang, P.-Y., Jeong, Y., Mangelsdorf, D.J., Anderson, R.G.W., Michaely, P., 2012. Sterol-dependent nuclear import of ORP1S promotes LXR regulated trans-activation of apoE. Exp. Cell Res. 318, 2128–2142. https://doi.org/10.1016/j.yexcr.2012.06.012
Lehto, M., Hynynen, R., Karjalainen, K., Kuismanen, E., Hyvärinen, K., Olkkonen, V.M., 2005. Targeting of OSBP-related protein 3 (ORP3) to endoplasmic reticulum and plasma membrane is controlled by multiple determinants. Exp. Cell Res. 310, 445–462. https://doi.org/10.1016/j.yexcr.2005.08.003
Lehto, M., Laitinen, S., Chinetti, G., Johansson, M., Ehnholm, C., Staels, B., Ikonen, E., Olkkonen, V.M., 2001. The OSBP-related protein family in humans. J. Lipid Res. 42, 1203–1213.
Lehto, M., Mayranpaa, M.I., Pellinen, T., Ihalmo, P., Lehtonen, S., Kovanen, P.T., Groop, P.-H., Ivaska, J., Olkkonen, V.M., 2008. The R-Ras interaction partner ORP3 regulates cell adhesion. J. Cell Sci. 121, 695–705. https://doi.org/10.1242/jcs.016964
Lehto, M., Tienari, J., Lehtonen, S., Lehtonen, E., Olkkonen, V.M., 2004. Subfamily III of mammalian oxysterol-binding protein (OSBP) homologues: the expression and intracellular localization of ORP3, ORP6, and ORP7. Cell Tissue Res. 315, 39–57. https://doi.org/10.1007/s00441-003-0817-y
Lemmon, M.A., Ferguson, K.M., 2001. Molecular determinants in pleckstrin homology domains that allow specific recognition of phosphoinositides. Biochem. Soc. Trans. 29, 377–384.
Lenoir, G., Williamson, P., Puts, C.F., Holthuis, J.C.M., 2009. Cdc50p Plays a Vital Role in the ATPase Reaction Cycle of the Putative Aminophospholipid Transporter Drs2p. J. Biol. Chem. 284, 17956–17967. https://doi.org/10.1074/jbc.M109.013722
Lev, S., 2010. Non-vesicular lipid transport by lipid-transfer proteins and beyond. Nat. Rev. Mol. Cell Biol. 11, 739–750. https://doi.org/10.1038/nrm2971
Levanon, D., Hsieh, C.-L., Francke, U., Dawson, P.A., Ridgway, N.D., Brown, M.S., Goldstein, J.L., 1990. cDNA cloning of human oxysterol-binding protein and localization of the gene to human chromosome 11 and mouse chromosome 19. Genomics 7, 65–74. https://doi.org/10.1016/0888-7543(90)90519-Z
Levine, A.J., Momand, J., Finlay, C.A., 1991. The p53 tumour suppressor gene. Nature 351, 453–456. https://doi.org/10.1038/351453a0

Levine, T.P., Munro, S., 2002. Targeting of Golgi-Specific Pleckstrin Homology Domains Involves Both PtdIns 4-Kinase-Dependent and -Independent Components. Curr. Biol. 12, 695–704. https://doi.org/10.1016/S0960-9822(02)00779-0
Levine, T.P., Munro, S., 2001. Dual Targeting of Osh1p, a Yeast Homologue of Oxysterol-binding Protein, to both the Golgi and the Nucleus-Vacuole Junction. Mol. Biol. Cell 12, 1633–1644. https://doi.org/10.1091/mbc.12.6.1633
Levine, T.P., Munro, S., 1998. The pleckstrin homology domain of oxysterol-binding protein recognises a determinant specific to Golgi membranes. Curr. Biol. 8, 729–739. https://doi.org/10.1016/S0960-9822(98)70296-9
Li, D., Dammer, E.B., Lucki, N.C., Sewer, M.B., 2013. cAMP-stimulated phosphorylation of diaphanous 1 regulates protein stability and interaction with binding partners in adrenocortical cells. Mol. Biol. Cell 24, 848–857. https://doi.org/10.1091/mbc.E12-08-0597
Li, Jianzong, Feng, Y., Wang, X., Li, Jing, Liu, W., Rong, L., Bao, J., 2015. An Overview of Predictors for Intrinsically Disordered Proteins over 2010–2014. Int. J. Mol. Sci. 16, 23446–23462. https://doi.org/10.3390/ijms161023446
Li, J.-W., Xiao, Y.-L., Lai, C.-F., Lou, N., Ma, H.-L., Zhu, B.-Y., Zhong, W.-B., Yan, D.-G., 2016. Oxysterol-binding protein-related protein 4L promotes cell proliferation by sustaining intracellular Ca2+ homeostasis in cervical carcinoma cell lines. Oncotarget 7, 65849–65861. https://doi.org/10.18632/oncotarget.11671
Li, P., Banjade, S., Cheng, H.-C., Kim, S., Chen, B., Guo, L., Llaguno, M., Hollingsworth, J.V., King, D.S., Banani, S.F., Russo, P.S., Jiang, Q.-X., Nixon, B.T., Rosen, M.K., 2012. Phase transitions in the assembly of multivalent signalling proteins. Nature 483, 336–340. https://doi.org/10.1038/nature10879
Linding, R., Jensen, L.J., Diella, F., Bork, P., Gibson, T.J., Russell, R.B., 2003. Protein Disorder Prediction. Structure 11, 1453–1459. https://doi.org/10.1016/j.str.2003.10.002
Lippincott-Schwartz, J., Snapp, E., Kenworthy, A., 2001. Studying protein dynamics in living cells. Nat. Rev. Mol. Cell Biol. 2, 444–456. https://doi.org/10.1038/35073068
Litvak, V., Dahan, N., Ramachandran, S., Sabanay, H., Lev, S., 2005. Maintenance of the diacylglycerol level in the Golgi apparatus by the Nir2 protein is critical for Golgi secretory function. Nat. Cell Biol. 7, 225–234. https://doi.org/10.1038/ncb1221
Liu, G., Coyne, A.N., Pei, F., Vaughan, S., Chaung, M., Zarnescu, D.C., Buchan, J.R., 2017. Endocytosis regulates TDP-43 toxicity and turnover. Nat. Commun. 8, 2092. https://doi.org/10.1038/s41467-017-02017-x
Liu, S.-L., Sheng, R., Jung, J.H., Wang, L., Stec, E., O'Connor, M.J., Song, S., Bikkavilli, R.K., Winn, R.A., Lee, D., Baek, K., Ueda, K., Levitan, I., Kim, K.-P., Cho, W., 2017. Orthogonal lipid sensors identify transbilayer asymmetry of plasma membrane cholesterol. Nat. Chem. Biol. 13, 268–274. https://doi.org/10.1038/nchembio.2268
Liu, X., Ridgway, N.D., 2014. Characterization of the Sterol and Phosphatidylinositol 4-Phosphate Binding Properties of Golgi-Associated OSBP-Related Protein 9 (ORP9). PLoS ONE 9, e108368. https://doi.org/10.1371/journal.pone.0108368
Liu, Y., Kahn, R.A., Prestegard, J.H., 2014. Interaction of Fapp1 with Arf1 and PI4P at a membrane surface: an example of coincidence detection. Struct. Lond. Engl. 1993 22, 421–430. https://doi.org/10.1016/j.str.2013.12.011
Loewen, C.J.R., Levine, T.P., 2005. A Highly Conserved Binding Site in Vesicle-associated Membrane Protein-associated Protein (VAP) for the FFAT Motif of Lipid-binding Proteins. J. Biol. Chem. 280, 14097–14104. https://doi.org/10.1074/jbc.M500147200
Loewen, C.J.R., Roy, A., Levine, T.P., 2003. A conserved ER targeting motif in three families of lipid binding proteins and in Opi1p binds VAP. EMBO J. 22, 2025–2035. https://doi.org/10.1093/emboj/cdg201
Lopez-Marques, R.L., Theorin, L., Palmgren, M.G., Pomorski, T.G., 2014. P4-ATPases: lipid flippases in cell membranes. Pflüg. Arch. - Eur. J. Physiol. 466, 1227–1240. https://doi.org/10.1007/s00424-013-1363-4

Losev, E., Reinke, C.A., Jellen, J., Strongin, D.E., Bevis, B.J., Glick, B.S., 2006. Golgi maturation visualized in living yeast. Nature 441, 1002–1006. https://doi.org/10.1038/nature04717
Lowe, E.D., Tews, I., Cheng, K.Y., Brown, N.R., Gul, S., Noble, M.E.M., Gamblin, S.J., Johnson, L.N., 2002. Specificity Determinants of Recruitment Peptides Bound to Phospho-CDK2/Cyclin A †, ‡. Biochemistry 41, 15625–15634. https://doi.org/10.1021/bi0268910
Lu, D., Sun, H., Wang, H., Barylko, B., Fukata, Y., Fukata, M., Albanesi, J.P., Yin, H.L., 2012. Phosphatidylinositol 4-Kinase IIα Is Palmitoylated by Golgi-localized Palmitoyltransferases in Cholesterol-dependent Manner. J. Biol. Chem. 287, 21856–21865. https://doi.org/10.1074/jbc.M112.348094
Luby-Phelps, K., 2013. The physical chemistry of cytoplasm and its influence on cell function: an update. Mol. Biol. Cell 24, 2593–2596. https://doi.org/10.1091/mbc.e12-08-0617
Luu, W., Sharpe, L.J., Capell-Hattam, I., Gelissen, I.C., Brown, A.J., 2016. Oxysterols: Old Tale, New Twists. Annu. Rev. Pharmacol. Toxicol. 56, 447–467. https://doi.org/10.1146/annurev-pharmtox-010715-103233
Macia, E., Paris, S., Chabre, M., 2000. Binding of the PH and Polybasic C-Terminal Domains of ARNO to Phosphoinositides and to Acidic Lipids. Biochemistry 39, 5893–5901. https://doi.org/10.1021/bi992795w
Maeda, K., Anand, K., Chiapparino, A., Kumar, A., Poletto, M., Kaksonen, M., Gavin, A.-C., 2013. Interactome map uncovers phosphatidylserine transport by oxysterol-binding proteins. Nature 501, 257–261. https://doi.org/10.1038/nature12430
Magdeleine, M., Gautier, R., Gounon, P., Barelli, H., Vanni, S., Antonny, B., 2016. A filter at the entrance of the Golgi that selects vesicles according to size and bulk lipid composition. eLife 5. https://doi.org/10.7554/eLife.16988
Manford, A.G., Stefan, C.J., Yuan, H.L., MacGurn, J.A., Emr, S.D., 2012. ER-to-Plasma Membrane Tethering Proteins Regulate Cell Signaling and ER Morphology. Dev. Cell 23, 1129–1140. https://doi.org/10.1016/j.devcel.2012.11.004
Manjarrés, I.M., Alonso, M.T., García-Sancho, J., 2011. Calcium entry-calcium refilling (CECR) coupling between store-operated Ca2+ entry and sarco/endoplasmic reticulum Ca2+-ATPase. Cell Calcium 49, 153–161. https://doi.org/10.1016/j.ceca.2011.01.007
Mao, A.H., Crick, S.L., Vitalis, A., Chicoine, C.L., Pappu, R.V., 2010. Net charge per residue modulates conformational ensembles of intrinsically disordered proteins. Proc. Natl. Acad. Sci. 107, 8183–8188. https://doi.org/10.1073/pnas.0911107107
Martin, S.J., 1995. Early redistribution of plasma membrane phosphatidylserine is a general feature of apoptosis regardless of the initiating stimulus: inhibition by overexpression of Bcl-2 and Abl. J. Exp. Med. 182, 1545–1556. https://doi.org/10.1084/jem.182.5.1545
Matsuo, H., 2004. Role of LBPA and Alix in Multivesicular Liposome Formation and Endosome Organization. Science 303, 531–534. https://doi.org/10.1126/science.1092425
Maxfield, F.R., van Meer, G., 2010. Cholesterol, the central lipid of mammalian cells. Curr. Opin. Cell Biol. 22, 422–429. https://doi.org/10.1016/j.ceb.2010.05.004
Mayinger, P., 2012. Phosphoinositides and vesicular membrane traffic. Biochim. Biophys. Acta BBA - Mol. Cell Biol. Lipids 1821, 1104–1113. https://doi.org/10.1016/j.bbalip.2012.01.002
McGuffee, S.R., Elcock, A.H., 2010. Diffusion, Crowding & Protein Stability in a Dynamic Molecular Model of the Bacterial Cytoplasm. PLoS Comput. Biol. 6, e1000694. https://doi.org/10.1371/journal.pcbi.1000694
McMahon, H.T., Gallop, J.L., 2005. Membrane curvature and mechanisms of dynamic cell membrane remodelling. Nature 438, 590–596. https://doi.org/10.1038/nature04396
Mesmin, B., Bigay, J., Moser von Filseck, J., Lacas-Gervais, S., Drin, G., Antonny, B., 2013. A Four-Step Cycle Driven by PI(4)P Hydrolysis Directs Sterol/PI(4)P Exchange by the ER-Golgi Tether OSBP. Cell 155, 830–843. https://doi.org/10.1016/j.cell.2013.09.056
Mesmin, B., Bigay, J., Polidori, J., Jamecna, D., Lacas-Gervais, S., Antonny, B., 2017. Sterol transfer, PI4P consumption, and control of membrane lipid order by endogenous OSBP. EMBO J. 36, 3156–3174. https://doi.org/10.15252/embj.201796687

Metzler, R., Jeon, J.-H., Cherstvy, A.G., 2016. Non-Brownian diffusion in lipid membranes: Experiments and simulations. Biochim. Biophys. Acta BBA - Biomembr. 1858, 2451–2467. https://doi.org/10.1016/j.bbamem.2016.01.022

Meutiawati, F., Bezemer, B., Strating, J.R.P.M., Overheul, G.J., Žusinaite, E., van Kuppeveld, F.J.M., van Cleef, K.W.R., van Rij, R.P., 2018. Posaconazole inhibits dengue virus replication by targeting oxysterol-binding protein. Antiviral Res. 157, 68–79. https://doi.org/10.1016/j.antiviral.2018.06.017

Meyer, K., Kirchner, M., Uyar, B., Cheng, J.-Y., Russo, G., Hernandez-Miranda, L.R., Szymborska, A., Zauber, H., Rudolph, I.-M., Willnow, T.E., Akalin, A., Haucke, V., Gerhardt, H., Birchmeier, C., Kühn, R., Krauss, M., Diecke, S., Pascual, J.M., Selbach, M., 2018. Mutations in Disordered Regions Can Cause Disease by Creating Dileucine Motifs. Cell 175, 239-253.e17. https://doi.org/10.1016/j.cell.2018.08.019

Milovanovic, D., De Camilli, P., 2017. Synaptic Vesicle Clusters at Synapses: A Distinct Liquid Phase? Neuron 93, 995–1002. https://doi.org/10.1016/j.neuron.2017.02.013

Milovanovic, D., Wu, Y., Bian, X., De Camilli, P., 2018. A liquid phase of synapsin and lipid vesicles. Science 361, 604–607. https://doi.org/10.1126/science.aat5671

Mochizuki, S., Miki, H., Zhou, R., Kido, Y., Nishimura, W., Kikuchi, M., Noda, Y., 2018. Oxysterol-binding protein-related protein (ORP) 6 localizes to the ER and ER-plasma membrane contact sites and is involved in the turnover of PI4P in cerebellar granule neurons. Exp. Cell Res. 370, 601–612. https://doi.org/10.1016/j.yexcr.2018.07.025

Mondal, M., Mesmin, B., Mukherjee, S., Maxfield, F.R., 2009. Sterols are mainly in the cytoplasmic leaflet of the plasma membrane and the endocytic recycling compartment in CHO cells. Mol. Biol. Cell 20, 581–588. https://doi.org/10.1091/mbc.e08-07-0785

Moreau, P., Cassagne, C., Keenan, T.W., Morré, D.J., 1993. Ceramide excluded from cell-free vesicular lipid transfer from endoplasmic reticulum to Golgi apparatus. Evidence for lipid sorting. Biochim. Biophys. Acta BBA - Biomembr. 1146, 9–16. https://doi.org/10.1016/0005-2736(93)90332-T

Morré, D.J., Ovtracht, L., 1977. Dynamics of the Golgi apparatus: membrane differentiation and membrane flow. Int. Rev. Cytol. Suppl. 61–188.

Moser von Filseck, J., opi, A., Delfosse, V., Vanni, S., Jackson, C.L., Bourguet, W., Drin, G., 2015. Phosphatidylserine transport by ORP/Osh proteins is driven by phosphatidylinositol 4-phosphate. Science 349, 432–436. https://doi.org/10.1126/science.aab1346

Muramatsu, N., Minton, A.P., 1988. Tracer diffusion of globular proteins in concentrated protein solutions. Proc. Natl. Acad. Sci. U. S. A. 85, 2984–2988.

Nachtergaele, S., Mydock, L.K., Krishnan, K., Rammohan, J., Schlesinger, P.H., Covey, D.F., Rohatgi, R., 2012. Oxysterols are allosteric activators of the oncoprotein Smoothened. Nat. Chem. Biol. 8, 211–220. https://doi.org/10.1038/nchembio.765

Naji, A., Levine, A.J., Pincus, P.A., 2007. Corrections to the Saffman-Delbruck mobility for membrane bound proteins. Biophys. J. 93, L49-51. https://doi.org/10.1529/biophysj.107.119222

Nakada, T., Kashihara, T., Komatsu, M., Kojima, K., Takeshita, T., Yamada, M., 2018. Physical interaction of junctophilin and the Ca $_{V}$ 1.1 C terminus is crucial for skeletal muscle contraction. Proc. Natl. Acad. Sci. 115, 4507–4512. https://doi.org/10.1073/pnas.1716649115

Nassa, M., Anand, P., Jain, A., Chhabra, A., Jaiswal, A., Malhotra, U., Rani, V., 2012. Analysis of human collagen sequences. Bioinformation 8, 26–33.

Ngo, M., Ridgway, N.D., 2009. Oxysterol binding protein-related Protein 9 (ORP9) is a cholesterol transfer protein that regulates Golgi structure and function. Mol. Biol. Cell 20, 1388–1399. https://doi.org/10.1091/mbc.e08-09-0905

Ngo, M.H., Colbourne, T.R., Ridgway, N.D., 2010. Functional implications of sterol transport by the oxysterol-binding protein gene family. Biochem. J. 429, 13–24. https://doi.org/10.1042/BJ20100263

Nickels, J.D., Smith, J.C., Cheng, X., 2015. Lateral organization, bilayer asymmetry, and inter-leaflet coupling of biological membranes. Chem. Phys. Lipids 192, 87–99. https://doi.org/10.1016/j.chemphyslip.2015.07.012
Nishimura, T., Inoue, T., Shibata, N., Sekine, A., Takabe, W., Noguchi, N., Arai, H., 2005. Inhibition of cholesterol biosynthesis by 25-hydroxycholesterol is independent of OSBP. Genes Cells 10, 793–801. https://doi.org/10.1111/j.1365-2443.2005.00879.x
Nissilä, E., Ohsaki, Y., Weber-Boyvat, M., Perttilä, J., Ikonen, E., Olkkonen, V.M., 2012. ORP10, a cholesterol binding protein associated with microtubules, regulates apolipoprotein B-100 secretion. Biochim. Biophys. Acta 1821, 1472–1484. https://doi.org/10.1016/j.bbalip.2012.08.004
Noland, B.J., Arebalo, R.E., Hansbury, E., Scallen, T.J., 1980. Purification and properties of sterol carrier protein2. J. Biol. Chem. 255, 4282–4289.
Nott, T.J., Petsalaki, E., Farber, P., Jervis, D., Fussner, E., Plochowietz, A., Craggs, T.D., Bazett-Jones, D.P., Pawson, T., Forman-Kay, J.D., Baldwin, A.J., 2015. Phase Transition of a Disordered Nuage Protein Generates Environmentally Responsive Membraneless Organelles. Mol. Cell 57, 936–947. https://doi.org/10.1016/j.molcel.2015.01.013
Olkkonen, V.M., Levine, T.P., 2004. Oxysterol binding proteins: in more than one place at one time? Biochem. Cell Biol. Biochim. Biol. Cell. 82, 87–98. https://doi.org/10.1139/o03-088
Olkkonen, V.M., Li, S., 2013. Oxysterol-binding proteins: Sterol and phosphoinositide sensors coordinating transport, signaling and metabolism. Prog. Lipid Res. 52, 529–538. https://doi.org/10.1016/j.plipres.2013.06.004
Ouimet, M., Hennessy, E.J., van Solingen, C., Koelwyn, G.J., Hussein, M.A., Ramkhelawon, B., Rayner, K.J., Temel, R.E., Perisic, L., Hedin, U., Maegdefessel, L., Garabedian, M.J., Holdt, L.M., Teupser, D., Moore, K.J., 2016. miRNA Targeting of Oxysterol-Binding Protein-Like 6 Regulates Cholesterol Trafficking and Efflux. Arterioscler. Thromb. Vasc. Biol. 36, 942–951. https://doi.org/10.1161/ATVBAHA.116.307282
Owen, D.J., Vallis, Y., Noble, M.E., Hunter, J.B., Dafforn, T.R., Evans, P.R., McMahon, H.T., 1999. A structural explanation for the binding of multiple ligands by the alpha-adaptin appendage domain. Cell 97, 805–815.
Pacheco, J., Dominguez, L., Bohórquez-Hernández, A., Asanov, A., Vaca, L., 2016. A cholesterol-binding domain in STIM1 modulates STIM1-Orai1 physical and functional interactions. Sci. Rep. 6. https://doi.org/10.1038/srep29634
Peretti, D., Dahan, N., Shimoni, E., Hirschberg, K., Lev, S., 2008. Coordinated lipid transfer between the endoplasmic reticulum and the Golgi complex requires the VAP proteins and is essential for Golgi-mediated transport. Mol. Biol. Cell 19, 3871–3884. https://doi.org/10.1091/mbc.e08-05-0498
Perry, R.J., Ridgway, N.D., 2006. Oxysterol-binding Protein and Vesicle-associated Membrane Protein–associated Protein Are Required for Sterol-dependent Activation of the Ceramide Transport Protein□D. Mol. Biol. Cell 17, 13.
Perttilä, J., Merikanto, K., Naukkarinen, J., Surakka, I., Martin, N.W., Tanhuanpää, K., Grimard, V., Taskinen, M.-R., Thiele, C., Salomaa, V., Jula, A., Perola, M., Virtanen, I., Peltonen, L., Olkkonen, V.M., 2009. OSBPL10, a novel candidate gene for high triglyceride trait in dyslipidemic Finnish subjects, regulates cellular lipid metabolism. J. Mol. Med. Berl. Ger. 87, 825–835. https://doi.org/10.1007/s00109-009-0490-z
Peters, R., Cherry, R.J., 1982. Lateral and rotational diffusion of bacteriorhodopsin in lipid bilayers: experimental test of the Saffman-Delbruck equations. Proc. Natl. Acad. Sci. 79, 4317–4321. https://doi.org/10.1073/pnas.79.14.4317
Praefcke, G.J.K., Ford, M.G.J., Schmid, E.M., Olesen, L.E., Gallop, J.L., Peak-Chew, S.-Y., Vallis, Y., Babu, M.M., Mills, I.G., McMahon, H.T., 2004. Evolving nature of the AP2 α-appendage hub during clathrin-coated vesicle endocytosis. EMBO J. 23, 4371–4383. https://doi.org/10.1038/sj.emboj.7600445
Prinz, W.A., 2014. Bridging the gap: Membrane contact sites in signaling, metabolism, and organelle dynamics. J. Cell Biol. 205, 759–769. https://doi.org/10.1083/jcb.201401126

Proszynski, T.J., Klemm, R.W., Gravert, M., Hsu, P.P., Gloor, Y., Wagner, J., Kozak, K., Grabner, H., Walzer, K., Bagnat, M., Simons, K., Walch-Solimena, C., 2005. A genome-wide visual screen reveals a role for sphingolipids and ergosterol in cell surface delivery in yeast. Proc. Natl. Acad. Sci. U. S. A. 102, 17981–17986. https://doi.org/10.1073/pnas.0509107102

Pulli, I., Lassila, T., Pan, G., Yan, D., Olkkonen, V.M., Törnquist, K., 2018. Oxysterol-binding protein related-proteins (ORPs) 5 and 8 regulate calcium signaling at specific cell compartments. Cell Calcium 72, 62–69. https://doi.org/10.1016/j.ceca.2018.03.001

Radhakrishnan, A., Ikeda, Y., Kwon, H.J., Brown, M.S., Goldstein, J.L., 2007. Sterol-regulated transport of SREBPs from endoplasmic reticulum to Golgi: Oxysterols block transport by binding to Insig. Proc. Natl. Acad. Sci. 104, 6511–6518. https://doi.org/10.1073/pnas.0700899104

Ramadurai, S., Holt, A., Krasnikov, V., van den Bogaart, G., Killian, J.A., Poolman, B., 2009. Lateral Diffusion of Membrane Proteins. J. Am. Chem. Soc. 131, 12650–12656. https://doi.org/10.1021/ja902853g

Raychaudhuri, S., Im, Y.J., Hurley, J.H., Prinz, W.A., 2006. Nonvesicular sterol movement from plasma membrane to ER requires oxysterol-binding protein-related proteins and phosphoinositides. J. Cell Biol. 173, 107–119. https://doi.org/10.1083/jcb.200510084

Rebbeck, R.T., Karunasekara, Y., Gallant, E.M., Board, P.G., Beard, N.A., Casarotto, M.G., Dulhunty, A.F., 2011. The β1a Subunit of the Skeletal DHPR Binds to Skeletal RyR1 and Activates the Channel via Its 35-Residue C-Terminal Tail. Biophys. J. 100, 922–930. https://doi.org/10.1016/j.bpj.2011.01.022

Ridgway, N.D., 1992. Translocation of oxysterol binding protein to Golgi apparatus triggered by ligand binding. J. Cell Biol. 116, 307–319. https://doi.org/10.1083/jcb.116.2.307

Rocha, N., Kuijl, C., van der Kant, R., Janssen, L., Houben, D., Janssen, H., Zwart, W., Neefjes, J., 2009. Cholesterol sensor ORP1L contacts the ER protein VAP to control Rab7–RILP–p150 ^{Glued} and late endosome positioning. J. Cell Biol. 185, 1209–1225. https://doi.org/10.1083/jcb.200811005

Romeo, G.R., Kazlauskas, A., 2008. Oxysterol and diabetes activate STAT3 and control endothelial expression of profilin-1 via OSBP1. J. Biol. Chem. 283, 9595–9605. https://doi.org/10.1074/jbc.M710092200

Romero, P., Obradovic, Z., Kissinger, C., Villafranca, J.E., Dunker, A.K., 1997. Identifying disordered regions in proteins from amino acid sequence, in: Proceedings of International Conference on Neural Networks (ICNN'97). Presented at the International Conference on Neural Networks (ICNN'97), IEEE, Houston, TX, USA, pp. 90–95. https://doi.org/10.1109/ICNN.1997.611643

Roosen-Runge, F., Hennig, M., Zhang, F., Jacobs, R.M.J., Sztucki, M., Schober, H., Seydel, T., Schreiber, F., 2011. Protein self-diffusion in crowded solutions. Proc. Natl. Acad. Sci. 108, 11815–11820. https://doi.org/10.1073/pnas.1107287108

Rusiñol, A.E., Cui, Z., Chen, M.H., Vance, J.E., 1994. A unique mitochondria-associated membrane fraction from rat liver has a high capacity for lipid synthesis and contains pre-Golgi secretory proteins including nascent lipoproteins. J. Biol. Chem. 269, 27494–27502.

Rustandi, R.R., Baldisseri, D.M., Weber, D.J., 2000. Structure of the negative regulatory domain of p53 bound to S100B(ββ). Nat. Struct. Biol. 7, 5.

Sahu, S.K., Gummadi, S.N., Manoj, N., Aradhyam, G.K., 2007. Phospholipid scramblases: An overview. Arch. Biochem. Biophys. 462, 103–114. https://doi.org/10.1016/j.abb.2007.04.002

Sato, K., Norris, A., Sato, M., Grant, B.D., 2014. C. elegans as a model for membrane traffic. WormBook Online Rev. C Elegans Biol. 1–47. https://doi.org/10.1895/wormbook.1.77.2

Schmid, E.M., Bakalar, M.H., Choudhuri, K., Weichsel, J., Ann, H.S., Geissler, P.L., Dustin, M.L., Fletcher, D.A., 2016. Size-dependent protein segregation at membrane interfaces. Nat. Phys. 12, 704–711. https://doi.org/10.1038/nphys3678

Schmid, E.M., McMahon, H.T., 2007. Integrating molecular and network biology to decode endocytosis. Nature 448, 883–888. https://doi.org/10.1038/nature06031

Schneiter, R., Brügger, B., Sandhoff, R., Zellnig, G., Leber, A., Lampl, M., Athenstaedt, K., Hrastnik, C., Eder, S., Daum, G., Paltauf, F., Wieland, F.T., Kohlwein, S.D., 1999. Electrospray Ionization Tandem Mass Spectrometry (Esi-Ms/Ms) Analysis of the Lipid Molecular Species Composition of Yeast Subcellular Membranes Reveals Acyl Chain-Based Sorting/Remodeling of Distinct Molecular Species En Route to the Plasma Membrane. J. Cell Biol. 146, 741–754. https://doi.org/10.1083/jcb.146.4.741

Seelig, J., 2004. Thermodynamics of lipid–peptide interactions. Biochim. Biophys. Acta BBA - Biomembr. 1666, 40–50. https://doi.org/10.1016/j.bbamem.2004.08.004

Sharma, R., Raduly, Z., Miskei, M., Fuxreiter, M., 2015. Fuzzy complexes: Specific binding without complete folding. FEBS Lett. 589, 2533–2542. https://doi.org/10.1016/j.febslet.2015.07.022

Simons, K., Van Meer, G., 1988. Lipid sorting in epithelial cells. Biochemistry 27, 6197–6202. https://doi.org/10.1021/bi00417a001

Simonsen, A., Wurmser, A.E., Emr, S.D., Stenmark, H., n.d. The role of phosphoinositides in membrane transport 8.

Singer, S.J., Nicolson, G.L., 1972. The fluid mosaic model of the structure of cell membranes. Science 175, 720–731.

Sorre, B., Callan-Jones, A., Manneville, J.-B., Nassoy, P., Joanny, J.-F., Prost, J., Goud, B., Bassereau, P., 2009. Curvature-driven lipid sorting needs proximity to a demixing point and is aided by proteins. Proc. Natl. Acad. Sci. U. S. A. 106, 5622–5626. https://doi.org/10.1073/pnas.0811243106

Spann, N.J., Glass, C.K., 2013. Sterols and oxysterols in immune cell function. Nat. Immunol. 14, 893–900. https://doi.org/10.1038/ni.2681

Stefan, C.J., Manford, A.G., Baird, D., Yamada-Hanff, J., Mao, Y., Emr, S.D., 2011. Osh Proteins Regulate Phosphoinositide Metabolism at ER-Plasma Membrane Contact Sites. Cell 144, 389–401. https://doi.org/10.1016/j.cell.2010.12.034

Stenmark, H., Aasland, R., Toh, B.H., D'Arrigo, A., 1996. Endosomal localization of the autoantigen EEA1 is mediated by a zinc-binding FYVE finger. J. Biol. Chem. 271, 24048–24054.

Stoica, R., De Vos, K.J., Paillusson, S., Mueller, S., Sancho, R.M., Lau, K.-F., Vizcay-Barrena, G., Lin, W.-L., Xu, Y.-F., Lewis, J., Dickson, D.W., Petrucelli, L., Mitchell, J.C., Shaw, C.E., Miller, C.C.J., 2014. ER-mitochondria associations are regulated by the VAPB-PTPIP51 interaction and are disrupted by ALS/FTD-associated TDP-43. Nat. Commun. 5, 3996. https://doi.org/10.1038/ncomms4996

Stone, S.J., Vance, J.E., 2000. Phosphatidylserine Synthase-1 and -2 Are Localized to Mitochondria-associated Membranes. J. Biol. Chem. 275, 34534–34540. https://doi.org/10.1074/jbc.M002865200

Strating, J.R.P.M., van der Linden, L., Albulescu, L., Bigay, J., Arita, M., Delang, L., Leyssen, P., van der Schaar, H.M., Lanke, K.H.W., Thibaut, H.J., Ulferts, R., Drin, G., Schlinck, N., Wubbolts, R.W., Sever, N., Head, S.A., Liu, J.O., Beachy, P.A., De Matteis, M.A., Shair, M.D., Olkkonen, V.M., Neyts, J., van Kuppeveld, F.J.M., 2015. Itraconazole inhibits enterovirus replication by targeting the oxysterol-binding protein. Cell Rep. 10, 600–615. https://doi.org/10.1016/j.celrep.2014.12.054

Suh, B.-C., Leal, K., Hille, B., 2010. Modulation of High-Voltage Activated Ca2+ Channels by Membrane Phosphatidylinositol 4,5-Bisphosphate. Neuron 67, 224–238. https://doi.org/10.1016/j.neuron.2010.07.001

Szabadkai, G., Bianchi, K., Várnai, P., De Stefani, D., Wieckowski, M.R., Cavagna, D., Nagy, A.I., Balla, T., Rizzuto, R., 2006. Chaperone-mediated coupling of endoplasmic reticulum and mitochondrial Ca^{2+} channels. J. Cell Biol. 175, 901–911. https://doi.org/10.1083/jcb.200608073

Tafesse, F.G., Huitema, K., Hermansson, M., van der Poel, S., van den Dikkenberg, J., Uphoff, A., Somerharju, P., Holthuis, J.C.M., 2007. Both Sphingomyelin Synthases SMS1 and SMS2 Are Required for Sphingomyelin Homeostasis and Growth in Human HeLa Cells. J. Biol. Chem. 282, 17537–17547. https://doi.org/10.1074/jbc.M702423200

Takeshima, H., Komazaki, S., Nishi, M., Iino, M., Kangawa, K., 2000. Junctophilins: a novel family of junctional membrane complex proteins. Mol. Cell 6, 11–22.
Taylor, F.R., Kandutsch, A.A., 1985. Oxysterol binding protein. Chem. Phys. Lipids 38, 187–194. https://doi.org/10.1016/0009-3084(85)90066-0
Theillet, F.-X., Kalmar, L., Tompa, P., Han, K.-H., Selenko, P., Dunker, A.K., Daughdrill, G.W., Uversky, V.N., 2013. The alphabet of intrinsic disorder: I. Act like a Pro: On the abundance and roles of proline residues in intrinsically disordered proteins. Intrinsically Disord. Proteins 1, e24360. https://doi.org/10.4161/idp.24360
Tompa, P., 2012. Intrinsically disordered proteins: a 10-year recap. Trends Biochem. Sci. 37, 509–516. https://doi.org/10.1016/j.tibs.2012.08.004
Tompa, P., 2002. Intrinsically unstructured proteins 7.
Tompa, P., Fuxreiter, M., 2008. Fuzzy complexes: polymorphism and structural disorder in protein–protein interactions. Trends Biochem. Sci. 33, 2–8. https://doi.org/10.1016/j.tibs.2007.10.003
Tompa, P., Han, K.-H., Bokor, M., Kamasa, P., Tantos, A., Fritz, B., Kim, D.-H., Lee, C., Verebelyi, T., Tompa, K., 2016. Wide-line NMR and DSC studies on intrinsically disordered p53 transactivation domain and its helically pre-structured segment. BMB Rep. 49, 497–501. https://doi.org/10.5483/BMBRep.2016.49.9.037
Tong, J., Manik, M.K., Im, Y.J., 2018. Structural basis of sterol recognition and nonvesicular transport by lipid transfer proteins anchored at membrane contact sites. Proc. Natl. Acad. Sci. 115, E856–E865. https://doi.org/10.1073/pnas.1719709115
Tong, J., Manik, M.K., Yang, H., Im, Y.J., 2016. Structural insights into nonvesicular lipid transport by the oxysterol binding protein homologue family. Biochim. Biophys. Acta BBA - Mol. Cell Biol. Lipids 1861, 928–939. https://doi.org/10.1016/j.bbalip.2016.01.008
Tong, J., Yang, Huiseon, Yang, Hongyuan, Eom, S.H., Im, Y.J., 2013. Structure of Osh3 Reveals a Conserved Mode of Phosphoinositide Binding in Oxysterol-Binding Proteins. Structure 21, 1203–1213. https://doi.org/10.1016/j.str.2013.05.007
Toulmay, A., Prinz, W.A., 2012. A conserved membrane-binding domain targets proteins to organelle contact sites. J. Cell Sci. 125, 49–58. https://doi.org/10.1242/jcs.085118
Trimble, W.S., Grinstein, S., 2015. Barriers to the free diffusion of proteins and lipids in the plasma membrane. J. Cell Biol. 208, 259–271. https://doi.org/10.1083/jcb.201410071
Udagawa, O., Ito, C., Ogonuki, N., Sato, H., Lee, S., Tripvanuntakul, P., Ichi, I., Uchida, Y., Nishimura, T., Murakami, M., Ogura, A., Inoue, T., Toshimori, K., Arai, H., 2014. Oligo-astheno-teratozoospermia in mice lacking ORP4, a sterol-binding protein in the OSBP-related protein family. Genes Cells 19, 13–27. https://doi.org/10.1111/gtc.12105
Uversky, V., 2016. p53 Proteoforms and Intrinsic Disorder: An Illustration of the Protein Structure–Function Continuum Concept. Int. J. Mol. Sci. 17, 1874. https://doi.org/10.3390/ijms17111874
Uversky, V.N., 2015. The intrinsic disorder alphabet. III. Dual personality of serine. Intrinsically Disord. Proteins 3, e1027032. https://doi.org/10.1080/21690707.2015.1027032
Uversky, V.N., 2013a. The alphabet of intrinsic disorder: II. Various roles of glutamic acid in ordered and intrinsically disordered proteins. Intrinsically Disord. Proteins 1, e24684. https://doi.org/10.4161/idp.24684
Uversky, V.N., 2013b. Disorder in the lifetime of a protein. Intrinsically Disord. Proteins 1, e26782. https://doi.org/10.4161/idp.26782
Uversky, V.N., Eliezer, D., 2009. Biophysics of Parkinson's disease: structure and aggregation of alpha-synuclein. Curr. Protein Pept. Sci. 10, 483–499.
van Meer, G., Stelzer, E.H., Wijnaendts-van-Resandt, R.W., Simons, K., 1987. Sorting of sphingolipids in epithelial (Madin-Darby canine kidney) cells. J. Cell Biol. 105, 1623–1635.
van Meer, G., Voelker, D.R., Feigenson, G.W., 2008. Membrane lipids: where they are and how they behave. Nat. Rev. Mol. Cell Biol. 9, 112–124. https://doi.org/10.1038/nrm2330
Vance, J., Steenbergen, R., 2005. Metabolism and functions of phosphatidylserine. Prog. Lipid Res. 44, 207–234. https://doi.org/10.1016/j.plipres.2005.05.001

Vance, J.E., 1990. Phospholipid synthesis in a membrane fraction associated with mitochondria. J. Biol. Chem. 265, 7248–7256.
Vihervaara, T., Uronen, R.-L., Wohlfahrt, G., Björkhem, I., Ikonen, E., Olkkonen, V.M., 2011. Sterol binding by OSBP-related protein 1L regulates late endosome motility and function. Cell. Mol. Life Sci. CMLS 68, 537–551. https://doi.org/10.1007/s00018-010-0470-z
von Filseck, J.M., Vanni, S., Mesmin, B., Antonny, B., Drin, G., 2015. A phosphatidylinositol-4-phosphate powered exchange mechanism to create a lipid gradient between membranes. Nat. Commun. 6. https://doi.org/10.1038/ncomms7671
Vonkova, I., Saliba, A.-E., Deghou, S., Anand, K., Ceschia, S., Doerks, T., Galih, A., Kugler, K.G., Maeda, K., Rybin, V., van Noort, V., Ellenberg, J., Bork, P., Gavin, A.-C., 2015. Lipid Cooperativity as a General Membrane-Recruitment Principle for PH Domains. Cell Rep. 12, 1519–1530. https://doi.org/10.1016/j.celrep.2015.07.054
Wang, C., Jebailey, L., Ridgway, N.D., 2002. Oxysterol-binding-protein (OSBP)-related protein 4 binds 25-hydroxycholesterol and interacts with vimentin intermediate filaments 12.
Wang, J., Bian, Y., Cao, X., Zhao, N., 2017. Understanding diffusion of intrinsically disordered proteins in polymer solutions: A disorder plus collapse model. AIP Adv. 7, 115120. https://doi.org/10.1063/1.5002710
Wang, J., Sun, H.-Q., Macia, E., Kirchhausen, T., Watson, H., Bonifacino, J.S., Yin, H.L., 2007. PI4P Promotes the Recruitment of the GGA Adaptor Proteins to the *Trans* -Golgi Network and Regulates Their Recognition of the Ubiquitin Sorting Signal. Mol. Biol. Cell 18, 2646–2655. https://doi.org/10.1091/mbc.e06-10-0897
Wang, P. -y., 2005. OSBP Is a Cholesterol-Regulated Scaffolding Protein in Control of ERK 1/2 Activation. Science 307, 1472–1476. https://doi.org/10.1126/science.1107710
Wang, Y., Benton, L.A., Singh, V., Pielak, G.J., 2012. Disordered Protein Diffusion under Crowded Conditions. J. Phys. Chem. Lett. 3, 2703–2706. https://doi.org/10.1021/jz3010915
Wang, Y., Li, C., Pielak, G.J., 2010. Effects of proteins on protein diffusion. J. Am. Chem. Soc. 132, 9392–9397. https://doi.org/10.1021/ja102296k
Wang, Y.J., Wang, J., Sun, H.Q., Martinez, M., Sun, Y.X., Macia, E., Kirchhausen, T., Albanesi, J.P., Roth, M.G., Yin, H.L., 2003. Phosphatidylinositol 4 Phosphate Regulates Targeting of Clathrin Adaptor AP-1 Complexes to the Golgi. Cell 114, 299–310. https://doi.org/10.1016/S0092-8674(03)00603-2
Weber-Boyvat, M., Kentala, H., Lilja, J., Vihervaara, T., Hanninen, R., Zhou, Y., Peränen, J., Nyman, T.A., Ivaska, J., Olkkonen, V.M., 2015. OSBP-related protein 3 (ORP3) coupling with VAMP-associated protein A regulates R-Ras activity. Exp. Cell Res. 331, 278–291. https://doi.org/10.1016/j.yexcr.2014.10.019
Weiß, K., Neef, A., Van, Q., Kramer, S., Gregor, I., Enderlein, J., 2013. Quantifying the Diffusion of Membrane Proteins and Peptides in Black Lipid Membranes with 2-Focus Fluorescence Correlation Spectroscopy. Biophys. J. 105, 455–462. https://doi.org/10.1016/j.bpj.2013.06.004
West, M., Zurek, N., Hoenger, A., Voeltz, G.K., 2011. A 3D analysis of yeast ER structure reveals how ER domains are organized by membrane curvature. J. Cell Biol. 193, 333–346. https://doi.org/10.1083/jcb.201011039
Wilkins, D.K., Grimshaw, S.B., Receveur, V., Dobson, C.M., Jones, J.A., Smith, L.J., 1999. Hydrodynamic Radii of Native and Denatured Proteins Measured by Pulse Field Gradient NMR Techniques †. Biochemistry 38, 16424–16431. https://doi.org/10.1021/bi991765q
Wirtz, K.W., Zilversmit, D.B., 1968. Exchange of phospholipids between liver mitochondria and microsomes in vitro. J. Biol. Chem. 243, 3596–3602.
Wirtz, K.W.A., Zilversmit, D.B., 1969. Participation of soluble liver proteins in the exchange of membrane phospholipids. Biochim. Biophys. Acta BBA - Biomembr. 193, 105–116. https://doi.org/10.1016/0005-2736(69)90063-7
Wright, P.E., Dyson, H.J., 1999. Intrinsically unstructured proteins: re-assessing the protein structure-function paradigm. J. Mol. Biol. 293, 321–331. https://doi.org/10.1006/jmbi.1999.3110

Wu, L., Bauer, C.S., Zhen, X., Xie, C., Yang, J., 2002. Dual regulation of voltage-gated calcium channels by PtdIns(4,5)P2. Nature 419, 947–952. https://doi.org/10.1038/nature01118

Wyles, J.P., Perry, R.J., Ridgway, N.D., 2007. Characterization of the sterol-binding domain of oxysterol-binding protein (OSBP)-related protein 4 reveals a novel role in vimentin organization. Exp. Cell Res. 313, 1426–1437. https://doi.org/10.1016/j.yexcr.2007.01.018

Wyles, J.P., Ridgway, N.D., 2004. VAMP-associated protein-A regulates partitioning of oxysterol-binding protein-related protein-9 between the endoplasmic reticulum and Golgi apparatus. Exp. Cell Res. 297, 533–547. https://doi.org/10.1016/j.yexcr.2004.03.052

Xie, J., Sun, B., Du, J., Yang, W., Chen, H.-C., Overton, J.D., Runnels, L.W., Yue, L., 2011. Phosphatidylinositol 4,5-bisphosphate (PIP2) controls magnesium gatekeeper TRPM6 activity. Sci. Rep. 1. https://doi.org/10.1038/srep00146

Xu, Y., Seet, L.-F., Hanson, B., Hong, W., 2001. The Phox homology (PX) domain, a new player in phosphoinositide signalling 18.

Yan, D., Mäyränpää, M.I., Wong, J., Perttilä, J., Lehto, M., Jauhiainen, M., Kovanen, P.T., Ehnholm, C., Brown, A.J., Olkkonen, V.M., 2008. OSBP-related Protein 8 (ORP8) Suppresses *ABCA1* Expression and Cholesterol Efflux from Macrophages. J. Biol. Chem. 283, 332–340. https://doi.org/10.1074/jbc.M705313200

Yeung, T., Gilbert, G.E., Shi, J., Silvius, J., Kapus, A., Grinstein, S., 2008. Membrane Phosphatidylserine Regulates Surface Charge and Protein Localization. Science 319, 210–213. https://doi.org/10.1126/science.1152066

Zhong, W., Qin, S., Zhu, B., Pu, M., Liu, F., Wang, L., Ye, G., Yi, Q., Yan, D., 2015. Oxysterol-binding protein-related protein 8 (ORP8) increases sensitivity of hepatocellular carcinoma cells to Fas-mediated apoptosis. J. Biol. Chem. 290, 8876–8887. https://doi.org/10.1074/jbc.M114.610188

Zhong, W., Zhou, Y., Li, S., Zhou, T., Ma, H., Wei, K., Li, H., Olkkonen, V.M., Yan, D., 2011. OSBP-related protein 7 interacts with GATE-16 and negatively regulates GS28 protein stability. Exp. Cell Res. 317, 2353–2363. https://doi.org/10.1016/j.yexcr.2011.05.028

Zhou, M., Morais-Cabral, J.H., Mann, S., MacKinnon, R., 2001. Potassium channel receptor site for the inactivation gate and quaternary amine inhibitors. Nature 411, 657–661. https://doi.org/10.1038/35079500

Zhou, Y., Li, S., Mäyränpää, M.I., Zhong, W., Bäck, N., Yan, D., Olkkonen, V.M., 2010. OSBP-related protein 11 (ORP11) dimerizes with ORP9 and localizes at the Golgi–late endosome interface. Exp. Cell Res. 316, 3304–3316. https://doi.org/10.1016/j.yexcr.2010.06.008

Zhou, Y., Robciuc, M.R., Wabitsch, M., Juuti, A., Leivonen, M., Ehnholm, C., Yki-Järvinen, H., Olkkonen, V.M., 2012. OSBP-Related Proteins (ORPs) in Human Adipose Depots and Cultured Adipocytes: Evidence for Impacts on the Adipocyte Phenotype. PLoS ONE 7, e45352. https://doi.org/10.1371/journal.pone.0045352

Zhou, Y., Srinivasan, P., Razavi, S., Seymour, S., Meraner, P., Gudlur, A., Stathopulos, P.B., Ikura, M., Rao, A., Hogan, P.G., 2013. Initial activation of STIM1, the regulator of store-operated calcium entry. Nat. Struct. Mol. Biol. 20, 973–981. https://doi.org/10.1038/nsmb.2625

Zhou, Y., Wohlfahrt, G., Paavola, J., Olkkonen, V.M., 2014. A vertebrate model for the study of lipid binding/transfer protein function: Conservation of OSBP-related proteins between zebrafish and human. Biochem. Biophys. Res. Commun. 446, 675–680. https://doi.org/10.1016/j.bbrc.2013.12.002

Zhuo, Y., Ilangovan, U., Schirf, V., Demeler, B., Sousa, R., Hinck, A.P., Lafer, E.M., 2010. Dynamic Interactions between Clathrin and Locally Structured Elements in a Disordered Protein Mediate Clathrin Lattice Assembly. J. Mol. Biol. 404, 274–290. https://doi.org/10.1016/j.jmb.2010.09.044

Zoncu, R., Perera, R.M., Sebastian, R., Nakatsu, F., Chen, H., Balla, T., Ayala, G., Toomre, D., De Camilli, P.V., 2007. Loss of endocytic clathrin-coated pits upon acute depletion of phosphatidylinositol 4,5-bisphosphate. Proc. Natl. Acad. Sci. 104, 3793–3798. https://doi.org/10.1073/pnas.0611733104

Zurzolo, C., Simons, K., 2016. Glycosylphosphatidylinositol-anchored proteins: Membrane organization and transport. Biochim. Biophys. Acta BBA - Biomembr. 1858, 632–639. https://doi.org/10.1016/j.bbamem.2015.12.018

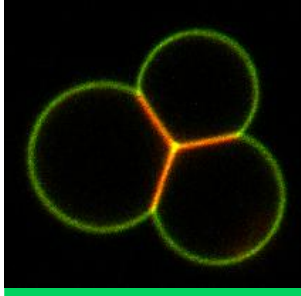

Appendix

APPENDIX

AUTHOR'S LIST OF PUBLICATIONS

Jamecna, D., Polidori, J., Mesmin, B., Bigay, J. and Antonny, B.

'An intrinsically disordered region in OSBP acts as an entropic barrier to control protein dynamics and orientation at membrane contact sites ', *(under revision in Dev Cell)*

Mesmin, B., Bigay, J., Polidori, J., **Jamecna, D**., Lacas-Gervais, S. and Antonny, B. (2017) 'Sterol transfer, PI4P consumption, and control of membrane lipid order by endogenous OSBP', *EMBO J,* 36(21), pp. 3156-3174.

Cattin, A. L., Burden, J. J., Van Emmenis, L., Mackenzie, F. E., Hoving, J. J., Garcia Calavia, N., Guo, Y., McLaughlin, M., Rosenberg, L. H., Quereda, V., **Jamecna, D**., Napoli, I., Parrinello, S., Enver, T., Ruhrberg, C. and Lloyd, A. C. (2015) 'Macrophage-Induced Blood Vessels Guide Schwann Cell-Mediated Regeneration of Peripheral Nerves', *Cell,* 162(5), pp. 1127-39.

An intrinsically disordered region in OSBP acts as an entropic barrier to control protein dynamics and orientation at membrane contact sites

Denisa Jamecna[1], Joël Polidori[1], Bruno Mesmin[1], Manuela Dezi[2,3], Daniel Levy[2,4], Joëlle Bigay[1] and Bruno Antonny[1]

1 : Université Côte d'Azur, CNRS, IPMC, 660 route des lucioles, 06560 Valbonne, France

2 : Laboratoire Physico Chimie Curie, Institut Curie, PSL Research University, CNRS UMR 168, 75005 Paris, France

3 : Institut de Minéralogie, de Physique des Matériaux et de Cosmochimie, UMR 7590, CNRS, UPMC, IRD, MNHN, 75005 Paris, France.

4 : Sorbonne Universités, UPMC, 75005, Paris, France

Correspondence: bigay@ipmc.cnrs.fr; antonny@ipmc.cnrs.fr

Lead contact: antonny@ipmc.cnrs.fr

Abstract

Lipid transfer proteins (LTPs) acting at membrane contact sites (MCS) between the ER and other organelles contain domains involved in heterotypic (e.g. ER to Golgi) membrane tethering as well as domains involved in lipid transfer. Here, we show that a long ≈ 90 aa intrinsically unfolded sequence at the N-terminus of oxysterol binding protein (OSBP) controls OSBP orientation and dynamics at MCS. This Gly-Pro-Ala-rich sequence, whose hydrodynamic radius is twice as that of folded domains, prevents the two PH domains of the OSBP dimer to homotypically tether two Golgi-like membranes and considerably facilitates OSBP in-plane diffusion and recycling at MCS. Although quite distant in sequence, the N-terminus of OSBP-related protein-4 (ORP4) has similar effects. We propose that N-terminal sequences of low complexity in ORPs form an entropic barrier that restrains protein orientation, limits protein density and facilitates protein mobility in the narrow and crowded MCS environment.

Keywords: Intrinsically disordered protein (IDP); low complexity sequence; Membrane Contact Site (MCS); OSBP-related protein (ORP), Lipid transfer protein (LTP).

Introduction

Oxysterol binding protein (OSBP) and OSBP-related proteins (ORPs) constitute a conserved family of lipid transfer proteins (LTPs) that transport key lipids such as cholesterol or phosphatidylserine between cellular membranes (Kim et al., 2013; Olkkonen and Li, 2013; Pietrangelo and Ridgway, 2018). LTPs contribute to the establishment of lipid gradients between organelles and counterbalance the homogenization in lipid composition that accompanies vesicular traffic or lipid signaling reactions (Kim et al., 2015; Saheki et al., 2016; Yadav et al., 2015). ORPs share an OSBP-related domain (ORD), which is responsible for the lipid transfer activity (Im et al., 2005) and functions in a directional manner by counter exchanging a specific lipid for the phosphoinositide PI(4)P (Chung et al., 2015; de Saint-Jean et al., 2011; Mesmin et al., 2013; Moser von Filseck et al., 2015a). Thus, OSBP transports cholesterol from the endoplasmic reticulum (ER) to the trans Golgi network (TGN) owing to back transfer of PI(4)P , which is synthesized in the TGN and hydrolyzed at the ER (Mesmin et al., 2013; 2017; Zewe et al., 2018).

In addition to the ORD, many ORPs carry targeting determinants for the ER and other organelles. These determinants allow ORPs to tether two membranes (e.g. ER and PM or ER and TGN), hence restricting the lipid exchange to membrane contact sites (MCSs), which are regions of close apposition between organelles (intermembrane distance ≈ 10-50 nm)(Levine, 2004; Mesmin et al., 2013). OSBP contains a N-terminal pleckstrin homology (PH) domain, which interacts with the TGN or endosomal phosphoinositide PI(4)P and a central FFAT (two phenylalanines in an acidic tract) motif, which interacts with the general ER receptor VAP-A/B (Furuita et al., 2010; Kaiser et al., 2005; Levine and Loewen, 2006; Levine and Munro, 2002; Loewen et al., 2003). Cellular observations as well as *in vitro* reconstitution experiments suggest that the tripartite PH-FFAT-ORD architecture of OSBP allows this protein to function as a ferry-bridge, bridging the TGN and the ER through its PH domain and FFAT motif, respectively, and

ferrying cholesterol between the ER and TGN through its ORD (Antonny et al., 2018; Mesmin et al., 2013).

Although the tripartite PH-FFAT-ORD architecture of OSBP explains its membrane tethering and lipid transfer activities, many mechanistic questions remain. The very nature of MCSs where two parallel membranes sandwich a thin layer of cytosol should create unique constraints. For example, it is not known whether the linker regions connecting the PH domain, FFAT motif, and ORD are long enough to allow simultaneous membrane tethering and ORD movement between membranes (Antonny et al., 2018; Dittman and Menon, 2017). The compatibility between the movements of folded domains and the linker length is a general issue in MCS, also applying to proteins such as the PI phosphatase Sac1, which hydrolyzes PI(4)P (Stefan et al., 2011; Zewe et al., 2018), and the extended synaptotagmins (Schauder et al., 2014). A second question is the degree of cooperativity between proteins at MCS. The establishment of MCS by some 'pioneered' tethers should indirectly favor the subsequent recruitment of other tethers of the same length. However, having too many proteins in MCS might create some steric hindrance. A recent study using artificial tethers made of fluorescent proteins held by elementary blocks of defined height has started uncovering the complex behavior of proteins at MCS, revealing the possibility of an exclusion mechanism based on the incompatibility between proteins of different lengths or *via* crowding effects (Schmid et al., 2016).

In this study, we focus on an overlooked feature of ORPs: the presence of a long N-terminal region (hereafter abbreviated as N-ter) of low amino-acid complexity upstream of the PH domain. Using OSBP and ORP4 as models, we show that the N-ter has two functions. First, it imposes the geometry of membrane tethering, favoring heterotypic membrane tethering between a VAP-containing membrane and a PI(4)P-containing membrane at the expense of the homotypic configuration where two PI(4)P-rich membranes are held by the two PH domains of OSBP or ORP4, which are dimers. Second, the N-ter prevents OSBP from being too concentrated at MCS, thereby facilitating protein diffusion within MCS and protein recycling between MCS.

Our work uncovers a new function of intrinsically unfolded regions in the functioning of multi-domain proteins.

Results

Bioinformatic analysis of the N-terminal region of OSBP and related proteins

The mammalian ORP family includes 12 members, many of which display a similar domain organization (**Figure 1A, S1A**). The N-terminal half (including PH domain and FFAT motif) is involved in membrane tethering while the C-terminal half (ORD) transfers lipids (Mesmin et al., 2013). For ORP5 and ORP8, which lack FFAT motif, ER tethering depends on a C-ter transmembrane segment (Yan *et al.*, 2008; Du *et al*., 2011). Intriguingly, most ORPs (OSBP, ORP3 - ORP8, ORP10 and ORP11) contain a long sequence upstream of their PH domain (**Figures 1A, S1 and S2**). The exceptions are ORP2, which only consists of the FFAT motif and ORD, and ORP9, which does not contain a sequence upstream of its PH domain. Phylogenetic analysis indicates that the N-ter of OSBP as well as the coiled-coils between the PH domain and FFAT motif appeared later and showed less sequence conservation than the PH domain and ORD (**Figure S2B**).

We assessed the order/disorder distribution along the ORP sequences using Predictor of Naturally Disordered Regions (PONDR®) (**Figure S1A**). We employed two algorithms, VL3 and VSL2, trained on a set of hundreds of disordered and ordered protein regions. Both predictors are based on attributes including amino acid frequencies, sequence complexity and averaged flexibility. The N-ter of OSBP, ORP3–8, ORP10 and ORP11 have a high disorder score (> 0.8), in contrast to the low disorder score of the PH domain and ORD. The low disorder score of the N-ter of ORP1 correlates with the presence of three ankyrin repeats that bind the small GTPase Rab7 on late endosomes (Johansson et al., 2003). The second region of high disorder was found in the linker between the PH domain and ORD. Thus, most ORPs contain long 60-140 aa N-terminal sequences that are predicted to be disordered.

We compared the aa composition of the N-ter of human ORPs using the PH domain and ORD as references for well-folded domains (**Figures 1A** and **S1B**; exact aa range of each region is shown in **Figure S2A**). Pie charts show that the aa composition of the PH domain and ORD is well distributed between the 20 aa, as generally observed for folded domains, whereas the N-terminal sequences display contrasting features (**Figure S1B**). Some N-ter are very rich in proline (black), the strongest disorder-promoting residue (Theillet et al., 2013). Others are enriched in glycine (dark grey), alanine (light grey) and/or in charged residues (red: negative; blue: positive). Common features for all N-ter are the paucity of large hydrophobic residues (Phe, Trp, Ile and Leu; yellow and green) and the abundance of serine (shown in light pink), which is after proline and glutamic acid the third most disorder-promoting residue (Theillet et al., 2013) (**Figure S1B**). Because sequences enriched in proline and in polar and charged residues at the expense of hydrophobic amino acids are not prone to fold, we hypothesized that most N-terminal sequences in ORPs are intrinsically disordered.

The N-terminal regions of OSBP/ORP4 strongly increase their hydrodynamic radii

In the following, we focused on the N-ter of OSBP and ORP4. This choice was motivated by two reasons. First, numerous *in vitro* and cellular assays have been developed for OSBP, thereby facilitating the analysis (Mesmin et al., 2013). Second, ORP4 is the closest OSBP orthologue, but its N-ter is quite different (**Figure 1A** and **S1B**). The N-ter of OSBP is almost entirely composed of Gly, Pro and Ala residues (GPA), which account for 75% of the sequence, whereas ORP4 N-ter is significantly longer and also rich in Ser and Glu. The comparison between ORP4 and OSBP could help defining the general *vs* peculiar properties of their N-ter.

Unstructured sequences occupy a larger volume than structured sequences of the same amino acid length. To estimate the contribution of N-ter to protein size, we performed gel filtration chromatography on purified constructs. The analysis was performed on the full-length protein (OSBP *vs* ΔN-OSBP) as well as on shorter constructs (**Figure 1B-D**). N-PH-FFAT and PH-

FFAT correspond to the first half of OSBP and can be used to recapitulate its tethering activity, independently of lipid transfer (Mesmin et al., 2013). N-PH-ΔCC-FFAT and PH-ΔCC-FFAT lack the predicted coiled-coil regions between the PH domain and FFAT motif and behave as monomers rather than as dimers in the gel-filtration column. In all cases, we observed that N-ter had a large impact on protein size, increasing the Stoke's radius by ~0.5 to 1 nm for OSBP constructs (OSBP *vs* ΔN-OSBP, N-PH-FFAT *vs* PH-FFAT; N-PH-ΔCC-FFAT *vs* PH-ΔCC-FFAT) and by ~1.3 nm for ORP4 constructs (N-PH-FFAT *vs* PH-FFAT) (**Figure 1D**). This increase was about 2-fold higher than what was expected from the slope of the calibration curve, which was established with folded globular standards. Because denaturation increases the hydrodynamic radius of well-folded proteins by ca. two-fold (Dutta and Bhattacharyya, 2001), this hydrodynamic analysis suggests that the N-ter of both OSBP and ORP4 are intrinsically unfolded.

The N-ter accelerates OSBP cellular dynamics

To assess the role of N-ter on OSBP subcellular localization, we transfected RPE1 and HeLa cells with the following C-terminally mCherry-tagged constructs: OSBP, ΔN-OSBP, N-PH-FFAT and PH-FFAT (**Figure 1B**). In both cell types, full-length OSBP localized mainly to the Golgi complex (as evidenced by co-localization with the marker BFP-GalT, **Figures 2A** and **S3A**) and, to a lesser extent, to late endosomes (colocalized with marker EGFP-Rab7, **Figure S3A**). However, a large fraction of OSBP was also found in the cytosol. Compared to OSBP, ΔN-OSBP displayed a 2-fold higher Golgi partitioning ratio, whereas both N-PH-FFAT and PH-FFAT localized almost completely to the Golgi complex with a very minor cytosolic fraction (**Figure 2A**). The large decrease in the apparent Golgi partitioning of the constructs containing the ORD (OSBP and ΔN-OSBP) as compared to the constructs lacking the ORD (N-PH-FFAT and PH-FFAT) is due to a negative feedback effect of the ORD, which by transferring PI(4)P destabilizes the interaction of OSBP with membranes (Mesmin et al., 2013).

We performed similar experiments with ORP4 N-PH-FFAT and ORP4 PH-FFAT (**Figure 2B**). In agreement with a previous report (Wang *et al.*, 2002), ORP4 constructs containing the ORD (ORP4 and ΔN-ORP4) co-localized with intermediate filaments (**Fig. S3B and C**) and only modestly stained the Golgi making their analysis complicated. We thus focused on ORP4 N-PH-FFAT and ORP4 PH-FFAT, which only partitioned between the cytosol and the Golgi. ORP4 PH-FFAT showed significantly higher Golgi partitioning than ORP4 N-PH-FFAT (**Figure 2B**). Thus, the N-ter of OSBP and ORP4 reduce the Golgi membrane partitioning of these proteins.

We assessed the dynamics of the OSBP and ORP4 constructs at the Golgi by fluorescence recovery after photobleaching (FRAP) experiments. As shown in **Figure 2C**, the rate of fluorescence recovery inversely correlated with the Golgi partitioning of the constructs: full-length (FL) > ΔN > N-PH-FFAT > PH-FFAT. In addition, the recovery kinetics of the OSBP constructs were systematically slower than that of the corresponding ORP4 constructs, in good agreement with the higher Golgi partitioning of OSBP *vs* ORP4 (**Figure 2A and B**). Importantly, all N-ter-harboring constructs manifested much faster (≈ 3-5-fold) fluorescence recovery than the corresponding ΔN-constructs, suggesting that the N-ter facilitates protein lateral motility at the membrane surface and/or exchange with the cytosolic pool (**Figure 2C**).

N-ter facilitates OSBP recycling under conditions of restricted PI(4)P synthesis

To further assess the role of N-ter in OSBP dynamics, we performed experiments in which we artificially forced OSBP to move within the TGN (Mesmin et al., 2017). For this, we inhibited the Golgi-associated kinase PI4KIIIβ, which co-localizes with OSBP and locally provides PI(4)P to the OSBP cycle. When PI4KIIIβ is inhibited by the specific inhibitor PIK93, OSBP exhibits travelling waves, which probably corresponds to movements of OSBP contact sites towards PI(4)P-rich regions produced by remote PI4-kinases (Mesmin et al., 2017). These waves are very regular, making them adapted to precise dynamics measurements. The experiments were performed in cells stably expressing GFP-PH_{OSBP}, which acts as a PI(4)P/Arf1

reporter at the Golgi. After silencing endogenous OSBP using specific siRNA, PIK93 no longer induced travelling waves of PH_{OSBP} indicating that OSBP is largely responsible for PI(4)P turnover at the Golgi (**Figure 3A-C**).

We performed rescue experiments by expressing siRNA-resistant forms of either full-length OSBP or ΔN-OSBP (OSBP-*res*-mCherry and ΔN-OSBP-*res*-mCherry, respectively). ΔN-OSBP-*res*-mCherry was more stably associated with the TGN than OSBP-*res*-mCherry (**Figure 3D-E**) in agreement with the steady state localization experiments (**Figure 2A-B**). Upon PIK93 addition, OSBP-*res*-mCherry restored the formation of large PH_{OSBP} travelling waves (green signal) and showed itself (red signal) travelling waves in phase with that of PH_{OSBP} (**Figure 3F**). In contrast, ΔN-OSBP-*res*-mCherry did not rescue the siRNA phenotype. Upon PIK93 addition, we observed a sharp decrease in GFP-PH_{OSBP} at the TGN suggesting that ΔN-OSBP consumed PI(4)P (compare the black trace in **Figure 3C** to the green trace in **Figure 3F lower panel**). However, this decrease was followed by waves of much smaller amplitude than that observed with full-length OSBP (**Figure 3F-G**).

Altogether, the experiments presented in **Figures 2** and **3** suggest that OSBP N-ter facilitates protein turnover within or between cellular membranes without affecting its PI(4)P transfer activity.

The N-ter of OSBP has no effect on its lipid transfer activity

The fact that the N-ter is not involved in PI(4)P transfer was confirmed by steady-state experiments where we analyzed the consequence of overexpressing OSBP or ΔN-OSBP on the Golgi/cytosol ratio of GFP-PH_{OSBP}. Both forms strongly diminished the level of the PI(4)P probe at the Golgi (**Figure S4A-B**).

To directly address the influence of the N-ter of OSBP on lipid transfer, we performed liposome-based reconstitution experiments. We followed the transfer of the naturally

fluorescent analog of cholesterol (DHE) from ER-like to Golgi-like liposomes (**Figure S4C**). Conversely, we followed the relocation of PI(4)P from Golgi-like liposomes (4mol% PI(4)P) to ER-like liposomes by monitoring the quenching of a PI(4)P probe (**Figure S4D**). OSBP was used in catalytic amount compared to PI(4)P (1 OSBP for 30 accessible PI(4)P molecules) but in large excess over the liposomes (≈ 60 OSBP molecules for one liposome). Therefore, equilibration of PI(4)P between the donor and acceptor liposomes required OSBP to undergo multiple rounds of lipid exchange on the same liposomes; without the need for OSBP to translocate between different liposomes. As shown in **Figure S4C-D**, OSBP and ΔN-OSBP were indistinguishable in their sterol and PI(4)P exchange activity. This similarity also applied when cholesterol and PI(4)P were initially present in the ER and Golgi liposomes, respectively (**Figure S4D**), a condition that considerably accelerated the rate of PI(4)P transfer due to coupling between forward cholesterol transfer and backward PI(4)P transfer (Mesmin et al., 2017; Moser von Filseck et al., 2015b). We concluded that the N-ter is not involved in the mechanism of sterol/PI(4)P exchange by OSBP.

The N-ter limits the membrane recruitment of the PH domain by a crowding effect

The above analysis suggests that the N-ter of OSBP is an inert appendage that does not interfere with the molecular mechanism of lipid transfer but controls OSBP dynamics on membranes. Given its low complexity sequence, its position in the protein and its effect on the hydrodynamic volume of the protein, we hypothesized that the N-ter could have a simple steric effect, controlling OSBP density on membranes by limiting the surface concentration of the downstream PH domain. To test this hypothesis, we compared the membrane-binding properties of N-PH-ΔCC-FFAT and PH-ΔCC-FFAT. We labeled N-PH-ΔCC-FFAT and PH-ΔCC-FFAT with the fluorophore Alexa488 and tested their binding to giant unilamellar vesicles (GUVs) of Golgi-like lipid composition containing 0.1% Atto390-DOPE and 4% PI(4)P. We incubated these GUVs with increasing concentrations of N-PH-ΔCC-FFAT or PH-ΔCC-FFAT (**Figure 4A-B**). N-PH-ΔCC-FFAT displayed lower recruitment on GUVs and saturated the

membrane at lower protein concentration, as indicated by the smaller increase in signal intensity with concentration, and stagnation of fluorescence signal above 400nM. On the contrary, PH-ΔCC-FFAT displayed a higher density on GUVs, and continued binding to GUVs at higher concentrations (**Figure 4B**). This observation suggested that the N-ter limits the surface density of OSBP on PI(4)P-containing membrane.

To further analyze this density effect, we performed liposome-based sedimentation assays. We increased the surface density of PI(4)P in liposomes from 1, 2, 5, 8, to 15 mol% while reciprocally decreasing the liposome concentration from 2, 1, 0.4, 0.25, to 0.13 mM, thereby keeping the total PI(4)P concentration constant (20 μM) (**Figure 4C-D**). After centrifugation and quantification of bound protein, we observed that N-PH-ΔCC-FFAT and PH-ΔCC-FFAT were equally recruited on liposomes with the lowest PI(4)P density (1 mol%). In the absence of PI(4)P, background binding was observed. Thus, the affinity of the PH domain for PI(4)P did not seem to be directly affected by N-ter. However, as the density of PI(4)P increased, N-PH-ΔCC-FFAT showed a stronger reduction in binding as compared to PH-ΔCC-FFAT. These observations suggest that the N-ter limits the membrane density of the adjacent PH domain by a crowding effect.

OSBP N-ter controls the geometry of membrane tethering

OSBP interacts not only, *via* its PH domain, with PI(4)P on Golgi membrane but also, *via* its FFAT motif, with the ER-resident protein VAP-A (Levine and Munro, 1998; Loewen *et al.*, 2003). This dual interaction allows OSBP to act as a membrane tether. To determine whether the N-ter influences OSBP and ORP4 tethering activities, we reconstituted membrane tethering using purified components (Mesmin et al., 2013). We prepared two liposome populations with a composition corresponding to that of the ER with 2% DGS-NTA-Ni and of the Golgi with 4% PI(4)P. The presence of DGS-NTA-Ni allowed recruitment of a histidine-tagged form of VAP-A onto the ER liposomes. Then, we mixed the two liposome populations, added purified N-PH-

FFAT or PH-FFAT and followed liposome aggregation in real time by dynamic light scattering (DLS).

In presence of all tethering determinants (Golgi + ER + VAP), we observed no difference in the tethering activity of N-PH-FFAT and PH-FFAT from both OSBP and ORP4 (**Figure 5A and S5A**). Surprisingly, when we removed VAP-A (**Figures 5B and S5B**) or when we replaced VAP-A with a mutant (VAP-A KM/DD) unable to interact with the FFAT motif (**Figure S5C**) we observed a striking difference between the two constructs: PH-FFAT caused liposome aggregation, whereas N-PH-FFAT did not.

We suspected that, in the absence of VAP-A, the ER-like liposomes might not be included in the aggregates promoted by PH-FFAT, which would instead promote homotypic tethering of Golgi liposomes. To distinguish homotypic (Golgi-Golgi) *vs* heterotypic (ER-Golgi) tethering, we labeled the Golgi-like liposomes with Texas Red-DOPE and the ER-like liposomes with Oregon Green-DOPE (Ho and Stroupe, 2015). As such, we could complement the DLS measurements with the visualization of liposome aggregates by confocal microscopy. When VAP-A was present, both N-PH-FFAT and PH-FFAT of OSBP or ORP4 promoted the tethering of ER with Golgi liposomes as the aggregates displayed the color of the two lipid probes (**Figure 5A and S5A**). When VAP-A was absent, N-PH-FFATs did not aggregate any liposome population, whereas PH-FFAT selectively promoted the tethering of the Golgi liposomes (**Figure 5B and S5B**). Indeed, under these conditions, we only observed red aggregates, revealing that N-ter-lacking constructs gained an unusual capacity in tethering liposomes in a Golgi-Golgi manner.

To investigate how PH-FFAT promotes the homotypic tethering of Golgi liposomes, we performed additional experiments. First, we replaced PH-FFAT or N-PH-FFAT by equivalent constructs lacking the coiled-coil region (i.e. PH-[ΔCC]-FFAT or N-PH-[ΔCC]-FFAT) (**Figure 5C-D**). Second, we removed PI(4)P from the Golgi liposomes (**Figure S6A-B**). In both cases, we observed no Golgi-Golgi homotypic tethering (**Figure 5D and S6A**), although PH-ΔCC-FFAT and

N-PH-ΔCC-FFAT kept the ability to tether ER liposomes to Golgi liposomes (**Figure 5C**). These observations demonstrate that the two PH domains of the PH-FFAT construct from OSBP, which forms homodimers, can simultaneously bind two PI(4)P-containing membranes, thereby causing homotypic tethering. When the PH domains are flanked by the N-ter, homotypic membrane tethering is prevented, whereas heterotypic membrane tethering is not affected.

CryoEM analysis of homotypic tethering by PH-FFAT

We visualized by cryoEM the homotypic membrane contacts induced by the PH-FFAT region of OSBP on PI(4)P-containing liposomes. In incubations with PH-FFAT but not with N-PH-FFAT, we observed large regions of juxtaposition between the liposomes (**Figures 5E and S6C**). In both cases, proteins as seen by dotted electron densities were present bound to the external lipid leaflet of the membrane (see inserts in **Figure 5E**). The contact sites induced by PH-FFAT had a well-defined intermembrane distance (15 ± 1 nm) and showed a thin band of protein electron density right in the middle of the two juxtaposed membranes, suggesting that PH-FFAT adopts a symmetric conformation to tether the two liposomes.

OSBP N-ter regulates protein enrichment and diffusion at homotypic membrane interfaces

Next, we investigated the influence of the N-ter on the distribution and mobility of OSBP constructs at membrane-membrane interfaces made by GUVs under the two main tethering conditions identified in this study, i.e. homotypic Golgi-Golgi and heterotypic ER-Golgi tethering. In all cases, the experiments consisted in adding GUVs of defined features (Golgi-like and/or ER-like) to solutions of fluorescent proteins (e.g. VAP-A, PH-FFAT, N-PH-FFAT, PH-ΔCC-FFAT, N-PH-ΔCC-FFAT). Two to three fluorescent dyes were used to visualize the GUVs and proteins by confocal microscopy and to analyze protein dynamics by FRAP experiments (**Figure 6**). Note that these assays were complementary to the bulk assays using LUVs and dynamic light scattering. The GUV assay provided unique information on the distribution and dynamics of the proteins at the membrane surface but was less quantitative in term of tethering activity than

bulk assays as it is difficult to master the GUV concentration and therefore the protein/lipid ratio.

We first incubated Golgi-like GUVs (labelled with the blue probe Atto 390 and containing 2 mol% PI(4)P) with either N-PH-FFAT or PH-FFAT (labeled with Alexa 488 or Alexa568 probes) (**Figure 6A**). With PH-FFAT, we observed large GUV-GUV contacts, as manifested by the mutual deformation of the tethered GUVs at the interfacial region. Surprisingly, we also observed GUV-GUV contacts in the presence of N-PH-FFAT, which seemed at odds with the results of the DLS experiments (**Figure 6A**). However, there was an obvious difference between N-PH-FFAT and PH-FFAT. Whereas PH-FFAT was greatly enriched at the GUV-GUV contact, N-PH-FFAT decorated all membrane surface and showed only a slight enrichment at the interface (**Figure 6A**). We also noticed that N-PH-FFAT was not perfectly pure. On SDS-PAGE, the protein exhibited some contaminants with a lower molecular weight than the major band (**Figures 1C and S7A**). An antibody against the C-terminal FFAT motif showed that all bands contained the C-terminus indicating that N-PH-FFAT was contaminated at a level of about 16% by fragments with a truncated N-ter, which could explain the tendency of the protein preparation to promote homotypic tethering in the GUV assay. In spite of this contamination, the comparison between N-PH-FFAT and PH-FFAT indicated that the presence of the N-ter favored a balanced protein distribution over all membrane surfaces, whereas the N-ter-lacking construct tended to accumulate at membrane interfaces (**Figure 6A**).

We compared the membrane diffusion rates of OSBP-derived constructs by FRAP on tethered GUVs (**Figure 6B**). The bleaching area was located either on the free GUV surface or in the center of the GUV-GUV contact site. For both constructs, the recovery on the free GUV surface was instantaneous ($k > 1\ s^{-1}$; Fig. S4B) (**Figure S7B**). In contrast, we could resolve protein recovery at the GUV-GUV interface and observed that recovery of N-PH-FFAT was much quicker than that of PH-FFAT (recovery time of ≈ 1 s and >> 100 s, respectively, **Figure 6B**).

Thus, the N-ter has a large impact on protein density and diffusion rate of the protein at the GUV-GUV interface.

In studies with fluorescent binding and nonbinding model proteins at the interface between GUVs, it has been reported that, small proteins that are able to transversally bind each other and establish a contact site can exclude larger non-binding proteins (Schmid et al., 2016). This exclusion is size-dependent and also influenced by protein crowding. Given the clear difference in membrane distribution and diffusion rate between PH-FFAT and N-PH-FFAT, we wondered if the effect of N-ter would also be evident under conditions where both proteins co-localize on the same GUV-GUV contact. We thus added GUVs to a 1:1 protein mixture of N-PH-FFAT and PH-FFAT, which could be distinguished from each other by different fluorescent dyes. After several hours of incubation, we observed a clear segregation between the two proteins: PH-FFAT concentrated in the GUV-GUV contact sites, whereas N-PH-FFAT predominantly localized on the free GUV surface (**Figure 6C**). Thus, the presence of the N-ter upstream of the PH domain is an effective way of regulating protein crowding/exclusion at membrane interfaces.

To confirm the effect of the N-ter on protein exclusion, we compared the ability of N-PH-FFAT or PH-FFAT to invade a membrane interface that was already occupied by the other protein. We first pre-incubated GUVs with either N-PH-FFAT or PH-FFAT labelled with one color and then added an excess of the other protein (PH-FFAT or N-PH-FFAT, respectively) labeled with a different fluorophore. Whereas N-PH-FFAT did not invade PH-FFAT-tethered membrane interfaces, PH-FFAT was able to invade and even replace N-PH-FFAT after a certain time (**Figure S7C**). This observation further underlines the impact of the N-ter on protein distribution and density at membrane interfaces.

OSBP N-ter regulates protein diffusion at heterotypic membrane interfaces

Last, we moved to conditions of heterotypic tethering by mixing the OSBP constructs with two populations of GUVs: ER-like GUVs containing 3% DOGS-NiNTA to promote the binding of histidine tagged VAP-A and Golgi-like GUVs containing 2% PI(4)P (**Figure 6D**). The former contained no probe and thus were visible only when a fluorescent protein was bound to them, whereas the latter were labelled with a blue lipid probe. In pilot experiments, we noticed that incubations with N-PH-FFAT of PH-FFAT constructs gave complex assemblies where the GUVs underwent both homotypic and heterotypic contacts, making the analysis complicated. To simplify the system and focus only on the role of the N-ter, we compared N-PH-ΔCC-FFAT and PH-ΔCC-FFAT. The lack of the coiled-coil domain made these constructs monomeric and thus only able to drive heterotypic tethering (see **Figures 1D and 5C-D**). Furthermore, their monomeric nature necessarily decreased the number of putative interactions with the GUVs, which should favor protein recycling and therefore FRAP analysis. **Figure 6D** presents confocal microscopy pictures of heterotypic ER-Golgi GUV-GUV contacts promoted by N-PH-ΔCC-FFAT or PH-ΔCC-FFAT. The heterotypic nature of these GUV-GUV contacts was manifested by the blue fluorescence distribution, which was present only on the Golgi-like GUVs. In all cases, we noticed a dramatic enrichment of both VAP-A and N-PH-ΔCC-FFAT or PH-ΔCC-FFAT at the ER-like Golgi-like GUV interface. However, FRAP analysis showed that N-PH-FFAT recovered within seconds in the GUV-GUV contact region, whereas PH-FFAT showed very slow recovery (**Figure 6E**). This striking difference in recovery rate was also observed for VAP-A in the GUV-GUV contact zone (**Figure 6F**). Thus, the N-ter also controls OSBP density and mobility under heterotypic tethering conditions, i.e. when the protein is engaged in a dual interaction with VAP-A on one membrane and PI(4)P on the other membranes.

Discussion

The geometry of MCS creates a confined (≈ 20 nm-thick) environment, which could impede protein dynamics. However, the function of MCS as privileged zones for material exchange between organelles suggests that proteins in MCS should keep some mobility. This is especially true for LTPs, which are responsible for massive lipid flows in the cell (Hanada et al., 2003; Mesmin et al., 2017). Our work reveals a key role for the long N-terminal tail of OSBP in its dynamics at MCS. The N-ter has no direct effect on the lipid transfer mechanism *per se*, but considerably accelerates OSBP mobility within the narrow MCS environment. In addition, the N-ter restricts the orientation of OSBP by favoring heterotypic over homotypic membrane tethering. These two observations suggest a model in which the N-ter acts as an entropic barrier to prevent OSBP mis-orientation and crowding at MCS (**Figure 7**).

As determined by FRAP experiments, the N-ter accelerates the apparent mobility of OSBP or of its PH-FFAT membrane tethering region by 3 to 10-fold, both in cells and in reconstituted lipid membrane-based systems. This effect is striking both by its trend and by its amplitude. Increasing the size of a protein generally decreases its mobility due to higher friction with the milieu; the cytoplasm in the case of a soluble protein, the surrounding lipid bilayer in the case of a transmembrane protein (Lippincott-Schwartz et al., 2001). However, the effect of protein size is generally modest: for spherical proteins, doubling the molecular weight decreases the diffusion coefficient by 1.25-fold given the cubic relationship between MW and radius (Lippincott-Schwartz et al., 2001). For transmembrane proteins, reconstitution experiments in model liposomes indicate that the diffusion of large multipass membrane proteins is only 1.5 slower than that of a single transmembrane helix (Ramadurai et al., 2009). These comparisons underline the remarkable effect of OSBP N-ter: it constitutes only one tenth (80 aa) of OSBP sequence (807 aa) and yet it increases the apparent mobility of OSBP/ORP4 and derived constructs in MCS by almost an order of magnitude (**Figures 2C, 6B and 6E**).

375 The complex arrangements of membranes at the Golgi makes the interpretation of FRAP
376 recovery curves in this region difficult (Lippincott-Schwartz et al., 2001). OSBP recovery could
377 occur by lateral diffusion within MCS as well as by exchange with the cytosol pool. Furthermore,
378 the lipid transfer activity of OSBP creates a negative feedback loop whereby PI(4)P transfer
379 weakens in turn OSBP membrane association (Mesmin et al., 2013). In contrast, the large and
380 simple geometry of reconstituted GUV-GUV contacts promoted by tethering constructs that
381 have no lipid exchange activity ((N)-PH-FFAT and (N)-PH-ΔCC-FFAT) facilitates the analysis.
382 Akin to what happens in cell-cell contacts (Bell, 1978; Wu et al., 2008), fluorescence recovery in
383 a central spot within a MCS probably occurs via a mixture of diffusive motions and
384 association/dissociation events. Fitting the recovery curves for N-PH-ΔCC-FFAT suggests an
385 apparent diffusion coefficient in the range of 0.15 $\mu m^2\ s^{-1}$, whereas no significant recovery was
386 observed when the construct lacked the N-ter. In addition, OSBP N-ter imposes the mobility of
387 VAP-A, suggesting a general effect on MCS dynamics.

388 When a tether molecule starts bridging two membranes, other similar molecules get
389 enriched in the forming MCS as their size matches the intermembrane distance (Schmid et al.,
390 2016). Although this cooperativity is advantageous for MCS formation, it could lead to an excess
391 of molecules in the MCS, which would in turn prevent their motion. Indeed, protein diffusion
392 under crowding conditions is no longer dominated by friction with the solvent but by protein-
393 protein collisions (Frick et al., 2007; Ramadurai et al., 2009). Akin to what has been described in
394 neurofilaments (Brown and Hoh, 1997), our experiments suggest that OSBP N-ter acts as an
395 entropic barrier whose thermal motion might set the limit for OSBP density at the membrane
396 surface, thereby preventing OSBP immobilization by crowding. Indeed, protein disorder has a
397 striking effect on the diffusion of model proteins (Wang et al., 2012). In the dilute regime, an
398 intrinsically unfolded protein diffuses slower than a folded protein of similar MW because the
399 former experiences higher friction with the solvent than the latter. Under high crowding regime,
400 the unfolded protein diffuses faster owing to higher intrinsic flexibility.

401 The second effect of the N-ter is to prevent the two PH domains of OSBP from bridging
402 two PI(4)P-containing membranes. This tethering geometry should be avoided as it diverts
403 OSBP from productive ER to Golgi sterol transfer. The N-ter could also prevent the binding of
404 OSBP to PI(4)P present in the ER before SAC1 hydrolysis. However, the possibility of homotypic
405 tethering pauses the question of the utility of OSBP dimerization. The coiled-coils between the
406 PH domain and the FFAT motif are probably dispensable for membrane tethering and lipid
407 transfer. For example, Osh3 displays the same triad organization as OSBP (PH domain - FFAT
408 motif – ORD), but the linker between the PH domain and the FFAT domain is predicted to form a
409 37 nm-long monomeric unstructured region (Tong et al., 2013). Similarly, phylogenetic analysis
410 of OSBP indicates that the N-ter and coiled-coil regions are recent features as compared to the
411 PH domain and ORD (**Figure S2B**). Because the advantage of coiled-coils *vs* flexible tethers is to
412 precisely set the intermembrane distance, we suggest that the appearance of the N-ter and
413 coiled-coils has allowed OSBP to finely adapt to the complex membrane organization of the
414 Golgi apparatus in higher organisms.

415 Many LTPs acting at MCS contain a low complexity N-ter region upstream their PH
416 domain. These include not only ORP proteins but also members of the Lam family of sterol
417 transporters (Ysp3p, Lam4P, Lam5p, Lam6p in yeast, GRAMD1A-C in human) (Gatta et al.,
418 2015). These sequences are different, which might reflect either additional functions or the
419 weak evolutionary pressure for sequence conservation in intrinsically disordered regions.
420 Nevertheless, the fact that two different N-ter (in OSBP and in ORP4) have similar effects on
421 protein mobility in a cellular context suggest than the mere control of protein orientation and
422 density is a plausible unifying role.

Acknowledgments

We thank N. Leroudier, D. Deblay, J. Cazareth and F. Brau for technical assistance, A. Di Cicco for cryo-EM image acquisition and for fruitful discussions, and A. Patel and A. Copic for comments on the manuscript. This work was supported by CNRS, Institut Curie and the Agence Nationale de la Recherche (ANR-15-CE11-0027-02 and ANR-11-LABX-0028-01). D.J. was supported by a PhD fellowship from the Signalife PhD Programme. We thank the Cell and Tissue Imaging (PICT-IBiSA), Institut Curie, member of the French National Research Infrastructure France-BioImaging (ANR10-INBS-04).

Author Contributions

Conceptualization, D.J., J.B., and B.A.; Methodology, D.J., J.P., M.D., B.M. and J.B; Investigation, D.J., J.P., B.M., M.D. and J.B; Writing - Original Draft, D.J and B.A.; Writing – Review & Editing, B.A.; Funding Acquisition, B.M., D.L. and B.A.; Supervision, J.B., D.L. and B.A.

Declaration of Interests

None

References

Antonny, B., Bigay, J., Mesmin, B., 2018. The Oxysterol-Binding Protein Cycle: Burning Off PI(4)P to Transport Cholesterol. Annu. Rev. Biochem. 87, 809–837. doi:10.1146/annurev-biochem-061516-044924

Bell, G., 1978. Models for the specific adhesion of cells to cells. Science 200, 618–627. doi:10.1126/science.347575

Brown, H.G., Hoh, J.H., 1997. Entropic exclusion by neurofilament sidearms: a mechanism for maintaining interfilament spacing. Biochemistry 36, 15035–15040. doi:10.1021/bi9721748

Chung, J., Torta, F., Masai, K., Lucast, L., Czapla, H., Tanner, L.B., Narayanaswamy, P., Wenk, M.R., Nakatsu, F., De Camilli, P., 2015. INTRACELLULAR TRANSPORT. PI4P/phosphatidylserine countertransport at ORP5- and ORP8-mediated ER-plasma membrane contacts. Science 349, 428–432. doi:10.1126/science.aab1370

de Saint-Jean, M., Delfosse, V., Douguet, D., Chicanne, G., Payrastre, B., Bourguet, W., Antonny, B., Drin, G., 2011. Osh4p exchanges sterols for phosphatidylinositol 4-phosphate between lipid bilayers. The Journal of Cell Biology 195, 965–978. doi:10.1083/jcb.201104062

Dittman, J.S., Menon, A.K., 2017. Speed Limits for Nonvesicular Intracellular Sterol Transport. Trends in Biochemical Sciences 42, 90–97. doi:10.1016/j.tibs.2016.11.004

Dutta, S., Bhattacharyya, D., 2001. Size of Unfolded and Dissociated Subunits versus that of Native Multimeric Proteins. J Biol Phys 27, 59–71. doi:10.1023/A:1011826525684

Frick, M., Schmidt, K., Nichols, B.J., 2007. Modulation of lateral diffusion in the plasma membrane by protein density. Current Biology 17, 462–467. doi:10.1016/j.cub.2007.01.069

Furuita, K., Jee, J., Fukada, H., Mishima, M., Kojima, C., 2010. Electrostatic interaction between oxysterol-binding protein and VAMP-associated protein A revealed by NMR and mutagenesis studies. J. Biol. Chem. 285, 12961–12970. doi:10.1074/jbc.M109.082602

Gatta, A.T., Wong, L.H., Sere, Y.Y., Calderón-Noreña, D.M., Cockcroft, S., Menon, A.K., Levine, T.P., 2015. A new family of StART domain proteins at membrane contact sites has a role in ER-PM sterol transport. eLife 4, 400. doi:10.7554/eLife.07253

Hanada, K., Kumagai, K., Yasuda, S., Miura, Y., Kawano, M., Fukasawa, M., Nishijima, M., 2003. Molecular machinery for non-vesicular trafficking of ceramide. Nature 426, 803–809. doi:10.1038/nature02188

Ho, R., Stroupe, C., 2015. The HOPS/class C Vps complex tethers membranes by binding to one Rab GTPase in each apposed membrane. Mol. Biol. Cell 26, 2655–2663. doi:10.1091/mbc.E14-04-0922

Im, Y.J., Raychaudhuri, S., Prinz2, W.A., Hurley, J.H., 2005. Structural mechanism for sterol sensing and transport by OSBP-related proteins. Nature 437, 154–158. doi:10.1038/nature03923

Johansson, M., Bocher, V., Lehto, M., Chinetti, G., Kuismanen, E., Ehnholm, C., Staels, B., Olkkonen, V.M., 2003. The Two Variants of Oxysterol Binding Protein-related Protein-1 Display Different Tissue Expression Patterns, Have Different Intracellular Localization, and Are Functionally Distinct. Mol. Biol. Cell 14, 903–915. doi:10.1091/mbc.e02-08-0459

Kaiser, S.E., Brickner, J.H., Reilein, A.R., Fenn, T.D., Walter, P., Brunger, A.T., 2005. Structural Basis of FFAT Motif-Mediated ER Targeting. Structure 13, 1035–1045. doi:10.1016/j.str.2005.04.010

Kim, Y.J., Guzman-Hernandez, M.L., Wisniewski, E., Balla, T., 2015. Phosphatidylinositol-Phosphatidic Acid Exchange by Nir2 at ER-PM Contact Sites Maintains Phosphoinositide Signaling Competence. Developmental Cell 33, 549–561. doi:10.1016/j.devcel.2015.04.028

Kim, Y.J., Hernandez, M.-L.G., Balla, T., 2013. Inositol lipid regulation of lipid transfer in specialized membrane domains. Trends in Cell Biology 23, 270–278. doi:10.1016/j.tcb.2013.01.009

Lehto, M., Laitinen, S., Chinetti, G., Johansson, M., Ehnholm, C., Staels, B., Ikonen, E., Olkkonen, V.M., 2001. The OSBP-related protein family in humans. The Journal of Lipid Research 42, 1203–1213.

Levine, T.P., 2004. Short-range intracellular trafficking of small molecules across endoplasmic reticulum junctions. Trends in Cell Biology 14, 483–490. doi:10.1016/j.tcb.2004.07.017

Levine, T.P., Loewen, C.J.R., 2006. Inter-organelle membrane contact sites: through a glass, darkly. Current Opinion in Cell Biology 18, 371–378. doi:10.1016/j.ceb.2006.06.011
Levine, T.P., Munro, S., 2002. Targeting of Golgi-specific pleckstrin homology domains involves both PtdIns 4-kinase-dependent and -independent components. Current Biology 12, 695–704.
Lippincott-Schwartz, J., Snapp, E., Kenworthy, A., 2001. Studying protein dynamics in living cells. Nature Reviews Molecular Cell Biology 2, 444–456. doi:10.1038/35073068
Loewen, C.J.R., Roy, A., Levine, T.P., 2003. A conserved ER targeting motif in three families of lipid binding proteins and in Opi1p binds VAP. The EMBO Journal 22, 2025–2035. doi:10.1093/emboj/cdg201
Mesmin, B., Bigay, J., Moser von Filseck, J., Lacas-Gervais, S., Drin, G., Antonny, B., 2013. A Four-Step Cycle Driven by PI(4)P Hydrolysis Directs Sterol/PI(4)P Exchange by the ER-Golgi Tether OSBP. Cell 155, 830–843. doi:10.1016/j.cell.2013.09.056
Mesmin, B., Bigay, J., Polidori, J., Jamecna, D., Lacas-Gervais, S., Antonny, B., 2017. Sterol transfer, PI4P consumption, and control of membrane lipid order by endogenous OSBP. The EMBO Journal 36, 3156–3174. doi:10.15252/embj.201796687
Moser von Filseck, J., Čopič, A., Delfosse, V., Vanni, S., Jackson, C.L., Bourguet, W., Drin, G., 2015a. INTRACELLULAR TRANSPORT. Phosphatidylserine transport by ORP/Osh proteins is driven by phosphatidylinositol 4-phosphate. Science 349, 432–436. doi:10.1126/science.aab1346
Moser von Filseck, J., Vanni, S., Mesmin, B., Antonny, B., Drin, G., 2015b. A phosphatidylinositol-4-phosphate powered exchange mechanism to create a lipid gradient between membranes. Nature Communications 6, 6671. doi:10.1038/ncomms7671
Olkkonen, V.M., Li, S., 2013. Oxysterol-binding proteins: sterol and phosphoinositide sensors coordinating transport, signaling and metabolism. PROGRESS IN LIPID RESEARCH 52, 529–538. doi:10.1016/j.plipres.2013.06.004
Pietrangelo, A., Ridgway, N.D., 2018. Bridging the molecular and biological functions of the oxysterol-binding protein family. Cell. Mol. Life Sci. 510, 48–20. doi:10.1007/s00018-018-2795-y
Ramadurai, S., Holt, A., Krasnikov, V., van den Bogaart, G., Killian, J.A., Poolman, B., 2009. Lateral diffusion of membrane proteins. J. Am. Chem. Soc. 131, 12650–12656. doi:10.1021/ja902853g
Saheki, Y., Bian, X., Schauder, C.M., Sawaki, Y., Surma, M.A., Klose, C., Pincet, F., Reinisch, K.M., De Camilli, P., 2016. Control of plasma membrane lipid homeostasis by the extended synaptotagmins. Nat Cell Biol. doi:10.1038/ncb3339
Schauder, C.M., Wu, X., Saheki, Y., Narayanaswamy, P., Torta, F., Wenk, M.R., De Camilli, P., Reinisch, K.M., 2014. Structure of a lipid-bound extended synaptotagmin indicates a role in lipid transfer. Nature 510, 552–555. doi:10.1038/nature13269
Schmid, E.M., Bakalar, M.H., Choudhuri, K., Weichsel, J., Ann, H., Geissler, P.L., Dustin, M.L., Fletcher, D.A., 2016. Size-dependent protein segregation at membrane interfaces. Nat Phys 12, 704–711. doi:10.1038/nphys3678
Stefan, C.J., Manford, A.G., Baird, D., Yamada-Hanff, J., Mao, Y., Emr, S.D., 2011. Osh proteins regulate phosphoinositide metabolism at ER-plasma membrane contact sites. Cell 144, 389–401. doi:10.1016/j.cell.2010.12.034
Theillet, F.-X., Kalmar, L., Tompa, P., Han, K.-H., Selenko, P., Dunker, A.K., Daughdrill, G.W., Uversky, V.N., 2013. The alphabet of intrinsic disorder: I. Act like a Pro: On the abundance and roles of proline residues in intrinsically disordered proteins. Intrinsically Disord Proteins 1, e24360. doi:10.4161/idp.24360
Tong, J., Yang, H., Yang, H., Eom, S.H., Im, Y.J., 2013. Structure of Osh3 reveals a conserved mode of phosphoinositide binding in oxysterol-binding proteins. Structure 21, 1203–1213. doi:10.1016/j.str.2013.05.007
Wang, Y., Benton, L.A., Singh, V., Pielak, G.J., 2012. Disordered Protein Diffusion under Crowded Conditions. J Phys Chem Lett 3, 2703–2706. doi:10.1021/jz3010915
Wu, J., Fang, Y., Zarnitsyna, V.I., Tolentino, T.P., Dustin, M.L., Zhu, C., 2008. A coupled diffusion-kinetics model for analysis of contact-area FRAP experiment. Biophys. J. 95, 910–919. doi:10.1529/biophysj.107.114439
Yadav, S., Garner, K., Georgiev, P., Li, M., Gomez-Espinosa, E., Panda, A., Mathre, S., Okkenhaug, H., Cockcroft, S., Raghu, P., 2015. RDGBα, a PtdIns-PtdOH transfer protein, regulates G-

protein-coupled PtdIns(4,5)P2 signalling during Drosophila phototransduction. Journal of Cell Science 128, 3330–3344. doi:10.1242/jcs.173476

Zewe, J.P., Wills, R.C., Sangappa, S., Goulden, B.D., Hammond, G.R., 2018. SAC1 degrades its lipid substrate PtdIns4P in the endoplasmic reticulum to maintain a steep chemical gradient with donor membranes. eLife 7, e35588. doi:10.7554/eLife.35588

Figures legends

Figure 1. Low complexity N-terminal sequences increase the hydrodynamic radius of OSBP and ORP4

(A) Scheme of the various domains and interactions of OSBP/ORP4 and sequence of the N terminal region.
(B) Constructs used in this study.
(C) SDS-PAGE analysis of the purified constructs. Staining: Sypro Orange.
(D) Stoke radius *vs* MW of OSBP/ORP4 constructs (colored symbols) and folded standards (black circles) as determined by gel-filtration. The N-ter increases the Stoke radius by a factor twice as much as that expected for a well-folded domain.

Figure 2 OSBP/ORP4 N-ter influence protein subcellular localization and dynamics

(A and B) Localization of OSBP-mCherry or ORP4-mCherry constructs overexpressed in HeLa cells. Left: representative confocal images. Bar = 20 µm. Right: ratio between mean Golgi signal and mean total cell signal. All localization experiments were also performed on RPE1 cells with similar results. Each point corresponds to one cell. At least two experiments were done on each cell type.
(C) FRAP recovery curves of OSBP-mCherry (left) and ORP4-mCherry (right) constructs in HeLa cells after bleaching a circular area (3 µm diameter) at the Golgi. At least 5 measurements of each construct from one representative experiment among three independent experiments are shown.

Figure 3. OSBP N-ter facilitates protein turnover under conditions of remote PI(4)P synthesis

(A-B) RPE1 cells stably expressing the PI(4)P probe GFP-PH_{OSBP} were treated with control siRNA (siNT, A) or with siRNA against OSBP (siOSBP, B). After 24 hours, widefield time-lapse imaging was performed. When indicated, PIK93 (500 nM) was added into the cell medium. Top: snapshots of cells taken at t=0 using an inverted grayscale lookup table (fluorescence in black). Scale bar = 20 µm. Bottom: kymographs taken from a rectangular TGN region ("K", ≈ 20 x 3 µm).

(C) Temporal analysis showing normalized mean fluorescence intensity of GFP-PH_{OSBP} from a circular TGN region (see "T" on cell images in A-B; diameter 8 µm) over time. Silencing of endogenous OSBP abolishes GFP-PH_{OSBP} oscillations (black line), in contrast to control siNT-treated cells (green line).

(D-E) RPE1 cells stably expressing GFP-PH_{OSBP} and treated with siOSBP were transfected with siRNA-resistant OSBP (OSBP-res-mCherry) or ΔN-OSBP (ΔN-OSBP-res-mCherry) for 24 h before imaging. The signal from both GFP-PH_{OSBP} and the mCherry construct was monitored by time-lapse microscopy.

(F) Temporal analysis. OSBP-res-mCherry rescued GFP-PH_{OSBP} oscillations, whereas ΔN-OSBP-res-mCherry did not.

(G) Quantification of GFP-PH_{OSBP} oscillations at TGN from recordings similar to that shown in (C) and (F).

Figure 4. OSBP/ORP4 N-ter limits protein density on PI(4)P-containing membranes

(A) Visualization of N-PH-ΔCC-FFAT or PH-ΔCC-FFAT (400 nM) on Golgi-like GUVs (2% PI(4)P). Bar = 5 μm.

(B) Quantification of protein recruitment from an experiment similar to that shown in (A). Each point corresponds to one GUV.

(C) Principle of the liposome sedimentation assay. To assess the effect of PI(4)P membrane density on N-PH-ΔCC-FFAT and PH-ΔCC-FFAT recruitment, PI(4)P concentration was held constant (20 μM) but PI(4)P was present at increasing surface concentration while the liposome concentration was decreased.

(D) Result of the liposome sedimentation assay from 5 independent experiments. PH-FFAT and N-PH-FFAT showed similar PI(4)P-dependent binding to liposomes at low PI(4)P density. When the surface density of PI(4)P increased, N-PH-FFAT dissociated from the liposomes more significantly than PH-FFAT suggesting exclusion by crowding.

Figure 5. Control of liposome tethering geometry by OSBP N-ter

(A-B) The samples initially contained 15 μM of ER-like liposomes (2% DGS-NTA-Ni) labelled with Oregon Green-DHPE, 15 μM of Golgi like liposomes (2% PI(4)P) labelled with Texas Red-DHPE, and either 300 nM VAP-A (which binds to ER-like liposomes, A) or no VAP-A (B). At t = 100 s, 600 nM of the indicated tethering construct (green: N-PH-FFAT, blue PH-FFAT) was added and liposome aggregation was followed over time by DLS. After kinetics completion, the DLS samples were visualized by confocal microscopy to determine the nature of the liposome aggregates. Bar =20 μm.

(C-D) Same as in (A-B) with N-PH-ΔCC-FFAT or PH-ΔCC-FFAT.

(E) Cryo EM analysis of Golgi-like liposomes (5% PI(4)P) after incubation with N-PH-FFAT or PH-FFAT. In both cases, liposomes were decorated with proteins (inset). With N-PH-FFAT, no liposome-liposome contact formed. With PH-FFAT, liposome-liposome contacts, often associated with membrane remodeling, formed with an interdistance of

15 ± 1 nm and a characteristic central dense layer of protein between them (white arrow head). Bar = 100 nm. Larger EM fields are shown in Figure S6C.

Figure 6. The N-ter controls OSBP distribution and lateral motility under homotypic and heterotypic tethering conditions

(A-C) Analysis of homotypic tethering

(A) GUVs containing 2% PI(4)P and labeled with Atto390-DOPE were incubated with 100 nM N-PH-FFAT or PH-FFAT (labelled with Alexa488 or Alexa568) as schematized. Enrichment index was calculated from line scans across the GUV-GUV interface and free GUV surface (see star methods and(Schmid et al., 2016)). Each point corresponds to one GUV-GUV interface. Bar = 5 µm.

(B) FRAP measurements of N-PH-FFAT (green trace) and PH-FFAT (blue trace). Photobleaching was performed on a circular area (diameter 2 µm) on the interface between tethered GUVs (see A). Measurements performed with proteins labelled with Alexa488 or Alexa568 gave similar results. Means ± SD of one representative experiment is shown (n: numbers of recordings per condition).

(C) 50 nM N-PH-FFAT labeled with Alexa488 (green) and 50 nM PH-FFAT labeled with Alexa568 (red) were incubated with Golgi-like GUVs (2% PI(4)P, Atto390-DOPE). After four hours, the suspension was visualized by confocal microscopy. Experiment was also performed with inverse color combination with similar results. Bar = 5 µm.

(D-F) Analysis of heterotypic tethering

(D) 50 nM N-PH-ΔCC-FFAT or PH-ΔCC-FFAT labeled with Alexa568 (red) was mixed with 50 nM VAP-A-His labeled with Alexa488 (green). Golgi-like GUVs (2% PI(4)P, Atto390-DOPE) and ER-like GUVs (2% DGS-NTA-Ni, no color) were added and the sample was very gently mixed. After 30 min, tethered GUVs were observed by confocal microscopy. Bar = 5 µm.

(E) FRAP measurements at 568 nm of N-PH-ΔCC-FFAT or PH-ΔCC-FFAT from GUV-GUV contacts similar to that shown in (D). Photobleaching was performed on a circular area (diameter 2 µm) in the middle of the GUV interface. Means ± SD of one representative experiment is shown (n = number of recordings per condition).

(F) Same as in (E) but FRAP was conducted on VAP-A-His labelled with Alexa-488.

Figure 7. Model for N-ter mediated regulation of OSBP tethering geometry and dynamics at MCS

By being intrinsically disordered, the N-ter of OSBP acts as an entropic barrier. It prevents the two PH domains from simultaneously bridging two PI(4)P-containing

membranes. It limits protein density under heterotypic tethering conditions, thereby facilitating OSBP in plane diffusion.

STAR methods

KEY RESOURCES TABLE

REAGENT or RESOURCE	SOURCE	IDENTIFIER
Antibodies		
Rabbit polyclonal anti OSBP	Atlas Antibodies	Cat# HPA039227, RRID:AB_2676401
Mouse monoclonal anti V9 Vimentin	Sigma-Aldrich	Cat# V6389, RRID:AB_609914
Secondary Alexa Fluor-conjugated	Thermo Fisher Scientific	Cat# A32723, RRID:AB_2633275
secondary HRP-conjugated	Jackson ImmunoResearch Labs	Cat# 111-035-047, RRID:AB_2337940
Bacterial and Virus Strains		
Escherichia coli BL21(DE3)	IPMC ressources	N/A
Escherichia coli DH10 Bac	Thermo Fisher Scientific	Cat# 10361012
Escherichia coli Bl21(DE3)pRIL-TEV	Kapust et al., 2001	N/A
Biological Samples		
Chemicals, Peptides, and Recombinant Proteins		
Egg PC	Avanti Polar Lipids	Cat# 840051C
Brain PS	Avanti Polar Lipids	Cat# 840032C
Brain PI(4)P	Avanti Polar Lipids	Cat# 840045X
Liver PE	Avanti Polar Lipids	Cat# 840026C
Liver PI	Avanti Polar Lipids	Cat# 840042C
Dansyl-PE	Avanti Polar Lipids	Cat# 810330C
Rhodamine-PE	Avanti Polar Lipids	Cat# 810158C
DGS-NTA(Ni)	Avanti Polar Lipids	Cat# 790404P
Cholesterol	Sigma-Aldrich	Cat# C8667
dehydroergosterol (DHE)	Sigma-Aldrich	Cat# 81025P
Methyl-β-cyclodextrin (MCD)	Sigma-Aldrich	Cat# C4555
G418	Sigma-Aldrich	Cat# G8168
PIK93	Sigma-Aldrich	Cat# SML0546
Texas Red-DHPE	Invitrogen	Cat# T1395MP
Oregon Green-DHPE	Invitrogen	Cat# O12650
Atto390-DHPE	Atto-TEC	Cat# AD 390-161
HisPur™ Cobalt Resin	Thermo Scientific	Cat# 89964
Lipofectamine 2000 reagent	Invitrogen	Cat# 11668-019
Amaxa Cell Line Nucleofector Kit V	Lonza	Cat# VCA-1003
Amaxa Cell Line Nucleofector Kit R	Lonza	Cat# VCA-1001
Complete-EDTA-free protease inhibitor	Roche	Cat# 05056489001
Critical Commercial Assays		
GeneArtTM Seamless Cloning and Assembly Enzyme Mix	Invitrogen	Cat# A14606
Deposited Data		
Experimental Models: Cell Lines		

hTERT-RPE1	ATCC	RRID:CVCL_4388
HeLa	Gift from Thierry Coppola	N/A
SF9	From lab	N/A
Experimental Models: Organisms/Strains		
Oligonucleotides		
ON-TARGETplus Human OSBP (5007) siRNA Target sequence : GCAAUGACUUGAUAGCUAA	Dharmacon (GE Healthcare)	Cat# J-009747-06-0020
ON-TARGETplus Non-targeting siRNA Target sequence : UGGUUUACAUGUUGUGUGA	Dharmacon (GE Healthcare)	Cat# D-001810-02-05
siRNA-resistant OSBP-For : CTT GAG CAC GTG CAA TGA TCT TAT AGC TAA GCA TGG C	This study	N/A
siRNA-resistant OSBP-Rev : GCC ATG CTT AGC TAT AAG ATC ATT GCA CGT GCT CAA G	This study	N/A
pFastBac-HTA-mod1-For: CTG TAT TTT CAG GGC GCC TAA TAG CCG GAA TTC AAA GGC CTA	This study	N/A
pFastBac-HTA-mod2-For : TCT CGG TCC GAA TAC CAT CAC CAT CAC CAT C	This study	N/A
Recombinant DNA		
pmCherry-N1-OSBP PH-FFAT (76-408)	Mesmin et al., 2013	N/A
pmCherry-N1-OSBP FL (1-807)	This study	N/A
pmCherry-N1-OSBP ΔN (86-807)	This study	N/A
pmCherry-N1-OSBP N-PH-FFAT (1-408)	This study	N/A
pmCherry-N1-ORP4 FL (1-878)	This study	N/A
pmCherry-N1-ORP4 ΔN (144-878)	This study	N/A
pmCherry-N1-ORP4 N-PH-FFAT (1-474)	This study	N/A
pmCherry-N1-ORP4 PH-FFAT (144-474)	This study	N/A
pmCherry-N1-*res*-OSBP FL (1-807)	This study	N/A
pmCherry-N1- *res*-OSBP ΔN (86-807)	This study	N/A
pENTD/R-OSBP FL (1-807)-SThr-6His	Mesmin et al., 2013	N/A
pFast-Bac-6His Cter (intermediate plasmide)	This study	N/A
pFB- OSBP ΔN (88-807)-SThr-6His	This study	N/A
pET.His6.StrepII.TEV.LIC (2HR-T)	gift from Scott Gradia	Addgene # 29718
pET.His10.TEV.LIC (2B-T-10)	gift from Scott Gradia	Addgene # 78173
pET16b. StrepII.TEV.OSBP N-PH-FFAT (1-408)	This study	N/A
pET16b. StrepII.TEV.OSBP PH-FFAT (76-408)	This study	N/A
pET16b.His10.TEV.LIC (intermediate plasmide)	This study	N/A
pET16b.His10.TEV. ORP4 N-PH-FFAT (1-475)	This study	N/A
pET16b.His10.TEV. ORP4 PH-FFAT (128-475)	This study	N/A
pGEX-4T3-PH_{FAPP1} (C37S/C94S/T13C/T100S)	Mesmin et al., 2013	N/A
pET-21b-VAP-A	Mesmin et al., 2013	N/A
pET-21b-VAP-A (K94D/M96D)	Mesmin et al., 2013	N/A
pEGFP-C1-PH_{OSBP}	Mesmin et al., 2013	N/A
pTagBFP-N-β-1,4-Galactosyltransferase-1 (1-82)	Mesmin et al., 2017	N/A
pEGFP-Rab7	Gift from Sylvain Feliciangeli	N/A
Software and Algorithms		

Predictor of Natural Disordered Regions (PONDR®)	Molecular Kinetics, Inc.	http://www.pondr.com/
ProtParam	ExPASy Bioinformatics Resource Portal, SIB	https://web.expasy.org/protparam/
Phylogeny.fr	Sebastien Santini - CNRS/AMU IGS UMR7256	http://www.phylogeny.fr/
Clustal Omega	Sievers et al., 2011	https://www.ebi.ac.uk/Tools/msa/clustalo/
COILS version 2.2 web server	Lupas et al., 1991	https://embnet.vital-it.ch/software/COILS_form.html
ImageJ 1.51w	NIH, USA	
Zen 2011	Carl Zeiss SAS	
MetaMorph Version 7.8.9.0	Molecular Devices LLC	
Dynamics v6.1	Protein Solutions	
SigmaPlot 14	Systat Software Inc.	
Canvas X	ACD System	
Other		

656

657

658

Reagents

Rabbit polyclonal antibody against OSBP (Atlas Antibodies Cat# HPA039227, RRID:AB_2676401)) and mouse monoclonal V9 Vimentin antibody (Sigma-Aldrich Cat# V6389, RRID:AB_609914) were from Sigma-Aldrich. Secondary Alexa Fluor-conjugated antibody (Thermo Fisher Scientific Cat# A32723, RRID:AB_2633275) were from Invitrogen and secondary HRP-conjugated antibody were from Jackson ImmunoResearch (Jackson ImmunoResearch Labs Cat# 111-035-047, RRID:AB_2337940).

Egg PC, brain PS, brain PI(4)P, liver PI, liver PE, dansyl-PE (1,2-dioleoyl-sn-glycero-3-phosphoethanolamine-N-(5-dimethylamino-1-naphthalenesulfonyl)), rhodamine-PE [1,2-dipalmitoyl-sn-glycero-3-phosphoethanolamine-N-(lissamine rhodamine B sulfonyl)], and DGS-NTA(Ni) [1,2-dioleoyl-sn-glycero-3-[(N-(5-amino-1-carboxypentyl) iminodiacetic acid) succinyl] (nickel salt)] were from Avanti Polar Lipids.

Cholesterol, dehydroergosterol (DHE), Methyl-β-cyclodextrin (MCD) and G418 were from Sigma-Aldrich.

Texas Red-DHPE, Oregon Green-DHPE and Atto390-DHPE were from Invitrogen.

Bioinformatic analysis

We used the following sequences of human ORPs (Uniprot access number): OSBP1 (P22059), OSBP2/ORP4 (Q969R2), ORP5 (Q9H0X9), ORP8L (Q9BZF1), ORP10 (Q9BXB5), ORP11 (Q9BXB4), ORP6 (Q9BZF3), ORP7 (Q9BZF2), ORP1 (Q9BXW6), ORP3 (Q9H4L5), ORP9 (Q96SU4). Notably, our ORP4 sequence (gift from N. Ridgway) started at M39 (as referred to UNIPROT Q969R2:ORP4-OSBP2 sequence), therefore, in all this study M1 corresponds to M39 of the UNIPROT reference sequence. Order/disorder composition of different ORPs was determined with "Predictor of Natural Disordered Regions (PONDR®)" web server (http://www.pondr.com/) using VL3-BA and VSL2 predictors. Amino acids % composition of selected domains was determined using Expasy/protparam web server (https://web.expasy.org/protparam/) and plotted as pie charts to highlight similarities and divergences between domains (N-terminus, PH domain, ORD). Limits of selected domains are details in Figure S2A.

For phylogenetic analysis, protein sequences of higher eukaryotes most similar to human OSBP were obtained from the UniProt database. The phylogenetic tree was created using the Phylogeny.fr server (Dereeper and Guignon et al., 2008). The sequences of each OSBP domain were then aligned and compared to that of the corresponding human domain using Clustal Omega (Sievers et al., 2011). A percent identity matrix was calculated for each domain. For the N-ter, sequences shorter than 20 amino acids were not included in the identity analysis. The

prediction of coiled-coils was done using the COILS 2.2 web server (Lupas et al., 1991). Only sequences located between the PH domain and the FFAT motif were evaluated..

Plasmids and cell transfection

Plasmid for OSBP PH-FFAT (residues 76-408) has been previously described (Mesmin et al., 2013).

Human OSBP sequences [full-length (residues 1-807), ΔN (residues 86-807), N-PH-FFAT (residues 1-408) and human ORP4 sequences [FL (residues 1-878), ΔN (residues 144-878), N-PH-FFAT (residues 1-474), PH-FFAT (residues 144-474)] were cloned into the BamHI site of pmCherry-N1 vector using the GeneArt™ Seamless Cloning and Assembly Kit (Invitrogen).

The siRNA-resistant OSBP constructs (full-length and ΔN) were prepared by PCR using the corresponding pmCherry-N1 plasmids as template with primers F: CTT GAG CAC GTG CAA TGA TCT TAT AGC TAA GCA TGG C and R: GCC ATG CTT AGC TAT AAG ATC ATT GCA CGT GCT CAA G.

For protein expression, cells were transfected with Lipofectamine 2000 reagent (Invitrogen) or by electroporation with Nucleofector Solution (Lonza) using the Amaxa Nucleofector device (Lonza), for 18-24 hrs.

Construction, expression and purification of OSBP and ΔN-OSBP

Full-length (1-807) human OSBP and ΔN-OSBP (88-807) were purified from baculovirus-infected Sf9 cells. The construct of full-length (1-807) human OSBP in pENTD/R was previously described (Mesmin et al., 2013). For ΔN-OSBP, the pFastBac™HTA vector (Invitrogen) was modified by successive mutations to allow the insertion of a PCR amplified sequence upstream and in frame with the 6His tag. These modifications were: 1) transformation of the original BamHI site into 2 stop codons (F oligo sequence: CTG TAT TTT CAG GGC GCC TAA TAG CCG GAA TTC AAA GGC CTA); 2) insertion of a new BamHI site upstream of the His tag (F oligo sequence: TCT CGG TCC GAA TAC CAT CAC CAT CAC CAT C). [OSBP ΔN (88-807) + thrombin site] DNA sequence was PCR amplified using the pENTR/D-(OSBP-FL-thrombin site) as matrix and cloned into the BamHI-digested pFastBac HTA modified vector using the GeneArt™ Seamless Cloning and Assembly Kit (Invitrogen). Recombinant vectors were then transformed into DH10 Bac *E.coli.* Recombinant bacmides were selected as described in Bac to Bac^{R} Expression System user manual (Invitrogen) and used to produce recombinant Baculovirus.

Full-length OSBP and ΔN-OSBP with a C-terminal 6His tag were purified from baculovirus-infected Sf9 cells as described (Mesmin et al., 2013). Cell pellets were resuspended in lysis buffer (20 mM Tris pH 7.5, 300 mM NaCl, 20 mM imidazole, EDTA-free protease inhibitors and phosphatases inhibitors) and lysed with Dounce homogenizer. After ultracentrifugation (125 000 g), OSBP or ΔN-OSBP from the supernatant was adsorbed on an HisPur™ Cobalt Resin

(Thermo Scientific), submitted to 3 washes with lysis buffer supplemented with 800, 550, and 300 mM NaCl, respectively, and then eluted with 250 mM imidazole-containing buffer. OSBP fractions were pooled, concentrated on Amicon Ultra (cut-off 30 kDa), and submitted to thrombin cleavage for 1 hr at 25°C to eliminate the His tag, then purified on a Sephacryl S300 HK16/70 column (GE Healthcare) using an AKTÄ chromatography system (GE Healthcare). All steps were performed at 4°C. The purified protein fractions were pooled, concentrated, supplemented with 10 % glycerol, flash-frozen in liquid nitrogen and stored at -80°C.

Construction, expression and purification of OSBP and ORP4 fragments

N-PH-FFAT and PH-FFAT fragments of OSBP and ORP4 were expressed in *E. Coli* BL21 (DE3). The corresponding constructs were prepared using pET.His6.StrepII.TEV.LIC (2HR-T, Addgene plasmid # 29718) and pET.His10.TEV.LIC (2B-T-10, Addgene plasmid # 78173) cloning vectors (gift from Scott Gradia).

OSBP N-PH-FFAT (1-408) and OSBP PH-FFAT (76-408) fragments were first inserted into pET.His6.StrepII.TEV.LIC vector, subcloned into pET16b, and then expressed as N-terminal 6His tag- StrepII-TEV site constructs.

ORP4 DNA sequences [ORP4(1-475)=N-PH-FFAT, ORP4(128-475)=PH-FFAT] were PCR amplified using the pmCherry-ORP4 FL as matrix. The host plasmid pET16b.His10.TEV.LIC was prepared from the pET16b.His6.StrepII.TEV.LIC OSBP(76-408) by replacing the fragment His6.StrepII.TEV.LIC OSBP(76-408) by a His10.TEV.LIC fragment. In addition, the SspI site of pET16b was mutated (AATATT into AATAGC). Last, the ORP4 N-PH-FFAT or PH-FFAT PCR fragments were inserted into the SspI digested pET16b.His10.TEV.LIC vector using GeneArtTM Seamless Cloning and Assembly Enzyme Mix (Invitrogen). After protein expression, bacteria were lysed with a French Press (SLM AMINCO) and incubated for 30 min on ice with DNAse and $MgCl_2$ (5mM) before ultracentrifugation (125 000 *g*). His tagged proteins were purified using HisPur™ Cobalt Resin (Thermo Scientific). Protein fractions were pooled and submitted to TEV protease cleavage overnight at 4°C. Digested proteins were purified on a SourceQ HR 10/10 column (GE Healthcare) with a 0-1M NaCl gradient in 25mM Tris pH7.5 followed by a Sephacryl S200 HK16/70 column (GE Healthcare) equilibrated in 25mM Tris pH7.5, 120 mM NaCl, 2mM DTT. Purified proteins were pooled, concentrated, supplemented with 10% glycerol, flash-frozen in liquid nitrogen and stored at -80°C.

N-PH-ΔCC-FFAT and PH-ΔCC-FFAT constructs were prepared from pGEX4.T1 (GE Healthcare) plasmids expressing the OSBP (1-408) or (76-408) sequence. A NaeI restriction was introduced by site directed mutagenesis to remove the coiled-coil (207-329) region by digestion / ligation taking advantage of another NaeI site. Proteins were expressed as N-terminal (GST-thrombin-

site) constructs in *E. coli* BL21(DE3). Purification was preformed using Glutathione Sepharose beads (GE Healthcare). GST was removed by thrombin clivage. The subsequent purification steps were the same as that used for N-PH-FFAT / PH-FFAT.

All new construct sequences were confirmed by sequencing.

Other protein constructs

The preparation of NBD-PH_{FAPP1} and VAP-A have been described previously (Mesmin et al., 2013). The TEV protease plasmid (gift from D. Waugh) (Kapust et al., 2001) was used to expressed the protein in Bl21(DE3)pRIL *E.coli* which was purified as described (Tropea et al., 2009).

Cell culture

HeLa cells were cultured in DMEM medium with glutaMAX (Gibco) supplemented with 10% fetal calf serum, 1% antibiotics (Zell Shield, Minerva Biolabs) and were incubated at 37°C in a 5% CO_2 humidified atmosphere. For hTERT-RPE1 cells (ATCC Cat# CRL-4000, RRID:CVCL_4388); hereafter RPE1 cells), DMEM was replaced by DMEM/F12 (Gibco). RPE1 cells stably expressing EGFP-PH_{OSBP} were selected using G418 (Sigma). Surviving colonies were isolated using cloning cylinders (Bel-Art), expanded and further sorted by FACS (FACSAria III, BD Biosciences). RPE1 cells stably expressing EGFP-PH_{OSBP}, EGFP-$P4M_{SidM}$ were cultured in medium supplemented with G418 (500 µg/ml). For microscopy, cells were seeded at suitable density to reach 50-90% confluence on the day of imaging. SF9 cells were cultured at 27°C in SF-900 II media supplemented with 1,5% FCS in absence of antibiotic. For protein expression SF9 cells were infected at 10^6 cells/ml and an MOI of 0.1 in 0.5 l CELLSPIN Spinner. After 72h, cells were collected by centrifugation at 300xg for 15 mn, washed in PBS and stored at -20°C.

RNA interference

For endogenous OSBP silencing and simultaneous expression of siRNA resistant OSBP, RPE-1 cells stably expressing GFP-PH^{OSBP} were electroporated with 90 pmol siRNA and 1 µg siRNA-resistant OSBP plasmid using RNAiMAX (Invitrogen) and plated on 6-well plate or on µ-$Dish^{35mm}$ (Ibidi). ON-TARGETplus Human OSBP siRNA was from Dharmacon (GE Healthcare, target sequence: GCAAUGACUUGAUAGCUAA). After 18-24 hrs cells were used for live-cell imaging or western blotting.

Liposome preparation

Lipids in chloroform or in chloroform:methanol (2:1) in the case of mixtures containing PI(4)P) were mixed at the desired molar ratio and the solvent was removed in a rotary evaporator. For

most assays, the lipid films were hydrated in 50 mM HEPES pH 7.2 and 120 mM potassium acetate (HK buffer, which was degassed before use) to give a suspension of large multilamellar liposomes (lipid concentration: 2-5 mM). In the case of sedimentation assay, the lipid films were hydrated (lipid concentration: 2mM) in 50 mM HEPES pH 7.2, sucrose 210 mM. The suspensions were then frozen in liquid nitrogen and thawed in a water bath (40°C) four times. Liposomes were extruded through 0.1 µm pore size polycarbonate filters using hand extruder (Avanti Polar Lipids) and were used within 1-2 days.

GUV Preparation

Giant unilamellar vesicles were generated by electro-formation. Lipids mixtures of the chosen composition (0.5 mg/ml) in chloroform or in 2:1 chloroform:methanol in the case of mixtures containing PI(4)P were deposited on indium tin oxide coated glass slides and dried at RT for 45 min to remove all solvents. Lipids were then hydrated in 250 mM sucrose osmotically equilibrated with buffers. GUVs were electroformed using Vesicle Prep Pro (Nanion Technologies) by applying an AC electric field (3 V and 5 Hz), at 37 °C for 60 min.

Liposomes aggregation measurements

Liposome aggregation induced by OSBP or ORP4 fragments was followed in real time by dynamic light scattering (DLS) using a DynaPro instrument (Protein Solutions) as described (Mesmin et al., 2013). Golgi-like liposomes (15 µM) containing 0 - 4% PI(4)P and ER-like liposomes containing 2% DGS-NTA(Ni) (15 µM) were mixed in HK buffer supplemented with 1 mM $MgCl_2$ and 1 mMDTT (HKMD buffer) and with VAP-A-His or VAP-A(KM-DD)-His (300 - 600 nM) as indicated. 10 DLS autocorrelation curves (= 10 x 10 seconds) were acquired to determine the initial size distribution of liposome suspension. Thereafter, 300 - 600 nM OSBP or ORP4 fragment was injected and liposome aggregation was followed in real time by acquiring one autocorrelation curve every 10 s. The temperature was set at 30°C. Data were analyzed using the Dynamics v6.1 software (Protein Solutions).

Microscopy, FRAP assays

Confocal microscopy of fixed cells was performed with a Zeiss LSM780 microscope run by ZEN software using a Plan-Apochromat 63X/1.4 Oil objective (Carl Zeiss). Confocal microscopy of liposomes or GUVs was performed using the same microscope. The liposome or GUV suspension in HKM buffer (50mM HEPES, 120mM potassium acetate and 1mM $MgCl_2$) was placed in 8-well Dish (Ibidi) coated by casein (Sigma Aldrich); imaging was performed at room temperature.

Fluorescence recovery after photobleaching recordings were performed with a Zeiss LSM780 microscope or with a Nicon Eclipse Ti microscope equipped with an UltraVIEW VoX spinning

disc imaging system (PerkinElmer) operated by Volocity software, and using a CFI Plan Apo 100X/1.4 Oil objective (Nikon). Cells were placed in phenol red-free medium supplemented with HEPES (Gibco) and FRAP assays were carried out at 37°C. Photobleaching was performed on circular areas of 3 µm within perinuclear regions positive for BFP-GalT signal. FRAP assays with liposomes/GUVs were performed in HKM buffer at room temperature. Photobleaching was performed on circular areas of 2 µm diameter in the middle of GUV-GUV interface.

Time-lapse widefield microscopy was performed using an Olympus IX83 inverted microscope equipped with a Z-drift compensator, a scanning stage SCAN IM (Märzhäuser) and an iXon3 camera (Andor). Cells plated in µ-Dish^{35mm} (Ibidi) were put into a stage chamber set at 37°C (Okolab). Tag BFP, EGFP and mCherry signal were detected using Chroma fluorescence filter sets (ref. 49000, 39002, 39010). Multidimensional acquisition and analysis was performed with MetaMorph software (Molecular Devices).

Image analysis

For TGN/cytosol ratio, two ROIs of the same area were applied in the TGN and in the cytosol. The average fluorescence was determined for each ROI and the ratio was then calculated. Kymographs were generated using the Metamorph software (Molecular Devices) from a line drawn on the image stack and projected across time of the complete time series. The lines were 72 pixels long (ca. 20 µm) with a width set to 10 pixels (ca. 3 µm), from which pixel values were averaged. Scan lines quantification on GUVs were generated using Image J software.

Analytical gel filtration

Purified proteins (100 µl, 5 µM) were applied on a Superose 12™column (GE Healthcare) and eluted at a flow rate of 0.5 ml.min^{-1} in 25 mM Tris pH 7.5, 120 mM NaCl and 1mM DTT. The column was calibrated using the following standards (MW/Stokes radius): Apoferritin (443 kDa/6.1 nm), Alcohol dehydrogenase (150 kDa/4.6 nm), Bovine serum albumin (67 kDa/3.5 nm), Carbonic anhydrase (25 kDa/2.1 nm) and Cytochrome C (12.4 kDa/ 1.7 nm). The elution volume and Stoke's radius of the standards were used to establish a first calibration curve, from which the Stoke's radius of the OSBP/ORP4 constructs were determined. Thereafter, we plotted the Stoke's radius as a function of MW for both protein standards and for OSBP/ORP4 constructs.

***In vitro* PI(4)P-transfer assays**

PI(4)P-transfer assays were performed as described previously using purified recombinant proteins and extruded liposomes mimicking ER and Golgi membranes (Mesmin et al., 2013; 2017). The default lipid composition of the ER and Golgi liposomes was egg PC/brain PS/DGS-

NTA(Ni)/cholesterol (93/5/2/0-15 mol%) and egg PC/liver PE/brain PS/liver PI/brain PI(4)P/ rhodamine-PE (64/17/5/12-8/0-4/2mol%), respectively. Measurements were carried out in a Jasco FP-8300 spectrofluorimeter using a cylindrical quartz cuvette (600 µl) equilibrated at 37°C and equipped with a magnetic bar for continuous stirring. The cuvette initially contained NBD-PH_{FAPP1} (300 nM) and VAP-A-His (3 µM) in HKM buffer. NBD emission was measured at 510 nm (excitation 460 nm). Golgi liposomes (300 µM lipid supplemented with 4% PI(4)P and 2% rhodamine-PE), ER liposomes (300 µM lipid, ± 15% cholesterol) and OSBP (0.1 µM) were then sequentially added at the indicated times.

Sedimentation assay

For sedimentation assays comparing the binding properties of N-PH-ΔCC-FFAT and PH-ΔCC-FFAT, we used sucrose-loaded Golgi-like liposomes containing (mol%) egg PC (61), liver PE (17), brain PS (5), cholesterol (10), Rhodamine-PE (2) and increasing amount of brain PI(4)P (0, 1, 2, 5, 8 or 15 mol%) at the expense of liver PI (15, 14, 13, 10, 7 or 0 mol%). Proteins (3 µM) and liposomes (up to 20 µM PI(4)P) were incubated in 50 mM Hepes (pH 7.2), 120 mM potassium acetate, and 1 mM $MgCl_2$ (HKM buffer) at room temperature for 30 min in a total volume of 50 μL. The samples were centrifuged at 240 000g in a TLA 120.1 (Beckman) rotor for 1 h. The pellets resuspended in 50µl HKM buffer before analysis on 13% SDS-PAGE by Sypro orange staining.

Cryo-EM experiments

Lipid mixture in $CHCl_3$ composed of Egg PC/brain PS/brain PI(4)P (85/15/5 molar ratio) were dried under a nitrogen flux for 5 minutes and further dried under vacuum for 60 minutes. Lipid film was rehydrated at 1 mM in 50 mM Hepes pH 7, 120 mM K-acetate and liposomes were formed by 2 minutes vortex. Liposomes were diluted at 30 µM with 600 nM N-PH-FFAT or PH-FFAT. After 5 minutes incubation, a 5 µL drop of the solution was deposited on a glow discharged lacey carbon electron microscopy grid (Ted Pella, USA). Blotting was carried out on the opposite side from the liquid drop and plunge frozen in liquid ethane (EMGP, Leica, Germany). Samples were imaged using a Tecnai G2 (Thermofisher, USA) microscope operated at 200 kV and equipped with a 4k x 4k CMOS camera (F416, TVIPS). Image acquisition was performed under low dose conditions of 10 $e^-/Å^2$ at a magnification of 50,000 or 29,500 with a pixel size of 2.13 Å and 3. Å, respectively.

Dereeper, A., Guignon, V., Blanc, G., Audic, S., Buffet, S., Chevenet, F., Dufayard, JF., Guindon, S., Lefort, V., Lescot, M., Claverie, JM., Gascuel, O., 2008. Phylogeny.fr: robust phylogenetic analysis for the non-specialist. Nucleic Acids Res. 2008 Jul 1;36(Web Server issue):W465-9. doi: 10.1093/nar/gkn180. Epub 2008 Apr 19.

de Saint-Jean, M., Delfosse, V., Douguet, D., Chicanne, G., Payrastre, B., Bourguet, W., Antonny, B., Drin, G., 2011. Osh4p exchanges sterols for phosphatidylinositol 4-phosphate between lipid bilayers. The Journal of Cell Biology 195, 965–978. doi:10.1083/jcb.201104062

Kapust, R.B., Tözsér, J., Fox, J.D., Anderson, D.E., Cherry, S., Copeland, T.D., Waugh, D.S., 2001. Tobacco etch virus protease: mechanism of autolysis and rational design of stable mutants with wild-type catalytic proficiency. Protein Eng. 14, 993–1000.

Lupas, A., Van Dyke, M., Stock, J., 1991. Predicting Coiled Coils from Protein Sequences. Science 252:1162-1164.

Mesmin, B., Bigay, J., Moser von Filseck, J., Lacas-Gervais, S., Drin, G., Antonny, B., 2013. A Four-Step Cycle Driven by PI(4)P Hydrolysis Directs Sterol/PI(4)P Exchange by the ER-Golgi Tether OSBP. Cell 155, 830–843. doi:10.1016/j.cell.2013.09.056

Mesmin, B., Bigay, J., Polidori, J., Jamecna, D., Lacas-Gervais, S., Antonny, B., 2017. Sterol transfer, PI4P consumption, and control of membrane lipid order by endogenous OSBP. The EMBO Journal 36, 3156–3174. doi:10.15252/embj.201796687

Sievers F., Wilm A., Dineen D.G., Gibson T.J., Karplus K., Li W., Lopez R., McWilliam H., Remmert M., Söding J., Thompson J.D., Higgins D., 2011. Fast, scalable generation of high-quality protein multiple sequence alignments using Clustal Omega. Molecular Systems Biology 7 Article number: 539 doi:10.1038/msb.2011.75

Tropea, J.E., Cherry, S., Waugh, D.S., 2009. Expression and purification of soluble His(6)-tagged TEV protease. Methods Mol Biol 498, 297–307. doi:10.1007/978-1-59745-196-3_19

Supplementary Figures legends

Figure S1. Intrinsically disordered regions in ORPs. Related to Figure 1

(A) Disorder prediction in ORPs. Scores were obtained using PONDR® web server (algorithms: VL3, grey; VSL2, blue) of the indicated ORPs, which were ordered according to subfamilies (Lehto et al., 2001). Regions corresponding to PH domain, ORD and ankyrin repeats are highlighted in yellow, green and pink, respectively.

(B) Amino acid composition of ORP N-ter (upper row), PH domain (middle row) and ORD (bottom row). For the aa range of each domain see Figure S2A

Figure S2. Intrinsically disordered regions in ORPs. Related to Figure 1

(A) Amino-acid range of the various domains and regions of ORPs.

(B) Phylogenetic tree of OSBP in higher eukaryotes. The bar plots show aa identity in the N-ter region and in the PH and ORD domains (see STAR method). N-terminal sequences shorter than 20 amino acids were excluded from the identity analysis (blank rows). The column showing the probability of coiled-coil formation between the PH domain and FFAT motif was built by scanning the corresponding sequences using three windows in the COILS software: (++): all scanning windows give a region with a coiled-coil probability score > 0.5; (+) one or two scanning window gives a coiled-coil probability score > 0.5. (0) all scanning windows give a coiled-coil probability score < 0.5.

Figure S3. OSBP colocalizes with endosome marker and ORP4 constructs containing the ORD interact with vimentin filaments. Related to Figure 2

(A) Overexpressed OSBP-mCherry colocalizes with TGN marker BFP-GalT and endosome marker GFP-Rab7 in RPE1 cells. Bar = 20 μm.

(B) Overexpressed ORP4 FL-mCherry colocalizes with TGN marker BFP-GalT and vimentin filaments (visualized with anti-vimentin antibody).

(C) ΔN-ORP4-mCherry overexpression causes reorganization of vimentin filaments with "bundles" of intermediate filaments appearing in perinuclear region and colocalizing with ΔN-ORP4-mCherry.

Figure S4. N-ter deletion does not affect lipid transfer by OSBP. Related to Figure 3

(A) Representative fluorescence images of RPE1 cells co-transfected with the PI(4)P probe GFP-PH_{OSBP} and OSBP-mCherry (red) or ΔN-OSBP-mCherry (orange), respectively. Bar = 5 μm.

(B) Quantification of experiments similar to (A). The two OSBP constructs cause a similar reduction in GFP-PH_{OSBP} at the Golgi. Each point corresponds to one cell. Data shown are representative from two independent experiments.

(C) Time course of DHE transfer from ER-like to Golgi-like liposomes by 100 nM OSBP or ΔN-OSBP.

(D) Transfer of PI(4)P from Golgi-like liposomes to ER-like liposomes by 100 nM OSBP or ΔN-OSBP. The experiment was performed either in the absence or in the presence of cholesterol (15 mol%) in the ER-like liposomes.

Figure S5. Homotypic liposome tethering by OSBP/ORP4 constructs and dependence on VAP-A interaction. Related to figure 5.

(A-B) Same analysis as in **Figure 5A-B** with N-PH-FFAT or PH-FFAT constructs from ORP4.

(C) Same analysis as in **Figure 5A** with a VAP mutant (KM-DD) unable to interact with the FFAT motif of OSBP.

Figure S6. Homotypic liposome tethering by PH-FFAT is dependent on PI(4)P and on the ability of PH-FFAT to dimerize. Related to Figure 5.

(A-B) Homotypic tethering mediated by PH-FFAT requires PI(4)P and protein dimerization. The sample contained 15 µM Golgi like liposomes (0% or 2% PI(4)P, as indicated) labelled with Oregon Green-DHPE and 15 µM of Golgi like liposomes (0% or 2% PI(4)P, as indicated) labelled with Texas Red-DHPE. At t=100 s, 300 nM PH-FFAT (A) or PH-ΔCC-FFAT (B) was added. Bar = 20 µm.

(C) Large Cryo EM fields at low magnification of Golgi-like liposomes (5% PI(4)P) after incubation with N-PH-FFAT or PH-FFAT. Bar = 500nm.

Figure S7. OSBP N-ter controls protein distribution and lateral motility on GUVs. Related to Figure 6.

(A) N-PH-FFAT (labeled with Alexa488) contains shorter constructs, resembling PH-FFAT. The protein was analyzed by western blot using antibody against FFAT motif (left) or directly visualized by Alexa488 fluorescence (right).

(B) FRAP measurements performed on the free surface of tethered GUVs. Measurements were performed on proteins labelled with Alexa488 or Alexa568, with similar results. Two measurements per condition from one experiment are shown.

(C) Golgi-like GUVs (2% PI(4)P, labeled with Atto390-DOPE) were preincubated with 50nM of N-PH-FFAT (Alexa488, green) or PH-FFAT (Alexa488, green). After 30 min, an excess of PH-FFAT (Alexa568, red) and N-PH-FFAT (Alexa568, red) was added, respectively. Confocal microscopy was performed after additional 30 min of incubation. Bar = 5 μm.

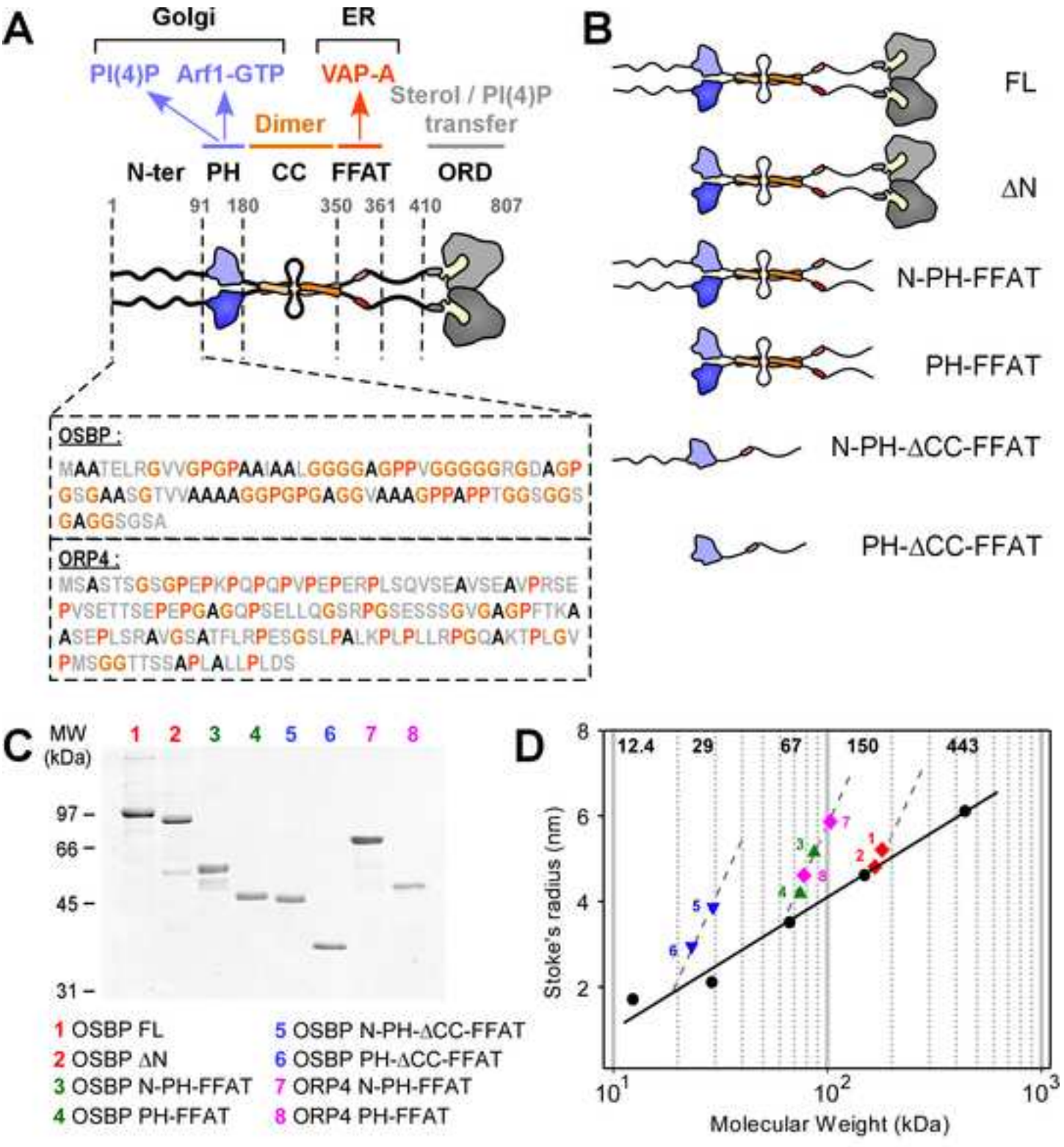

Figure 1

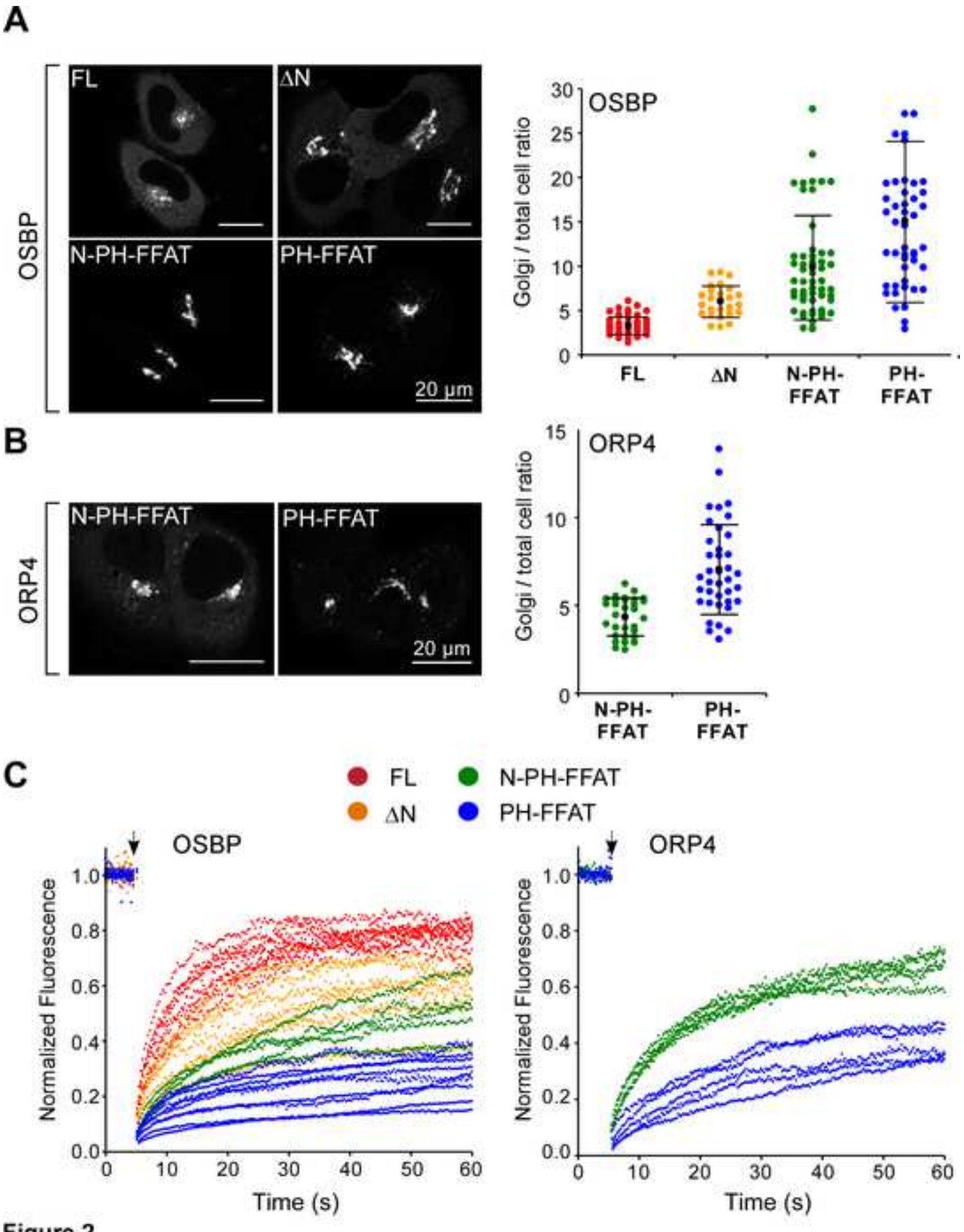

Figure 2

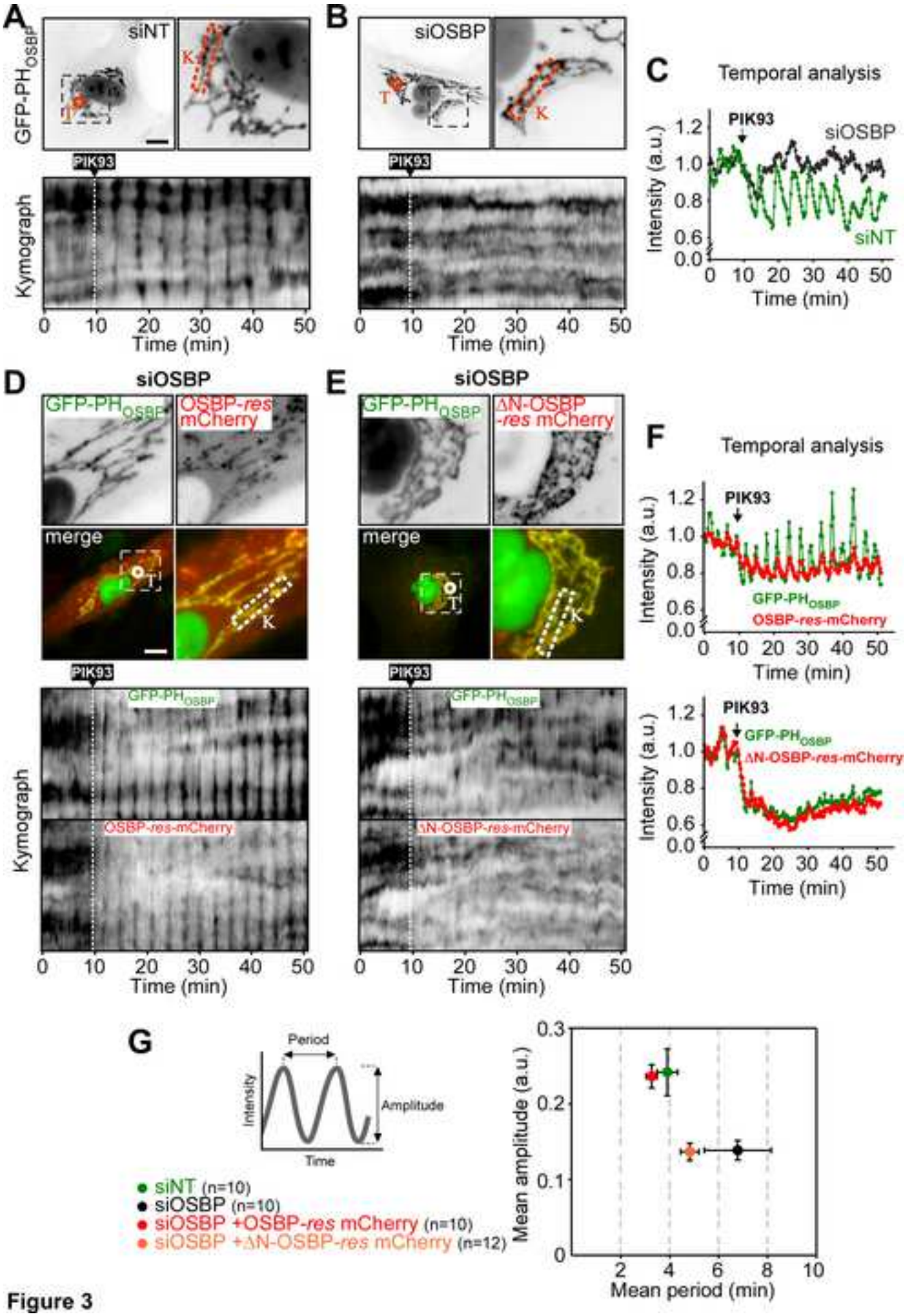

Figure 3

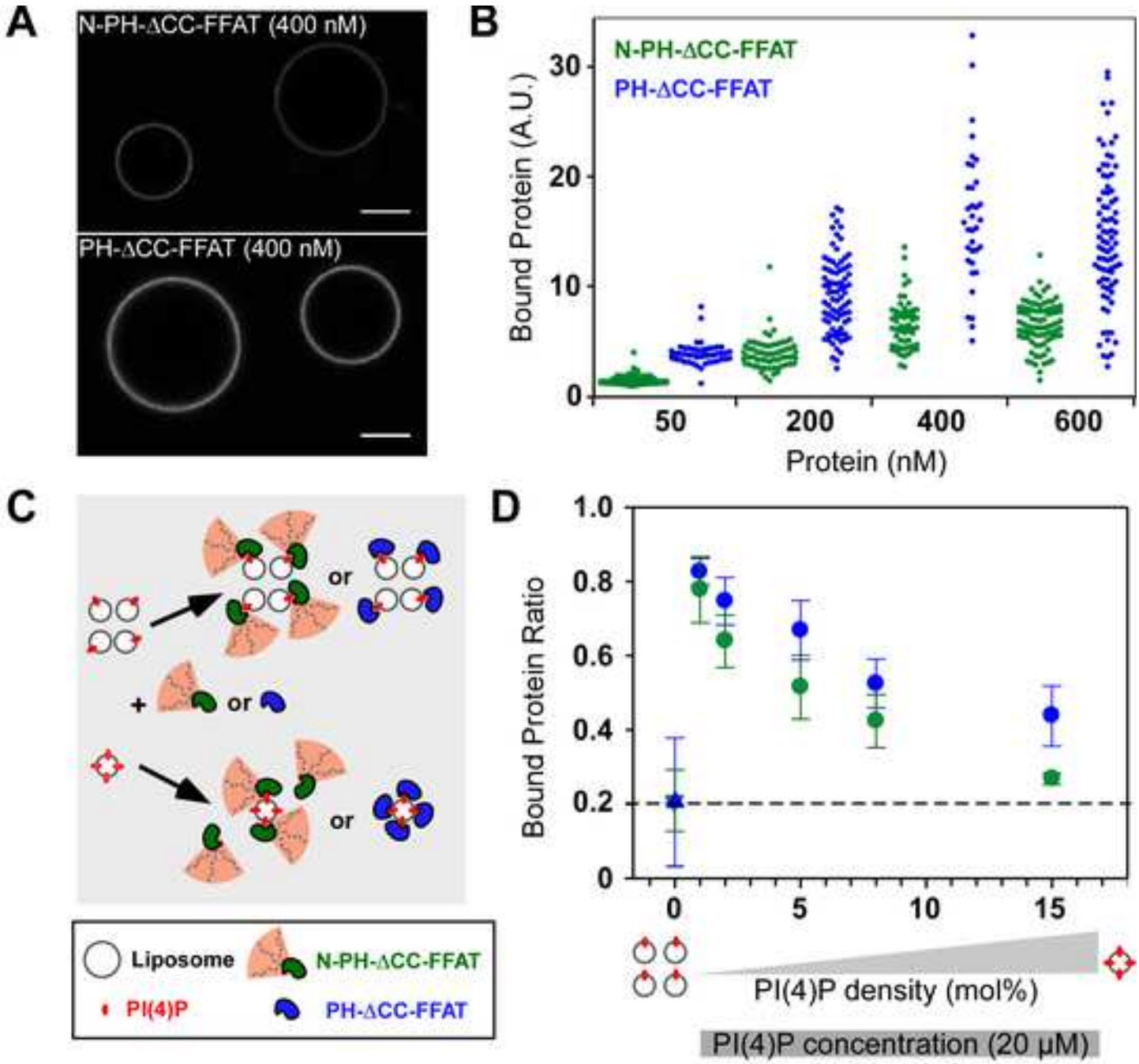

Figure 4

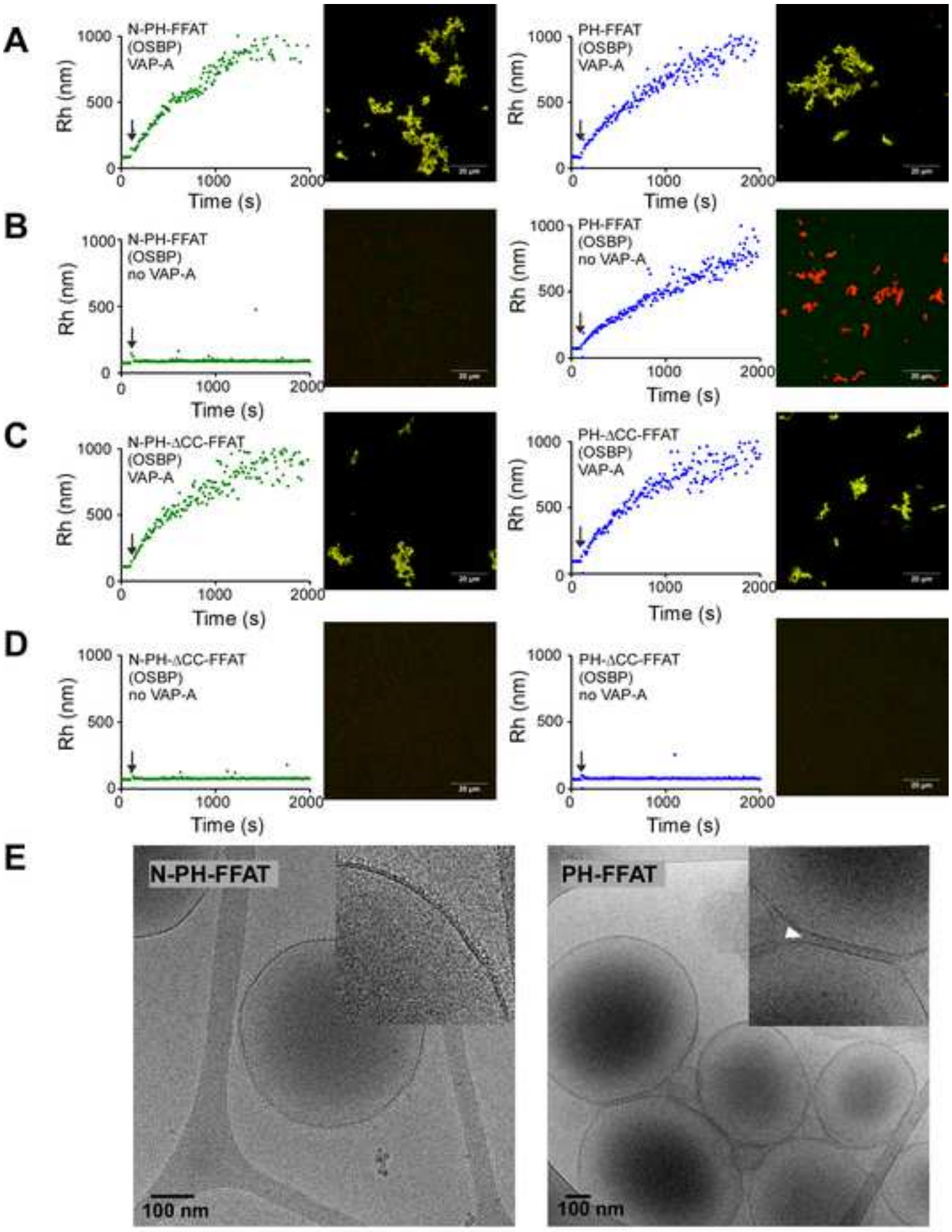

Figure 5

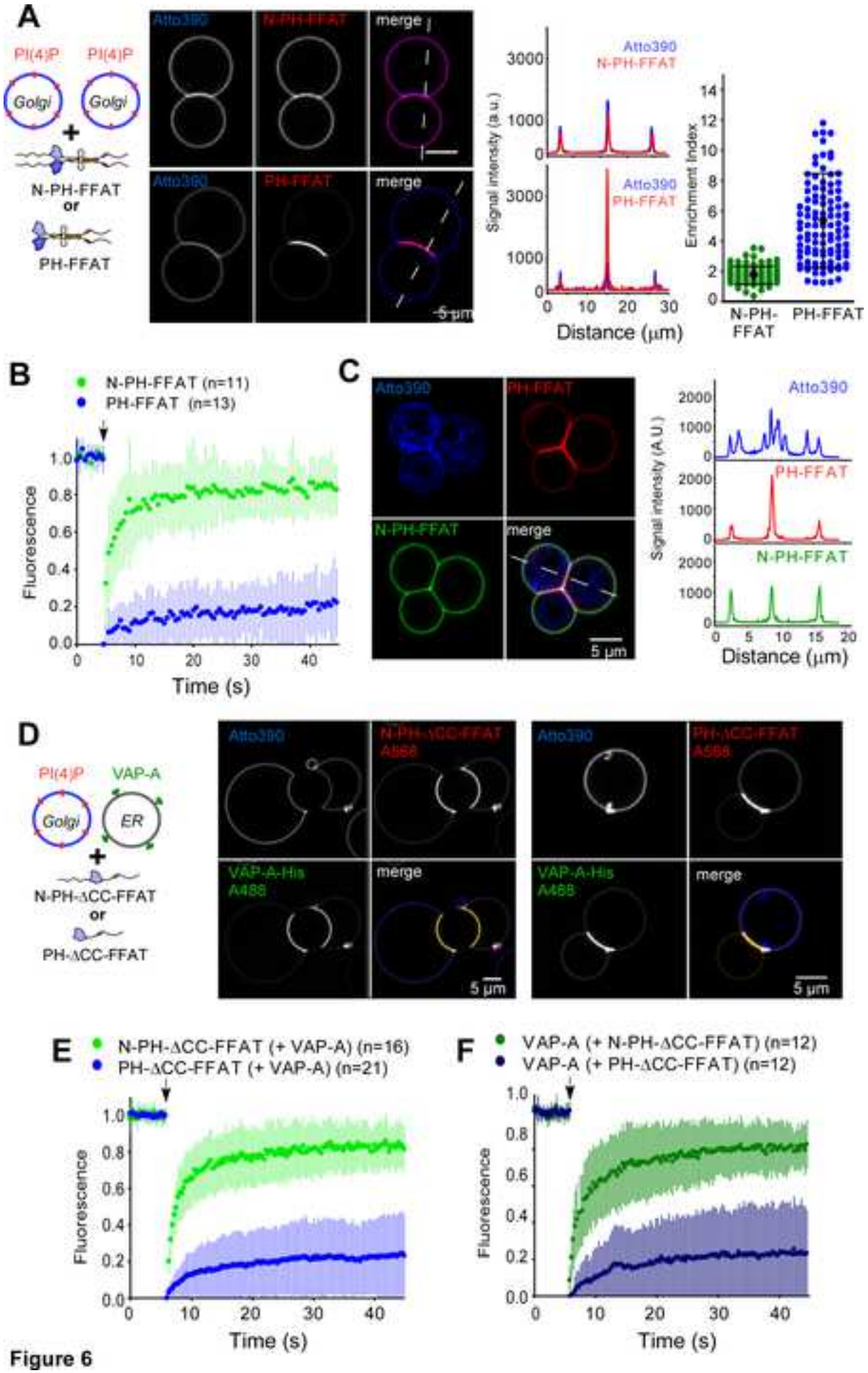

Figure 6

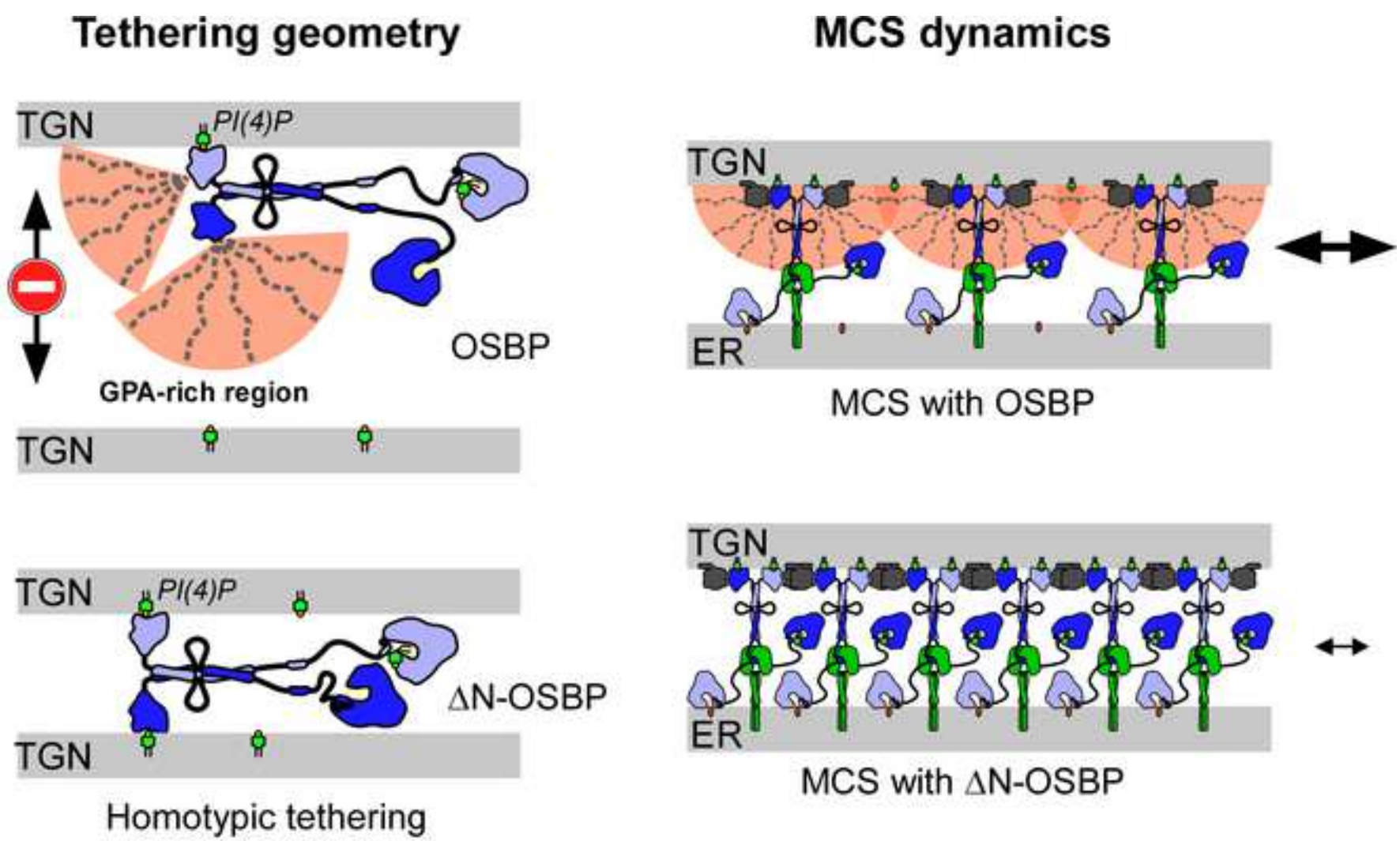

Figure 7

Figure S1

Click here to access/download;Supplemental Text and Figures;Fig S1 LZW.tif

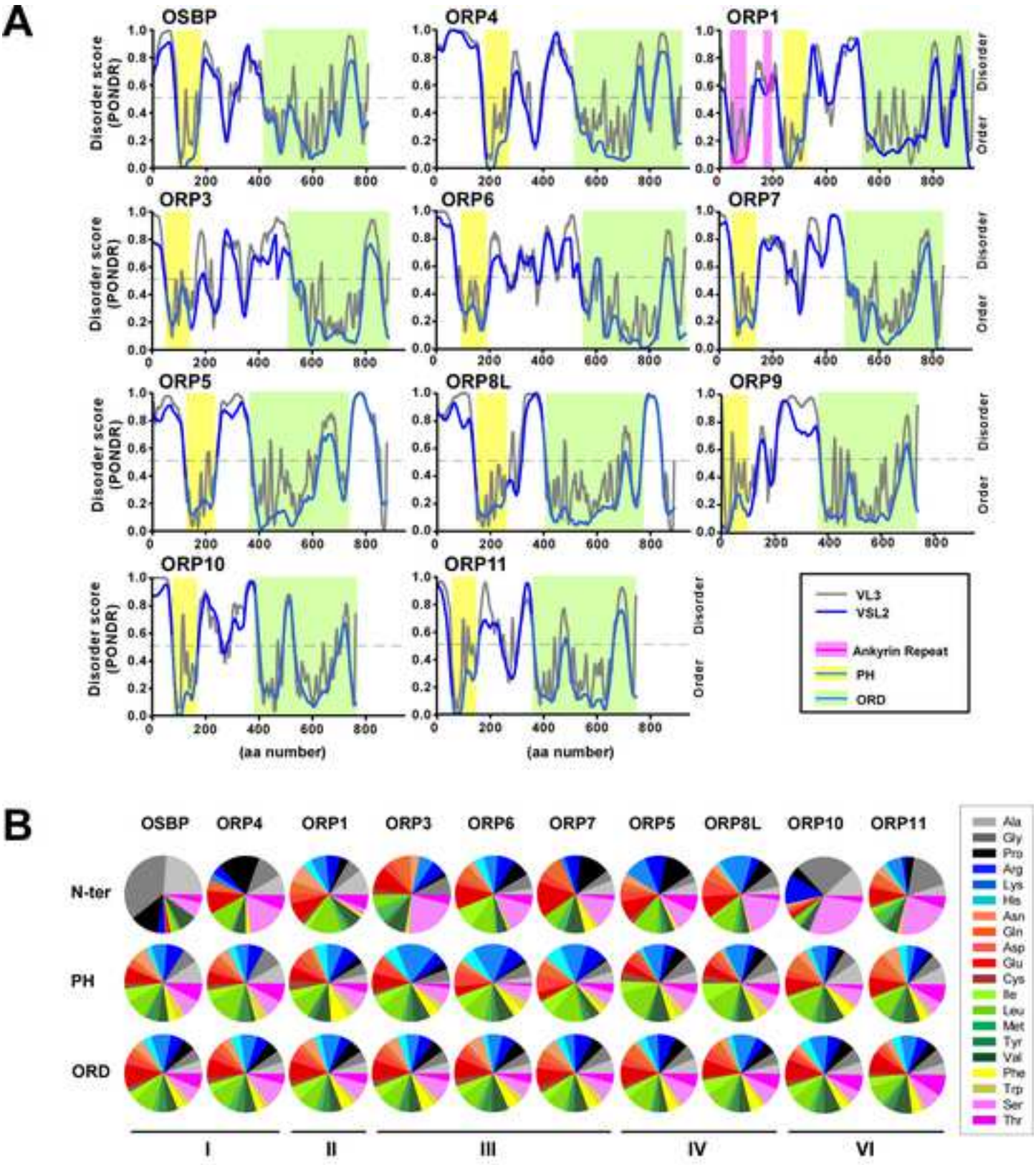

Sup. Figure 1

Figure S2

Click here to access/download;Supplemental Text and Figures;Fig S2 LZW.tif

A

Human ORP	UNIPROT Accession Number	Total AA	N-ter Seq	PH Seq	ORD Seq
OSBP 1	P22059	1-807	1-91	92-183	410-807
ORP 4	Q969R2	1-878	1-147	148-238	476-878
ORP 1	Q9BXW6	1-950	1-234	235-334	537-950
ORP 3	Q9H4L5	1-887	1-50	51-146	516-887
ORP 6	Q9BZF3	1-934	1-89	90-190	559-934
ORP 7	Q9BZF2	1-842	1-50	51-142	467-842
ORP 5	Q9H0X9	1-879	1-125	126-243	359-748
ORP 8L	Q9BZF1	1-889	1-147	148-265	395-780
ORP 9	Q96SU4	1-736		1-99	365-736
ORP 10	Q9BXB5	1-764	1-73	74-171	387-764
ORP 11	Q9BXB4	1-747	1-58	59-160	357-747

B

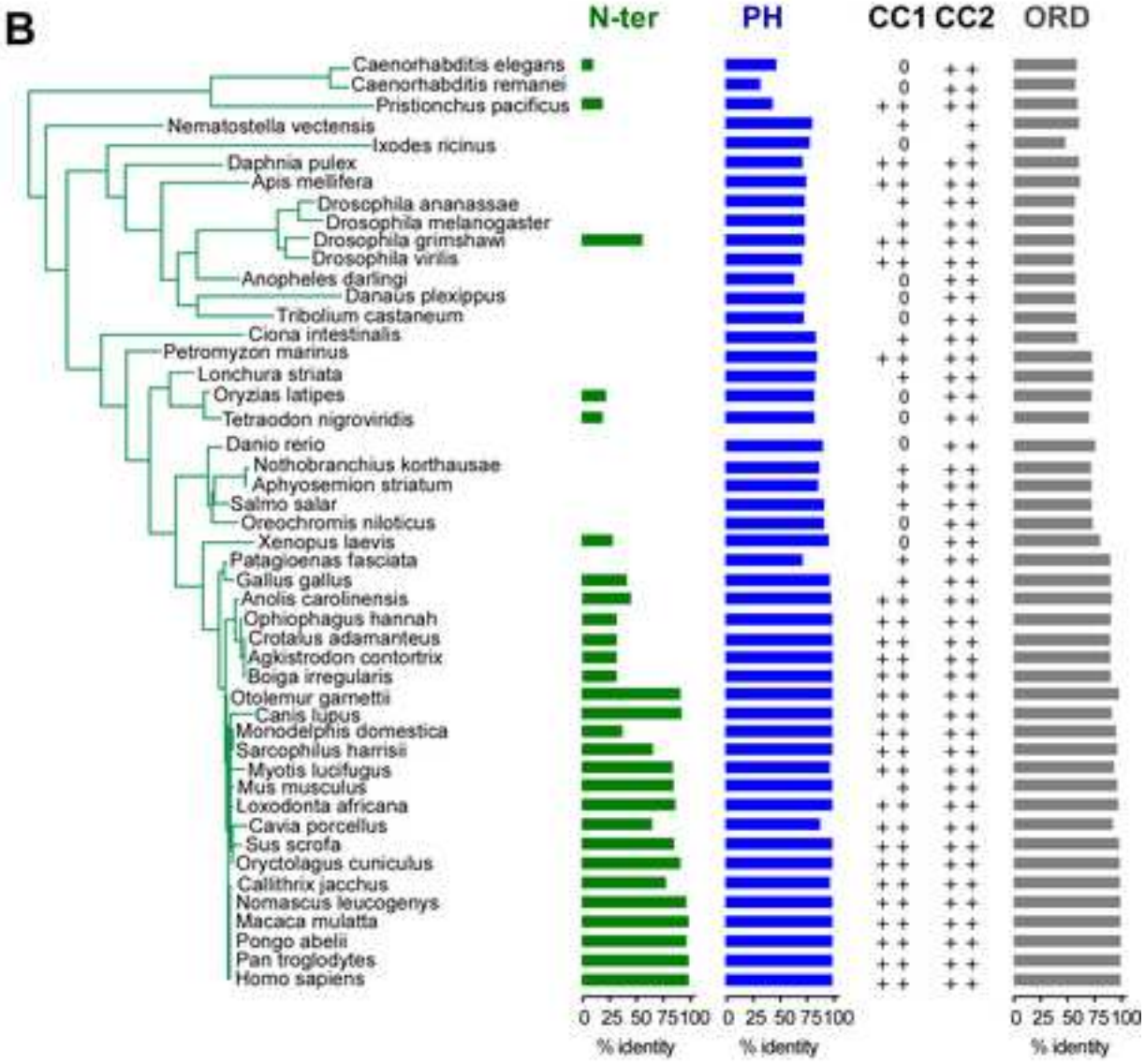

Sup. Figure 2

Figure S3

Click here to access/download;Supplemental Text and Figures;Fig S3 LZW.tif

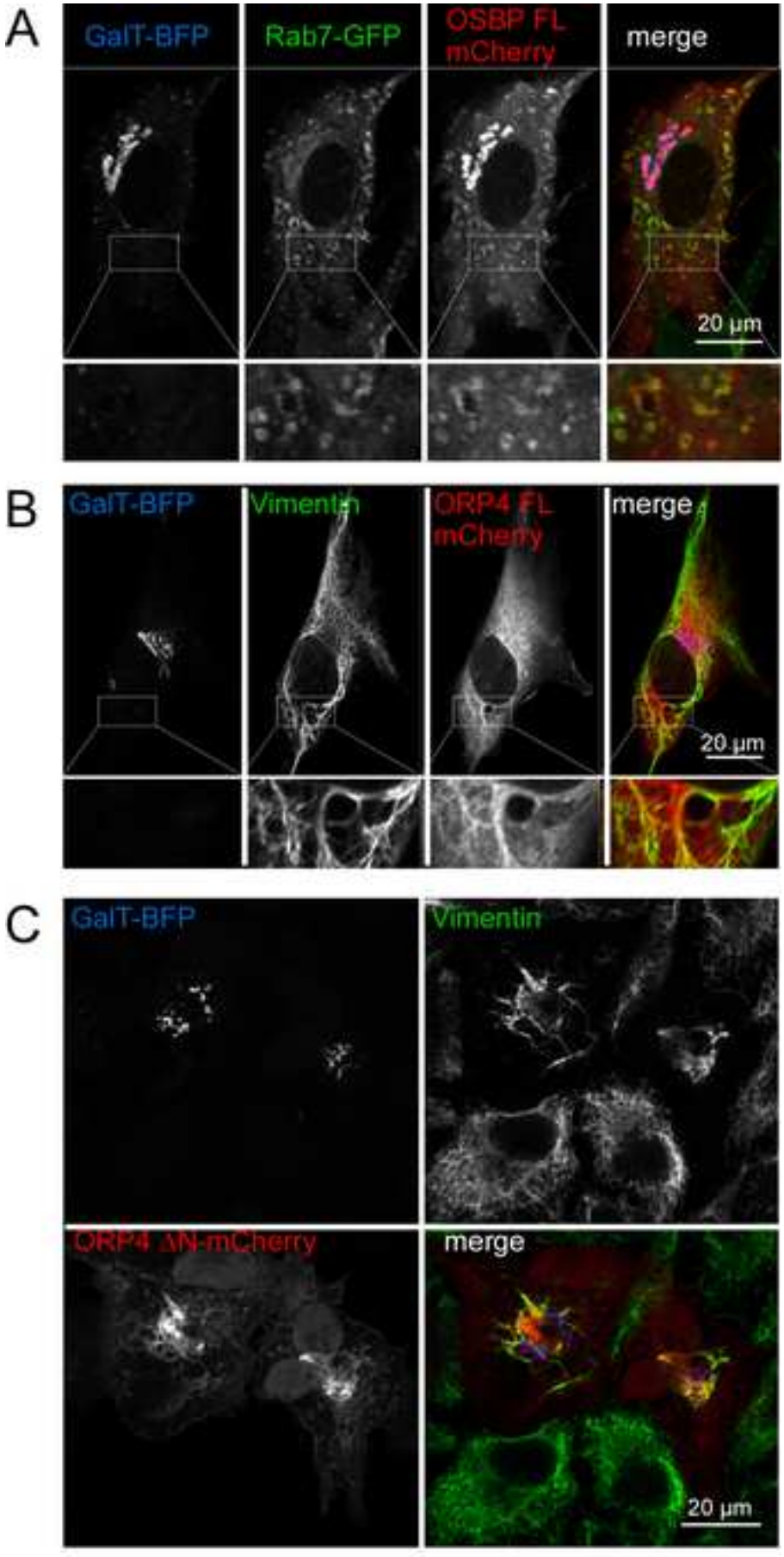

Sup. Figure 3

Figure S4

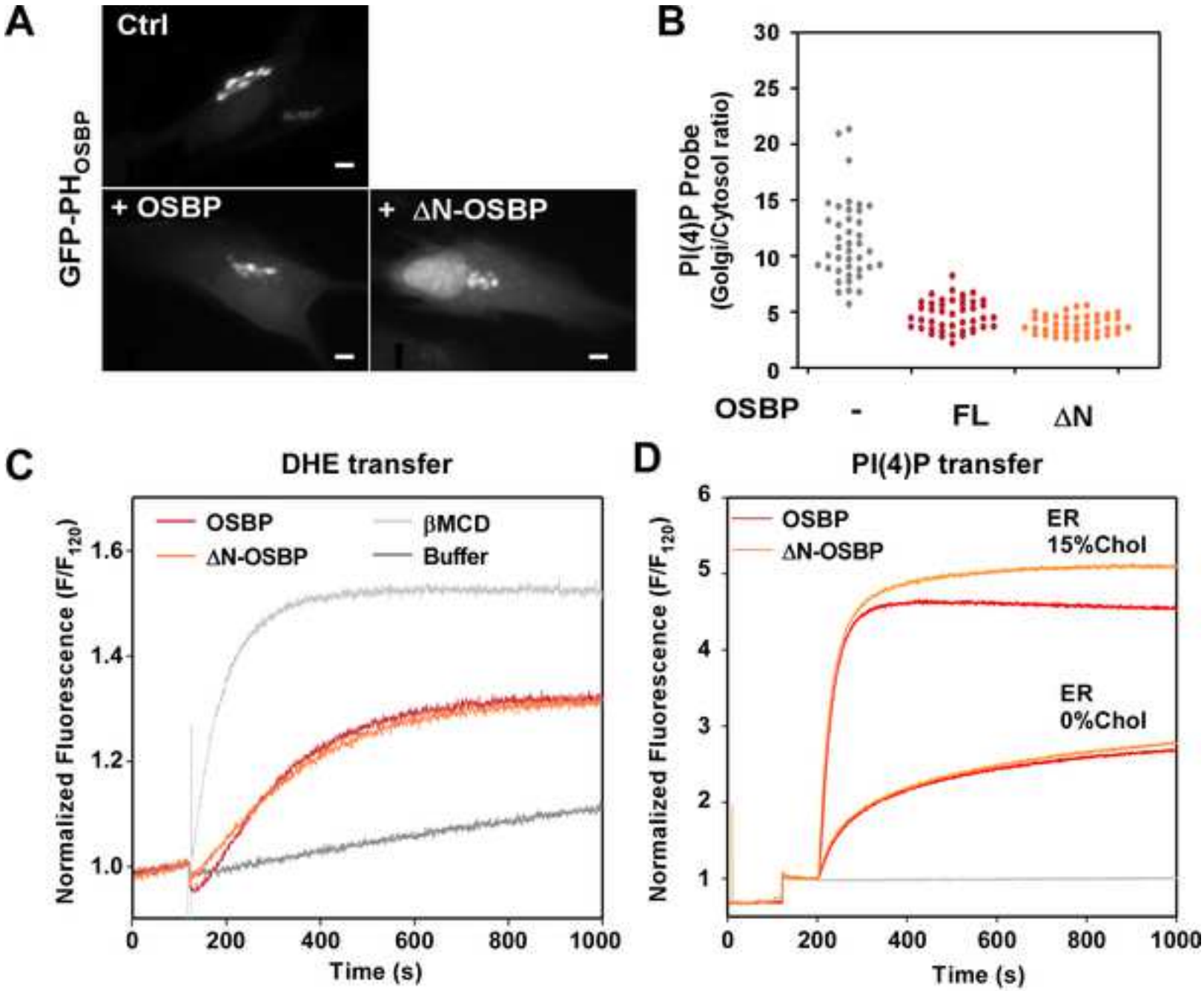

Sup. Figure 4

Figure S5

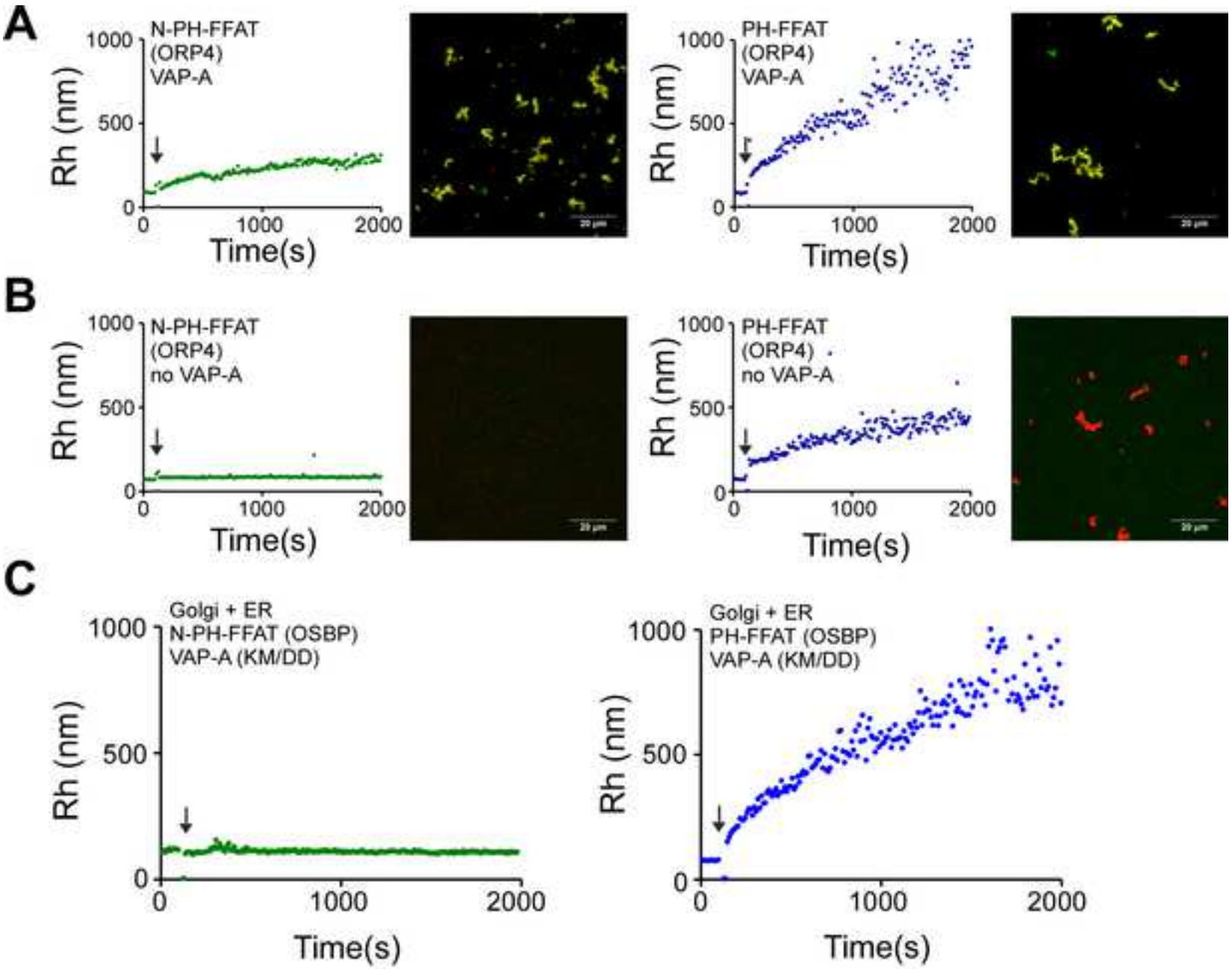

Sup. Figure 5

Figure S6

Click here to access/download;Supplemental Text and Figures;Fig S6 LZW.tif

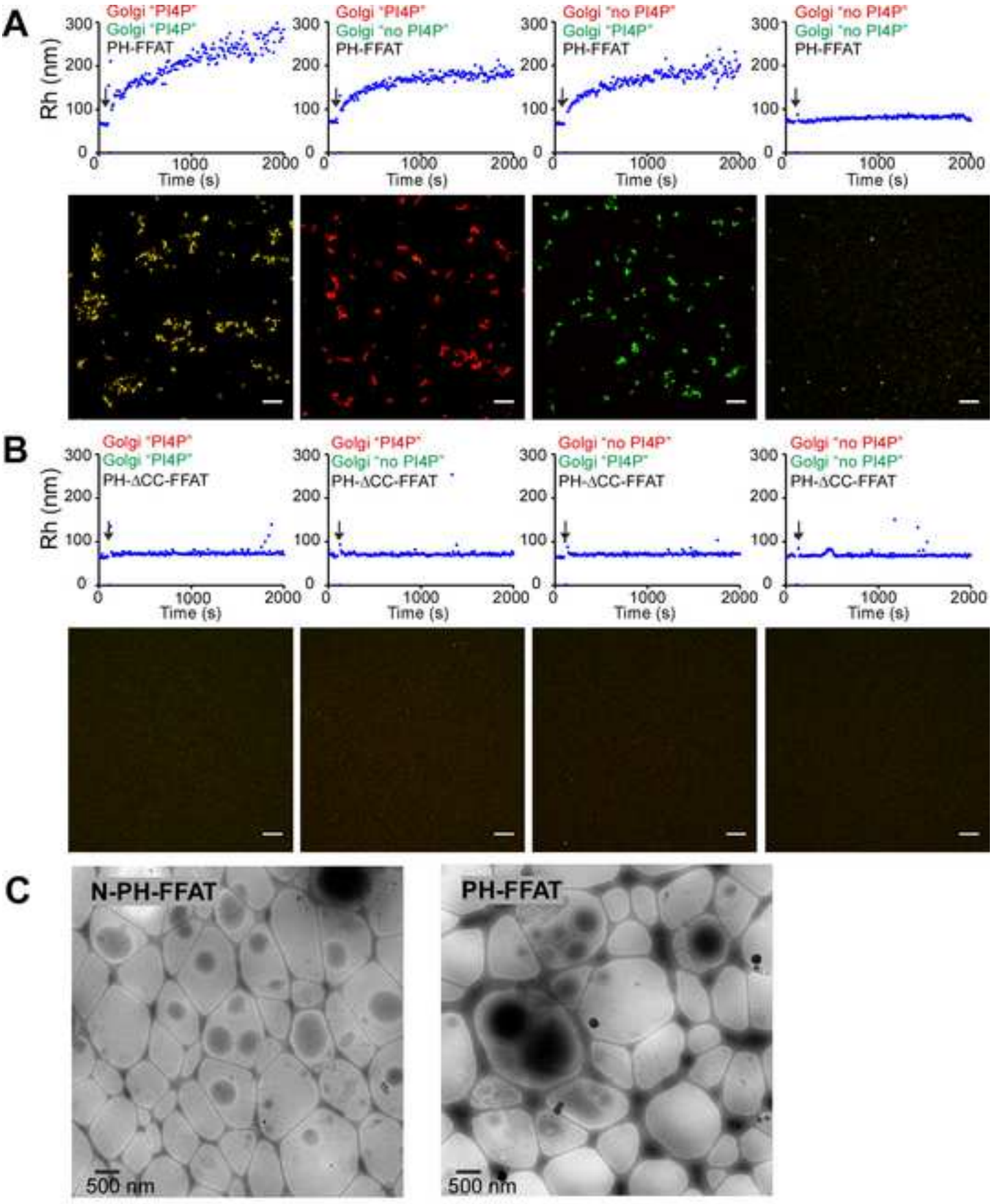

Sup. Figure 6

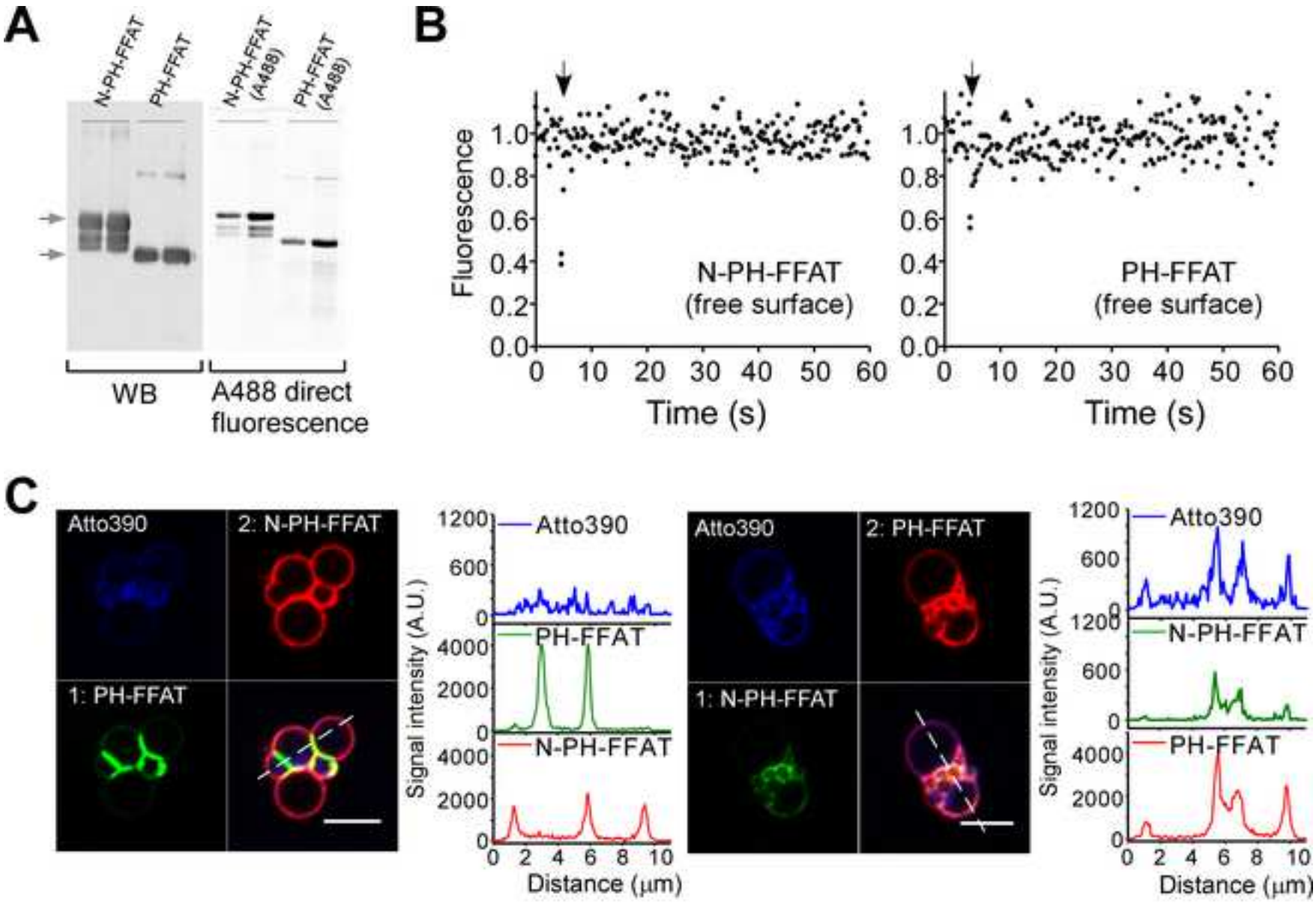

Sup. Figure 7